Simplified Seismic Design for Mid-Rise Buildings with Vertical Combination of Framing Systems

by

Xiaoli Yuan

A thesis
presented to the University of Waterloo
in fulfillment of the
thesis requirement for the degree of
Doctor of Philosophy
in
Civil Engineering

Waterloo, Ontario, Canada, 2016

Author’s Declaration

I hereby declare that I am the sole author of this thesis. This is a true copy of the thesis, including any required final revisions, as accepted by my examiners.

I understand that my thesis may be made electronically available to the public.

Abstract

The mid-rise building with vertical combination of framing systems consists of a structural system in which the seismic-force-resisting-system (SFRS) of the upper structure is commonly a lightweight structural system such as cold-formed steel (CFS) frame or wood frame, while the SFRS associated with the lower one adopts a traditional structural system, such as reinforced concrete (RC) or structural steel frame. In current practice, the presence of: (a) vertical irregularities on mass and stiffness, and (b) damping difference between lower and upper structures creates challenges for the seismic design of such buildings. Presented in this thesis is research with aiming to solve the challenges arising from the foregoing two aspects in relatively simple and practical ways.

Because of the mass irregularity in the vertical direction, the stiffness arrangement for the lower and upper structures in the combined framing system is quite different from that of the "regular" building. A simplified approach is proposed for the determination of storey-stiffness arrangements of such buildings based on the pre-determined mass distribution and specified storey drift limit. In addition, by considering both the mass and stiffness irregularities, two manually-based simplified methods, i.e., modified equivalent lateral force procedure (ELF) and two-stage analysis procedures, are proposed to evaluate seismic loads of the combined framing systems. The simplified approaches to determine the required storey-stiffness arrangements and compute seismic loads are developed based on the USA standard American Society of Civil Engineers 7 (ASCE 7) (ASCE, 2010) at first. Then, by considering the difference in seismic design provisions between ASCE 7 and the Canadian code National Building Code of Canada 2010 (NBCC 2010) (NBCC, 2010), several modifications are made on the simplified approaches based on ASCE 7 for their Canadian application.

In the proposed approach to evaluate the storey-stiffness arrangements, the effects of the interaction between the lower and upper structures in terms of mass and stiffness on the seismic load are investigated. The feasible stiffness arrangements can be obtained based on the required relationship between the stiffness of the lower structure and that of the upper one determined by the proposed approach. Two examples are presented to demonstrate the efficiency of the proposed approach. The result obtained from the proposed approach is justified by the code-specified modal response spectrum analysis. The two examples demonstrate that the relative seismic weight between the lower and upper structures has a significant influence on the required stiffnesses of the lower and upper structures. In general, when the number of the storey and total seismic weight associated with the lower structure are much greater than those of the upper one, the required stiffness of the upper structure will be greatly affected by the interaction between lower and upper structures in terms of

mass and stiffness. On the other hand, if the number of the storey and total seismic weight associated with the lower structure are much smaller than those of the upper one, such interaction has less effect on the required stiffness of the upper structure. In such case, the required stiffness of the upper structure is based primarily on the characteristics of the upper structure.

The modified ELF procedure is applied to the combined framing systems in which there is only one-storey upper structure. Both the applicable requirements and seismic load distributions associated with the modified ELF procedure are proposed. If the storey-stiffness ratio between lower and upper structures is less than a specific value designated as r_{kb1}, the lower structure is dominated primarily by the first mode and the traditional ELF procedure can be used to approximate the seismic load of the lower structure. However, the seismic load of the one-storey upper structure may still be underestimated as the behaviour of the upper structure may be dominated by higher vibration modes of the entire structure. Consequently, the shear force of the one-storey upper structure cannot be estimated based on the traditional ELF procedure. Equations for evaluating the shear force of the one-storey upper structure are presented in the modified ELF procedure.

The two-stage analysis procedure prescribed in ASCE 7 (ASCE, 2006; 2010) ignores the interaction between lower and upper structures in terms of mass and stiffness and permits the lower and upper structure to be analyzed by the conventional ELF procedure, separately. New applicable requirements and seismic load distributions associated with the two-stage analysis procedures are proposed. The proposed procedure is compared with that prescribed in ASCE 7. It is found the stiffness requirement of ASCE 7 two-stage analysis procedure may be inappropriate, which may result in the underestimation of the base shear force of the upper structure in certain cases. Furthermore, the shear force for the top storey of the upper structure may also be considerably underestimated by the ASCE 7 two-stage analysis procedure. Therefore, an additional top shear force is to be applied to the top of upper structure. Equations to compute the additional top shear force are also provided. The accuracy of the proposed two-stage analysis procedure, either the one based on both ASCE 7 or the one based on NBCC 2010, is greatly improved compared to that prescribed in ASCE 7 (ASCE, 2006; 2010).

Finally, damping difference between lower and upper structures in the combined framing system is investigated. By assuming the combined framing systems are classically damped, i.e., the damping matrix of the combined framing systems is orthogonal to the un-damped mode shape, an analytical method to approximate the equivalent modal damping ratio for the case where lower and upper structures have different damping ratios is proposed. However, as the combined framing system in fact is non-classically damped, if the lower and upper structures have different damping ratios, the

proposed approximation of the equivalent modal damping ratio may lead to significant errors on seismic load in certain cases. Therefore, errors on seismic loads resulted from the classical damping approximation, which determine whether the proposed equivalent modal damping ratio is acceptable or not, are investigated. It is found large errors of seismic response associated with the proposed equivalent modal damping ratio usually occur when the dominating modes of the structures have closely spaced natural frequencies. However, for most combined framing systems in practice, the dominating modes have well separated natural frequencies and the proposed equivalent modal damping ratio is applicable to evaluate the seismic response of the combined framing systems. In addition, a new index of damping non-proportionality is suggested in this study to quantify the extent of non-proportional damping.

Acknowledgements

At first I would like to express my sincere appreciation to my supervisor Professor Lei Xu for his guidance and supervision. His insightful discussions, comments and suggestions are sincerely appreciated. His support, both academically and financially, during the completion of this research is invaluable.

I would also like to thank Professor Wei-Chau Xie, Dr. Steven R. Fox, and Professor Armaghan Salehian for serving as my thesis committee members and for their comments and constructive suggestions to this research. Special thanks are given to Professor Colin A. Rogers from University of McGill, for serving as the external examiner and for improving the quality of my thesis.

I greatly appreciate Professor Scott Walbridge for serving as my comprehensive committee member and for his valuable comments and suggestions on this thesis. I also greatly appreciate the assistance and help from my colleagues in the structural group at the University of Waterloo, and the help from my previous colleagues who are currently working in the steel structural group at Chongqing University, China.

The financial support I have received is greatly appreciated: the research assistantships provided by the Natural Sciences and Engineering Research Council of Canada, the University of Waterloo Graduate Scholarship, the Reinhold M. Schuster Graduate Scholarship, the Teaching Assistantship granted by the Department of Civil and Environmental Engineering, and the Doctoral Scholarship granted by China Scholarship Council.

I would like to thank the UW library for the help of providing me invaluable reference materials.

Thanks to my family and friends for their support and encouragement during my Ph.D. studies.

Last but not least, I dedicate this thesis to my husband Weikai Qi. Without his encouragement and support, this thesis would not be possible.

Table of Contents

List of Figures

List of Tables

Nomenclature

m_U	storey-mass of upper structure
k_U	storey-stiffness of upper structure
T_{singU}	single storey-period of upper structure
m_L	storey-mass of lower structure
k_L	storey-stiffness of lower structure
T_{singL}	single storey-period of lower structure
N_L	number of storeys of lower structure
N_U	number of storeys of upper structure
M_U	total mass of upper structure
K_U	overall stiffness of upper structure with the base fixed to the ground
T_U	first mode period of upper structure with the base fixed to the ground
M_L	total mass of lower structure
K_L	overall stiffness of lower structure with the base fixed to the ground
T_L	first mode period of lower structure with the base fixed to the ground
r_m	storey-mass ratio of lower and upper structures, $r_m=m_L/m_U$
r_k	storey-stiffness ratio of lower and upper structures, $r_k=k_L/k_U$
R_m	overall mass ratio of lower and upper structures, $R_m=M_L/M_U$
R_k	overall stiffness ratio of lower and upper structures, $R_k=K_L/K_U$
R	seismic response modification factor
C_d	deflection amplification factor
Δ_U	storey drift associated with the first storey of upper structure
$\Delta_{U\lim}$	storey-drift limit of upper structure
C_{NE}	scale factor of response spectrum acceleration
ω_i	ith-mode natural frequency
T_i	ith-mode period
T_S	period at which the horizontal and descending curves of the response spectrum in ASCE 7-10 intersects
S_a	response spectrum acceleration
α_U	shear-force-amplification factor of the upper structure
r_{kU1}	minimum storey-stiffness ratio
r_{kU2}	the minimum storey-stiffness ratio at which the shear-force-amplification factor $\alpha_U=\alpha_{U\max}$

r_{kU3}	the maximum storey-stiffness ratio at which the shear-force-amplification factor $\alpha_U = \alpha_{U\max}$
$r_{kU2\text{stg}}$	two-stage storey-stiffness ratio of the upper structure
R_{kU1}	minimum overall stiffness ratio
R_{kU2}	the minimum overall stiffness ratio at which the shear-force-amplification factor $\alpha_U = \alpha_{U\max}$
R_{kU3}	the maximum overall stiffness ratio at which the shear-force-amplification factor $\alpha_U = \alpha_{U\max}$
$R_{kU2\text{stg}}$	overall two-stage stiffness ratio of the upper structure
$r_{k2\text{stg}}$	two-stage storey-stiffness ratio of the entire structure
$R_{k2\text{stg}}$	overall two-stage stiffness ratio of the entire structure
r_{kb1}	storey-stiffness ratio at which the effective mass of the entire building associated with the first mode is equal to 90% of the total mass
R_{kb1}	overall stiffness ratio at which the effective mass of the entire building associated with the first mode is equal to 90% of the total mass
$\alpha_{U\max}$	value of α_U when R_k lies between R_{kU2} and R_{kU3}
α_{U1}	value of α_U when $R_k = R_{kU1}$
$\alpha_{U2\text{stg}}$	two-stage shear-force-amplification factor of the upper structure, value of α_U when $R_k \geq R_{kU2stg}$
φ_{ij}	*i*th-DOF mode shape value of the *j*th-mode, where the first subscript *i* represents the *i*th-DOF, and the second subscript *j* represents the *j*th-mode
M_{ij}^*	*j*th-mode effective modal mass of the *i*th-DOF
M_{ij}	normalized *j*th-mode effective modal mass of the *i*th-DOF
M_{Uj}^*	*j*th-mode effective modal mass of the upper structure
M_{Uj}	normalized *j*th-mode effective modal mass of the upper structure
M_{Lj}^*	*j*th-mode effective modal mass of the lower structure
M_{Lj}	normalized *j*th-mode effective modal mass of the lower structure
M_{bj}^*	*j*th-mode effective modal mass of the entire building
M_{bj}	normalized *j*th-mode effective modal mass of the entire building
F_i	lateral seismic force for *i*th-storey of the entire building
V_{Lb}	base shear force of lower structure
V_{Ub}	base shear force of upper structure
V_{Li}	shear force for *i*th-storey of the lower structure

V_{Ui}	shear force for *i*th-storey of the upper structure
V_y	yield shear force
F_{Li}	lateral seismic force for *i*th-storey of the lower structure
F_{Ui}	lateral seismic force for *i*th-storey of the upper structure
F_U	lateral seismic force of the upper structure in the simplified 2DOF model
F_L	lateral seismic force of the lower structure in the simplified 2DOF model
h_n	storey height
h_i	height from the ground base to the *i*th-storey of the entire building
h_{Ui}	height from the base of the upper structure to the *i*th-storey of the upper structure
h_{Li}	height from the ground base to the *i*th-storey of the lower structure
γ	the ratio between the applied additional top shear force and the base shear force of the upper structure
γ_{reg}	the ratio between the applied additional top shear force and the base shear force of a "regular" structure
$\gamma_{\text{reg,NBCC}}$	value of γ_{reg} prescribed in National Building Code of Canada
γ_{intr}	the ratio between the applied additional top shear force and the base shear force of the upper structure, where the additional top shear force is resulted from the interaction of higher vibration modes between lower and upper structures
κ	force distribution exponent associated with the ELF procedure prescribed in ASCE 7
$\mathbf{M}$	mass matrix of the entire building
$\mathbf{K}$	stiffness matrix of the entire building
$\mathbf{C}$	damping matrix of the entire building
$\mathbf{M}_L$	mass matrix of the entire building with the assumption that that storey-mass of the upper structure is zero
$\mathbf{K}_L$	stiffness matrix of the entire building with the assumption that that lateral storey-stiffness of the upper structure is zero
$\mathbf{M}_U$	mass matrix of the entire building with the assumption that that storey-mass of the lower structure is zero
$\mathbf{K}_U$	stiffness matrix of the entire building with the assumption that that lateral storey-stiffness of the lower structure is zero
$\boldsymbol{\Xi}$	modal damping matrix
$\mathbf{x}$	displacement vector
$\mathbf{q}$	modal coordinate vector
ς_L	damping ratio of lower structure

ς_U	damping ratio of upper structure
ς_{eqi}	equivalent damping ratio associated with the *i*th-mode
D_i	displacement response associated with the *i*th-mode
$D_{max,i}$	maximum displacement response associated with the *i*th-mode
Γ_i	participation factor of the *i*th-mode
β_{ij}	period ratio between the *i*th- and *j*th-modes
ρ_{ij}	correlation coefficient between the *i*th- and *j*th- modes
p	peak factor
r_{max}	maximum seismic response for the quantity *r*
$r_{max,i}$	maximum seismic response for the quantity *r* associated with the *i*th-mode
δ_r	error of r_{max} induced by the proposed equivalent modal damping ratio
δ_i	error of r_{max} associated with the *i*th-mode

Chapter 1 Introduction

1.1 Background

The mid-rise building with vertical combination of framing systems consists of a structural system in which the seismic-force-resisting-system (SFRS) of the upper structure is commonly a lightweight structural system such as cold-formed steel (CFS) frame or wood frame while the SFRS associated with the lower one adopts a traditional structural system, such as reinforced concrete (RC) or structural steel frame. In current practice, the combined framing systems are typically adopted in new residential or mixed residential-commercial buildings where the lower structure requires accommodating open spaces with heavier loads such as retail stores or parking garages, as shown in Figure 1.1 (a). Such combined framing systems are also used in the case of adding additional storeys on the top of existing buildings, as shown in Figure 1.1 (b). Existing buildings and their foundations designed based on load combinations without additional levels may not possess adequate axial and seismic capacity when additional storeys are constructed with traditional heavy construction materials. Therefore, additional levels often consist of lightweight materials, such as CFS or wood, to reduce the structural weight and expedite construction progress.

Considering different SFRSs are adopted for lower and upper structures, the seismic design of mid-rise buildings with vertical combination of framing systems are quite different from that of regular ones. Engineers in North America will face following challenges when designing such combined framing systems:

(a) three-storey steel parking garage with nine-storey CFS residential units

(b) five-storey CFS residential units built on an existing two-storey retail building

Figure 1.1: Application of buildings with vertical combination of framing systems (courtesy of Worthington Construction Group)

(1) Due to the difference of structural forms and intended occupancies between lower and upper structures, the storey-masses of lower and upper structures are different. In accordance with current standards ASCE 7 (ASCE, 2010) and NBCC 2010 (NBCC, 2010), the combined framing systems may be designated as having vertical irregularity on mass. In order to satisfy the seismic design requirement, the vertical irregularities on mass may then result in the stiffness arrangement of such buildings to be quite different from that of regular ones. In seismic design of mid-rise building structures with vertical combination of framing systems, storey-masses of lower and upper structures can be approximately evaluated once the structural forms and intended occupancies are determined. After that, however, a trial-and-error procedure, as shown in Figure 1.2, has to be carried out to obtain feasible storey-stiffness distributions for both lower and upper structures. By following this dynamic-analysis-based trial-and-error procedure, Liu et al. (2008) designed a seven-storey building, with the lower one-storey structure being the structural steel moment frame (SMF) and the upper six-storey one being the wood frame. In order to find out the feasible stiffness distributions for both lower and upper structures, multiple designs were tried, which leads this design procedure to be quite tedious. Consequently, it is of great necessity to develop a simplified approach for the engineering practice to replace this lengthy dynamic-analysis-based trial-and-error design procedure to obtain the feasible stiffness distribution.

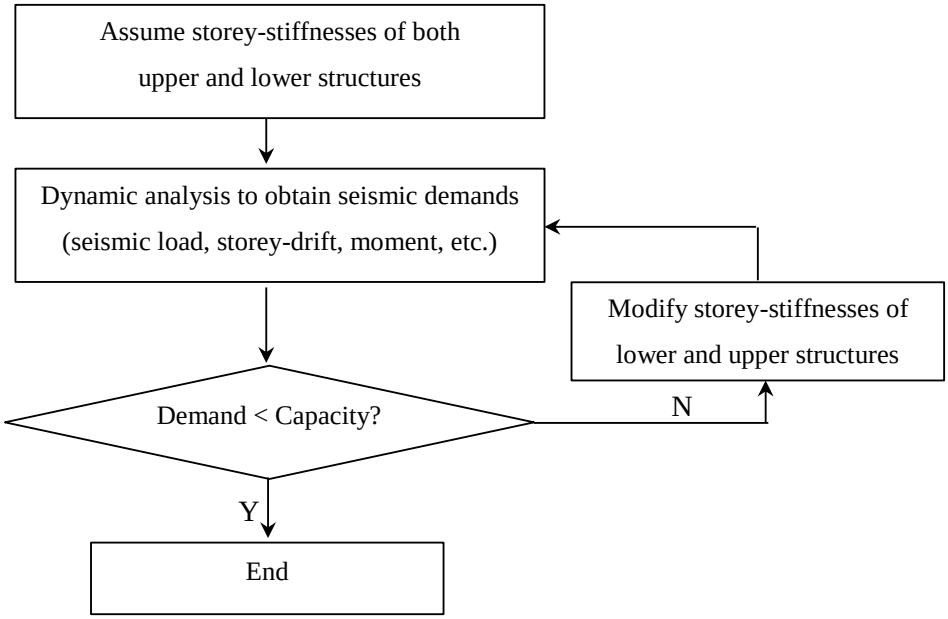

Figure 1.2: Trial-and-error design procedure

(2) Owing to the mass irregularity, the designed structure is usually designated as having stiffness irregularity (ASCE, 2010; NBCC, 2010) as well. With both mass and stiffness irregularities, the dynamic properities of such combined framing structures are quite different from those of "regular" ones. Xiong et al. (2008) carried out full scale shake table tests to investigate the influence of the stiffness irregularity on the seismic behavior of buildings with lower and upper structures being reinforced concrete and wood frames, respectively. It was concluded that the seismic response of such combined framing systems may be influenced by higher vibration modes other than the first mode. Therefore, the traditional equivalent lateral force (ELF) procedure specified in ASCE 7 (ASCE, 2010) and NBCC 2010 (NBCC, 2010), which is applied to analyze "regular" structures, may be no longer generally applicable. Note the ELF procedure is called the equivalent static force (ESF) procedure in NBCC 2010 (NBCC, 2010). The terminology "ELF" is adopted in this thesis to maintain consistency.

Although the traditional ELF procedure may not be applicable for the combined framing systems because of the mass and stiffness irregularities in the vertical direction, there is one unique type of the combined framing system that the ELF procedure may still be applicable with appropriate modification of the procedure. Such unique combined framing system is commonly used in so-called "appendage-style" building, in which there is only one-storey upper structure and the upper structure can be treated as an "appendage" to the lower one. If the upper "appendage" does not have a significant effect on the lower structure, the lower structure can be considered as an independent "regular" building and the ELF procedure is still applicable to estimate its seismic load. However, the challenge arises as to for such "appendage-style" building, what is the applicable requirement of the ELF procedure? Meanwhile, if the seismic load of the lower structure can be approximated by the ELF procedure, how to approximate the seismic load of the upper "appendage"?

In addition to the ELF procedure, the two-stage analysis procedure is another simplified method prescribed in ASCE 7 (ASCE, 2006; 2010) to approximate the seismic load of the combined framing system. The two-stage analsyis procedure allows lower and upper structures be analyzed by the ELF procedure separately if: (a) the stiffness of the lower structure is at least 10 times the stiffness of the upper structure, and (b) the period of the entire structure is not greater than 1.1 times the period of the upper structure considered as a separate structure fixed at the base (ASCE, 2006). Structural engineers have performed the two-stage analysis procedure for the combined framing system since its introduction to the 1988 Uniform Building Code (ICBO, 1988). However, the application of the two-stage analysis procedure primarily limits to the building in which the storey number of the lower structure is one or two (Allen, Chung, Tran & Zepeda, 2013). For the case where the storey number of the lower structure is greater than two, the two-stage analysis procedure is rarely applied. In fact,

recent research suggested that the two-stage analysis procedure prescribed in ASCE 7 (ASCE, 2006) may underestimate the seismic load of the upper structure for certain cases (Xu & Yuan, 2015).

Note the two-stage analysis procedure is only provided in the USA standard ASCE 7 (ASCE, 2006, 2010). The Canadian code NBCC 2010 (NBCC, 2010) does not specify any simplified method similar to the two-stage analysis procedure to analyze the building with vertical combination of framing systems. In accordance with NBCC 2010, the combined framing systems should be analyzed and designed by dynamic analysis.

With the advance in computer capacity and speed and the availability of dynamic analysis procedure in commercially available softwares, it is believed that the elastic dynamic analysis, especially the elastic modal response spectrum analysis (Chopra, 2007), is the most viable means currently to deal with the combined framing systems with mass and stiffness irregularity. Nevertheless, simplified approaches to evaluate seismic loads are still of importance for practical applications. The approaches provide basic dynamic properties of the combined framing systems to help structural engineers have a better understanding on the behavior of such system in resisting seismic loading. Meanwhile, results from the simplified approaches can also serve as a benchmark to check whether the results obtained from the software are reasonable or not. As the possible two simplified analysis methods for the combined framing system, however, the ELF and two-stage analysis procedures in fact cannot be directly applied to the combined framing system because of the previously discussed challenges. To facilitate the application of the these two simplified seismic loading methods, it is necessary to: (a) modify the traditional ELF procedure such that the modified procedure can be applied to the "appendage-style" buildings which satisfy the applicable requirement proposed in this study; (b) develop new applicable requirements and seismic load distribution methods for the two-stage analysis procedure based on ASCE 7 (ASCE, 2010); and (c) propose a two-stage analysis procedure similar to that was developed based on ASCE 7 but to be complied with NBCC 2010 (NBCC, 2010).

(3) Considering lower and upper structures use different materials and SFRSs in the combined framing systems, damping ratios of lower and upper structures may be different. Consequently, the damping matrix of the entire building generally does not satisfy the Caughey-O'Kelly condition (1965). The entire structure is non-classically damped and has complex eigenproperties. Strictly speaking, the seismic response of the non-classically damped systems cannot be obtained from the conventional modal analysis that is based on the classical damping assumption and un-damped eigenproperty. Researchers have developed various modal combination rules, based on damped (Sinha & Igusa, 1995) or un-damped eigenproperty (Falsone & Muscolino, 1999; 2004), to compute

the seismic demand of the non-classically damped system. However, these methods are quite complicated and are rarely applied in practical analysis. Meanwhile, the current design standards ASCE 7 (ASCE, 2010) and NBCC 2010 (NBCC, 2010) do not provide provisions on how to determine the damping ratio in modal response spectrum analysis if lower and upper structures have different damping ratios. In practice, engineers tend to use the conventional modal response spectrum analysis together with a conservative damping ratio, which adopts the smaller one of the damping values associated with lower and upper structures, to design the building. Nevertheless, this approach may lead too conservative results. A more reasonable method to approximate the equivalent damping ratio is needed.

1.2 Research objective

Presented in this thesis is research regarding to solving the foregoing three design challenges discussed in the previous section. The objectives of this research are:

- Propose a simplified approach to evaluate feasible stiffness distributions for the lower and upper structures based on the pre-determined mass distribution and code-specified storey drift limit.
- Overcome the difficulties of applying ELF and two-stage analysis procedures to the combined framing systems by: (a) proposing applicable requirements of the ELF procedure to be applied to the "appendage-style" building and suggesting a method to approximate the seismic load of the upper "appendage"; and (b) developing new applicable requirements and seismic load distribution methods for the two-stage analysis procedure.
- Develop a simplified approach to approximate the equivalent damping ratio by accounting for the damping difference between lower and upper structures.

The proposed simplified approach to evaluate the feasible stiffness distributions of the lower and upper structures and the proposed simplified approach to compute the seismic loads of the combined framing systems are affected by the design standards. As certain difference in seismic design provisions exists between the US standard ASCE 7 (ASCE, 2010) and the Canadian code NBCC 2010 (NBCC, 2010), simplified approaches that can be used together with each standard are developed, respectively. The difference in seismic design provisions between the US standard and the Canadian code, which has certain effect on the proposed simplified approaches, is also discussed in this thesis.

1.3 Applicability of the study

1.3.1 Assumptions

For the reason of simplicity and engineering practice, following assumptions are made in this thesis:

(1) The idealized stick model, as shown in Figure 1.3 (a), is adopted as the analytical model of the combined framing systems.

(2) Code specified modal response spectrum analysis with CQC (complete quadratic combination) rule to evaluate the combination of peak modal responses, as prescribed in ASCE 7 (ASCE, 2010) and NBCC 2010 (NBCC, 2010), is adopted to assess the seismic responses of the building. Damping irregularity is not considered in Chapters 3 ~ 5 but will be accounted for in Chapter 6. The damping ratio for each vibration mode is taken as 5% in Chapters 3 ~ 5, which is the value adopted in both ASCE 7 (ASCE, 2010) and NBCC 2010 (NBCC, 2010) to obtain the default spectrum.

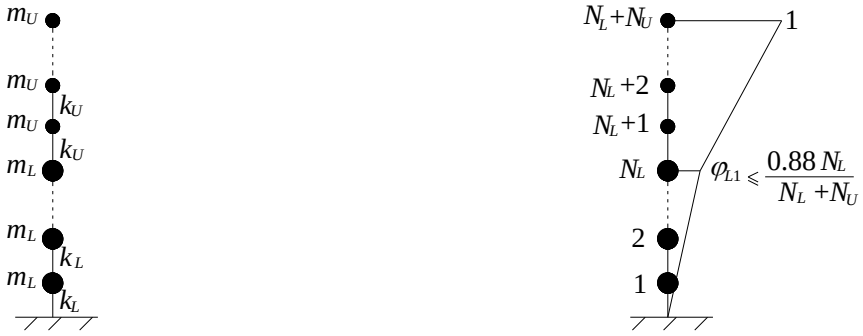

(a) analytical model

(b) first mode shape for combined framing systems with stiffer lower structure

Figure 1.3: Analytical model of the mid-rise building with vertical combination of framing systems

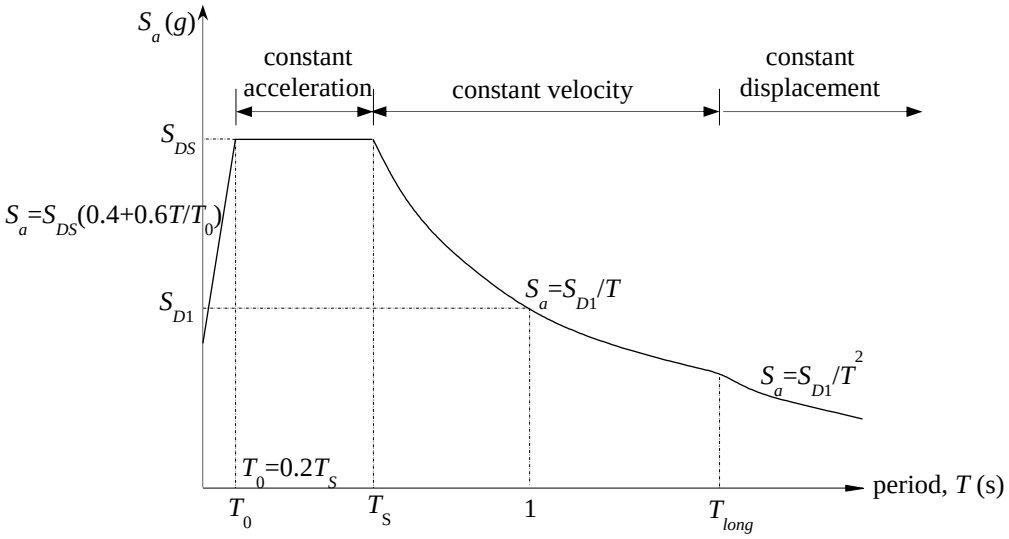

Figure 1.4: ASCE 7-10 design spectrum (ASCE, 2010)

1.3.2 Scope

Buildings with vertical combination of framing systems investigated in this study are limited to the following:

(1) The total number of storeys of the building is not greater than ten, i.e.,$(N_L+N_U)\leq 10$, where N_L and N_U represent numbers of storeys of lower and upper structures, respectively; the storey-masses and lateral storey-stiffnesses of the lower and upper structures, designated as (m_L and m_U) and (k_L and k_U), respectively, are uniformly distributed, as shown in Figure 1.3 (a).

(2) Single storey-periods of the lower and upper structures, denoted as T_{singL} and T_{singU}, are both limited to the range between $0.2T_S$ and $1.1T_S$, where T_S is the period at which the horizontal and descending curves of the ASCE 7 design spectrum intersects, as shown in Figure 1.4. As prescribed in ASCE 7 (ASCE, 2010), the period of a regular structure T should not exceed the product of the upper limit coefficient C_U and the calculated empirical period T_a, where $T_a=C_t(h_n)^x$. Given that (a) the storey height h_n of the structure is generally less than 3.3 m, (b) for the most flexible structures, $C_t=0.0724$ and $x=0.8$, (c) the maximum C_U for high risk seismic zones is 1.4, and (d) the minimum T_S can be assumed to be 0.24 second (USGS, 2014), it is obtained that the maximum T_{singL} or $T_{singU}=1.4\times0.0724\times3.3^{0.8}=0.263$ s$<1.1\times0.24$ s$=1.1T_S$, which indicates both T_{singL} and T_{singU} are not greater than $1.1T_S$.

The NBCC 2010 (NBCC, 2010) has similar prescriptions on the period of a regular structure T. However, the value of the upper limit coefficient C_U and the equation to calculate the empirical period T_a are different. The NBCC considers the steel moment frame as the most flexible structure. The corresponding equation to compute the empirical period of the frame T_a is $T_a=C_t(h_n)^x$, where $C_t=0.085$ and $x=0.75$, and the associated upper limit coefficient $C_U=1.5$. Therefore, it is obtained that based on the NBCC 2010, the maximum T_{singL} or $T_{singU}=1.5\times0.075\times3.3^{0.75}=0.31$ s.

(3) Storey-mass ratio r_m and storey-stiffness ratio r_k of the lower and upper structures are limited to $1\leq r_m\leq 3$ and $\max(1, r_{kU1})\leq r_k\leq 20$, respectively, where $r_m=m_L/m_U$ and $r_k=k_L/k_U$, and r_{kU1}, called as the minimum storey-stiffness ratio, is calculated as follows:

$$r_{kU1}=\left[\frac{r_m N_L\left(0.12N_L+N_U\right)}{\left(N_L+N_U\right)N_U}+\frac{0.12N_L+N_U}{0.88N_L}\right]\frac{N_U}{N_L}\left(\frac{\bar{\omega}_{1U}}{\bar{\omega}_{1L}}\right)^2 \tag{1.1}$$

where $\bar{\omega}_{1L}$ ($\bar{\omega}_{1U}$) is the normalized first mode natural frequency of an N_L(N_U)-storey structure. For an N-storey structure with constant storey-mass and storey-stiffness being m and k, respectively, if the first mode natural frequency is ω_1, then $\bar{\omega}_1=\omega_1(m/k)^{0.5}$. Numerical values of $\bar{\omega}_1$ for one- to ten-storey of such structures are listed in Table 1.1.

Table 1.1: Normalized first mode natural frequency of uniform structures

number of storey N	1	2	3	4	5	6	7	8	9	10
$\bar{\omega}_1$	1	0.618	0.445	0.347	0.285	0.241	0.209	0.185	0.165	0.150

The solution for the minimum storey-stiffness ratio r_{kU1} is derived based on the assumption that the maximum storey-drift ratio of the complete building occurs at the first storey of the upper structure. This assumption is established based on the fact that the application of a stiff lower and a relative soft upper structure is a typical combination, such as the one with reinforced concrete frames as the lower structure and CFS or wood frames as the upper one. Meanwhile, since soft and weak lower structures are detrimental in seismic events (Tena-Colunga, 2004), it is required that the lower structure be stiffer than the upper one. By limiting N_L, N_U, r_m, T_{singU}/T_S and T_{singL}/T_S to the ranges specified previously, it is found the first mode shape should satisfy the relationship $\varphi_{L1} \leq 0.88N_L/(N_L+N_U)$ to ensure the maximum storey-drift ratio occurs at the first storey of the upper structure, as shown in Figure 1.3 (b). Then, as discussed in Appendix C.1, by setting $\varphi_{L1}=0.88N_L/(N_L+N_U)$, the solution for the minimum storey-stiffness ratio r_{kU1} is obtained as shown in Eq.(1.1).

1.4 Thesis organization

The thesis is organized into seven chapters as follows:

- Chapter 2 presents a review on the seismic behavior of structures with mass, stiffness, strength or damping irregularity in the vertical direction.
- Chapter 3 proposes a simplified approach on how to evaluate feasible stiffness distribution in accordance with the pre-determined mass distribution for the combined framing systems. The approach is established based on ASCE 7 (ASCE 7, 2010). The obtained feasible stiffness distribution accounts for the interactions between lower and upper structures in terms of mass and stiffness and ensures that the storey drift requirement can be satisfied.
- Chapter 4 focuses on the critical issues associated with the two simplified seismic analysis methods, i.e., modified ELF and two-stage analysis procedures, to be applied to the combined framing systems. Both the applicable requirements and seismic load distributions associated with the two procedures are developed based on ASCE 7 (ASCE 7, 2010). Meanwhile, the proposed two-stage analysis procedure developed in this study is also compared with the two-stage analysis procedure prescribed in ASCE 7 (ASCE, 2006; 2010).
- Chapter 5 extends the simplified approaches proposed in Chapters 3 and 4, which are established based on ASCE 7 (ASCE, 2010), to be complied with NBCC 2010 (NBCC, 2010).

Differences in seismic design provisions between the NBCC 2010 and the ASCE 7, which result in that the approaches have to be developed as country specific, are investigated and discussed.

- Chapter 6 presents an analytical method to approximate the equivalent modal damping ratio by assuming that buildings with vertical combination of framing systems are classically damped. However, as the combined framing system in fact is a non-classically damped system, errors resulted from the classical damping approximation are also quantitatively analyzed. It is found the classical damping approximation is reasonable for most practical buildings with vertical combination of framing systems.
- Chapter 7 presents the conclusions drawn from the study. Recommendations for the future research concerning buildings with vertical combination of framing systems are outlined.

Chapter 2 Literature survey

2.1 Introduction

Presented in this chapter are previous researches on the seismic behavior of buildings with vertical combination of framing systems. Moreover, considering the similarities on the stiffness, mass and strength distributions between buildings with vertical combination of framing systems and buildings with setbacks, previous researches on the seismic behavior of setback structures are also reviewed.

2.2 Buildings with vertical combination of framing systems

There are limited researches on the seismic behavior of the building with vertical combination of framing systems. These researches primarily focus on two issues: (a) mass, stiffness and strength irregularities induced by different intended occupancies and SFRSs between lower and upper structures; and (b) damping irregularity induced by the different damping ratios associated with the lower and upper structures.

2.2.1 Vertical irregularities on mass, stiffness and strength

The influence of the stiffness irregularity on the seismic response of the combined framing system was investigated by Xiong et.al (2008) through full scale shaking table tests. The tested buildings consisted of a one-storey reinforced concrete lower structure and a two-storey wood frame upper structure. It was concluded that as the increase of storey-stiffness ratio between the lower and upper structures, the seismic response of the lower reinforced concrete structure would be influenced by the second vibration mode, and the seismic response of the upper structure would decrease. The author also pointed out that hold-downs at the corners and around openings at the interface of the upper and lower structures should be carefully designed to prevent the separation of wall studs and sill plates. Based on the experimental results, elastic numerical analysis for the combined framing system was subsequently conducted. The numerical results suggested using the elastic modal response spectrum analysis and the linear time history analysis to evaluate the elastic shear forces of the combined framing system.

Owing to the mass irregularity in the vertical direction, the stiffness design of the combined framing system is quite different from that of regular ones. Liu (2008) proposed a performance based seismic design (PBSD) procedure, which was based on multiple nonlinear time history analyses, for a seven-storey combined framing system. The lower one storey and the upper six storeys of the tested building were constructed by the steel moment frame (SMF) and the wood frame, respectively. The general idea of the proposed PBSD procedure is that with the preliminary design of the wood upper

structure being known, the effective stiffness of the SMF can be determined based on the desired performance, which was assumed to be correlated with the storey drift.

As the lower and upper structures adopt different SFRSs, the ductility ratio μ and ductility-related force modification factor R_d for the lower and upper structures may be different. The current code NBCC (NRCC, 2010) suggests using the lowest R_d factor of the two SFRSs for the entire structure design. However, the study conducted by Chen et.al (2013) showed that the use of a R_d value higher than the lowest R_d factor of the two SFRSs may be justifiable. Equations to estimate the ductility ratio μ and ductility-related force modification factor R_d for the combined framing system, which were constructed of wood portal frames and wood shear walls in the vertical direction, were also proposed by Chen et.al (2013).

2.2.2 Damping irregularity

When the lower and upper structures adopt different materials, the damping ratios of lower and upper structures may be different, and the damping matrix of the entire building generally does not satisfy the Caughey-O'Kelly condition (Caughey and O'Kelly, 1965). The entire structure is non-classically damped, or called as non-proportional damped in some references. The elastic dynamic response of non-classically damped system normally should be analyzed by complex modal superposition method in terms of complex eigenproperties (Perotti, 1994). Similar to the CQC modal combination rules for the classically damped system (Chopra, 2007), modal combination rules associated with the complex modal analysis were also proposed (Sinha & Igusa, 1995). However, the complex eigenvalue problem involves complex algebra and the size of the complex eigenvalue problem is twice the size of that for classically damped one. In order to avoid the complex eigenvalue analysis, Falsone et.al (Falsone & Muscolino, 1999; 2004) suggested using the classical modal property together with a proposed correlation coefficient, which accounts for the non-classical damping effect, to calculate the structural response. By assuming the earthquake ground motion is a white noise process, an analytical solution for the correlation coefficient was obtained. However, the new proposed correlation coefficient is quite different from that of a classically damped system. The calculation of the correlation coefficient involves evaluating the inversion of a matrix, the size of which is n times of that of the damping matrix, where n is the number of the degree of freedom of the entire system. Therefore, it can be seen procedures to evaluate the structural response by both complex modal superposition method (Sinha & Igusa, 1995) and the method proposed by Falsone et.al (1999; 2004) are quite complicated and time consuming. The both are not practically accepted in current engineering process.

Due to the complexity of the complex modal analysis, a decoupling procedure, which neglects the off-diagonal terms of the modal damping matrix, was suggested to approximate the elastic dynamic response. By adopting the decoupling procedure and simplifying the multi-degree-of-freedom model to an equivalent two-degree-of-freedom model, Huang et.al (1996) presented an analytical solution to evaluate the equivalent modal damping ratio of a composite TV tower in which the lower and upper parts were constructed by RC and steel mast, respectively. Although the decoupling procedure is quite convenient for practical application, its main drawback is that it may induce uncertain error. Such errors have been investigated by other researchers (Hasselman, 1976; Warburton & Soni, 1977; Bhaskar, 1994; Morzfeld, Ajavakom & Ma, 2009). It is generally believed that errors due to the decoupling approximation should be negligible if the modal damping matrix is diagonally dominant. Errors are expected to decrease as the modal damping matrix becomes more diagonally dominant. However, it is shown in recent research (Morzfeld , Ajavakom & Ma, 2009) that errors due to the decoupling approximation can increase monotonically at any specified rate while the modal damping matrix becomes more diagonally dominant. Any error-criterion based solely upon the diagonal dominance of the modal damping matrix would not be accurate. In fact, the decoupling error is dependent both on the modal damping matrix and on the excitation frequency. This is the reason why small off-diagonal elements in the modal damping matrix are not sufficient to ensure small decoupling errors. To account for the effect of the excitation frequency, Hasselman (1976) and Warburton et.al (1977) adopted the frequency-domain approach to establish criteria for determining whether a non-classically damped system may be regarded as practically decoupled. It was concluded that for greatly separated frequencies and small damping, the error due to the decoupling approximation in each mode is small. However, Hasselman (1976) and Warburton et.al (1997) only provided qualified indices, which have certain relationship with the possible error of the decoupling method. The error was not analytically quantified.

Owing to the possible error and its lack of analytical quantification associated with the decoupling procedure, some researchers suggested the classical modal properties should be used together with the equivalent modal damping ratios to reduce the error. Papageorgiou and Gantes (2010) suggested the equivalent modal damping ratios be evaluated by complex eigenvalue analysis (Perotti, 1994). They also suggested using an equivalent uniform damping ratio for buildings with vertical combination of concrete and structural steel frames (Papageorgiou & Gantes, 2011). The equivalent uniform damping ratio was obtained by an error minimization procedure through the nonlinear time history analysis between the non-classically damped structure and the equivalent classically damped structure. However, both the equivalent modal damping ratio and the equivalent uniform damping ratio were calculated based on the equivalent two-degree-of-freedom model. The authors pointed out the

transition from actual multi-degree-freedom model to the equivalent two-degree-of-freedom model might not yield satisfactory accuracy in some irregular and complex structural configurations. The authors also addressed that more research was needed to assess the effect of structural irregularity in terms of mass and stiffness distributions. It is recommended in the commercial software Midas Gen (MIDAS/Gen Program, 2000) that the equivalent modal damping ratio be computed as the sum of the damping ratio of each component weighted by the modal strain energy ratio of each component to that of total system (Raggett, 1975). However, no evidence signifies that the composite damping rule method leads to more accurate results than that of the decoupling procedure.

2.3 Setback structures

Comparing to that of the building with vertical combination of framing system, a large number of researches have been carried out to investigate the seismic behavior of setback structures as such type of structures are commonly seen in practice.

Many researchers investigated the influences of mass and stiffness irregularities on the elastic seismic behavior of setback structures. Similar to the combined framing system, setback structures usually exhibit a sudden reduction in storey-mass, storey-stiffness and in some cases in storey strength as well. In a setback structure with a single setback, the lower structure below the setback is usually called the "base", while the upper structure above the setback is called the "tower" (Al-Ali, 1998). Penzien and Chopra (1965) investigated the seismic behavior of buildings with light-weight appendages or towers, and it was concluded that the tower response was found to be greatly accentuated when the natural period of the tower was close to one of the mode periods of the base. Humar (1977) concluded the contribution of higher vibration modes to the base shear force was not negligible when the tower was very slender. In addition, storey drifts and shear coefficients at the level of setback and in the upper storeys of the tower for the setback structure show a pronounced increase compared to those for regular ones. Tso et.al (1994) also found for setback structures, the influence of higher vibration modes on the base shear force was significant. The foregoing researches have demonstrated that higher vibration modes have a significant contribution to the elastic seismic responses of setback structures, such as storey shear forces and storey drifts, and the seismic demands of setback structures cannot be assessed by the ELF procedure.

However, other researches demonstrated that the ELF procedure can be adopted for the seismic design of setback structures. In order to determine whether dynamic analysis was really needed for setback structures, as stipulated by major seismic codes such as NBCC 2005 (NRCC, 2005), Tremblay and Poncet (2005) evaluated the influence of the mass irregularity on the seismic behavior

of setback structures. They concluded that even with strong mass irregularity (200% and 300% storey-mass ratios with setbacks at 25, 50 and 75% of the building height, respectively), setback structures designed with the ELF procedure did not result in significant negative effects on the seismic responses. In addition, adopting a code-specified modal response spectrum analysis in design does not significantly improve the seismic performance, as the peak store drifts obtained from the nonlinear time history analysis are similar regardless of which design procedure was used.

Experimental studies were also conducted to investigate whether dynamic analysis was needed for the seismic design of setback structures. Wood (1985; 1992) carried out shaking table tests for two small-scale (approximately one-fifteenth scale) reinforced concrete setback structures. One (tower structure) has a seven-storey tower on a two-storey base, and another one (stepped structure) has an unsymmetrical arrangement of a three-storey tower, a three-storey middle section, and a three-storey base. The study concluded that the maximum storey shear force could be well represented by the ELF distribution. Moreover, it was observed that the setback frames were not more susceptible to damage or more susceptible to higher mode effects than the frames with uniform profiles. Shahrooz and Moehle (1990) carried out shaking table tests for a six-storey, two-bay by two-bay reinforced concrete moment resisting-frame structure with a 50% setback at the mid-height. The test results demonstrated the dynamic behavior of setback structures were similar to those of regular ones. However, modest concentrations of inelastic behavior were observed in some of the tower members. This concentration was not a manifestation of the dynamics of the configuration, but was explicable in static terms. Moreover, both the conventional modal response spectrum analysis and the ELF procedure were inadequate to prevent this configuration-caused nonlinear damage concentration. It is noted that the results from Shahrooz and Moehle (1990) contradict those from Wood (1985;1992).

Because of the poor seismic performance of setback structures which has been observed during past earthquakes (Shahrooz & Moehle, 1990), many researchers investigated the seismic capacity of setback buildings which were designed by applicable seismic design standards. Two irregular fourteen-storey reinforced concrete moment resisting frame buildings, with one or two-bay frames in the short direction of plan dimension, were studied by Tena-Colunga (2004). In this case, the setback structures were designed by the model response spectrum analysis procedure. Then, nonlinear time history analyses were conducted for these structures. The nonlinear time history results demonstrated that setback structures with only one-bay frame in the short direction was extremely vulnerable in terms of seismic capacity, while the seismic capacity of the two-bay frame setback structure was much improved. Therefore, the author suggested that seismic design standards should penalize buildings with a single-bay frame in the short direction of plan dimension. The influence of setbacks

on the seismic performance of reinforced concrete buildings was evaluated by Athanassiadou (2008) as well. The buildings were designed in accordance with the provisions of the Eurocode 8 (CEN, 2004) for the high and medium ductility class. The nonlinear time history results indicated the seismic performance of all irregular frames appear to be equally satisfactory, not inferior to (and in some cases superior than) that of the regular ones, even for ground motions twice as strong as the design earthquake. These researches indicated if it is designed appropriately, the seismic capacity of the setback structure is equally satisfactory with that of the regular one.

2.4 Comments on previous researches

At first, previous researches on both the combined framing system and setback structure primarily focused on whether dynamic analysis is needed to design such structures. To date, almost no research focused on simplified seismic design for such type of irregular structures has been performed. For example, when determining the stiffness arrangements of lower and upper structures based on the pre-determined mass distribution, the proposed methods were based on nonlinear time history analyses (Liu, van de Lindt & Pryor, 2008), as shown in Figure 1.2. No simplified method to determine such feasible stiffness arrangement was proposed previously.

Secondly, although a lot of researches were conducted for setback structures, there were conflicting conclusions. Some researchers argued that the ELF procedure could not be adopted for the seismic design of setback structures while others held opposite opinions. The potential reason for conflicting conclusions is that almost all conclusions were obtained by case study, and the results are only applicable to the structure with the particular configuration. Therefore, results obtained from different structural configurations contradict each other. From a general aspect, the ELF procedure cannot always ensure a safe design and dynamic analysis should be conducted for setback structures. However, it may still be applicable if the combined framing system satisfies certain requirements. For example, if the combined framing system is dominated by the first mode and the first mode shape is almost linearly distributed along the height, the ELF procedure may still be applicable. Therefore, it is of great necessity to propose applicable requirements of the ELF procedure for its application to the combined framing system. On the other hand, the two-stage analysis procedure has been proposed in building codes of United States for almost forty years (SEAOC, 1973; ATC, 1978). Nevertheless, the applicable requirements and seismic load distribution methods associated with the two-stage analysis procedure have never been systematically evaluated by any research. Its accuracy is questionable. Consequently, the applicable requirements and seismic load distribution methods associated with the two-stage analysis need to be systematically investigated. In order to avoid conflicting conclusions

and make the conclusions be general, the structural model should accommodate various practical structural configurations as discussed in section 1.3.2.

Finally, the damping issue associated with the combined framing system is not satisfactorily solved. The proposed various modal combination rules, based on classical (Sinha & Igusa, 1995) or complex eigenproperty (Falsone & Muscolino, 1999; 2004), to compute the seismic demand of non-classically damped system, are very complicated. Previous researchers only provided qualified indices (Hasselman, 1976; Warburton & Soni, 1977), which have certain relationship with the possible error of the decoupling procedure, to demonstrate the error associated with the decoupling procedure. Errors induced by the decoupling procedure have never been analytically quantified. Furthermore, these indices were proposed based on frequency domain analysis rather than analysis under the earthquake ground motion. In addition to the decoupling procedure, the composite damping rule method (Raggett, 1975) is another popular method to estimate the equivalent modal damping ratio. However, no evidence can signify that the composite damping rule method leads to more accurate results than the decoupling procedure. Another significant topic associated with the combined framing system is how to construct the damping matrix of the entire structure. Nevertheless, almost no discussion on this issue has been conducted previously. Consequently, it is of great necessity to propose an effective and simplified method to solve for these damping issues associated with the combined framing system.

It is also worth noting that researches conducted by Shahrooz (1990) and Tena-Colunga (2004) demonstrated that code-specified modal response spectrum analysis, which estimates the seismic response based on the modal response spectrum analysis together with the adoption of the seismic performance factors, cannot always ensure a safe design when structural members are in the inelastic range. Nevertheless, research by Tena-Colunga (2004) also demonstrated that if appropriate conceptual design is conducted, the code-specified modal response spectrum analysis is still applicable for such setback structures. For example, if one-bay frame in the short direction of plan dimension is prohibited, using modal response spectrum analysis to design setback structures can still lead to satisfactory seismic performance. Therefore, in this study, it is assumed that the conceptual design is appropriately conducted, and the code-specified modal response spectrum analysis can always ensure a safe design.

Chapter 3 A simplified approach to evaluate stiffness distributions for lower and upper structures

3.1 Introduction

A simplified approach for evaluating feasible lateral stiffness distributions of lower and upper structures based on the pre-determined mass distribution, developed in accordance with ASCE 7 (ASCE 7, 2010), is presented in this chapter. At first, a set of applicable design equations are introduced to evaluate the feasible storey-stiffness distributions for both lower and upper structures while the derivation of these equations is discussed in Appendices A ~ D. A proposed design procedure is then presented. Finally, the proposed approach was applied to two design examples to illustrate the accuracy and efficiency of the proposed approach.

3.2 Formulation of design equation I: design criterion

The simplified seismic design approach is developed to ensure that the specified storey-drift limit to be satisfied. The storey-drift-ratio limits specified in ASCE 7 (ASCE, 2010) for the lower and upper structures are identical. Meanwhile, as discussed in section 1.3, the largest storey-drift-ratio occurs at the first storey of the upper structure. Therefore, if the storey drift associated with the first storey of the upper structure satisfies the specified limit, other storey drifts of the upper structures should be within the specified limit.

The storey drift associated with the first storey of the upper structure, Δ_U, can be evaluated as

$$\Delta_U = \frac{V_{Ub}}{k_U}\frac{C_d}{R} \tag{3.1}$$

where V_{Ub} is the elastic base shear force of the upper structure, k_U is the storey-stiffness of the upper structure, as shown in Figure 3.1 (a), and R and C_d are the seismic response modification coefficient and the deflection amplification coefficient, respectively. For the case where the lower and upper structures have different R values, the seismic design coefficients (R, C_d) associated with the system that has the lower of the two R values is suggested to be used in Eq.(3.1). As the shear force V_{Ub} is affected by the interaction between lower and upper structures in terms of mass and stiffness, the following factor is proposed to quantify such interaction:

$$\alpha_U = \frac{V_{Ub}}{m_U N_U S_a\left(T_U\right)} \tag{3.2}$$

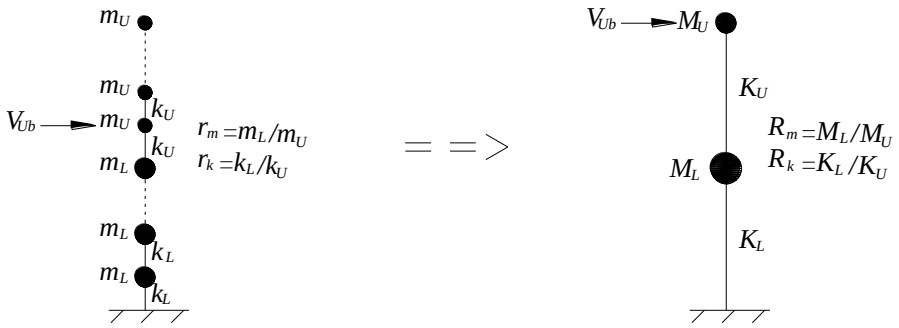

(a) MDOF model (b) 2DOF model

Figure 3.1: Model simplification

where m_U and N_U are the storey-mass and storey number of the upper structure, respectively, T_U is the vibration period of the upper structure when the base fixed to the ground, and $S_a(T_U)$ is the design spectral acceleration associated with the period T_U. Since the factor α_U accounts for the shear-force-amplification effect contributed by the lower structure to the upper one, it is called as shear-force-amplification factor of the upper structure. Based on Eq. (3.2), the elastic base shear force V_{Ub} can be calculated as follows:

$$V_{Ub} = \alpha_U m_U N_U S_a(T_U) \tag{3.3}$$

By substituting V_{Ub} in Eq.(3.1) with Eq.(3.3), and assuming the drift Δ_U is within the specified limit, the governing equation of the simplified design is

$$\alpha_U \le \frac{R}{C_d} \frac{k_U \Delta_{U\,\mathrm{lim}}}{m_U N_U S_a(T_U)} \tag{3.4}$$

where $\Delta_{U\mathrm{lim}}$ is the code specified storey-drift limit for the upper structure (ASCE, 2010). The factor α_U on the left hand side of Eq.(3.4) is related to the storey-mass and storey-mass stiffness distributions of both lower and upper structures. In seismic design of mid-rise buildings with vertical combination of framing systems, storey-stiffnesses of the upper and lower structures, k_U and k_L, should conform to certain relationship to ensure Eq.(3.4) is satisfied. In order to solve for Eq.(3.4) and obtain such required relationship, an analytical study is firstly conducted in section 3.3 to develop empirical equations of evaluating the factor α_U. Then, based on the proposed empirical equations of evaluating the factor α_U, Eq.(3.4) is solved and corresponding design equations are provided in section 3.4.

3.3 Formulation of design equation II: analytical study on factor α_U

Illustrated in Figure 3.2 is the process about how an analytical study is carried out to obtain empirical equations for evaluating the factor α_U. At first, a simplified two-degree-of-freedom (2DOF) model is

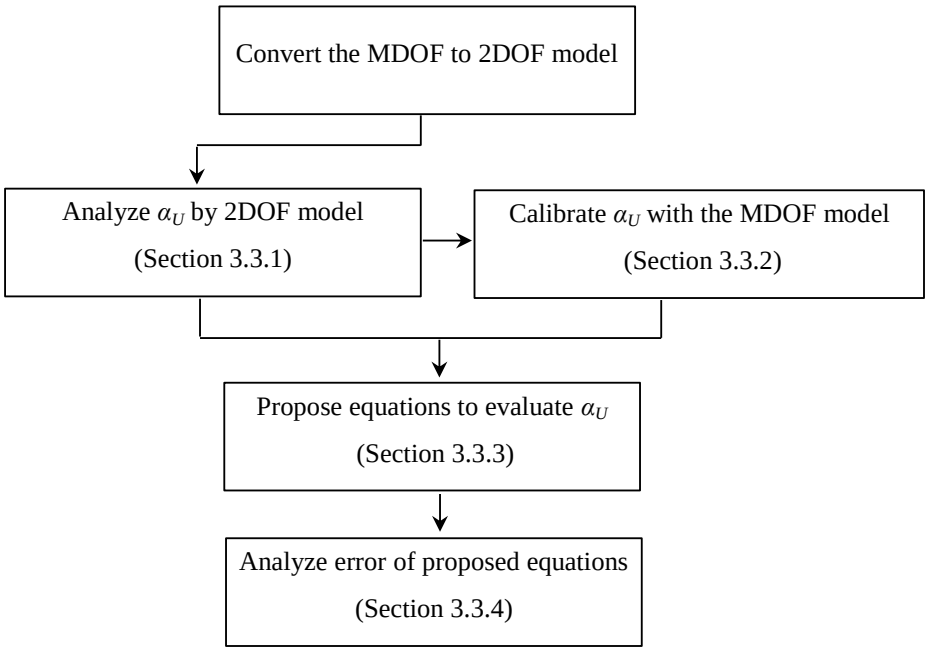

Figure 3.2: Flowchart illustrating the process to investigate the factor α_U

proposed to estimate the seismic behavior of the multi-degree-of-freedom (MDOF) model with mass and stiffness irregularities as shown in Figure 3.1. For any building having an N_L-storey lower structure and an N_U-storey upper structure, with storey-masses and lateral storey-stiffnesses of the lower and upper structures being (m_L and m_U) and (k_L and k_U), respectively, the overall masses and stiffnesses for the upper and lower structures of the simplified 2DOF model are approximated as follows:

$$M_U = m_U N_U \tag{3.5 a}$$

$$K_U = \left(\bar{\omega}_{1U}\sqrt{k_U / m_U}\right)^2 M_U \tag{3.5 b}$$

$$M_L = m_L N_L \tag{3.5 c}$$

$$K_L = \left(\bar{\omega}_{1L}\sqrt{k_L / m_L}\right)^2 M_L \tag{3.5 d}$$

where $\bar{\omega}_{1L}$ ($\bar{\omega}_{1U}$) is the normalized first mode natural frequency of an N_L(N_U)-storey structure as listed in Table 1.1. Then, the analytical study on the factor α_U is carried out based on the simplified 2DOF model. As the model simplification to convert the MDOF to a simplified 2DOF model is an empirical process, analytical results of α_U obtained from the simplified 2DOF model are calibrated by that of the MDOF model. Finally, empirical equations to evaluate the factor α_U are proposed in section 3.3.3. Error analysis is also carried out to assess the practicability of the proposed equations.

3.3.1 Analytical results based on simplified 2DOF model

With modal response spectrum analysis, the equation to evaluate the shear-force-amplification factor α_U based on the simplified 2DOF model is presented in Eq. (A.16) of Appendix A. As discussed in Appendix A, the factor α_U evaluated based on the simplified 2DOF model is associated with the overall mass ratio R_m, overall stiffness ratio R_k and period ratio T_U/T_S, where T_S is the period at which the horizontal and descending curves of the design spectrum intersects, as shown in Figure 1.4, and R_m, R_k and T_U are defined as

$$R_m = \frac{M_L}{M_U} = \frac{r_m N_L}{N_U} \tag{3.6}$$

$$R_k = \frac{K_L}{K_U} = r_k \left(\frac{N_L}{N_U} \right) \left(\frac{\bar{\omega}_{1L}}{\bar{\omega}_{1U}} \right)^2 \tag{3.7}$$

$$T_U = \frac{2\pi}{\bar{\omega}_{1U}} \sqrt{\frac{m_U}{k_U}} \tag{3.8}$$

Effects of overall stiffness ratio R_k

For given values of overall mass ratio R_m and period ratio T_U/T_S, the variations of the factor α_U with respect to the ratio R_k , i.e., α_U-R_k curve, are shown in Figures 3.3 (a) ~ (c). As discussed in Appendix B.1, the effects of R_k on the factor α_U can be summarized as follows:

(1) When the lower structure is extremely flexible compared to the upper one ($R_k \rightarrow 0$), the factor $\alpha_U \rightarrow 0$, which indicates there is no seismic load applied to the upper structure and in such case the lower structure acts similar to a damper as illustrated in Figure 3.4 (a).

(2) When the lower structure is much stiffer than the upper one, the factor $\alpha_U \rightarrow 1$. For this case, the lower structure has no influence on the upper one, and the upper structure behaves as it is fixed to the ground base as shown in Figure 3.4 (b). In such case, the two-stage analysis procedure prescribed in ASCE 7 (ASCE, 2010) is applicable to analyze the combined framing system.

For a given overall mass ratio R_m, let R_{kU2stg}, the smallest value of the overall stiffness ratio that results in α_U=1, be the two-stage stiffness ratio of the upper structure. As discussed in Appendix C.2, R_{kU2stg} can be evaluated as

$$R_{kU2stg} = \begin{cases} 0.826R_m + 4.76 & R_m \le 0.71 \\ 11.029R_m - 2.5 & R_m > 0.71 \end{cases} \tag{3.9}$$

(3) As the ratio R_k increases from zero to R_{kU2stg}, the factor α_U either monotonically increases from zero to unity; or initially increases from zero to a maximum value and then decreases to unity, as shown in Figures 3.3 (a) ~ (c).

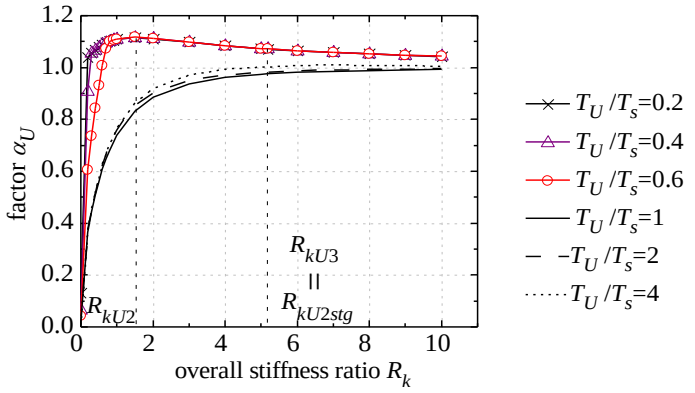

(a) R_m=0.5

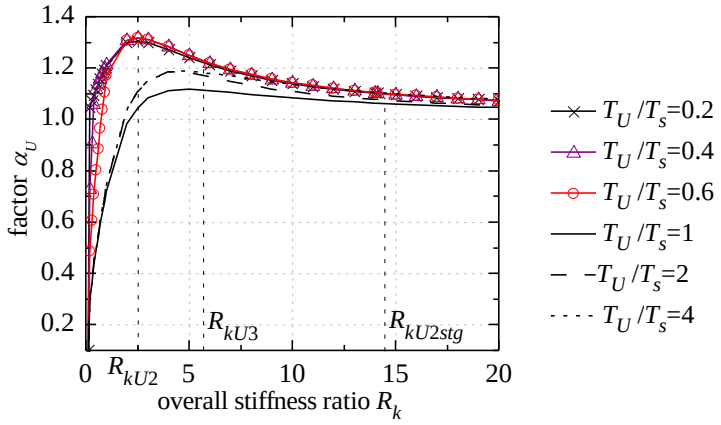

(b) R_m=1.5

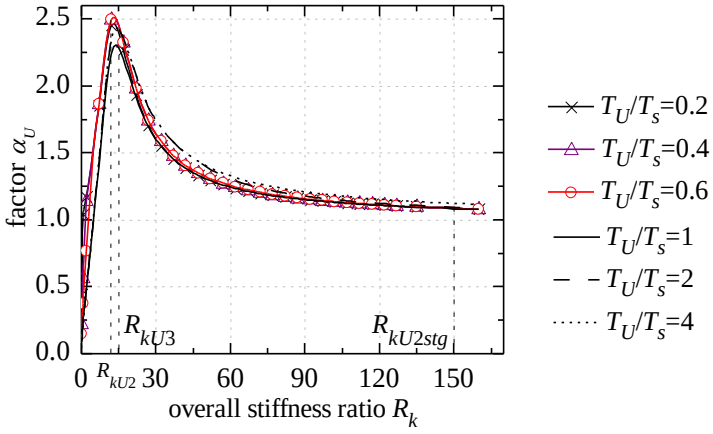

(c) R_m=12

Figure 3.3: Variation of the shear-force-amplification factor of the upper structure

(a) extremely flexible lower structure ($R_k \to 0$) (b) extremely stiff lower structure ($R_k \geq R_{kU2stg}$)

Figure 3.4: Physical interpretation of extremely flexible and stiff lower structure

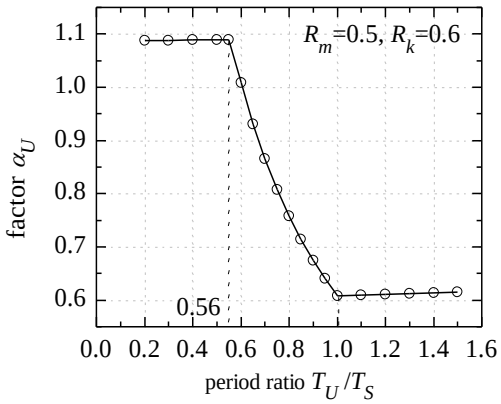

Figure 3.5: Effect of period ratio T_U/T_S on the factor α_U

Effects of overall mass ratio R_m

The effects of the overall mass ratio R_m on the factor α_U is discussed in Appendix B.2. As shown in Figures 3.3 (a) ~ (c), the maximum α_U on each α_U-R_k curve increases as the increase of the ratio R_m. The maximum α_U is close to unity when R_m is small (Figure 3.3 a). However, when the mass of the lower structure is relatively heavy, i.e. R_m is large, as illustrated in Figure 3.3 (c), the maximum α_U on the α_U-R_k curve is far greater than unity.

Effects of period ratio T_U/T_S

The effects of the period ratio T_U/T_S on the factor α_U is discussed in Appendix B.3 and the following are observed:

(1) The ratio T_U/T_S has no influence on the factor α_U when $(T_U/T_S) \leq (T_U/T_1)$ or $(T_U/T_S) \geq 1$, while the factor α_U decreases as the increase of the ratio T_U/T_S if $(T_U/T_1) < (T_U/T_S) < 1$, where T_1 is the first-mode period of the simplified 2DOF model. For example, for the case where R_m=0.5 and R_k=0.6, the calculated period ratio T_U/T_1 based on Eqs.(A.7) and (A.8) of Appendix A is 0.56. As shown in Figure 3.5, the factor α_U keeps as a constant when $(T_U/T_S) \leq 0.56$ or $(T_U/T_S) \geq 1$; while the factor α_U gradually decreases as the ratio T_U/T_S increases from 0.56 to unity.

(2) As to each α_U-R_k curve, the overall stiffness ratio R_k at which the factor α_U reaches the maximum value generally increases as the increase of the ratio T_U/T_S when $(T_U/T_S)\leq 1$, as shown in Figures 3.3 (a) ~ (c). Let R_{kU2} and R_{kU3} be the overall stiffness ratios at which the factor α_U reaches the maximum value for $T_U/T_S=0.2$ and $T_U/T_s\geq 1$, respectively. As discussed in Appendix C.5, ratios R_{kU2} and R_{kU3} can be determined as follows:

$$R_{kU2} = R_m + 1 \tag{3.10}$$

$$R_{kU3} = \begin{cases} R_{kU2stg} & R_m \leq 0.71 \\ -0.26R_m + 5.52 & 0.71 < R_m < 1 \\ R_m + 3 & R_m \geq 2 \end{cases} \tag{3.11}$$

From Eqs. (3.10) ~(3.11), it can be seen for the case where $R_m\geq 2$, R_{kU2} and R_{kU3} are located close to each other, as shown in Figure 3.3 (c). Meanwhile, based on $T_U/T_L=(R_k/R_m)^{0.5}$, where T_L is the period of the lower structure, it is obtained that the factor α_U reaches the maximum value when $T_U \approx T_L$ if $R_m\geq 2$. Such amplification effect of the lower structure on the upper one is similar to the resonance observed in the response of a single-degree-of-freedom (SDOF) system to harmonic excitations (Chopra, 2007).

However, for the case where $R_m<2$, values of R_{kU2} and R_{kU3} may be of great difference due to the influence of T_U/T_S. Especially when $R_m\leq 0.71$, the ratio R_{kU3} is equal to the overall two-stage stiffness ratio R_{kU2stg}, which indicates the factor α_U will monotonically increase to unity as the increase of the ratio R_k for the case when $T_U/T_S\geq 1$, as shown in Figure 3.3 (a). Despite of the difference between the value of R_{kU2} and the value of R_{kU3} for the case where $R_m<2$, there is not a significant change for the value of factor α_U on each α_U-R_k curve if the ratio R_k lies between R_{kU2} and R_{kU3}, as shown in Figures 3.3 (a) and (b).

3.3.2 Analytical results calibration with the MDOF model

With N_L, N_U, r_m, r_k, T_{singU}/T_S and T_{singL}/T_S being limited to ranges specified in section 1.3.2, the factor α_U evaluated based on the MDOF model (Eq.(D.1) in Appendix D.1) is compared with that evaluated based on the simplified 2DOF model (Eq.(A.16) in Appendix A). As discussed in Appendix D.1, the error associated with the simplified 2DOF model is primarily affected by the storey-stiffness ratio r_k. Let r_{kU2}, r_{kU3} and r_{kU2stg} be critical storey-stiffness ratios of the MDOF model, which are calculated from ratios R_{kU2}, R_{kU3} and R_{kU2stg} of the simplified 2DOF model through Eq.(3.7), respectively. Errors associated with the simplified 2DOF model are in the range -43.58% ~22.41%, 0% ~22.41% and -8.27% ~20.24% for cases where $r_k<r_{kU1}$, $r_{kU2}\leq r_k\leq r_{kU3}$ and $r_k>r_{kU3}$, respectively. With the negative and

positive error signifying the simplified 2DOF model underestimating and overestimating the factor α_U, respectively, it is concluded:

(1) When $r_k<r_{kU2}$, as the simplified 2DOF model may greatly underestimate the factor α_U, the factor α_U should be estimated from the MDOF model rather than the simplified 2DOF model because of the significance of the error.

(2) When $r_{kU2}\leq r_k\leq r_{kU3}$, the factor α_U can be estimated from the simplified 2DOF model.

(3) When $r_k>r_{kU3}$, the error of the simplified 2DOF model is acceptable; however, for the case where the simplified 2DOF model may underestimate the factor α_U, minor modifications should be introduced to avoid such underestimation.

3.3.3 Proposed equations to evaluate the shear-force-amplification factor α_U

The general concept of using proposed equations, Eqs.(3.12) ~(3.23), to evaluate the shear-force-amplification factor α_U is to convert the MDOF model with mass and stiffness irregularity into a simplified 2DOF model. With the determination of R_m, R_k and T_U/T_S, the factor α_U can be determined by following empirical equations:

$$\alpha_U=\begin{cases}\alpha_{U1}\left(R_k/R_{kU1}\right)^{x_1} & R_{kU1}\leq R_k<R_{kU2} \quad \text{(a)}\\ \alpha_{U\max} & R_{kU2}\leq R_k\leq R_{kU3} \quad \text{(b)}\\ \alpha_{U\max}\left(R_k/R_{kU3}\right)^{x_2} & R_{kU3}<R_k<R_{kU2stg} \quad \text{(c)}\\ \alpha_{U2stg} & R_k>R_{kU2stg} \quad \text{(d)}\end{cases} \tag{3.12}$$

where

$$x_1=\frac{\ln(\alpha_{U\max}/\alpha_{U1})}{\ln(R_{kU2}/R_{kU1})} \tag{3.13}$$

$$x_2=\frac{\ln(\alpha_{U2stg}/\alpha_{U\max})}{\ln(R_{kU2stg}/R_{kU3})} \tag{3.14}$$

$$\alpha_{U1}=\begin{cases}\alpha_{U11} & T_U/T_S\geq 1\\ \alpha_{U12} & T_U/T_S\leq\sqrt{\left(N_U+0.12N_L\right)/\left(N_U+N_L\right)}\\ \alpha_{U11}\left(T_U/T_S\right)^{x_3} & \sqrt{\left(N_U+0.12N_L\right)/\left(N_U+N_L\right)}<T_U/T_S<1\end{cases} \tag{3.15}$$

$$x_3=\frac{\ln(\alpha_{U12}/\alpha_{U11})}{0.5\ln\left[\left(N_U+0.12N_L\right)/\left(N_U+N_L\right)\right]} \tag{3.16}$$

$$\alpha_{U\max}=\begin{cases}\alpha_{U\max1} & T_U/T_S\geq 1\\ \alpha_{U\max2} & T_U/T_S\leq 0.769\left(R_m\right)^{0.059}\\ \alpha_{U\max1}\left(T_U/T_S\right)^{x_4} & 0.769\left(R_m\right)^{0.059}<T_U/T_S<1\end{cases} \tag{3.17}$$

$$x_4 = \frac{\ln(\alpha_{U\max 2} / \alpha_{U\max 1})}{\ln\left[0.769\left(R_m\right)^{0.059}\right]} \tag{3.18}$$

$$\alpha_{U\max 1} = \begin{cases} 0.03R_m + 1.0 & R_m \le 0.71 \\ 0.17R_m + 0.90 & 0.71 < R_m \le 4.5 \\ -0.005R_m^2 + 0.190R_m + 0.91 & 4.5 < R_m \le 16 \\ 0.047R_m + 1.918 & R_m > 16 \end{cases} \tag{3.19}$$

$$\alpha_{U\max 2} = \begin{cases} 1.1 & R_m \le 0.40 \\ 0.35R_m + 0.96 & 0.40 < R_m \le 0.71 \\ 0.209R_m + 1.061 & 0.71 < R_m \le 4.5 \\ -0.0025R_m^2 + 0.145R_m + 1.40 & 4.5 < R_m < 21 \\ 0.0335R_m + 2.639 & R_m \ge 21 \end{cases} \tag{3.20}$$

$$\alpha_{U2stg} = \begin{cases} 1.1 & R_m \le 1.4 \\ 0.14R_m + 0.918 & 1.4 < R_m \le 2.3 \\ -0.08R_m + 1.424 & 2.3 < R_m < 4.1 \\ 1.1 & R_m \ge 4.1 \end{cases} \tag{3.21}$$

In Eqs. (3.12) ~ (3.14), R_{kU2} and $R_{kU2\text{stg}}$ are computed based on Eqs.(3.10) and (3.11), respectively; and R_{kU1} is the overall stiffness ratio corresponding to the minimum storey-stiffness ratio r_{kU1} prescribed in section 1.3.2. By substituting r_k in Eq.(3.7) with r_{kU1} that is expressed by Eq.(1.1), R_{kU1} is then expressed by Eq.(3.22). Meanwhile, R_{kU3} in Eqs.(3.12) ~ (3.14) are evaluated based on Eq.(3.23).

$$R_{kU1} = \frac{R_m\left(0.12N_L + N_U\right)}{N_L + N_U} + \frac{0.12N_L + N_U}{0.88N_L} \tag{3.22}$$

$$R_{kU3} = \begin{cases} 4.13R_m + 2 & R_m \le 0.8 \quad \text{(a)} \\ -0.26R_m + 5.52 & 0.8 < R_m < 2 \quad \text{(b)} \\ R_m + 3.0 & R_m \ge 2 \quad \text{(c)} \end{cases} \tag{3.23}$$

The effects of R_m, R_k and T_U/T_s on the factor α_U, which are discussed in section 3.3.1, are all accounted for in the proposed equations for evaluating the factor α_U, i.e., Eqs.(3.12) ~ (3.23). Furthermore, for the case where the simplified 2DOF model may underestimate the shear-force-amplification factor α_U, as discussed in section 3.3.2, minor modifications are made.

Effects of overall stiffness ratio R_k

Based on Figures 3.3 (a) ~ (c), proposed α_U-R_k curves are summarized as shown in Figures 3.6 (a) ~ (c). For each α_U-R_k curve, it is divided into four regions. As shown in Eq.(3.12), for regions 1 ($R_{kU1} \le R_k < R_{kU2}$) and 3 ($R_{kU3} < R_k < R_{kU2stg}$), the α_U-R_k relationship is fitted by a power function, while for

regions 2 ($R_{kU2} \leq R_k \leq R_{kU3}$) and 4 ($R_k \geq R_{kU2stg}$), constant values of $\alpha_{U\max}$ and α_{U2stg} are proposed, respectively. For simplicity, the value of $\alpha_{U\max}$ is set to be the maximum value of α_U when R_k is located in region 2 ($R_{kU2} \leq R_k \leq R_{kU3}$).

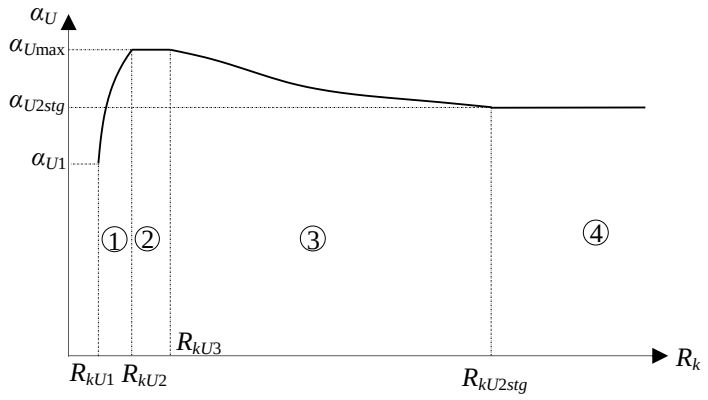

(a) $R_{kU1} < R_{kU2}$

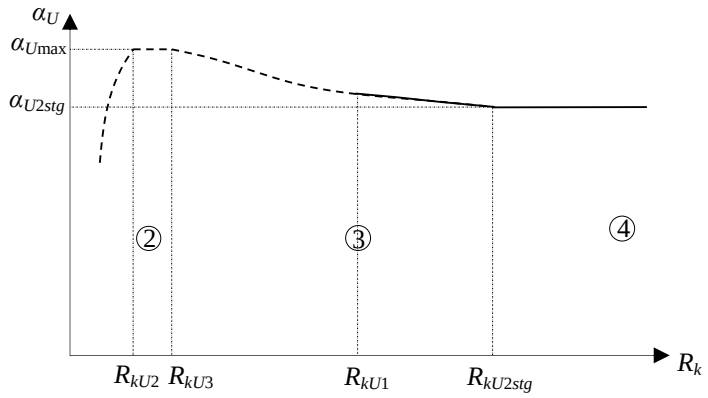

(b) $R_{kU1} \geq R_{kU2}$, $\alpha_{U\max} > \alpha_{U2stg}$

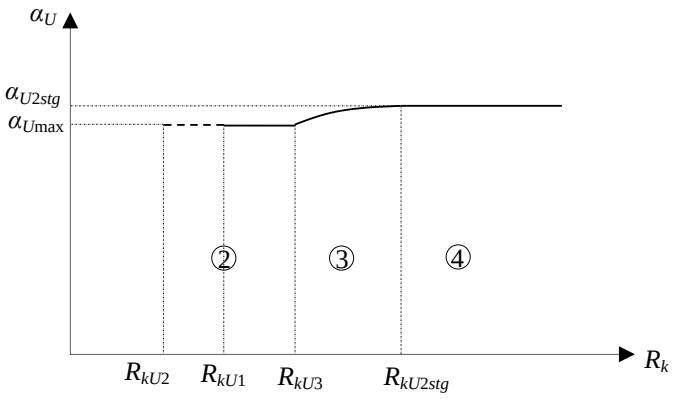

(c) $R_{kU1} \geq R_{kU2}$, $\alpha_{U\max} \leq \alpha_{U2stg}$

Figure 3.6: Proposed α_U-R_k relationship

Note for the case where the calculated R_{kU1} in Eq.(3.22) is smaller than R_{kU2} of Eq.(3.10), α_U is set to be α_{U1} when $R_k=R_{kU1}$, as shown in Figure 3.6 (a). However, if $R_{kU1}\geq R_{kU2}$, as shown in Figures 3.6 (b) ~ (c), α_U should be computed in accordance with the magnitude of R_{kU1} through Eqs.(3.12) (b) ~ (d) when $R_k=R_{kU1}$.

Effects of period ratio T_U/T_S

Considering the influence of T_U/T_S on the factor α_U being discussed in section 3.3.1, values of α_{U1} and $\alpha_{U\max}$ are evaluated by Eqs.(3.15) and (3.17), respectively. When $T_U/T_S\leq T_U/T_1$ or $T_U/T_S\geq 1$, α_{U1} is correspondingly set to be a constant α_{U11} and α_{U12}, and $\alpha_{U\max}$ is set to be a constant $\alpha_{U\max1}$ and $\alpha_{U\max2}$, respectively. When $T_U/T_1<T_U/T_S<1$, a power function is introduced to approximate the relationship between $\alpha_{U1}(\alpha_{U\max})$ and T_U/T_S.

Note in Eqs.(3.15) and (3.17), values of T_U/T_1 are calculated through Eq.(A.8) by setting $R_k=R_{kU1}$ and $R_k=R_{kU2}$, respectively, and it is then obtained that $T_U/T_1=[(N_U+0.12N_L)/(N_U+N_L)]^{0.5}$ and $0.769(R_m)^{0.059}$, respectively.

Effects of overall mass ratio R_m

Values of α_{U11}, α_{U12}, $\alpha_{U\max1}$ and $\alpha_{U\max2}$ are only associated with R_m. Values of $\alpha_{U\max1}$ and $\alpha_{U\max2}$ are evaluated based on the simplified 2DOF model by using Eq.(A.16) of Appendix A. By setting $T_U/T_S=1$ and $T_U/T_S=0.769(R_m)^{0.059}$, the maximum value of α_U for $R_{kU2}\leq R_k\leq R_{kU3}$ is set to be $\alpha_{U\max1}$ and $\alpha_{U\max2}$, respectively. Then, by curve fitting, empirical equations to calculate $\alpha_{U\max1}$ and $\alpha_{U\max2}$ are provided in Eqs. (3.19) and (3.20), respectively, as shown in Figure 3.7 (a).

For the case where $r_{kU1}<r_{kU2}$ in the MDOF model, which corresponds to $R_{kU1}<R_{kU2}$ in the simplified 2DOF model, the simplified 2DOF model may greatly underestimate the factor α_U if $r_k<r_{kU2}$, as discussed in section 3.3.2. Therefore, values of α_{U11} and α_{U12} in Eq.(3.15) cannot be estimated from the simplified 2DOF model. For possible upper and lower storey combinations that would result in $R_{kU1}<R_{kU2}$, values of α_{U11} and α_{U12} are calculated based on the elastic modal response spectrum analysis of the MDOF model by setting $T_U/T_S=1$ and $T_U/T_S=[(N_U+0.12N_L)/(N_U+N_L)]^{0.5}$, respectively. The calculated results are provided in Table 3.1. Since Table 3.1 only lists for cases r_m=1, 2 and 3, for other r_m values, values of α_{U11} and α_{U12} can be linearly interpolated by the magnitude of r_m.

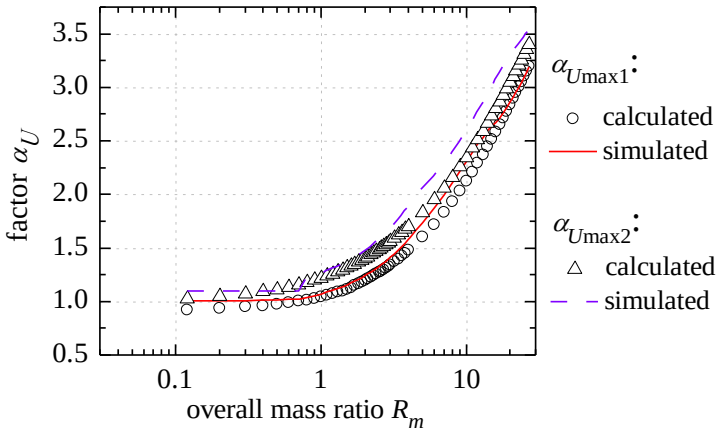

(a) values of α_{Umax1} and α_{Umax2}

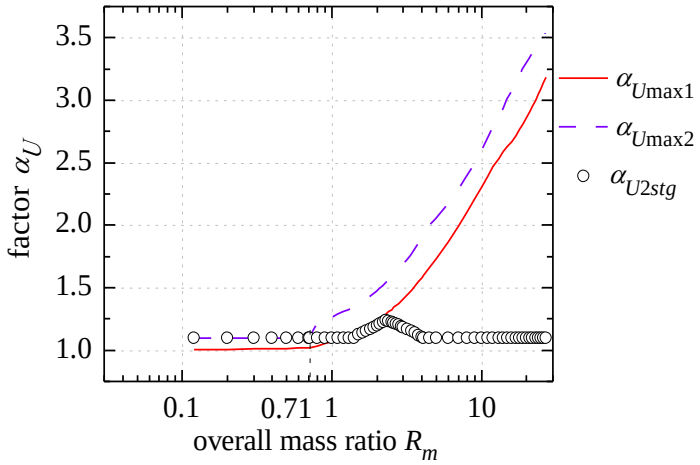

(b) comparison among α_{Umax1}, α_{Umax2} and α_{U2stg}

Figure 3.7: Numerical values for critical shear-force-amplification factors

Theoretically, the value of α_{U2stg} shown in Eq.(3.12 d) should be unity as discussed in section 3.3.1. However, a 10% increase is proposed for the reason of being conservative, i.e., α_{U2stg}=1.1. Moreover, as the simplified 2DOF model ignores the interaction of higher vibration modes between lower and upper structures, the simplified 2DOF model may underestimate the factor α_U when R_k>R_{kU3} as discussed in Appendix D.1. Consequently, the value of α_{U2stg}, which corresponds to the value of α_U when R_k>R_{kU2stg}, may be underestimated by the simplified 2DOF model. For cases where the simplified 2DOF model may underestimate the factor α_U, value of α_{U2stg} may need to be increased. For mid-rise buildings satisfying the limitation stated in section 1.3.2, numerical analyses indicate when 1.4<R_m<4.1, the value of α_{U2stg} should be increased in accordance with Eq.(3.21), as shown in Figure 3.7 (b).

Table 3.1: Values of α_{U11} and α_{U12} for case where $R_{kU1}<R_{kU2}$

N_L	N_U	r_m=1		r_m=2		r_m=3	
		α_{U11}	α_{U12}	α_{U11}	α_{U12}	α_{U11}	α_{U12}
1	1	0.986	1.258	1.162	1.435	1.281	1.572
2	1	0.990	1.468	1.179	1.681	1.296	1.818
3	1	0.979	1.550	1.165	1.757	1.267	1.874
4	1	0.985	1.609	1.163	1.801	1.253	1.899
5	1	0.993	1.652	1.165	1.826	1.248	1.910
6	1	1.007	1.686	1.175	1.846	1.252	1.921
7	1	0.929	1.556	1.077	1.692	1.145	1.754
8	1	0.942	1.575	1.086	1.703	1.154	1.761
9	1	0.956	1.593	1.100	1.716	1.168	1.771
2	2	0.905	1.237	1.086	1.412	1.222	1.555
3	2	0.893	1.314	1.088	1.516	1.221	1.663
4	2	0.944	1.452	1.150	1.674	1.283	1.823
5	2	0.943	1.500	1.147	1.720	1.269	1.856
6	2	0.948	1.541	1.148	1.754	1.260	1.877
7	2	0.954	1.574	1.148	1.778	1.250	1.888
8	2	0.959	1.600	1.145	1.793	1.239	1.892
3	3	0.872	1.223	1.051	1.391	1.190	1.532
4	3	0.869	1.278	1.064	1.470	1.200	1.617
5	3	0.921	1.400	1.127	1.615	1.267	1.769
6	3	0.925	1.441	1.131	1.661	1.267	1.809
7	3	0.927	1.476	1.134	1.696	1.262	1.836
3	4	0.918	1.231	1.066	1.373	1.204	1.502
4	4	0.905	1.285	1.092	1.459	1.240	1.605
5	4	0.903	1.331	1.106	1.525	1.250	1.678
6	4	0.907	1.370	1.114	1.577	1.256	1.732
4	5	0.901	1.223	1.054	1.383	1.197	1.515
5	5	0.892	1.193	1.077	1.385	1.225	1.548

Finally, note when $R_m \leq 0.71$, $R_{kU3} = R_{kU2\text{stg}}$ based on Eq.(3.11); however, the proposed $\alpha_{U\max}$ evaluated by Eqs.(3.17) ~ (3.20) is not always equal to α_{U2stg} evaluated by Eq.(3.21), as shown in Figure 3.7 (b). This may result in a discontinuity of the proposed α_U-R_k curve. To avoid such discontinuity, R_{kU3} is reduced for the case where $R_m \leq 0.8$ to ensure the corresponding $R_{kU3}<R_{kU2stg}$, as shown in Eq. (3.23 a). In fact, for the case where the value of R_k, which corresponds to the maximum α_U in the α_U-R_k curve of the simplified 2DOF model, is greater than that of the proposed R_{kU3} calculated by Eq. (3.23 a), the following is observed: (a) the factor α_U will monotonically increase from zero to unity on the α_U-R_k curve, as shown in Figure 3.3 (a); and (b) on the other hand, $\alpha_{U\max}$ is

smaller than α_{U2stg} in the proposed α_U-R_k curve for such cases as shown in Figure 3.6 (c). Therefore, by comparing Figure 3.3 (a) to Figure 3.6 (c), it is clear that the proposed reduction on R_{kU3} warrants the proposed method to be conservative.

The case $\alpha_{U\max} \leq \alpha_{U2stg}$ usually occurs when $R_m<1$. For the possible upper and lower storey combinations that may result in $R_{kU1}<R_{kU2}$, the calculated R_m is usually greater than unity, and the calculated $\alpha_{U\max}$ is therefore greater than α_{U2stg} as shown in Figure 3.6 (a).

3.3.4 Error analysis

Results obtained from the proposed approach are compared with those from the elastic response spectrum analysis procedure of the MDOF model with CQC rule to combine the peak modal responses (Chopra, 2007). The maximum and minimum errors for the buildings with an N_L-storey lower structure and an N_U-storey upper structure, as shown in Table 3.2 and Table 3.3 are obtained based on all the possible combinations of r_m, r_k, T_{singU}/T_S and T_{singL}/T_S. The positive and negative error in the table represents the proposed approach overestimates and underestimates the amplification factor α_U, respectively. From Table 3.2 and Table 3.3, it can be seen the errors associated with the proposed method for the factor α_U are in the range of -0.9% to 35.8%. The error of 35.8% is comparable with that of the conventional ELF procedure (ASCE, 2010) which is applied for "regular" structures. Take a ten-storey building as example. Assume: (a) the storey-mass of the lower four-storey structure m_L is approximately 1.3 times that of the upper six-storey one m_U (m_L =1.3m_U), and the storey-stiffness of the lower structure k_L is 1.2 times that of the upper one k_U (k_L =1.2k_U); (b) k_U=1366.04m_U/s^2, which then results in the period of the ten-storey structure is 1.09 second, a quite reasonable period for a practical ten-storey structure; and (c) the building is located in Los Angeles, California with type B soil condition, which results in the design spectrum being S_{DS}=1.632g and S_{D1}=0.572g. In accordance with the standard ASCE 7 (ASCE, 2010), this building can be considered as a "regular" structure and the ELF procedure can be used to evaluate the seismic load. It is found the shear force of the fifth-storey evaluated based on the ELF procedure prescribed in ASCE 7 and the modal response spectrum analysis is 47.48 m_U and 36.47 m_U, respectively. In this case, the ELF procedure overestimates the shear force by about 30%.

Table 3.2: Maximum errors of the proposed method on factor α_U (ASCE 7 spectrum)

N_L \ N_U	1	2	3	4	5	6	7	8	9
1	13.8%	15.7%	20.9%	23.7%	24.8%	25.6%	26.0%	26.2%	26.2%
2	18.8%	25.2%	21.9%	22.0%	24.6%	27.0%	28.5%	28.9%	N/A
3	21.2%	25.3%	30.6%	27.9%	25.9%	24.9%	25.8%	N/A	N/A
4	23.1%	25.2%	29.8%	33.5%	32.1%	29.0%	N/A	N/A	N/A
5	24.1%	25.2%	28.7%	32.5%	35.8%	N/A	N/A	N/A	N/A
6	23.6%	25.7%	27.9%	31.3%	N/A	N/A	N/A	N/A	N/A
7	15.3%	23.0%	26.1%	N/A	N/A	N/A	N/A	N/A	N/A
8	15.0%	19.6%	N/A	N/A	N/A	N/A	N/A	N/A	N/A
9	15.0%	N/A	N/A	N/A	N/A	N/A	N/A	N/A	N/A

Note: N/A denotes the proposed method is not applicable for the combination of the lower and upper structures.

Table 3.3: Minimum errors of the proposed method on factor α_U (ASCE 7 spectrum)

N_L \ N_U	1	2	3	4	5	6	7	8	9
1	-0.9%	1.9%	3.0%	5.9%	11.1%	12.4%	13.2%	13.8%	14.1%
2	3.6%	3.7%	3.4%	0.0%	2.0%	5.4%	6.3%	7.7%	N/A
3	1.9%	3.4%	3.6%	1.8%	0.9%	-0.1%	1.1%	N/A	N/A
4	0.9%	7.4%	3.7%	1.2%	0.6%	1.4%	N/A	N/A	N/A
5	1.0%	6.9%	6.6%	3.4%	1.0%	N/A	N/A	N/A	N/A
6	1.5%	5.4%	9.1%	3.7%	N/A	N/A	N/A	N/A	N/A
7	0.4%	7.0%	9.0%	N/A	N/A	N/A	N/A	N/A	N/A
8	1.4%	7.7%	N/A	N/A	N/A	N/A	N/A	N/A	N/A
9	1.9%	N/A	N/A	N/A	N/A	N/A	N/A	N/A	N/A

Note: N/A denotes the proposed method is not applicable for the combination of the lower and upper structures.

The error associated with the proposed approach is primarily resulted from two aspects: (a) the conversion of a MDOF model to a simplified 2DOF model; and (b) the approximations adopted in Eqs.(3.12) ~(3.23). Generally, the positive error is associated with the overestimation of $\alpha_{U\max}$, which is primarily induced by model conversion; whereas the error induced by approximation of $\alpha_{U\max}$ in Eqs.(3.17) ~ (3.20) will not exceed 17.2% for any cases. Take the building with N_L=5, N_U=5, T_{singU}/T_S=0.3, r_m=1 and r_k=2 as example. The error of $\alpha_{U\max}$ associated with model conversion is 20.1%, while the error results from the approximation of $\alpha_{U\max}$ is only 13.1%. Consequently, the resulted maximum error of the proposed approach for this case is 35.8%, as shown in Table 3.3.

3.4 Formulation of design equation III: stiffness evaluation

In order to solve for Eq.(3.4) and obtain the required stiffnesses of the upper and lower structures, firstly express the spectral acceleration $S_a(T_U)$ corresponding to the period of the upper structure T_U as follows:

$$S_a(T_U)=\begin{cases} S_{DS} & T_U/T_S \le 1 \\ S_{D1}/T_U & T_U/T_S > 1 \end{cases} \tag{3.24}$$

where S_{D1} and S_{DS} are design spectral accelerations when T=1.0 second and T=T_S, respectively, as shown in Figure 1.4. Note in accordance with scope of this study presented in section 1.3.2, the period of the upper structure T_U in (3.24) is not less than the transition period $0.2T_S$ .Secondly, substitute T_U evaluated based on Eq.(3.8) into Eqs. (3.15), (3.17) and (3.24). Then, substitute R_k, α_{U1}, $\alpha_{U\max}$, and α_{U2stg} evaluated respectively based on Eqs.(3.7), (3.15), (3.17) and (3.21) into Eq.(3.12). Finally, by substituting α_U and the spectrum acceleration $S_a(T_U)$ evaluated respectively based on Eqs.(3.12) and (3.24) into Eq.(3.4) and based on the definition of the storey-stiffness ratio r_k (r_k=k_L/k_U), it is obtained that the stiffness k_U of Eq.(3.4) should satisfy the following requirement:

$$k_U \ge k_{U\min} \tag{3.25}$$

If

$$k_U \ge k_{U\max} \tag{3.26}$$

there is no specific requirement on k_L as long as the value of k_L satisfies Eqs.(3.40) and (3.41) discussed later on in this section to ensure the assumptions stated in section 1.3.2 are satisfied. However, if k_U is limited between k_{Umin} and k_{Umax} (k_{Umin}<k_U <k_{Umax}), the k_L should satisfy the following requirement:

(1) R_{kU1}<R_{kU2} (Figure 3.6 a)

$$k_L \le \left(\frac{\alpha_{U\lim}}{\alpha_{U1}}\right)^{1/x_1} R_{kU1}\frac{N_U}{N_L}\left(\frac{\bar{\omega}_{1U}}{\bar{\omega}_{1L}}\right)^2 k_U \quad \text{or} \quad k_L \ge \left(\frac{\alpha_{U\lim}}{\alpha_{U\max}}\right)^{1/x_2} R_{kU3}\frac{N_U}{N_L}\left(\frac{\bar{\omega}_{1U}}{\bar{\omega}_{1L}}\right)^2 k_U \tag{3.27}$$

(2) $R_{kU1}\ge R_{kU2}$, $\alpha_{U\max}$>$\alpha_{U2\text{stg}}$ (Figure 3.6 b)

$$k_L \ge \left(\frac{\alpha_{U\lim}}{\alpha_{U\max}}\right)^{1/x_2} R_{kU3}\frac{N_U}{N_L}\left(\frac{\bar{\omega}_{1U}}{\bar{\omega}_{1L}}\right)^2 k_U \tag{3.28}$$

(3) $R_{kU1}\ge R_{kU2}$, $\alpha_{U\max}\le\alpha_{U2\text{stg}}$ (Figure 3.6 c)

$$k_L \le \left(\frac{\alpha_{U\lim}}{\alpha_{U\max}}\right)^{1/x_2} R_{kU3}\frac{N_U}{N_L}\left(\frac{\bar{\omega}_{1U}}{\bar{\omega}_{1L}}\right)^2 k_U \tag{3.29}$$

In Eqs.(3.25) ~ (3.29),

$$\alpha_{U\lim}=\frac{R}{C_d}\frac{k_U\Delta_{U\lim}}{m_U N_U S_a(T_U)} \tag{3.30}$$

$$k_{U\max}=\begin{cases}\max\left(k_{\alpha U1},\ k_{\alpha U\max},\ k_{\alpha U2stg}\right) & R_{kU1}<R_{kU2}\\ \max\left(\ k_{\alpha U\max},\ k_{\alpha U2stg}\right) & R_{kU1}\geq R_{kU2}\end{cases} \tag{3.31}$$

$$k_{U\min}=\begin{cases}\min\left(k_{\alpha U1},\ k_{\alpha U\max},\ k_{\alpha U2stg}\right) & R_{kU1}<R_{kU2}\\ \min\left(\ k_{\alpha U\max},\ k_{\alpha U2stg}\right) & R_{kU1}\geq R_{kU2}\end{cases} \tag{3.32}$$

In Eqs. (3.31) and (3.32),

$$k_{\alpha U1}=\begin{cases}m_U\left[\alpha_{U11}N_U\dfrac{\bar{\omega}_{1U}}{2\pi}\dfrac{C_d}{R}\dfrac{S_{D1}}{\Delta_{U\lim}}\right]^2 & k_{\alpha U1}\leq k_{US1}\\ \alpha_{U12}m_UN_U\dfrac{C_d}{R}\dfrac{S_{DS}}{\Delta_{U\lim}} & k_{\alpha U1}\geq k_{US3}\\ m_U\left[\alpha_{U11}N_U\left(\dfrac{2\pi}{\bar{\omega}_{1U}T_S}\right)^{x_3}\dfrac{C_d}{R}\dfrac{S_{DS}}{\Delta_{U\lim}}\right]^{\frac{1}{1+0.5x_3}} & k_{US1}<k_{\alpha U1}<k_{US3}\end{cases} \tag{3.33}$$

$$k_{\alpha U\max}=\begin{cases}m_U\left[\alpha_{U\max1}N_U\dfrac{\bar{\omega}_{1U}}{2\pi}\dfrac{C_d}{R}\dfrac{S_{D1}}{\Delta_{U\lim}}\right]^2 & k_{\alpha U\max}\leq k_{US1}\\ \alpha_{U\max2}m_UN_U\dfrac{C_d}{R}\dfrac{S_{DS}}{\Delta_{U\lim}} & k_{\alpha U\max}\geq k_{US2}\\ m_U\left[\alpha_{U\max1}N_U\left(\dfrac{2\pi}{\bar{\omega}_{1U}T_S}\right)^{x_4}\dfrac{C_d}{R}\dfrac{S_{DS}}{\Delta_{U\lim}}\right]^{\frac{1}{1+0.5x_4}} & k_{US1}<k_{\alpha U\max}<k_{US2}\end{cases} \tag{3.34}$$

$$k_{\alpha U2stg}=\begin{cases}m_U\left[\alpha_{U2stg}N_U\dfrac{\bar{\omega}_{1U}}{2\pi}\dfrac{C_d}{R}\dfrac{S_{D1}}{\Delta_{U\lim}}\right]^2 & k_{\alpha U\max}\leq k_{US1}\\ \alpha_{U2stg}m_UN_U\dfrac{C_d}{R}\dfrac{S_{DS}}{\Delta_{U\lim}} & k_{\alpha U\max}\geq k_{US1}\end{cases} \tag{3.35}$$

where

$$k_{US1}=m_U\left[2\pi/\left(\bar{\omega}_{1U}T_S\right)\right]^2 \tag{3.36}$$

$$k_{US2}=1.691\left(R_m\right)^{-0.118}k_{US1} \tag{3.37}$$

$$k_{US3}=\left[\left(N_U+N_L\right)/\left(N_U+0.12N_L\right)\right]^2k_{US1} \tag{3.38}$$

Note when R_k=R_{kU1}, the factor α_U is set to be α_{U1} only for the case where R_{kU1}<R_{kU2}, as discussed in section 3.3.3. Therefore, only for the case where R_{kU1}<R_{kU2}, values of $k_{\alpha U1}$ and k_{US3} are required to be calculated by Eqs.(3.33) and (3.38), respectively. If $R_{kU1}\geq R_{kU2}$, values of $k_{\alpha U1}$ and k_{US3} are not required

to be calculated, and the critical storey-stiffnesses $k_{U\max}$ and $k_{U\min}$ are computed only based on $k_{\alpha U\max}$ and $k_{\alpha U2stg}$, as shown in Eqs.(3.31) and (3.32). Considering single storey-periods, T_{singU} and T_{singL}, are both limited to the range between $0.2Ts$ and $1.1Ts$ and $\max(1, r_{kU1})\le r_k\le 20$, as discussed in section 1.3.2, k_U and k_L should also satisfy following requirements:

$$m_U\left[2\pi/(1.1T_S)\right]^2 \le k_U \le m_U\left[2\pi/(0.2T_S)\right]^2 \tag{3.39}$$

$$m_L\left[2\pi/(1.1T_S)\right]^2 \le k_L \le m_L\left[2\pi/(0.2T_S)\right]^2 \tag{3.40}$$

$$\max\left(r_{kU1}k_U, k_U\right) \le k_L \le 20k_U \tag{3.41}$$

3.5 Design procedure

Prior to provide procedures to evaluate feasible storey-stiffnesses k_U and k_L such that the specified limit on the storey-drift is satisfied, it is worthy to discuss how to determine design accelerations $S_a(T_U)$ in Eq.(3.4). According to FEMA P695 (FEMA, 2009), the average value of collapse probability for buildings designed based on ASCE 7 (ASCE, 2010) is 10% under the maximum considered earthquake. This indicates the non-existence (NE) probability of the storey drift greater than the storey-drift limit $\Delta_{U\lim}$ is 90%. However, the design acceleration specified in ASCE 7 represents the median demand (50%) for the specified hazard level. In order to design for a target NE probability of storey drift greater than the median, which is 90%, the design acceleration must be scaled up to reflect an increase of NE probability. The design acceleration adjusted for NE probability is

$$\bar{S}_a = C_{NE}S_a \tag{3.42}$$

where S_a (median) is the code specified acceleration value and the scale factor C_{NE} is assumed to be log-normal distributed with a median value of 1.0 and a logarithmic standard deviation, β_R, which accounts for the uncertainty of the ground motions as well as the uncertainty associated with the design procedure. According to the investigation of Pang et.al (2011), it is reasonable to let β_R be 0.75. Therefore, the corresponding scale factor is $C_{NE}=\exp[\Phi^{-1}(0.9)\times 0.75+\ln(1)]=2.61$.

With the method to adjust the design spectral acceleration, the procedure on how to evaluate feasible storey-stiffnesses k_U and k_L can be carried out as follows:

Step 1: Evaluate the effective seismic weight distribution (m_L and m_U); calculate the storey-mass ratio r_m ($r_m=m_L/m_U$) and the overall mass ratio R_m based on Eq. (3.6).

Step 2: Determine critical overall stiffness ratios R_{kU1}, R_{kU2}, R_{kU3} and R_{kU2stg} according to Eqs.(3.22), (3.10), (3.23) and (3.9), respectively.

Step 3: Obtain the values of α_{U11} and α_{U12} from Table 3.1 and the exponent x_3 in accordance with Eq. (3.16) if $R_{kU1}<R_{kU2}$; then, calculate values of $\alpha_{U\max1}$, $\alpha_{U\max2}$ and the exponent x_4 in accordance with Eqs .(3.19), (3.20) and (3.18), respectively; and calculate α_{U2stg} from Eq.(3.21).

Step 4: Calculate the critical storey-stiffness $k_{\alpha U1}$ by Eq.(3.33) if $R_{kU1}<R_{kU2}$; compute the critical storey-stiffnesses $k_{\alpha U\max}$ and $k_{\alpha U2stg}$ from Eqs. (3.34) and (3.35), respectively; and determine the critical storey-stiffnesses k_{Umax} and k_{Umin} based on Eqs. (3.31) and (3.32), respectively. Note if $R_{kU1}\geq R_{kU2}$, k_{Umax} and k_{Umin} are determined only based on $k_{\alpha U\max}$ and $k_{\alpha U2stg}$, as shown in Eqs. (3.31) and (3.32); therefore, $k_{\alpha U1}$, and α_{U11} and α_{U12} that are used to compute $k_{\alpha U1}$ based on Eq.(3.33), are not required to be calculated.

Step 5: Select the feasible storey-stiffness of upper structure k_U based on the value of k_{Umin} computed in step 4. Note that the value of k_U also needs to satisfy Eq. (3.39).

Step 6: With the value of k_U selected in step 5, calculate the period of the upper structures T_U from Eq.(3.8); then, compute values of α_{U1} and $\alpha_{U\max}$ based on Eqs. (3.15) and (3.17), respectively; finally, the corresponding value of storey-stiffness of lower structure k_L can be selected to satisfy Eqs. (3.26) ~ (3.29) and as well as Eqs. (3.40) and (3.41). Note that α_{U1}, which is the value of α_U when $R_k=R_{kU1}$, is only required to be calculated if $R_{kU1}<R_{kU2}$. If $R_{kU1}\geq R_{kU2}$, the value of α_U when $R_k=R_{kU1}$ should be computed in accordance with the magnitude of R_{kU1} through Eqs. (3.12) (b) ~ (d).

Once the feasible storey-stiffnesses k_U and k_L are obtained, the initial layout of the SFRSs of the lower and upper structures can be determined based on the selected storey-stiffness distribution. Then, with such initial lateral design, other seismic response parameters, such as seismic loads and overturning moment can be further evaluated. The final SFRSs' design should satisfy both the requirements on storey-drift limit and seismic load, and as well as the overturning moment.

3.6 Examples

Discussions on the determination of storey-stiffness distributions of two hypothetical mid-rise buildings with vertical combination of framing systems are presented in the following to illustrate the proposed design approach. The buildings are assumed to be located in Los Angeles, California.

3.6.1 Example 3-1

It is a nine-storey building with a vertical combination of framing system. The SFRSs of the upper three-storey and lower six-storey are cold-formed steel (CFS) framing with shear walls sheathed with oriented strand board (OSB) panels and special RC moment frame, respectively. The floor layout of the lower six-storey is shown in Figure 3.8. The storey-height and specified dead load of the lower

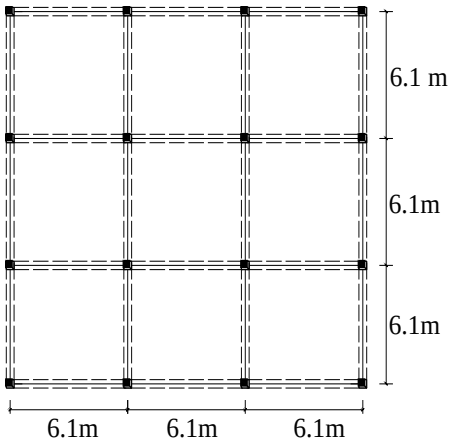

Figure 3.8: Floor plan of the lower RC structure

and upper structures are (3.3m and 3.06m) and (2.87 kPa and 6.550 kPa), respectively. The soil condition for the building is assumed as Class B and the building risk category is category II.

Assume compressive strength and elastic stiffness of the concrete are f_c=30MPa and E_c=3.0×10^{4}MPa, respectively. The column size is 600mm×600mm, and the lateral storey-stiffness of the lower structure per column with beam-to-column moment connection k_{LperC} can be calculated as per FEMA 356 (FEMA, 2000), which specifies the flexural stiffness $(EI)_{stf}$ should be 0.5 times of the actual component flexural stiffness if the axial load ratio is not greater than 0.3. Therefore, the storey-stiffness of the lower structures per column is k_{LperC}=5.41×10^{4}kN/m. In addition, assume the upper structure adopts CFS shear wall sheathed with double-sided 11mm OSB panel and CFS wall studs are adequately designed. The initial stiffness of such CFS shear wall can be approximately set as 3836 kN/m per meter (Branston, 2004).

The permissible storey drift of the CFS shear wall system is $0.02h_n$, and therefore, $\Delta_{U\text{lim}}$=0.02×3.06×1000=61.2mm. According to Table 12.2-1 of ASCE 7 (ASCE, 2010), the response modification factor R=6.5 and the deflection amplification factors C_d=4 for the CFS framed shear walls sheathed with wood structural panels, and R=8 and C_d=5.5 for the special RC moment frames. Therefore, in accordance with section 12.2.3.1 of ASCE 7 (ASCE, 2010), R=6.5 and C_d=4 are applied for the entire building. The site spectrum S_S =2.447 g and S_1 =0.858 g and the long transition period T_{Long}=8 s, which result in the design spectrum being S_{DS}=1.632 g and S_{D1}=0.572 g and the factored design response spectrum being $\bar{S}_{DS} = 2.61 \times 1.632 = 4.26$ g and $\bar{S}_{D1} = 2.61 \times 0.572 = 1.49$ g.

By following steps 1 ~ 5 described in section 3.5, it is firstly calculated: m_U=2.87×6.1^2×9/10=96,113 kg, m_L=6.550×6.1^2×9/10=219,352 kg, r_m=2.28, R_m=4.56, $k_{U\max}$=2.43×10^{5}kN/m, and $k_{U\min}$=1.14×10^5 kN/m. The initial feasible k_U is limited between 1.14×10^{5}kN/m and 7.72×10^5 kN/m. Then, based on step 6, it is finally determined storey-stiffness k_U

is limited between 1.31×10^5 kN/m and 3.99×10^5 kN/m. For each given value of k_U limited in this range, the requirement on the lateral stiffness k_L can be evaluated accordingly. By representing the obtained feasible storey-stiffnesses k_U and k_L in terms of required CFS shear wall length and number of columns in the RC moment frame, respectively, the domain of feasible SFRS designs of lower and upper structures are illustrated in the shaded area of Figure 3.9 (a). Note the stiffness combinations of the lower and upper structures shown in the shaded area of Figure 3.9 (a) requires $T_{singL}\geq0.2T_S$, $T_{singL}\geq0.2T_S$ and $r_k\leq20$ as discussed in section 1.3.2, where T_{singL} and T_{singU} are single storey-periods of lower and upper structures, respectively. Additionally, based on the floor layout of the building as shown in Figure 3.8, the number of columns in the RC moment frame and the CFS shear wall length in this example are limited to 16 and 73.2 m, respectively. The ranges of stiffness combinations of the lower and upper structure for the combined framing systems investigated in this example are shown in Figure 3.9 (b). For initial design, any combination of the shear wall length and the number of columns of the RC moment frame from the shaded area of Figure 3.9 (b) is a feasible design.

However, to better illustrate how the interaction between the lower and upper structures affect the required stiffness distributions, the limitations $T_{singL}\geq0.2T_S$, $T_{singU}\geq0.2T_S$ and $r_k\leq20$ are eliminated and results are shown in Figure 3.9 (c). Note the required stiffness distributions of the lower and upper structures are affected by the shape of the proposed α_U-R_k curve. Based on the relative magnitudes of R_{kU1} and R_{kU2}, and the relative magnitudes of $\alpha_{U\max}$ and α_{U2stg}, there are three possible shapes for α_U-R_K curve, as shown in Figures 3.6 (a) ~ (c). The calculated critical shear-force-amplification factors and overall stiffness ratios for this example are shown in Table 3.4 and Table 3.5. From these tables, it is seen that $\alpha_{U\max}>\alpha_{U2stg}$ and $R_{kU1}<R_{kU2}$. Therefore, the α_U-R_k relationship for this example conforms to that of Figure 3.6 (a).

The shaded areas 1 ~ 4 in Figure 3.9 (c) correspond to areas 1~ 4 in Figure 3.6 (a), respectively. From Figure 3.9 (c), it is seen the minimum required CFS shear wall length should not be less than 29.6 m. When the CFS shear wall length is not less than 29.6 m, the feasible stiffness distributions of the lower and upper structures have the following characteristics:

(1) When the CFS shear wall length ranges from 29.6 m to 33.47 m, the upper structure is relatively flexible. To ensure that the storey-drift limit of the upper structure is satisfied, the shear-force-amplification factor α_U should be limited to a certain small value otherwise the storey-drift limit may be violated, as shown in Eq.(3.4). From Figure 3.6 (a), it is seen that to limit the factor α_U to a certain small value, the overall stiffness ratio between the lower and upper structure R_k should be located in any area of 1, 3 or 4 rather than 2. However, it is found that if the CFS shear wall length is within the

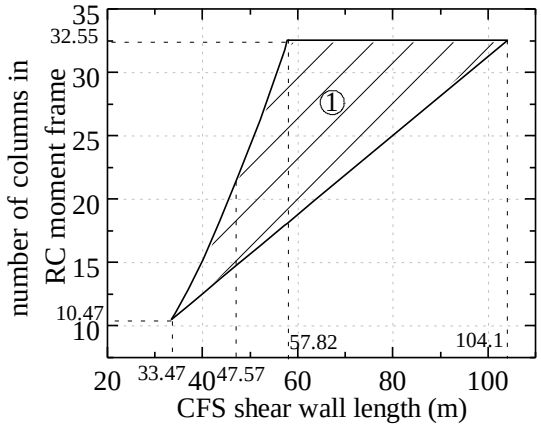

(a) considering $T_{singL} \geq 0.2T_S$, $T_{singU} \geq 0.2T_S$ and $r_k \leq 20$

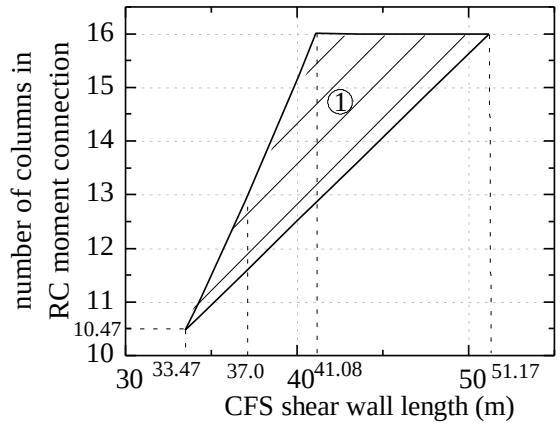

(b) considering floor layout

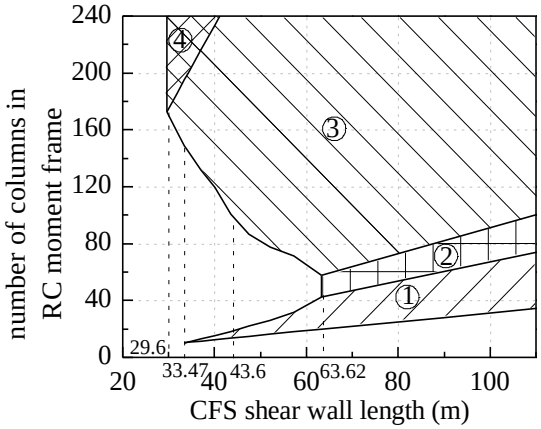

(c) all possible stiffness combinations

Figure 3.9: Feasible SFRS designs of lower and upper structures of Example 3-1

Table 3.4: Critical shear-force-amplification factors for Examples 3-1 and 3-2

	α_{U1}		$\alpha_{U\max}$		α_{U2stg}
	α_{U11}	α_{U12}	$\alpha_{U\max1}$	$\alpha_{U\max2}$	
Example 3-1	1.169	1.702	1.672	2.009	1.100
Example 3-2	N/A	N/A	1.029	1.220	1.100

Note: N/A denotes α_{U11} and α_{U12} do not exist since $R_{kU1} \geq R_{kU2}$.

Table 3.5: Critical stiffness ratios for Examples 3-1 and 3-2

	critical overall stiffness ratios				critical storey-stiffness ratios			
	R_{kU1}	R_{kU2}	R_{kU3}	R_{kU2stg}	r_{kU1}	r_{kU2}	r_{kU3}	r_{kU2stg}
Example 3-1	2.59	5.56	7.56	47.79	4.41	9.47	12.88	81.41
Example 3-2	4.14	1.76	5.14	5.88	1.89	0.80	2.35	2.69

range of 29.6 m to 33.47 m, the value of R_k selected from area 1 of Figure 3.6 (a) results in a large factor α_U and the storey-drift limit being violated. Therefore, only the value of R_k selected from either area 3 or 4 of Figure 3.6 (a) is permitted. To ensure R_k be located in area 3 or 4 of Figure 3.6 (a), the lower structure must be much stiffer than that of the upper one. Consequently, if the CFS shear wall length ranges from 29.6 m to 33.47 m, the required number of the columns in the RC moment frame becomes considerably large, as shown in Figure 3.9 (c).

In fact, the minimum required CFS shear wall length 29.6 m is derived by setting the three-storey CFS frame fix at the base. Therefore, when the CFS shear wall length is 29.6 m, the lower structure must be stiff enough so that the lower structure has no effect on the upper one. This is the case that the required number of columns in the RC moment frame is located in area 4 of Figure 3.9 (c), the area that the two-stage analysis procedure is applicable.

(2) If the selected CFS shear wall length ranges from 33.47 m to 63.62 m, the shear-force-amplification factor α_U should also be limited to a certain small value so that the storey-drift limit is not violated. Nevertheless, different from the case that the CFS shear wall length ranges between 29.6 m to 33.47 m, the value of R_k selected from area 1 of Figure 3.6 (a) is also permitted. Only the value of R_k selected from area 2 of Figure 3.6 (a) is not permitted. Therefore, the selection of the required number of columns in the RC moment frame becomes quite tricky. To exclude the value of R_k be located in area 2 of Figure 3.6 (a), the required number of columns has to be either greater or less than certain values depending on the selected length of CFS shear wall length. For example, if the CFS shear wall length is 43.60 m, the required number of columns in the RC moment frame is greater than 100.49 or lies in the range between 13.63 and 18.17, as shown in Figure 3.9 (c). The number of columns cannot be between 18.17 and 100.49. This is because if the number of columns in the RC moment frame lies between 18.17 and 100.49, the overall stiffness ratio between the lower and upper structures are closer to area 2 of Figure 3.6 (a) where the factor α_U reaches the maximum value. With the maximum factor α_U, the governing design equation, i.e., (3.4), is not satisfied and the storey-drift limit is violated.

(3) When the CFS steel shear wall length is greater than 63.62 m, the upper structure is stiff enough so that the storey-drift limit can always be satisfied regardless of the magnitudes of the shear-force-amplification factor α_U. Even if the overall stiffness ratio R_k is located in area 2 of Figure 3.6 (a) and the factor α_U reaches the maximum value, the governing design equation, i.e., Eq.(3.4), is satisfied due to the large storey-stiffness of the upper structure. Therefore, the storey-drift limit can always be satisfied. There is no specific requirement on the required number of columns in the RC moment frame as long as the storey-stiffness of the lower structure k_L is not less than $r_{kU1}k_U$, i.e., $k_L \geq r_{kU1}k_U$. As

discussed in section 1.3.2, the requirement $k_L \geq r_{kU1} k_U$ is to ensure that the maximum storey-drift occurs at the upper structure. In Figures 3.9 (a) ~ (c), the lower bound of area 1 represents that $k_L = r_{kU1} k_U$.

Based on Figure 3.9 (c), it is seen that for the combined framing system, there are many theoretical feasible stiffness combinations, which ensure the storey-drift limit to be satisfied. However, many of the feasible stiffness combinations may not be applicable for design practice. In this example, a stiffness combination that the CFS shear wall length is 29.6 m and the required number of columns in the RC moment frame is 172.8 is a theoretically feasible solution. However, to construct such a stiff lower structure is neither economical nor practically feasible as the maximum number in the RC concrete frame in this example is limited to 16, as shown in the floor plan view of Figure 3.8. With consideration of the structural layout of the building, the number of feasible and practical stiffness combinations of lower and upper structures is limited. In this example, the region of the feasible and practical stiffness combinations is that shown in Figure 3.9 (b).

By comparing Figure 3.9 (b) to 3.9 (c), it is seen all feasible and practical stiffness combinations are located in area 1 for this example. As shown in Figure 3.6 (a), when the overall stiffness ratio R_k is located in area 1, the factor α_U increases as the overall stiffness ratio R_k increases. Therefore, to limit the factor α_U, there is an upper limit associated with the stiffness of the lower structure as shown in Figure 3.9 (b). For example, if the CFS shear wall length is first selected as 37.0 m, the maximum required number of columns in the RC moment frame is theoretically 12.9. However, for being conservative, one may select all 16 columns in the floor plan to have a moment connection; but it results in that the storey-drift limit being violated. Therefore, by increasing the stiffness of the lower structure with the intention of reducing the mass and stiffness interactions between the lower and upper structure and limiting the maximum storey drift of the upper structure, it may not always yield to an effective and feasible design.

3.6.2 Example 3-2

The floor layout, storey-height, specified dead load, column size in the RC moment frame and CFS framing for the lower RC and upper CFS structures of the building in this example are all the same as those of Example 3-1, except that this is an eight-storey building. The SFRS of the lower two-storey structure is the special RC moment frame while that that of the upper six-storey is CFS framing with shear walls sheathed with oriented strand board (OSB) panels.

The storey-masses of the lower and upper structures in this building are identical to those of the previous example. Then, by following steps 1 ~ 6 described in section 3.5, the domain of feasible

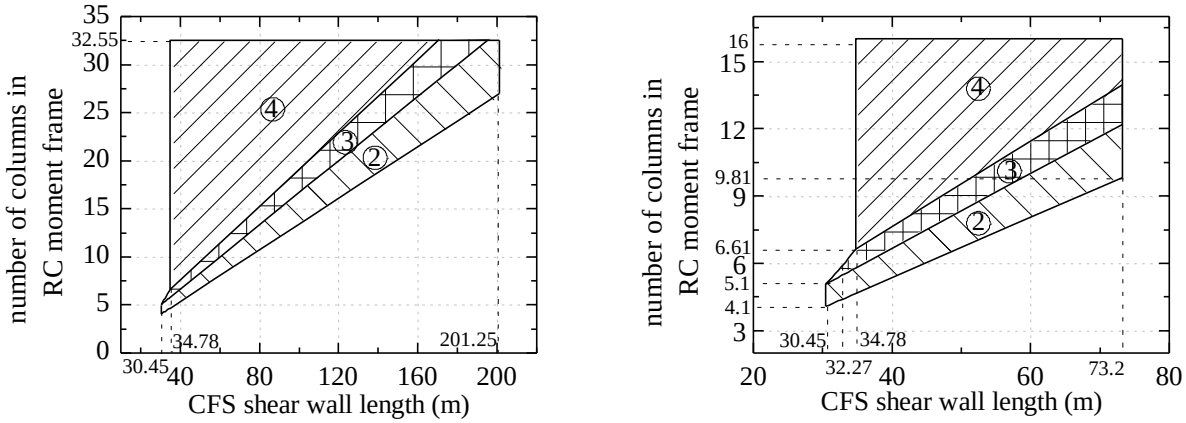

(a) considering $T_{singL} \geq 0.2T_S$, $T_{singU} \geq 0.2T_S$ and $r_k \leq 20$ (b) considering floor layout

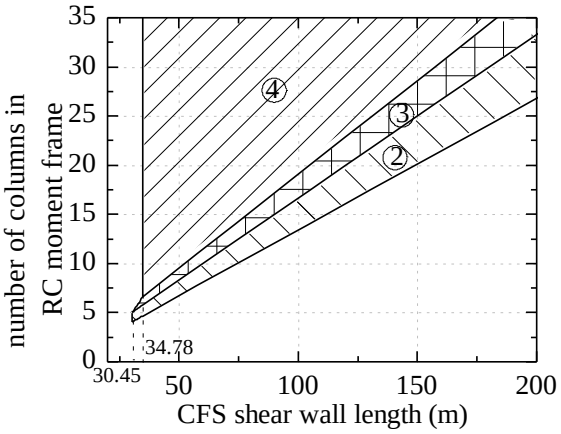

(c) all possible stiffness combinations

Figure 3.10: Feasible SFRS designs of lower and upper structures of Example 3-2

SFRS designs of lower and upper structures are illustrated in the shaded area in of Figure 3.10 (a). Similar to that of the previous example, the stiffness combinations of lower and upper structures shown in the shaded area of Figure 3.10 (a) have to satisfy $T_{singL} \geq 0.2T_S$, $T_{singU} \geq 0.2T_S$ and $r_k \leq 20$. Based on the floor plan layout, the maximum number of columns in the RC moment frame cannot be greater than 16 and the CFS shear wall length cannot be greater than 73.2 m (Figure 3.8). The feasible and practical stiffness combinations of lower and upper structures for this example are shown in Figure 3.10 (b).

Similar to that in Figure 3.9 (c), the limitations $T_{singL} \geq 0.2T_S$, $T_{singU} \geq 0.2T_S$ and $r_k \leq 20$ are eliminated in Figure 3.10 (c). Based on Table 3.4 and Table 3.5, it is seen that $R_{kU1} > R_{kU2}$ but the relative magnitude of $\alpha_{U\max}$ and α_{U2stg} is not certain. If $\alpha_{U\max} = \alpha_{U\max 1}$, $\alpha_{U\max} < \alpha_{U2stg}$; however, if $\alpha_{U\max} = \alpha_{U\max 2}$, $\alpha_{U\max} > \alpha_{U2stg}$. Therefore, depending on the relative magnitude of $\alpha_{U\max}$ and α_{U2stg}, the α_U-R_k relationship may conform to that shown in Figure 3.6 (b), but it may also conform to that shown in Figure 3.6 (c).

The shaded areas 2 to 4 in Figure 3.9 (c) are respectively corresponding to the areas of 2 to 4 in Figure 3.6 (b) or (c). From Figure 3.9 (c), it is seen that the minimum required CFS shear wall length is 30.45 m. When the CFS shear wall length is not less than 30.45 m, the feasible stiffness combinations of the lower and upper structures have the following characteristics:

(1) When the CFS shear wall length ranges from 30.45 m to 34.78 m, the upper structure is relatively flexible. The shear-force-amplification factor α_U should be limited to a certain small value. In addition, the period of the upper structure T_U is greater than the transition period T_S of the ASCE 7 spectrum if the CFS shear wall length lies between 30.45 m to 34.78 m. Based on Eq.(3.17), the critical shear-force-amplification factor $\alpha_{U\max}=\alpha_{U\max 1}$; and therefore, the α_U-R_k relationship conforms to that shown in Figure 3.6 (c) since $\alpha_{U\max 1}<\alpha_{U2stg}$, as shown in Table 3.4 and Table 3.5. From the proposed α_U-R_k curve shown in Figure 3.6 (c), the factor α_U associated with areas 2 and 3 is less than that of area 4 for the combined framing systems. Consequently, to limit the factor α_U, the overall stiffness ratio between lower and upper structures R_k should be selected from either area 2 or 3, but not 4. To ensure that the overall stiffness ratio R_k is located in either area 2 or 3, depending on the selected CFS shear length, the number of columns should be less than a certain value, as shown in Figure 3.9 (c). For example, if the CFS shear wall length is 32.27 m, the required number of columns in the RC moment frame should lie between 4.32 and 5.69. The maximum number 5.69 is to ensure the ratio R_k be located in areas 2 and 3 so that the storey-drift limit will not be violated; while the minimum number 4.32 is to ensure that the storey-stiffness of the lower structure k_L is not less than $r_{kU1}k_U$, i.e., $k_L \geq r_{kU1}k_U$, as discussed in section 1.3.2. The lower bound of area 2 in Figure 3.9 (a) ~ (c) represents that $k_L=r_{kU1}k_U$.

(2) If the CFS shear wall length is greater than 34.78 m, the upper structure is stiff enough and the storey-drift limit can always be satisfied regardless of the magnitude of the factor α_U. Therefore, there is no requirement on the required number of columns in the RC moment frame as long as the storey-stiffness of the lower structure k_L is not less than $r_{kU1}k_U$, i.e., $k_L \geq r_{kU1}k_U$.

3.6.3 Design validation

Elastic-analysis-based modal response spectrum analysis (Chopra, 2007) is carried out for the buildings investigated in Examples 3-1 and 3-2 as MDOF models, as shown in Figure 1.3, with the corresponding effective storey-masses and storey-stiffness evaluated previously. For all combinations of the CFS shear wall length and the number of columns in the RC moment frame shown in the shaded areas of Figure 3.9 (a) and 3.10 (a), the storey drifts of the first storey of CFS shear walls calculated from the elastic-analysis-based modal response spectrum analyses are less than 1.8% of the storey height for both buildings. Since the specified storey-drift limit for both buildings is 2% of the

storey height, all combinations the CFS shear wall length and the number of columns in the RC moment frame obtained from the proposed procedure are conservative.

3.6.4 Design comparison

The feasible and practical stiffness combinations of the lower and upper structures shown in Figure 3.9 (b) of Example 3-1 is compared with those shown in Figure 3.10 (b) of Example 3-2. From Figure 3.9 (b), it is seen that majority of the feasible and practical stiffness combinations of the lower and upper structures of Example 3-2 will result in that the overall stiffness ratio R_k to be located in area 4 of Figure 3.6 (b) or (c). The area 4 signifies that the two-stage analysis procedure is applicable. As previously discussed in section 3.3, if the overall stiffness ratio R_k is located in area 4, the lower structure has no effect on the upper one, and the upper structure can be considered as an independent building fixed to ground. Therefore, there is almost no interaction between the lower and upper structures in terms of mass and stiffness. The drift limit of the upper 6-storey CFS frame of Example 3-2 can be satisfied by considering the stiffness of CFS shear wall alone. However, all the feasible and practical stiffness combinations of Example 3-1 have yielded that the overall stiffness ratio between the lower and upper structures R_k to be located in area 1 of Figure 3.6 (a), as shown in Figure 3.9 (b). As previous discussed in section 3.3.1 and 3.3.3, if the overall stiffness ratio is located in the area 1 of Figure 3.6 (a), the interactions between lower and upper structure in terms of mass and stiffness should be accounted for in the design and analysis. Therefore, the feasible stiffness combinations of the lower and upper structures of Example 3-1 are greatly affected by the interactions between lower and upper structures in terms of mass and stiffness.

The difference of the stiffness combination characteristics between the two examples is primarily resulted from the difference of the mass associated with the lower structures between the two buildings. Considering the numbers of storey of the lower structure are 6 and 2 for the buildings in Examples 3-1 and 3-2, respectively, the resulted overall mass ratio between the lower and upper structures, R_m, of the building in Example 3-1 is 4.56, which is much greater than that of Example 3-2, i.e., 0.76, as shown in Table 3.6. Recall that the effect of the overall mas ratio R_m on the shear-force-amplification factor α_U discussed in section 3.3.1. A larger value of the overall mass ratio R_m would result in a more significant amplification of the shear force for the upper structure. Therefore, the calculated critical shear-force-amplification factors of Example 3-1 are much greater than those of Example 3-2, as shown in Table 3.4. In addition, with a larger value of the overall mass ratio, the critical storey-stiffness ratios of the upper structure of Example 3-1 are also much greater than those of Example 3-2, especially for the storey-stiffness ratio of the upper structure associated with the two-

Table 3.6: Design comparison between Examples 3-1 and 3-2

	lower structure	upper structure	R_m	CFS shear wall length (m)	number of columns in RC moment frame
Example 3-1	6-storey RC frame	3-storey CFS frame	4.56	33.47 ~ 51.17	10.47 ~16.0
Example 3-2	2-storey RC frame	6-storey CFS frame	0.76	30.45 ~ 73.20	4.10 ~ 16.0

stage analysis procedure r_{kU2stg}. The storey-stiffness ratio of the upper structure associated with the two-stage analysis procedure r_{kU2stg} for Example 3-1 is significantly greater than that of Example 3-2 with the values of r_{kU2stg} for Example 3-1 and Example 3-2 respectively being 81.41 and 2.69, as shown Table 3.5. With larger values of shear-force-amplification factors and critical storey-stiffness ratios, the interactions between the lower and upper structures in terms of mass and stiffness associated with Example 3-1 have a more significant effect on the stiffness combinations compared to that of Example 3-2.

Intuitively, people may think that the minimum required CFS shear wall length for the 3-storey CFS frame in Example 3-1 should be less than that for the 6-storey CFS frame in Example 3-2. However, due to the large shear-force-amplification effect associated with Example 3-1, the minimum required CFS shear wall length for the 3-storey CFS structure in Example 3-1 is greater than that for the 6-storey CFS structure in Example 3-2, with each of them respectively being 33.47 m and 30.45m, as shown in Table 3.6. Nevertheless, the maximum feasible and practical CFS shear wall length of Example 3-1, i.e., 51.71 m, is less than that of Example 3-2, i.e., 73.2 m, as shown in Table 3.6. The maximum CFS shear wall lengths for both examples are limited by the structure layout, as shown Figure 3.8. The maximum CFS shear wall length 6.1m × 3 ×4 = 73.2 m of Example 3.2 is limited by the total available wall length, while the maximum CFS shear wall length 51.71 m for Example 3-2 is limited by the total number of columns in the RC frame. To ensure that the maximum storey-drift occur at the upper structure, the storey-stiffness ratio should not be less than the calculated r_{kU1}, as discussed in section 1.3.2. The value of r_{kU1} for Example 3-1, i.e., 4.41, is greater than that of Example 3-2, i.e., 1.89, as shown in Figure 3.5. As to Example 3-1, if the CFS shear wall length is greater than 51.71 m, to ensure the storey-stiffness of the lower structure k_L be not less than $r_{kU1}k_U$, the required number of columns in the RC moment frame becomes greater than 16. Therefore, the maximum CFS shear wall length for Example 3-1 is limited to 51.71 m rather than 73.2m. As to Example 3-2, since value of the minimum storey-stiffness ratio r_{ku1} is relatively small, the required number of column can be less than 16 even if the CFS shear wall length is 73.2m, as shown in Figure 3.9 (b).

From the previous discussion, it is seen since the number of the storey and total seismic weight of the lower structure is greater than those of the upper structure in Example 3-1, the required stiffness of the upper structure is greatly affected by the interactions between lower and upper structures in terms of mass and stiffness. However, as to Example 3-2, since the number of the storey and total seismic weight of the lower structure is less than those of the upper structure, such interactions have less effect on the required stiffness of the upper structure. The required lateral stiffness of the upper structure can be determined without considering the influence of the lower structure.

3.7 Conclusion

Presented in this chapter is a simplified seismic design approach for the determination of storey-stiffness distribution of mid-rise buildings with vertical combination of framing systems based on the specified storey drift limit. Unlike the two-stage analysis procedure prescribed in ASCE 7, the effects of the interaction between the lower and upper structures in terms of mass and stiffness on the seismic load are considered. In order to quantify effects of such interaction on the base shear force of the upper structure, which is the key issue that governs the determination of the storey-stiffness distribution, the shear-force-amplification factor α_U is proposed to account for the effect of shear force amplification contributed by the lower structure to the upper one. The following conclusions are obtained:

(1) The overall stiffness ratio R_k between the lower and upper structures has a significant influence on the factor α_U: (a) when the lower structure is much stiffener than the upper one, $\alpha_U \approx 1$, which indicates the lower structure has no influence on the upper one, and the upper structure behaves as it is fixed to the ground base; however, (b) when periods of the lower and upper structures are close to each other, e.g., $T_U \approx T_L$, a large amount of the mass from the lower structure will contribute to the shear force associated with the upper structure and the factor α_U will reach the maximum value, which is usually greater than unity; and (c) when T_U is far more less than T_L, the lower structure may act similar to a damper to dissipate the energy generated by earthquakes, which results in $\alpha_U < 1$.

(2) Applicable equations to evaluate the shear-force-amplification factor α_U are proposed. And errors of the proposed equations are limited to the range between -0.9% and 35.8%, which is comparable with conventional ELF procedure for regular structures.

(3) The relative seismic weight between the lower and upper structures has a significant influence on the design of the lower and upper structures. In general, when the number of the storey and total seismic weight associated with the lower structure is much greater than those of the upper one, the required stiffness of the upper structure will be greatly affected by the interaction between lower and

upper structures in terms of mass and stiffness. On the other hand, if the number of the storey and total seismic weight associated with the lower structure are less than that of the upper structure, such interaction has less effect on the required stiffness of the upper structure. In such case, the required lateral stiffness of the upper structure is primarily based on the characteristics of the upper structure.

(4) The proposed simplified seismic design approach generally yields a conservative design, which has been demonstrated in the two illustrated examples.

Chapter 4 Simplified methods for evaluating seismic loading of mid-rise buildings with vertical combination of framing systems

4.1 Introduction

Two simplified methods for evaluating seismic loading of mid-rise buildings with vertical combination of framing systems, i.e., modified ELF and two-stage analysis procedures, are investigated in this chapter. Applicable requirements and seismic load distributions associated with the two simplified methods are proposed, respectively, based on the USA standard ASCE 7 (ASCE 7, 2010). Meanwhile, the proposed two-stage analysis procedure is also compared with the existing two-stage analysis procedure prescribed in ASCE 7 (ASCE, 2006; 2010). Finally, three design examples are presented to illustrate the efficiency of the two simplified methods.

4.2 Modified ELF procedure

4.2.1 Background of modified ELF procedure

The modified ELF procedure presented herein is applicable to the "appendage-style" building, in which the upper structure only has one storey. To modify or extend the conventional ELF procedure to be applicable to the "appendage-style" building, modal analyses based on the simplified 2DOF model are carried out. As to the "appendage-style" building, when the lower structure is relatively soft compared to the upper one, the effective mass distribution of the 2DOF model is shown in Figures 4.1 (b) and (c). From the figure, it is observed that: (a) the lower structure is dominated by the first mode; and (b) the upper "appendage" may be dominated by the second mode in addition to the first mode. However, as the seismic weight of the upper "appendage" is much less than that of the lower one, the second mode does not have a significant effect on the seismic load of the lower structure. Therefore, the lower structure can be treated as an independent "regular" building with the base fixed to the ground, and the conventional ELF procedure can be directly adopted to evaluate the seismic load of the lower structure. The base shear force of the lower structure V_{Lb} can be evaluated as follows:

$$V_{Lb} = \left(M_L + M_U\right) S_a\left(T_1\right) \tag{4.1}$$

Based on the simplified 2DOF model, the first mode period T_1 in Eq.(4.1) can be approximated by Eq.(A.5) of Appendix A.

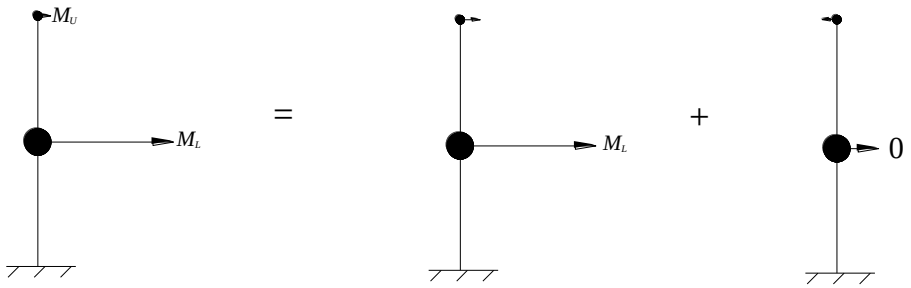

(a) mass distribution of 2DOF model (b) first mode (c) second mode

Figure 4.1: Effective mass distribution of simplified 2DOF model when ELF procedure is applicable to "appendage-style" building

4.2.2 Applicable requirement

As shown in Figure 4.1, to ensure the ELF procedure is applicable for the "appendage-style" building, it is required that the effective mass of the lower structure is primarily concentrated in the first mode. For a given overall mass ratio R_m, let R_{kb1} be the overall stiffness ratio at which the effective mass of the entire building associated with the first mode in the simplified 2DOF model is 90% of the total mass. As discussed in Appendix C.6, if the overall stiffness ratio R_k is less than R_{kb1}, the effective mass of entire building associated with the first mode in the simplified 2DOF model will be greater than 90% of the total mass and therefore, the modified ELF procedure can be adopted to approximate the seismic load. The critical overall stiffness ratio R_{kb1} is computed as follows:

$$R_{kb1} = \begin{cases} 0.386R_m + 1.1 & \text{if } 1 \le R_m \le 2 \\ 0.65R_m + 0.58 & \text{if } R_m > 2 \end{cases} \tag{4.2}$$

Then, based on Eq.(3.7), the critical storey-stiffness ratio associated with the modified ELF procedure to be applicable for the "appendage-style" building, r_{kb1}, can be computed as follows:

$$r_{kb1} = R_{kb1}\left(\frac{N_U}{N_L}\right)\left(\frac{\bar{\omega}_{1U}}{\bar{\omega}_{1L}}\right)^2 \tag{4.3}$$

where $\bar{\omega}_{1L}$ ($\bar{\omega}_{1U}$) is the normalized first mode natural frequency of an N_L(N_U)-storey structure as listed in Table 1.1. For practical "appendage-style" combined framing systems stated in section 1.3.2, values of r_{kb1} obtained in accordance with Eq. (4.3) are listed in Table 4.1. As long as the storey-stiffness ratio r_k is not greater than the value of r_{kb1} listed in Table 4.1, the modified ELF procedure presented in the section 4.2.4 is applicable for evaluating the seismic load of the "appendage-style" building. From the table, it is seen as the increase of the number of storeys associated with the lower structure, the value of r_{kb1} increases. As the number of storeys of the lower structure increases, the

Table 4.1: Values of r_{kb1} and errors associated with modified ELF procedure (ASCE 7)

N_L	N_U	r_{kb1}			error of shear force			
					lower structure		upper structure	
		r_m=1	r_m=2	r_m=3	maximum	minimum	maximum	minimum
2	1	2.45	4.16	5.87	23.9%	11.8%	18.8%	4.8%
3	1	4.26	7.54	10.82	28.2%	12.6%	19.7%	2.0%
4	1	6.59	11.98	17.37	31.7%	13.2%	19.6%	0.9%
5	1	9.46	17.48	25.51	33.7%	13.7%	19.2%	1.0%
6	1	12.84	24.03	35.21	35.3%	14.0%	20.7%	1.5%
7	1	16.76	31.63	46.49	35.0%	14.2%	14.0%	0.4%
8	1	21.22	40.32	59.41	34.3%	14.5%	15.0%	1.4%
9	1	26.18	50.00	73.81	30.9%	14.8%	15.0%	1.9%

upper one-storey structure will act more like an "appendage", and its effect on the lower structure will be less significant. Therefore, the applicable requirement of the modified ELF procedure in terms of r_{kb1} are less stringent as the number of storeys of the lower structure increases. In fact, when the number of storeys of the lower structure is eight or nine, as shown in Table 4.1, the value of r_{kb1} is greater than the assumed maximum storey-stiffness ratio 20. Therefore, the modified ELF procedure is always applicable to the "appendage-style" building if the number of storeys of the lower structure is not less than eight. Note listed in Table 4.1 are only values of r_{kb1} for cases where r_m=1, 2 or 3. For other r_m values, values of r_{kb1} can be linearly interpolated by the magnitude of r_m.

4.2.3 Seismic load distribution

4.2.3.1. Lower structure

By using the conventional ELF procedure, the lateral seismic force along the entire height of the building is distributed through the method prescribed in ASCE 7 (ASCE, 2010), as shown in Figure 4.2. The lateral seismic force associated with the *i*th-storey F_i is calculated as

$$F_i = \frac{m_i h_i^{\kappa}}{\sum_{i=1}^{N_L+N_U} m_i h_i^{\kappa}} V_{Lb} \tag{4.4}$$

where m_i is the mass associated with the *i*th-storey, h_i is the height from the ground to the *i*th-storey, and κ is an exponent related to the structural period (ASCE, 2010), which is calculated as

$$\kappa = \begin{cases} 1 & T_1 \le 0.5\ s \\ 2 & T_1 \ge 2.5\ s \\ 0.5T_1 + 0.75 & 0.5\ s < T_1 < 2.5\ s \end{cases} \tag{4.5}$$

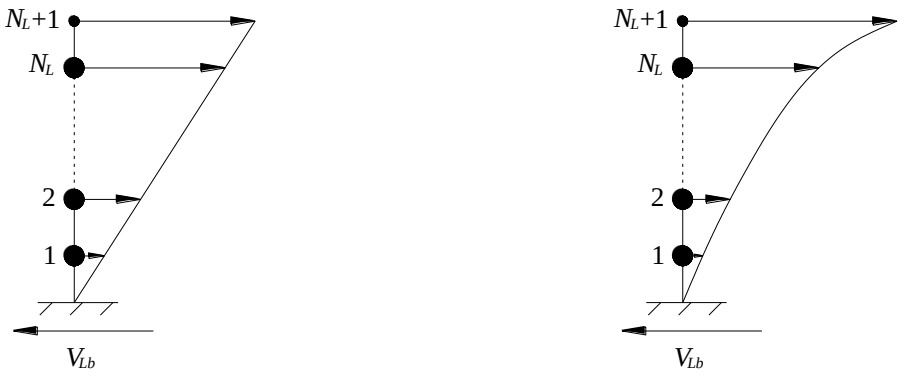

(a) κ=1 (b) κ=2

Figure 4.2: Lateral seismic force distribution associated with ELF procedure (ASCE, 2010)

The traditional "regular" building is primarily dominated by the first mode and the first mode shape is almost linearly distributed along the height. However, a few storeys near the top of the "regular" building may still be affected by higher vibration modes other than the first mode, and such effect becomes more significant as the period of the "regular" building elongates. To account for such higher vibration modes effects on the upper few storeys, the exponent κ is introduced in the ELF procedure. As shown in Figure 4.2 (b), when κ=2, the distributed lateral seismic forces associated with the top storey increases considerably. In this way, the effect of higher vibration modes on the seismic load of the few storeys near the top is accounted for.

With the calculated lateral seismic force, the shear force of the lower structure can be equivalently computed based on the lateral seismic force distribution as follows:

$$V_{Li} = \sum_{j=i}^{N_L} F_i + F_{N_L+1} \tag{4.6}$$

Note V_{Li} is the *i*th-storey of the lower structure, while F_i represents the lateral seismic force associated with the *i*th-storey of the entire building.

4.2.3.2. Upper Appendage

As presented in section 4.2.1, when the storey-stiffness ratio r_k is less than the value of r_{kb1} listed in Table 4.1, the seismic response of the upper "appendage" may be greatly affected by higher vibration modes other than the first mode. Consequently, the seismic load of the upper "appendage" cannot be estimated from the conventional ELF procedure as discussed in section 4.2.3.1. It is suggested that the base shear force of the upper "appendage" be calculated based on the shear-force-amplification-factor α_U proposed in Chapter 3 as follows:

$$V_{Ub} = \alpha_U m_U S_a(T_U) \tag{4.7}$$

where the factor α_U is determined by Eq.(3.12) and the period T_U is determined based on Eq.(3.8).

4.2.4 Modified ELF procedure

By adopting the modified ELF procedure, the seismic load of the "appendage-style" building can be evaluated as follows:

Step 1: Evaluate the effective seismic weight and stiffness distributions, (m_L and m_U) and (k_L and k_U), respectively; and calculate r_m (r_m=m_L/m_U) and r_k (r_k=k_L /k_U).

Step 2: Determine the value of r_{kb1} in accordance with Table 4.1.

Step 3: Check if the storey-stiffness ratio r_k is less than or equal to the value of r_{kb1}. If $r_k \leq r_{kb1}$, go to step 4; otherwise, the modified ELF procedure is not applicable.

Step 4: Calculate the base shear force of the lower structure V_{Lb} in accordance with Eq.(4.1); then, evaluate the lateral seismic force and shear force for each storey of the lower structure based on Eqs.(4.4) and (4.6), respectively; finally, determine the shear force of the upper "appendage", V_{Ub}, by Eq.(4.7).

4.2.5 Error analysis

Results obtained from the modified ELF procedure are compared with those from the elastic modal response spectrum analysis of the MDOF model with CQC rule to combine the peak modal responses (Chopra, 2007). The maximum and minimum errors for each storey combination, as shown in Table 4.1, are obtained based on all the possible combinations of r_m, r_k, T_{singU}/T_s and T_{singL}/T_s as stated in section 1.3.2. The positive and negative errors represent that the modified ELF procedure overestimates and underestimates the shear force, respectively. From Table 4.1, it is seen errors induced from the modified ELF procedure for the lower and upper structures are in the range 11.8%~35.3% and 0.4%~20.7%, respectively. The error of shear force for the lower structure is in general larger than that for the upper structure. However, the maximum error for the lower structure, i.e., 35.3%, is comparable with that of the conventional ELF procedure (ASCE, 2010) for "regular" structures, as discussed in section 3.3.4. Therefore, the modified ELF procedure can be adopted to analyze the "appendage-style" combined framing system.

4.3 Proposed two-stage analysis procedure

4.3.1 Background of proposed two-stage analysis procedure

The basic principle associated with the two-stage analysis procedure is that seismic forces of lower and upper structures can be computed by the ELF procedure separately (ASCE, 2006; 2010). This principle can be revealed by carrying out modal analysis for the simplified 2DOF model. When the

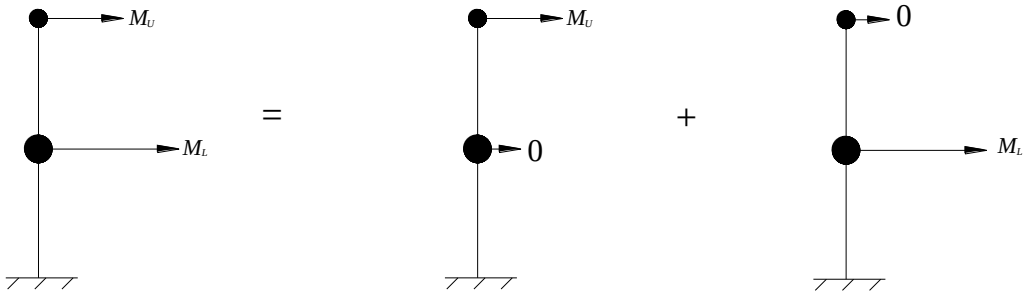

(a) mass distribution of 2DOF model (b) first mode ($T_1 \approx T_U$) (c) second mode ($T_2 \approx T_L$)

Figure 4.3: Effective mass distribution of simplified 2DOF model with extremely stiff lower structure

lower structure is much stiffer than the upper one, the effective mass distribution of the 2DOF model is shown in Figure 4.3. From the figure, it is observed that: (a) the upper structure is dominated by the first mode, with the period of the first mode of the building being equivalent to that of the upper structure T_U, and (b) the lower structure is dominated by the second mode, with the period of the second mode of the building being equivalent to that of the lower structure T_L, as shown in Figures 4.3 (b) and (c). Therefore, based on the modal response spectrum analysis (Chopra, 2007), lateral seismic forces of the lower and upper structures, designated as F_U and F_L, respectively, can be calculated as

$$F_U = M_U S_a\left(T_U\right) \tag{4.8}$$

$$F_L = M_L S_a\left(T_L\right) \tag{4.9}$$

From Eqs.(4.8) and (4.9), it is seen the two-stage analysis procedure ignores the possible mass and stiffness interaction between lower and upper structures. The lateral seismic forces associated with the lower and upper structures can be calculated separately as the structures are directly fixed to the ground base.

4.3.2 Applicable requirement

To ensure the proposed two-stage analysis procedure is applicable to evaluate the seismic loading of the combined framing system, Eqs.(4.8) and (4.9) should be satisfied simultaneously. For a given overall mass ratio R_m, let R_{k2stg}, the smallest value of overall stiffness ratio that ensures Eqs.(4.8) and (4.9) be satisfied simultaneously, be the overall two-stage stiffness ratio. As discussed in Appendix C.3, R_{k2stg} can be calculated as

$$R_{k\,2stg} = \begin{cases} 1.637R_m + 9.07 & R_m \le 1.23 \\ 11.029R_m - 2.5 & R_m > 1.23 \end{cases} \tag{4.10}$$

Table 4.2: Values of r_{k2stg} and errors associated with proposed two-stage analysis procedure

N_L	N_U	r_{k2stg}			error of shear force			
					upper structure		lower structure	
		r_m=1	r_m =2	r_m =3	maximum	minimum	maximum	maximum
1	1	10.71	19.56	30.59	11.6%	-0.4%	5.1%	-2.0%
1	2	7.55	8.18	10.73	24.5%	2.0%	26.5%	1.5%
2	2	10.71	19.56	30.59	20.3%	3.5%	36.3%	10.9%
3	2	18.06	39.33	60.60	13.5%	6.4%	40.5%	22.5%
1	3	5.71	6.04	6.36	32.8%	1.3%	35.6%	11.9%
2	3	7.90	9.49	15.21	28.4%	-0.3%	51.6%	13.2%
3	3	10.71	19.56	30.59	27.4%	-0.4%	59.2%	18.4%
4	3	15.03	33.14	51.24	21.9%	2.4%	63.0%	22.4%
1	4	4.57	4.77	4.97	35.9%	1.0%	44.5%	7.3%
2	4	6.25	6.76	8.87	30.5%	-0.5%	64.9%	14.1%
3	4	8.36	11.41	18.12	30.2%	-0.2%	74.0%	17.1%
4	4	10.71	19.56	30.59	29.0%	-0.5%	78.8%	19.7%
5	4	13.45	29.87	46.29	19.8%	-0.1%	81.0%	22.0%
1	5	3.81	3.94	4.07	35.9%	-0.1%	50.7%	8.2%
2	5	5.16	5.50	5.85	32.1%	-0.3%	67.3%	13.6%
3	5	6.85	7.52	11.83	31.8%	-0.4%	74.7%	17.0%
4	5	8.71	12.71	20.12	32.0%	-0.8%	81.1%	17.4%
5	5	10.71	19.56	30.59	24.9%	-0.1%	82.6%	19.2%
1	6	3.26	3.35	3.45	36.7%	-0.2%	56.5%	8.4%
2	6	4.39	4.64	4.89	33.0%	-0.9%	72.5%	14.8%
3	6	5.81	6.29	8.24	36.9%	-0.8%	81.1%	16.4%
4	6	7.35	8.82	14.14	35.0%	-0.5%	87.0%	17.7%
1	7	2.85	2.92	2.99	36.7%	0.1%	57.4%	8.5%
2	7	3.82	4.01	4.20	34.4%	-0.5%	75.4%	15.4%
3	7	5.03	5.40	6.02	37.3%	-0.4%	83.5%	16.5%
1	8	2.53	2.58	2.64	37.9%	1.1%	58.7%	8.7%
2	8	3.38	3.53	3.67	34.8%	0.1%	76.5%	15.6%
1	9	2.27	2.32	2.36	38.0%	-0.8%	60.6%	8.7%

Note R_{k2stg} in Eq.(4.10) is different from the R_{kU2stg} presented in Eq.(3.9). R_{kU2stg} is the smallest value of overall stiffness ratio that only ensures Eq.(4.8) be satisfied, while R_{k2stg} is the smallest overall stiffness ratio that satisfies Eqs.(4.8) and (4.9), simultaneously. Then, based on Eq.(3.7), the critical storey-stiffness ratio associated with the proposed two-stage analysis procedure, r_{k2stg}, for the combined framing systems can be computed as follows:

$$r_{k2stg} = R_{k2stg}\left(\frac{N_U}{N_L}\right)\left(\frac{\bar{\omega}_{1U}}{\bar{\omega}_{1L}}\right)^2 \tag{4.11}$$

As to the combined framing systems which satisfy the requirements stated in section 1.3.2, possible storey combinations of lower and upper structures that may be analyzed by the proposed two-stage analysis procedure and the corresponding threshold values of r_{k2stg} are listed in Table 4.2. As long as the storey-stiffness ratio r_k is not less than the value of r_{k2stg} listed in Table 4.2, the proposed two-stage analysis procedure is applicable for evaluating the seismic load of the combined framing system. From the table, it is seen the proposed two-stage analysis procedure is usually applied to the combined framing system in which the number of the storey of the lower structure is less than that of the upper one. For example, for the case where N_L=1 and N_U =9, as shown in Table 4.2, the corresponding threshold value of r_{k2stg} is quite small regardless magnitudes of storey-mass ratio r_m; consequently, for most cases, the proposed two-stage analysis procedure is applicable for such storey combination. In fact, for the case where the number of the storey of the lower structure is considerably less than that of the upper one, the lower structure can be treated as a "podium" to the upper one, and the upper structure usually behaves as it is fixed to the ground base directly.

4.3.3 Seismic load distribution

4.3.3.1. Upper structure

The seismic load of the upper structure can be calculated as it is fixed to the ground base directly. The base shear force of the upper structure V_{Ub} is computed as

$$V_{Ub} = \alpha_{U2stg} m_U N_U S_a(T_U) \tag{4.12}$$

where the factor α_{U2stg} is calculated in accordance with Eq.(3.21). Then, the lateral seismic force at the ith-storey of the upper structure, F_{Ui}, is linearly distributed along the height as shown in Figure 4.4 (b). F_{Ui} can be calculated as follows:

$$F_{Ui} = \frac{m_U h_{Ui}}{\sum_{j=1}^{N_U} m_U h_{Uj}} \left(V_{Ub} - F_t\right) \tag{4.13}$$

where h_{Ui} is the height measured from the base of the upper structure to the ith-level of the upper structure, and F_t is the proposed additional top shear force, which will be discussed later in section 4.4. The shear force of the upper structure associated with any level i, V_{Ui}, can be equivalently computed from Figure 4.4 (b) as follows:

$$V_{Ui} = \sum_{j=i}^{N_U} \left(F_{Ui} + F_t\right) \tag{4.14}$$

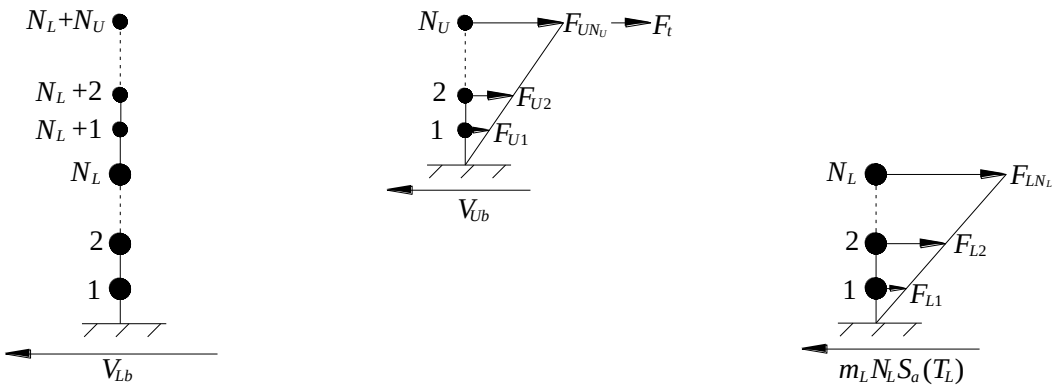

(a) entire building (b) upper structure (c) lower structure

Figure 4.4: Lateral seismic force distribution of proposed two-stage analysis procedure

4.3.3.2. Lower structure

The seismic load of the lower structure is also determined as it is fixed to the ground base. The lateral seismic force at any level of the lower structure, F_{Li}, is also linearly distributed along the height, as shown in Figure 4.4 (c). F_{Li} is computed as follows:

$$F_{Li} = \frac{m_L h_{Li}}{\sum_{i=1}^{N_L} m_L h_{Li}} m_L N_L S_a(T_L) \tag{4.15}$$

where h_{Li} is the height from the base of the lower structure to the ith-level of the lower structure. The shear force of the lower structure associated with any level i, V_{Li}, are equivalently computed from the lateral seismic force distribution shown in Figure 4.4 (c) and then combined with V_{Ub} as follows:

$$V_{Li} = \sqrt{\left[V_{Ub}\right]^2 + \left(\sum_{j=i}^{N_L} F_{Lj}\right)^2} \tag{4.16}$$

4.3.4 Proposed two-stage analysis procedure

By adopting the proposed two-stage analysis procedure, the seismic load of the combined framing system can be calculated as follows:

Step 1: Evaluate the effective seismic weight and stiffness distributions, (m_L and m_U) and (k_L and k_U), respectively; and calculate r_m (r_m=m_L/m_U) and r_k (r_k=k_L /k_U).

Step 2: Determine the value of r_{k2stg} based on Eq.(4.11).

Step 3: Check if the storey-stiffness ratio r_k is not less than the value of r_{k2stg}. If $r_k \geq r_{k2stg}$, go to step 4; otherwise, the proposed two-stage analysis procedure is not applicable.

Step 4: Calculate the base shear force of the upper structure V_{Ub} by Eq.(4.12); and, evaluate the proposed additional top shear force F_t in accordance with Eq.(4.17) in section 4.4; then, compute the lateral seismic force and shear force for each storey of the upper structure based on Eqs.(4.13) and (4.14), respectively; and finally, evaluate the lateral seismic force and shear forces for each storey of the lower structure based on Eqs.(4.15) and (4.16), respectively.

4.3.5 Error analysis

Similar to that of the modified ELF procedure, results obtained from the proposed two-stage analysis procedure are also compared with those from the elastic modal response spectrum analysis of the MDOF model with CQC rule to combine the peak modal responses (Chopra, 2007). The maximum and minimum errors for each storey combination are shown in Table 4.2. Again, the positive and negative errors represent that the proposed two-stage analysis procedure overestimates and underestimates the shear force, respectively. From Table 4.2, it is seen errors of the shear force induced by the proposed two-stage analysis procedure for the upper structure are in the range between -0.9% ~ 38.0%, which is comparable to that of the conventional ELF procedure (ASCE, 2010) for "regular" structures, as discussed in section 3.3.4.

The proposed two-stage analysis procedure may overestimate the shear force of the lower structure considerably, as shown in Table 4.2. However, compared to the two-stage analysis procedure prescribed in ASCE 7 (ASCE, 2006), which will be discussed later in section 4.5.2.1, the accuracy of the proposed procedure in this study is greatly improved. Since a weak or flexible lower structure is prohibited in practice, conservative design on the lower structure may be acceptable. Considering the amount of the work associated with the design of a combined framing system with a MDOF model, despite that it is conservative, the proposed two-stage analysis procedure is adopted to evaluate the seismic load of the lower structure as long as the applicable requirement of the two-stage analysis procedure is satisfied.

4.4 Top storey loading

The applicable requirement of the proposed two-stage analysis procedure, which is expressed in terms of the threshold value of r_{k2stg}, is derived based on the simplified 2DOF model, as discussed in sections 4.3.1 and 4.3.2. Since dynamic properties of the simplified 2DOF model are obtained based on first vibrations modes of the lower and upper structures, as shown in Eqs. (3.5 a) ~ (3.5 d), the simplified 2DOF model only accounts for the interaction of the first modes of the lower and upper structures. Therefore, satisfying the applicable requirement of the two-stage analysis procedure only ensures that the interaction of the first modes of the lower and upper structures is not significant so

that it can be ignored. However, in the MDOF model, the interaction of other vibration modes between the lower and upper structures, especially the interaction of the first mode of the lower structure and other higher vibration modes of the upper structure, may not be ignored. The effect of such interaction on the base shear force of the upper structure has been accounted for in the proposed two-stage amplification factor α_{U2stg} shown in Eq.(3.21). Nevertheless, as discussed in Appendix D.2.1, the amplification effect of such interaction on the shear force associated with the top storey of the upper structure is far more significant than that on the base shear force of the upper structure. Such phenomenon also occurs in "regular" buildings. The seismic response of the top storey associated with the "regular" building is more likely to be affected by higher vibration modes. In order to account for the "extra" amplification effects on the top storey of the upper structure, an additional shear force, F_t, as shown in Figure 4.4 (b), is applied to the top storey. Similar to the additional top shear force for the "regular" building prescribed in the NBCC 2010 (NBCC, 2010), the additional top shear force associated with the proposed two-stage analysis procedure for the combined framing system is calculated as follows:

$$F_t = \gamma V_{Ub} \tag{4.17}$$

where V_{Ub} is the base shear force of the upper structure calculated by Eq.(4.12), and the parameter γ is evaluated as

$$\gamma = \gamma_{\text{reg}} + \gamma_{\text{intr}} \tag{4.18}$$

In Eq.(4.18), γ_{reg} represents the additional top shear force that should be applied to the upper structure if it is fixed to the ground base directly; and γ_{intr} represents the additional top shear force that is induced by the interaction of the first mode of the lower structure and other higher vibration modes of the upper structure.

4.4.1 Determination of γ_{reg}

To account for the effect of higher vibration modes on the shear force of the top storey, the national building code NBCC 2010 (NBCC, 2010) specifies equations on how to calculate the additional top shear force in the "regular" building. By transferring the additional top shear force prescribed in NBCC in terms of the parameter γ_{reg}, $\gamma_{\text{reg-NBCC}}$ is calculated as follows:

$$\gamma_{\text{reg-NBCC}} = \begin{cases} 0 & T_1 \le 0.7\ s \\ 0.07T_1 & 0.7\ s < T_1 < 3.6\ s \\ 0.25 & T_1 \ge 3.6\ s \end{cases} \tag{4.19}$$

From Eq.(4.19), it is seen the NBCC considers $\gamma_{\text{reg,NBCC}}$ as a function of the first mode period T_1. In fact, the standard ASCE 7 (ASCE, 2010) also considers the effect of higher vibration modes on the

shear force of the top storey in the "regular" building as a function of T_1, as shown in Eq.(4.5). Although Eqs.(4.5) and (4.19) have been respectively adopted by ASCE 7 and NBCC for "regular" structures for a long time, the both equations may not be as accurate as one thought. This is because the both equations only account for the first mode period. The effect of higher vibration modes on the shear force of the top storey in "regular" building is not only related to the first mode period T_1, but also dependent on the predominant period of the earthquake ground motion in the field. In accordance with the standard ASCE 7 (ASCE, 2010), the predominant period of the earthquake ground motion can be represented by the period T_S in the response spectrum curve as shown in Figure 1.4. Therefore, for an N-storey "regular" structure, an accurate estimation of γ_{reg} should include both T_1 and T_S.

For an N-storey "regular" structure with the storey-mass being m, the parameter γ_{reg} can be evaluated as follows based on the MDOF modal response spectrum analysis (Chopra, 2007):

$$\gamma_{\text{reg}} = \frac{\sqrt{\sum_{i=1}^{N}\sum_{j=1}^{N}\rho_{ij}M_{Ni}^{*}S_a\left(T_i\right)M_{Nj}^{*}S_a\left(T_j\right)}\Big/\left[mNS_a\left(T_1\right)\right]-\left(mh_N\right)\Big/\left(\sum_{i=1}^{N}mh_i\right)}{1-\left(mh_N\right)\Big/\left(\sum_{i=1}^{N}mh_i\right)} \tag{4.20}$$

where h_N is the height from the ground base to the top storey; ρ_{ij} is the correlation coefficient between the ith- and jth-modes; and M_{Ni}^{*} is the effective modal mass of the top storey associated with the ith-mode. From Eq.(4.20), it is seen for an N-storey "regular" structure, all parameters on the right hand side of Eq.(4.20) are constants except the spectrum ratio $S_a(T_i)/ S_a(T_1)$. From the response spectrum curve shown in Figure 1.4, the spectrum ratio $S_a(T_i)$ $S_a(T_1)$ is not only related with the period ratio T_i/T_1, but also related with the period ratio T_1/T_S. However, the period ratio T_i/T_1 can be considered as a constant for an N-storey "regular" structure. Therefore, the only parameter that affects the value of γ_{reg} is the ratio T_1/T_S. For an N_U-storey upper structure with the base fixed to the ground, as shown in Figure 4.4 (b), the first mode period T_1 can be represented by its single storey-period T_{singU}. Consequently, the value of γ_{reg} for the N_U-storey upper structure is related to the period ratio T_{singU}/T_S. Such, both the effect of T_1 and T_S on γ_{reg} has been accounted for. Note the consideration of the first mode period of the upper structure T_1 is represented by the single storey-period of the upper structure T_{singU}.

Numerical values of γ_{reg} are provided in Table 4.3. For values of T_{singU}/T_S that are not listed in the table, the corresponding γ_{reg} can be linearly interpolated by the magnitude of T_{singU}/T_S.

Table 4.3: Values of γ_{reg} for "regular" upper structures

N_U \ T_{singU}	$0.2T_S$	$0.3T_S$	$0.4T_S$	$0.5T_S$	$0.6T_S$	$0.7T_S$	$0.8T_S$	$0.9T_S$	$1.0T_S$	$1.1T_S$
2	0.00	0.00	0.00	0.00	0.00	0.00	0.00	0.00	0.00	0.00
3	0.00	0.00	0.00	0.00	0.00	0.00	0.00	0.00	0.00	0.00
4	0.00	0.00	0.00	0.00	0.00	0.00	0.00	0.00	0.00	0.00
5	0.00	0.00	0.00	0.00	0.00	0.00	0.00	0.01	0.02	0.02
6	0.00	0.00	0.00	0.00	0.00	0.01	0.02	0.03	0.04	0.04
7	0.00	0.00	0.00	0.00	0.01	0.02	0.03	0.04	0.05	0.05
8	0.00	0.00	0.00	0.00	0.02	0.03	0.04	0.05	0.05	0.06
9	0.00	0.00	0.00	0.02	0.03	0.04	0.05	0.05	0.06	0.06

4.4.2 Determination of γ_{intr}

For a combined framing system with an N_L-storey lower and N_U-storey upper structure, the value of γ_{intr} is computed as follows:

$$\gamma_{intr} = 1 - \eta_{intr} \tag{4.21}$$

The parameter η_{intr} ranges between zero and unity. With η_{intr}=1, it represents that the interaction of the first mode of the lower structure and higher vibration modes of the upper structure does not induce an additional top shear force. The smaller the value of η_{intr}, the larger the additional top shear force.

In order to investigate how the value of η_{intr} is affected by the interaction of the first mode of the lower structure and higher vibration modes of the upper structure, errors of the seismic load associated with the top storey by setting γ_{intr}=0, i.e., η_{intr}=1, are discussed in Appendix D.2.1. From the discussion it is seen the error of the seismic load for the top storey with γ_{intr}=0 is generally affected by the period ratio T_U/T_S and the period ratio between lower and upper structures T_U/T_L. Considering the influence of ratios T_U/T_S and T_U/T_L, the value of η_{intr} is proposed to be estimated as follows in this study:

$$\eta_{intr} = \begin{cases} 1 & T_U / T_S \le (T_U / T_S)_{CRT} \\ \eta_{\min} \left[\dfrac{T_U / T_S}{T_U / T_L} \right]^{x_5} & (T_U / T_S)_{CRT} < T_U / T_S < T_U / T_L \\ \eta_{\min} & T_U / T_S \ge T_U / T_L \end{cases} \tag{4.22}$$

where numerical values of $(T_U/T_S)_{CRT}$ are listed in Table 4.4; and the exponent x_5 and the minimum value of η, η_{min}, are computed as follows:

$$x_5 = \ln\left(\eta_{\min}\right) / \ln\left[\frac{T_U / T_L}{\left(T_U / T_S\right)_{CRT}}\right] \tag{4.23}$$

$$\eta_{\min} = \begin{cases} \eta_{\min 1}\left[\dfrac{T_U / T_L}{\sqrt{R_{k2stg} / R_m}}\right]^{x_6} & T_U / T_L < \left(T_U / T_L\right)_{CRT1} \\ \eta_{\min 2} & \left(T_U / T_L\right)_{CRT1} \le T_U / T_L \le \left(T_U / T_L\right)_{CRT2} \\ \eta_{\min 2}\left[\dfrac{T_U / T_L}{\left(T_U / T_L\right)_{CRT2}}\right]^{x_7} & \left(T_U / T_L\right)_{CRT2} < T_U / T_L < \left(T_U / T_L\right)_{CRT3} \\ 1 & T_U / T_L \ge \left(T_U / T_L\right)_{CRT3} \end{cases} \tag{4.24}$$

where R_{k2stg} is calculated based on Eq.(4.10), and exponents x_6 and x_7 are calculated as

$$x_6 = \frac{\ln\left(\eta_{\min 2} / \eta_{\min 1}\right)}{\ln\left[\left(T_U / T_L\right)_{CRT1} / \sqrt{R_{k2stg} / R_m}\right]} \tag{4.25}$$

$$x_7 = \frac{\ln\left(\eta_{\min 2}\right)}{\ln\left[\left(T_U / T_L\right)_{CRT2} / \left(T_U / T_L\right)_{CRT3}\right]} \tag{4.26}$$

In Eqs. (4.24) ~ (4.26), values of $(T_U/T_L)_{CRT1}$, $(T_U/T_L)_{CRT2}$ and $(T_U/T_L)_{CRT3}$ are shown in Table 4.4, and values of $\eta_{\min 1}$ and $\eta_{\min 2}$ for possible storey combinations of the lower and upper structures that the two-stage analysis procedure may be applicable for are shown in Table 4.5.

Effects of T_U/T_S

The relationship between the period ratio T_U/T_S and the parameter η_{intr} presented in Eq.(4.22) is established in accordance with the effect of T_U/T_S on the error of the top shear force evaluated by setting γ_{intr}=0, as shown in Figure D.2 (g) of Appendix D.2.1. Based on the definition of the η_{intr} shown in Eq.(4.21), it is seen the positive error in Figure D.2 (g) represents no additional top shear force will be resulted from the interaction of higher vibration modes and η_{intr}=1. On the other hand, the negative error means an additional top shear force will be induced by the interaction of higher vibration modes and η_{intr}<1. Furthermore, as the magnitude of the negative error increases, value of the parameter η_{intr} decreases. From Figure D.2 (g), it is seen:

(1) When the period ratio of the upper structure T_U/T_S is less than a certain value, i.e., $(T_U/T_S)_{CRT}$ in Eq.(4.22), the error of the top shear force is positive; therefore, no addition top shear force will be induced by the interaction of higher vibration modes and η_{intr}=1.

(2) Then, as the increase of T_U/T_S, the effect of the interaction between the first mode of the lower structure and other higher vibration modes of the upper structures on the top storey shear force

Table 4.4: Empirical values of $(T_U/T_L)_{CRT1}$, $(T_U/T_L)_{CRT2}$, $(T_U/T_L)_{CRT3}$ and $(T_U/T_S)_{CRT}$

N_U	$(T_U/T_L)_{CRT1}$	$(T_U/T_L)_{CRT2}$	$(T_U/T_L)_{CRT3}$	$(T_U/T_S)_{CRT}$
3	2.34	3.18	4.71	1.00
4	3.06	4.25	7.44	1.00
5	3.74	4.61	9.3	1.05
6	4.44	5.87	10.92	1.24
7	4.6	6.4	10.7	1.43
8	4.83	6.64	12.97	1.63
9	4.86	7.82	13.08	1.82

Table 4.5: Values η_{min1} and η_{min2} for proposed two-stage analysis procedure

N_L	N_U	r_m=1		r_m=2		r_m =3	
		η_{min1}	η_{min2}	η_{min1}	η_{min2}	η_{min1}	η_{min2}
1	1	1.00	1.00	1.00	1.00	1.00	1.00
1	2	1.00	1.00	1.00	1.00	1.00	1.00
2	2	1.00	1.00	1.00	1.00	1.00	1.00
3	2	1.00	1.00	1.00	1.00	1.00	1.00
1	3	1.00	1.00	0.91	0.91	0.70	0.7
2	3	0.95	0.95	0.57	0.57	0.55	0.55
3	3	0.68	0.68	0.49	0.49	N/A	N/A
4	3	0.60	0.6	0.46	0.46	N/A	N/A
1	4	1.00	1.00	0.86	0.86	0.74	0.74
2	4	0.90	0.90	0.68	0.68	0.55	0.55
3	4	0.78	0.78	0.56	0.56	0.55	0.55
4	4	0.72	0.72	0.42	0.42	N/A	N/A
5	4	0.68	0.65	0.51	0.51	N/A	N/A
1	5	1.00	1.00	0.89	0.89	0.79	0.79
2	5	0.91	0.91	0.70	0.70	0.63	0.63
3	5	0.83	0.83	0.63	0.61	0.53	0.53
4	5	0.77	0.75	0.55	0.55	0.47	0.47
5	5	0.68	0.68	0.49	0.49	N/A	N/A
1	6	1.00	1.00	0.90	0.90	0.83	0.83
2	6	0.93	0.93	0.81	0.78	0.70	0.69
3	6	0.88	0.86	0.73	0.68	0.52	0.52
4	6	0.84	0.78	0.60	0.59	0.50	0.50
1	7	1.00	1.00	0.92	0.92	0.87	0.85
2	7	0.95	0.95	0.84	0.80	0.74	0.72
3	7	0.88	0.87	0.77	0.74	0.62	0.58
1	8	1.00	1.00	0.92	0.92	0.86	0.86
2	8	0.95	0.95	0.82	0.82	0.73	0.73
1	9	1.00	1.00	0.94	0.94	0.89	0.89

Note: N/A indicates the proposed two-stage analysis procedure is not applicable.

becomes more and more significant. The error turns to be negative and the magnitude of the negative error gradually increases. Therefore, the value of η_{intr} decreases exponentially as shown in Eq.(4.22).

(3) Finally, when the period ratio T_U/T_S is equal to the period ratio between the lower and upper structures, i.e, $T_U/T_S=T_U/T_L$, the magnitude of negative error reaches to the minimum value and remains as invariant as the further increase of T_U/T_S. Therefore, when $T_U/T_S=T_U/T_L$, the value of η_{intr} reaches to the minimum value, i.e., η_{min} in Eq.(4.22), and after that, the value of η_{intr} remains as invariant the as the further increase of T_U/T_S.

The value of critical period ratio $(T_U/T_S)_{CRT}$ shown in Eq. (4.22) is investigated by the numerical study. It is found $(T_U/T_S)_{CRT}$ is primarily affected by the number of the storey of the upper structure N_U, as shown in Table 4.4.

Effects of T_U/T_L

The relationship between the period ratio T_U/T_L and the value of η_{min} presented in Eq.(4.24) is constructed based on the effect of T_U/T_L on the error of top shear force by setting $\gamma_{intr}=0$, as shown in Figure D.2 (h) of Appendix D.2.1. From Figure D.2 (h), it is seen:

(1) As the initial increase of T_U/T_L, the magnitude of negative error gradually increases; therefore, values of η_{min} firstly decreases exponentially, as shown in Eq.(4.24).

(2) As the further increase of T_U/T_L, the negative error of the top storey shear force remains as the constant being minimum value; therefore, the value of η_{min} remains the constant minimum value $\eta_{min2,}$ as shown in Eq.(4.24).

(3) As the continuing increase of T_U/T_L, the interaction between the first mode of the lower structure and higher vibration modes of the upper structure becomes less significant, and the magnitude of the negative error gradually decreases; consequently, the value of η_{min} gradually increases from η_{min2} to unity as shown in Eq.(4.24).

(4) Finally, the effect of the interaction between the lower and upper structures vanishes. The assumption $\gamma_{intr}=0$ can well approximate the shear force of the upper structure. Therefore, η_{min} remains as unity as shown in Eq.(4.24).

In fact, the value of T_U/T_L determines which mode of the upper structure should be interacted with the first mode of the lower structure. For example, for the case where $N_L=2$, $N_U=8$ and $r_m=3$ as discussed in Appendix D.2.1, the first mode period of the lower structure is close to the fourth mode period of the upper structure if T_U/T_L =6.11, and the interaction is primarily associated with the first mode of the lower structure and the fourth mode of the upper structure. Therefore, critical period

ratios between the lower and upper structures in Eq.(4.24), i.e., $(T_U/T_L)_{CRT1}$, $(T_U/T_L)_{CRT2}$ and $(T_U/T_L)_{CRT3}$, are primarily influenced by the number of the storey of the upper structures, as shown in Table 4.4. From Table 4.4, it is seen as the number of the storey of the upper structures increases, critical period ratios $(T_U/T_L)_{CRT1}$, $(T_U/T_L)_{CRT2}$ and $(T_U/T_L)_{CRT3}$ increase. When the number of the storey of the upper structure increases, the number of its vibration modes increases correspondingly. In general, higher vibration modes have shorter periods if the first mode period of the upper structure, i.e., T_U, remains as a constant. When the first mode of the lower structure is interacted with these higher vibration modes of the upper structure, the first mode period of the lower structures, i.e., T_L, is approximately equivalent to the period associated with these higher vibration modes of the upper structure. Therefore, as the number of the storey of the upper structure increases, critical period ratios $(T_U/T_L)_{CRT1}$, $(T_U/T_L)_{CRT2}$ and $(T_U/T_L)_{CRT3}$ increase due to the decrease of periods associated with higher vibration mode of the upper structure.

For each storey combination of the lower and upper structures that the proposed two-stage analysis procedure is applicable, the two critical values of $\eta_{\min}$, i.e., $\eta_{\min 1}$ and $\eta_{\min 2}$ in Eq.(4.24), are obtained in accordance with numerical study and are listed in Table 4.5. Since Table 4.5 only lists $\eta_{\min 1}$ and $\eta_{\min 2}$ for cases r_m=1, 2 and 3, for other cases of r_m, values of $\eta_{\min 1}$ and $\eta_{\min 2}$ can be linearly interpolated by the magnitude of r_m.

4.5 Evaluation of two-stage analysis procedure prescribed in ASCE 7

4.5.1 Evaluation of applicable requirement

As discussed Appendix C.4, the overall two-stage stiffness ratio associated with ASCE 7 (ASCE, 2006), $R_{k2stg\text{-}ASCE}$, is calculated as

$$R_{k2stg} = \max\left(0.826R_m + 4.76,\ 10\right) \tag{4.27}$$

By comparing Eqs.(4.10) to (4.27) , it can be seen considerable difference exists on the applicable requirements of the two-stage analysis procedure between the prescribed one in ASCE 7 and the proposed in this study. When the overall mass ratio R_m is greater than 1.23, as shown in Figure 4.5, the proposed overall two-stage stiffness ratio R_{k2stg} is considerably greater than that prescribed in ASCE 7 (ASCE, 2006). For the design located in the shaded area of Figure 4.5, this study concludes that the two-stage analysis procedure is not applicable but ASCE 7 permits the use of the two-stage analysis procedure to analyze buildings with combined framing systems.

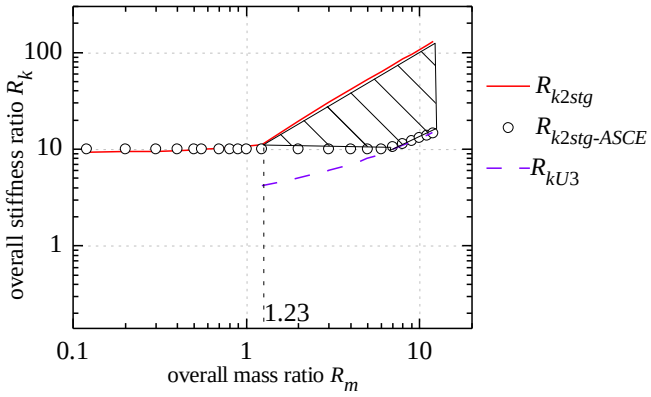

Figure 4.5: Comparison of overall two-stage stiffness ratios between ASCE 7 (ASCE, 2006) and proposed approach

Based on Eq.(3.7), the critical storey-stiffness ratio associated with the two-stage analysis procedure prescribed in ASCE 7, $r_{k2stg\text{-}ASCE}$, for the combined framing systems can be computed as follows:

$$r_{k2stg-ASCE} = R_{k2stg-ASCE}\left(\frac{N_U}{N_L}\right)\left(\frac{\bar{\omega}_{1U}}{\bar{\omega}_{1L}}\right)^2 \tag{4.28}$$

As to possible storey combinations of the lower and upper structures that may be analyzed by the proposed two-stage analysis procedure, values of r_{k2stg} and $r_{k2stg\text{-}ASCE}$ are compared in Table 4.6. It can be seen for the possible storey combination of the lower and upper structures that may result in the overall mass ratio R_m >1.23, considerable difference exists between the values of $r_{k2stg\text{-}ASCE}$ and r_{k2stg}. For example, when N_L=4, N_U=3, and r_m=3, based on the proposed method, r_{k2stg}=51.24; however, based on ASCE 7(ASCE, 2006), $r_{k2stg\text{-}ASCE}$ =12.31. Nevertheless, for the traditional "podium" building, in which the number of storey of the lower structure is considerably less than that of the upper one, there is not much difference between values of $r_{k2stg\text{-}ASCE}$ and r_{k2stg}. For example, when N_L=1 and N_U=6, values of $r_{k2stg\text{-}ASCE}$ and r_{k2stg} are almost the same, as shown in Table 4.6.

4.5.2 Evaluation of seismic load distribution

4.5.2.1. Base shear force of lower structure

Recall Eq.(4.16). It is seen the peak base shear forces of the lower structure associated with the first and second modes are combined by the SRSS (square-root-of-sum-of-square) rule. However, as prescribed in ASCE 7 (ASCE, 2006; 2010), the peak base shear forces of the lower structure associated with the first and second modes are combined by the absolute sum (ABSSUM) rule as follows:

$$V_{Lb-ASCE7} = M_U S_a\left(T_U\right) + M_L S_a\left(T_L\right) \tag{4.29}$$

Table 4.6: Comparison of two-stage storey-stiffness ratio between proposed approach and ASCE 7

N_L	N_U	r_m=1		r_m =2		r_m =3	
		proposed r_{k2stq}	ASCE 7 $r_{k2stq\text{-}ASCE}$	proposed r_{k2stq}	ASCE 7 $r_{k2stq\text{-}ASCE}$	proposed r_{k2stq}	ASCE 7 $r_{k2stq\text{-}ASCE}$
1	1	10.71	10.00	19.56	10.00	30.59	10.00
1	2	7.55	7.64	8.18	7.64	10.73	7.64
2	2	10.71	10.00	19.56	10.00	30.59	10.00
3	2	18.06	12.86	39.33	12.86	60.60	12.86
1	3	5.71	5.94	6.04	5.94	6.36	5.94
2	3	7.90	7.78	9.49	7.78	15.21	7.78
3	3	10.71	10.00	19.56	10.00	30.59	10.00
4	3	15.03	12.31	33.14	12.31	51.24	12.31
1	4	4.57	4.82	4.77	4.82	4.97	4.82
2	4	6.25	6.32	6.76	6.32	8.87	6.32
3	4	8.36	8.12	11.41	8.12	18.12	8.12
4	4	10.71	10.00	19.56	10.00	30.59	10.00
5	4	13.45	11.91	29.87	11.91	46.29	11.91
1	5	3.81	4.05	3.94	4.05	4.07	4.05
2	5	5.16	5.30	5.50	5.30	5.85	5.30
3	5	6.85	6.82	7.52	6.82	11.83	6.82
4	5	8.71	8.39	12.71	8.39	20.12	8.39
5	5	10.71	10.00	19.56	10.00	30.59	10.00
1	6	3.26	3.49	3.35	3.49	3.45	3.49
2	6	4.39	4.57	4.64	4.57	4.89	4.57
3	6	5.81	5.87	6.29	5.87	8.24	5.87
4	6	7.35	7.23	8.82	7.23	14.14	7.23
1	7	2.85	3.06	2.92	3.06	2.99	3.06
2	7	3.82	4.01	4.01	4.01	4.20	4.01
3	7	5.03	5.15	5.40	5.15	6.02	5.15
1	8	2.53	2.72	2.58	2.72	2.64	2.72
2	8	3.38	3.57	3.53	3.57	3.67	3.57
1	9	2.27	2.46	2.32	2.46	2.36	2.46

The ABSSUM modal combination rule is not popular in structural design, and often leads to much larger results than the accurate ones (Chopra, 2007). In fact, as discussed in Appendix D.2.2, since the proposed two-stage analysis procedure does not account for the interaction of higher vibration modes between the lower and upper structures on the shear force of the lower structure, Eq.(4.16) may greatly overestimate the seismic load of the lower structure. The two-stage analysis procedure prescribed in ASCE 7 (ASCE, 2006; 2010) also does not account for the effect of such interaction on the shear force of the lower structure. In addition, ASCE 7 selects the ABSSUM rule to combine the peak modal response. Therefore, the two-stage analysis procedure prescribed in ASCE 7 often leads

to overly conservative base shear force of the lower structure. Compared to the two-stage analysis procedure prescribed in ASCE 7 (ASCE, 2006), the accuracy of the proposed procedure on the base shear force of the lower structure is improved, as shown in Figures D.3 (a) ~ (d) in Appendix D.2.2.

4.5.2.2. Base shear force of upper structure

As shown in Figure 4.5, for the shadow area where $R_m \geq 1.23$: (a) the two-stage analysis procedure is applicable and $\alpha_U=1$ in accordance with ASCE 7 (ASCE, 2006); but (b) based on this study, the factor α_U can be greater than unity, as shown in Figures 3.6 (a) ~ (b). Therefore, the two-stage analysis procedure prescribed in ASCE 7 may underestimate the factor α_U and consequently the base shear force of the upper structure V_{Ub} for cases $R_m \geq 1.23$.

For each combination of R_m and R_k shown in the shadow area of Figure 4.5, elastic model response spectrum analysis with CQC rule of combining the peak modal responses (Chopra, 2007) is carried out for the 2DOF model to calculate the factor α_U and further investigate the possible error associated with ASCE 7 (ASCE, 2006). By limiting the period T_U to the range between $0.2T_S$ and T_S, the possible maximum and minimum errors of the factor α_U for each combination of R_m and R_k, are shown in Figure 4.6. Note that the negative error represents that the two-stage analysis procedure of ASCE 7 underestimates the factor α_U. It can be seen the two-stage analysis procedure prescribed in ASCE 7 always leads to a smaller value of the factor α_U. The underestimation can be as large as 70.1%. The magnitudes of the errors are greatly affected by ratios R_m and R_k. When the ratio R_k gradually increases from the proposed R_{kU3} to R_{k2stg}, the magnitude of the error gradually decreases. Meanwhile, the magnitude of the error also gradually increases as R_m increases.

The underestimation of the base shear for the upper structure associated with ASCE 7 (ASCE, 2006) is primarily induced by the over-relaxed stiffness requirement of the two-stage analysis procedure for the case $R_m \geq 1.23$. In ASCE 7-10 (ASCE, 2010), the second applicable requirement for the two-stage analysis procedure in ASCE 7-05 (ASCE, 2006) is revised from "*the period of the entire structure shall not be greater than 1.1 times the period of the upper portion considered as a separate structure fixed at the base*" to "*the period of the entire structure shall not be greater than 1.1 times the period of the upper portion considered as a separate structure supported at the transition from the upper to the lower portion*". However, as "*transition boundary condition*" is implicitly prescribed, it creates a difficulty to its application.

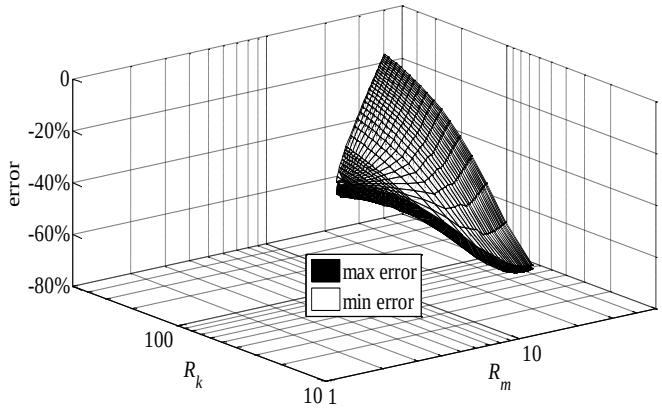

Figure 4.6: Possible maximum and minimum errors of factor α_U associated with two-stage analysis procedure in ASCE 7 (ASCE, 2006)

4.5.2.3. Seismic load distribution

The ASCE 7 (ASCE, 2006; 2010) assumes seismic loads the upper and lower structure can be calculated by the ELF procedure, separately. However, as discussed in sections 4.3.3.1 and 4.4, due to the interaction of the first mode of the lower structure and other higher vibration modes of the upper structure, the ELF procedure prescribed in ASCE 7 may underestimate the seismic load of the top storey. The proposed two-stage analysis approach of this study applies an additional top shear force to limit the underestimation within an acceptable range. Meanwhile, due to the overly conservative estimation for the base shear force of the lower structure as discussed in section 4.5.2.1, shear force for other stories in the lower structure may be greatly overestimated by ASCE 7 as well, which will be demonstrated by examples presented in section4.6.2.

4.6 Examples

4.6.1 Example 4-1

It is a seven-storey building with the combined framing systems located in Los Angeles, California. The SFRSs of the upper one-storey and lower six-storey are the cold-formed steel (CFS) framing with shear walls sheathed with oriented strand board (OSB) panels and the special RC moment frame, respectively. The floor layout, storey-height, specified dead load, column size and frame configuration for the lower RC and upper CFS structures in this example are all the same with those discussed in section 3.6.1. All columns shown in Figure 3.8 are selected as the columns in the RC moment frame and the corresponding CFS shear wall length is 14.42 m. With the lateral stiffness for each column in the RC moment frame being 5.41×10^4kN/m, the lateral storey-stiffness of the lower structure is $k_L=5.41\times10^4\times16=8.66\times10^5$kN/m. Meanwhile, the lateral storey-stiffness of the upper structure is $k_U=3836\times14.4=5.52\times10^4$kN/m, with 3836 being the lateral stiffness per meter of the CFS

shear frame (Branston, 2004). The mass and stiffness of the combined framing systems are summarized in Table 4.7.

Based on the modified ELF procedure stated in section 4.2.4, it is first calculated that $r_m=m_L/m_U$=219352/96113=2.28 and $r_k=k_L/k_U$=86.6/5.52=15.67. Then, from Table 4.1, it is seen that the critical storey-stiffness ratio associated with the modified ELF procedure, r_{kb1}=27.16. As the storey-stiffness ratio r_k is less than r_{kb1}, the proposed equations corresponding to the modified ELF procedure are applicable to compute the shear force. The shear forces of the combined framing system calculated by the modified ELF procedure are shown in Figure 4.7. Also shown in this figure are results evaluated from the ELF procedure prescribed ASCE 7 (ASCE, 2010). In addition, the accurate result shown in the figure is calculated from the elastic modal response spectrum analysis (Chopra, 2007). From the figure, it is seen the modified ELF procedure provides a good approximation for the shear forces of both the lower structure and upper "appendage". The ELF procedure prescribed ASCE 7 (ASCE, 2010) yields a good estimation for the shear force of the lower structure, but the shear force of the upper "appendage" is underestimated by 6%.

Table 4.7: Structural properties of Example 4-1

	storey number	storey-mass (kg)	SFRS	storey-stiffness (kN/m)
lower structure	6	219,352	RC moment frame, 16 columns in moment frame	8.66×10^5
upper structure	1	96,113	CFS shear wall, with shear wall length being 14.4 m	5.52×10^4

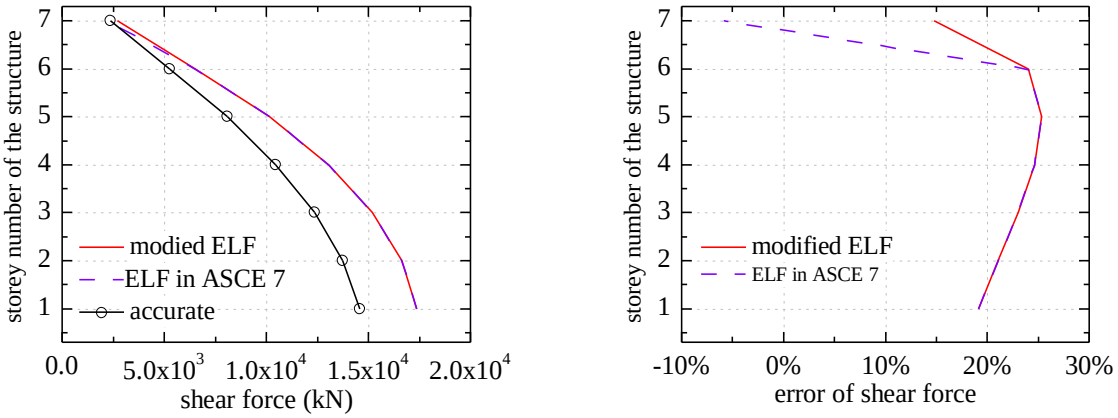

Figure 4.7: Results comparison of Example 4-1

4.6.2 Example 4-2

The building investigated in section 3.6.2, which is located in Los Angeles, California, is selected an example to illustrate how the proposed two-stage analysis procedure is applied to estimate the shear force of the combined framing system. In accordance with the obtained feasible lateral designs for the lower RC and upper CFS structures shown in Figure 3.9 (b), all columns shown in Figure 3.8 are selected as the columns in the RC moment frame and the corresponding CFS shear wall length is 43.2 m. The mass and stiffness properties of the combined framing systems are summarized in Table 4.8.

Table 4.8: Structural properties of Example 4-2

	storey number	storey-mass (kg)	SFRS	storey-stiffness (kN/m)
lower structure	2	219,352	RC moment frame, 16 columns in moment frame	8.66×10^5
upper structure	6	96,113	CFS shear wall, with shear wall length being 43.2 m	1.66×10^5

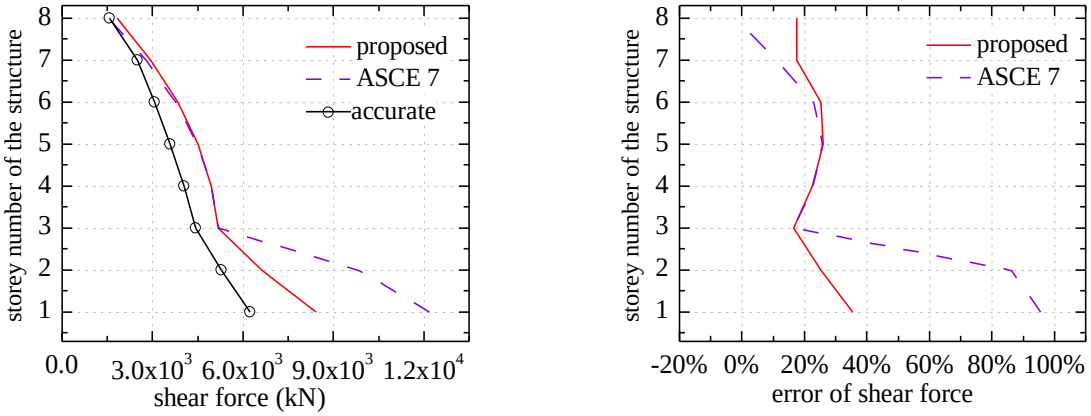

(a) Los Angeles, California

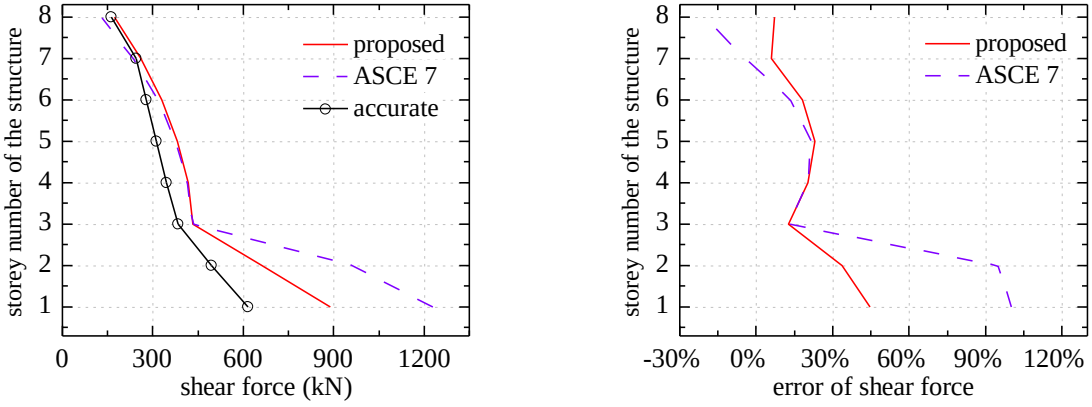

(b) Washington D.C.

Figure 4.8: Results comparison of Example 4-2

Based on the proposed two-stage analysis procedure stated in section 4.3.4, it is first calculated that $r_m=m_L/m_U$=219352/96113=2.28 and $r_k=k_L/k_U$=8.66/1.66=5.22. Then, from Table 4.2, it is seen that that the critical storey-stiffness ratio associated with the proposed two-stage analysis procedure, r_{k2stg}=4.71. As the storey-stiffness ratio r_k is greater than r_{k2stg}, the equations corresponding to the proposed two-stage analysis procedure can be adopted to compute the shear force of the combined framing system. Finally, based on step 4 of the proposed analysis procedure presented in section 4.3.4, the additional top shear force is obtained as F_t=0.1V_{Ub}. Shear forces for each level of the combined framing system calculated by the proposed two-stage analysis methods are shown in Figure 4.8 (a). Also shown in the figure are the shear force calculated by the two-stage analysis procedure prescribed in ASCE 7 (ASCE, 2006). From the figure, it is seen the proposed two-stage analysis procedure provides good approximations for the shear forces of the both lower and upper structures. At the meantime, the procedure associated with ASCE 7 estimates the shear force of the upper structure well, but it is overly conservative for the lower structure. As shown in Figure 4.8 (a), the base shear force of the lower structure estimated from the procedure associated with ASCE 7 is almost twice as much as that of the accurate result. One reason for such overestimation is that the ASCE 7 procedure adopts the ABSSUM rule to combine the peak modal responses, as discussed in section 4.5.2.1. Another reason for the overestimation is that the interaction of higher vibration modes between lower and upper structures, as discussed Appendix D.2.2, is not accounted for.

Now assume this building is located in Washington D.C. rather than Los Angeles. The site spectrum of Washington D.C. are S_S =0.278 g and S_1 =0.072 g and the long transition period T_{Long}=6 s, which results in the corresponding design spectrum being S_{DS}=0.185 g and S_{D1}=0.048 g. Compared to that of California, the earthquake magnitude of Washington D.C. is much less. Therefore, the building that is designed for California should satisfy the storey drift requirement if it is in Washington D.C.. Based on the proposed two-stage analysis procedure, it is found the additional top shear force F_t=0.16$V_{Ub.}$ The shear force for each storey of the combined framing system calculated by the both proposed two-stage analysis procedure and the two-stage analysis procedure prescribed in ASCE 7 (ASCE, 2006) are shown in Figure 4.8 (b). From Figure 4.8 (b), it is seen the shear force of the upper structure evaluated by the proposed two-stage analysis procedure is a good approximation to the accurate one. However, the procedure prescribed in ASCE 7 underestimates the shear force of the top storey by almost 20%. The main reason for such underestimation is that the procedure prescribed in ASCE 7 does not account for the amplification effect associated with the interaction between the first mode of the lower structure and higher vibration modes of the upper structures on the shear force of the top storey. The transition period T_S, as shown in Figure 1.4, for Washington D.C., i.e.,0.26 s, is much less than that for Los Angeles, i.e.,0.35s. With the same framing system, the period ratio T_U/T_S

of the building located in Washington D.C. is much larger than that in Los Angeles. As discussed in section 4.4.2, the amplification effect contributed by the interaction between the first mode of the lower structure and higher vibration modes of the upper structure on the top storey shear force becomes more significant as the increase of the period ratio T_U/T_S. As the procedure prescribed in ASCE 7 does not account for such amplification effect, it underestimates the top storey shear force, which is not acceptable in practice.

4.6.3 Example 4-3

The building discussed in section 3.6.1 is selected to be further investigated. However, the lateral stiffness distributions for both the lower and upper structure are not selected from the feasible ones shown in Figure 3.9 (b). The mass and stiffness properties of the combined framing systems in this example are summarized in Table 4.9.

Based on Eq.(4.28), it is calculated that the critical storey-stiffness ratio prescribed in ASCE 7 is $r_{k2stg\text{-}ASCE}$=17.2. The storey-stiffness ratio of the combined framing system is $r_k=k_L/k_U$=86.6/4.60=18.8, which is greater than 17.2. Therefore, ASCE 7 permits the two-stage analysis procedure to be applied to evaluate the seismic load of the upper structure, and the corresponding results are shown in Figure 4.9. From the figure, it is seen ASCE 7 underestimates shear forces of all storeys of the upper structure, of which the maximum error occurs at the base of the upper structure, being 18%. The primary reason for such underestimation is that ASCE 7 overly relaxes the stiffness requirement of the two-stage analysis procedure for the case $R_m \geq 1.23$, as discussed in section 4.5.2.1. In fact, in accordance with the two-stage analysis procedure proposed in this study, r_{k2stg}=81.41 based on Eq.(4.11) , which is much greater than the requirement set by ASCE 7, i.e., $r_{k2stg\text{-}ASCE}$= 17.2.

Table 4.9: Structural properties of Example 4-3

	storey number	storey-mass (kg)	SFRS	storey-stiffness (kN/m)
lower structure	6	219,352	RC moment frame, 16 columns in moment frame	8.66×10^5
upper structure	3	96,113	CFS shear wall, with shear wall length being 12 m	4.60×10^4

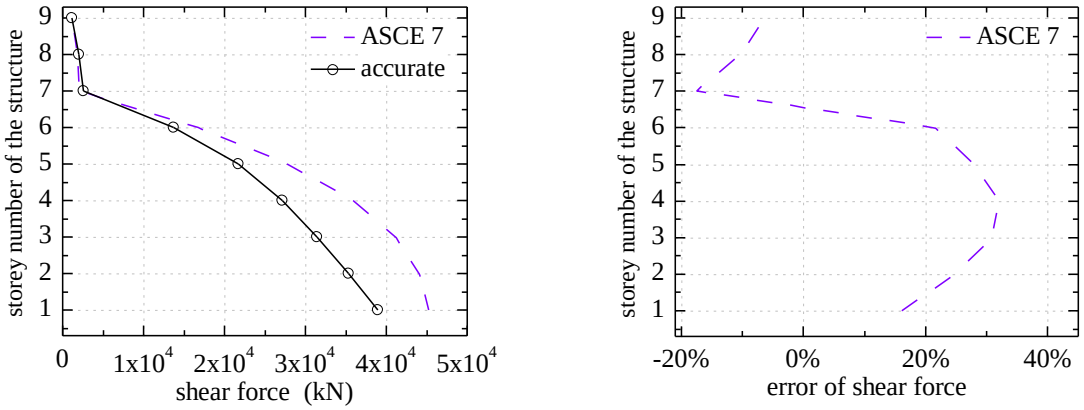

Figure 4.9: Results comparison of Example 4-3

4.7 Conclusion

Presented in this chapter are two simplified methods, i.e., modified ELF and two-stage analysis procedures, for evaluating seismic loading of the mid-rise building with vertical combination of framing systems. Applicable stiffness requirements and procedures of evaluating seismic load distributions associated with the two simplified methods are proposed. In addition, the proposed two-stage analysis procedure is also compared with the two-stage analysis procedure prescribed in ASCE 7 (ASCE, 2006; 2010). The following conclusions are obtained from this study:

(1) For the "appendage-style" building in which there is only one-storey upper structure, it is found if the storey-stiffness ratio between lower and upper structures is less than the proposed r_{kb1} value, the one-storey upper structure almost has no effect on the effective mass distribution of the lower structure. The lower structure is dominated by the first mode and the modified ELF procedure is applicable to approximate the seismic load of the upper structure. Errors of shear forces of the combined framing system associated with modified ELF procedure is in the range between 1.0% and 35.3%, which is comparable to the error of the conventional ELF procedure that is applicable for "regular" buildings.

(2) New applicable requirements and seismic load distributions of the two-stage analysis procedures are proposed. It is found that even when the applicable requirement of the proposed two-stage analysis procedure is satisfied, the shear force of the top storey of the upper structure, which is calculated by setting the upper structure fixed to the ground base, may still be underestimated. In order to eliminate such underestimation, an additional top shear force is proposed to be applied to the top of upper structure. Equations to compute the additional top shear force are provided.

(4) The two-stage analysis procedure and applicable requirements prescribed in ASCE 7 (ASCE, 2006; 2010) are also evaluated. The investigation indicates the stiffness requirement of the ASCE two-stage analysis procedure may be overly-relaxed, and therefore, the procedure may underestimate the seismic load in certain cases.

(3) Errors of shear forces of the upper structure associated with the proposed two-stage analysis procedure are in the range between -0.9% and 38.0%, which is comparable to the that associated with the conventional ELF procedure that is applicable for "regular" buildings in current practice. Although the shear forces of the lower structure may be overestimated by the proposed two-stage analysis procedure, compared to the overestimation associated with the two-stage analysis procedure prescribed in in ASCE 7 (ASCE, 2006; 2010), the accuracy of the proposed two-stage analysis procedure is greatly improved.

Chapter 5 Canadian simplified approaches to evaluate stiffness distributions and seismic loads

5.1 Introduction

The foregoing simplified approaches presented in Chapters 3 and 4 are derived based on the USA standard ASCE 7 (ASCE, 2010) and they are not applicable in Canada. Presented in this chapter is the development of simplified approaches similar to the approaches in Chapter 3 and 4 based on the NBCC 2010 (NBCC, 2010). At first, differences in seismic design provisions between the NBCC 2010 and the ASCE 7 that need to be addressed in the development of the simplified approaches are investigated. Then, based on the identified differences between the two standards, several modifications are made on the simplified approaches proposed in Chapters 3 and 4 such that the modified approaches are complied with the NBCC 2010. Finally, four design examples are presented to illustrate the efficiency of the Canadian simplified approaches. Since the proposed simplified approaches for evaluating the required stiffness distributions involves the nonlinear structural behavior of the combined framing systems, nonlinear time history analyses are also carried to investigate the nonlinear structural behavior of the combined framing systems.

5.2 Comparison between Canadian code and USA standard

The simplified approaches proposed in Chapters 3 and 4 are related highly to the corresponding seismic design provisions in following two aspects: (a) the seismic performance factors, and (b) the design response spectrum. In order to modify the simplified approaches for the Canadian application, the differences in the foregoing two aspects between the NBCC 2010 (NBCC, 2010) and the ASCE 7 (ASCE, 2010) are discussed in the following.

5.2.1 Seismic performance factors

The primary seismic performance factors prescribed in ASCE 7 (ASCE, 2010) include the response modification factor R, the overstrength factor Ω_0, and the deflection amplification factor C_d. The interpretation of the performance factors is illustrated in Figure 5.1. As shown in the figure, let V_e represent the shear force that is calculated based on the elastic modal response spectrum analysis with use of response spectra that are representative of the anticipated earthquake ground motions. Since the structural system can dissipate certain earthquake energy through the inelastic deformation, the design shear force V can be significantly reduced from the elastic shear force V_e by dividing the response modification factor R. In general, the system with high level of ductility has a larger value of R (Chopra, 2007). Then, the elastic deformation calculated under the reduced design shear force V,

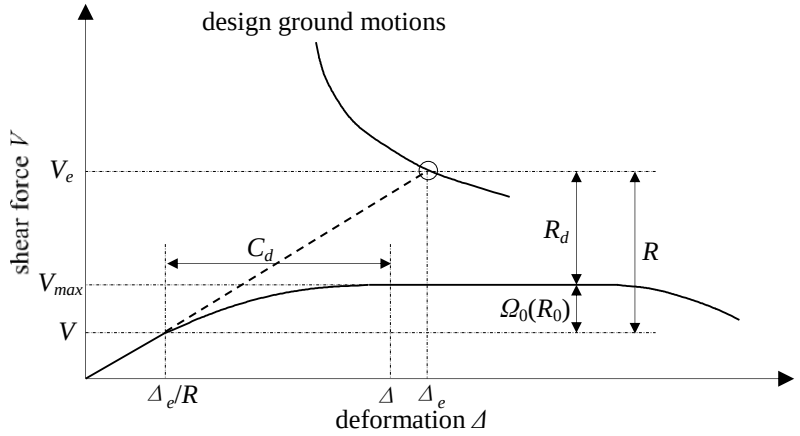

Figure 5.1: Illustration of seismic performance factors (FEMA, 2009)

i.e., Δ_e/R, should be amplified by a deflection amplification factor C_d to calculate the anticipated nonlinear deformation Δ, as shown in Figure 5.1. This is the typical elastic-analysis-based modal response spectrum analysis that is adopted in current practice. The nonlinear seismic response of the structural system is estimated by elastic analysis together with the adoption of seismic performance factors rather than a nonlinear time history analysis.

The first difference between the two standards is related to the response modification factor R. The seismic response modification factor R essentially accounts for two aspects: the ductility-related force modification factor R_d and the overstrength factor Ω_0, with $R=R_d\Omega_0$ (FEMA, 2009). Note the overstrength factor Ω_0 is termed as the overstrength-related force modification R_0 in the NBCC 2010 (NBCC, 2010). The factor R_d reflects the capability of a structure to dissipate energy through reversed cyclic inelastic behavior, while the factor R_0 (or Ω_0) accounts for reserve and redundant strength of the structure, as shown in Figure 5.1. The ASCE 7 (ASCE, 2010) directly specifies the value of R for each commonly used SFRS. However, starting from 2005, the NBCC (NBCC, 2005) attempts to quantify the relative contribution of the overstrength (R_0) and the inelastic behavior (R_d) to the permissible reduction in design strength (FEMA, 2004; Mitchell, et al., 2010). Therefore, for the commonly used SFRSs, values of R_d and R_0 are provided separately by the NBCC 2010 (NBCC, 2010).

Another difference between the two standards is that the NBCC 2010 assumes that the deflection amplification factor C_d is equal to the response modification R, i.e.,$C_d=R=R_dR_0$. Such assumption is based on the Newmark's "equal displacement rule" (Cuesta, Mark, & Fajfar, 2003), which assumes that the inelastic displacement is approximately equivalent to the elastic displacement. However, in

ASCE 7 (ASCE, 2010), the value of C_d for the commonly applied SFRS is provided separately, and the provided value of C_d is usually not equal to the response modification factor *R*, i.e., $C_d \neq R$.

5.2.2 Design response spectrum

The NBCC 2010 (NBCC, 2010) and ASCE 7 (ASCE, 2010) adopt different approaches to construct the design response spectrum. The ASCE 7 design spectrum is established based on the spectral shape proposed by Newmark and Hall (FEMA, 1997). It consists of primarily three segments: constant acceleration, constant velocity and constant displacement. As shown in Figure 1.4, the response acceleration associated with the constant acceleration segment is equal to a constant acceleration S_{DS}; and the response accelerations associated with the constant velocity and displacement segments are proportional to the reciprocal of the building period ($1/T$) and $1/T^2$, respectively. Besides the three segments, in the very short period range in which $T<T_0$, the response acceleration increases rapidly from the effective peak ground acceleration for infinite stiff structures to the constant response acceleration S_{DS} (FEMA, 1997; FEMA, 2009). By adopting the Newmark and Hall spectral shape, the design spectrum of ASCE 7 (ASCE, 2010) can be uniquely constructed by providing the following three parameters: the design response spectral accelerations at short period (S_{DS}) and one second period (S_{D1}), and the long-period transition period (T_{long}), as shown in Figure 1.4. The design response accelerations S_{DS} and S_{D1} are computed from the mapped values of S_S and S_1, respectively. Mapped values of S_S and S_1 provided in ASCE 7 are determined based on both the probabilistic seismic hazard analysis (PSHA) and fragility analysis to ensure that the collapse probability of the building is 1% in 50 years (FEMA 2009; Luco et.al, 2007).

However, the NBCC 2010 (NBCC, 2010) does not adopt the Newmark and Hall spectrum. It is believed that if the design spectrum is constructed based on a predetermined spectral shape, such as Newmark and Hall design spectral shape, the resulting spectrum does not have a uniform of probability of exceedance at all periods (Adams & Atkinson, 2003). Therefore, the spectral acceleration at each period in the NBCC 2010 is directly calculated by the PSHA to ensure the spectrum have a uniform probability of exceedance at different periods, which is 2% in 50 years. Such spectrum is called as "uniform hazard spectrum (UHS)". As the spectral ordinates at difference periods are determined directly at each geographical location with the specified probability of exceedance, the differences in spectral shape across the country are reflected. The Canadian UHS spectrum provides more site-specific descriptions of the earthquake spectrum and ensures a uniform hazard level at all periods (NBCC, 2010).

The NBCC 2010 uses spectral values of 0.2, 0.5, 1.0 and 2.0 seconds, denoted as S_a (0.2), S_a(0.5), etc. to establish the design spectrum. It is deemed that these four spectral values are sufficient to

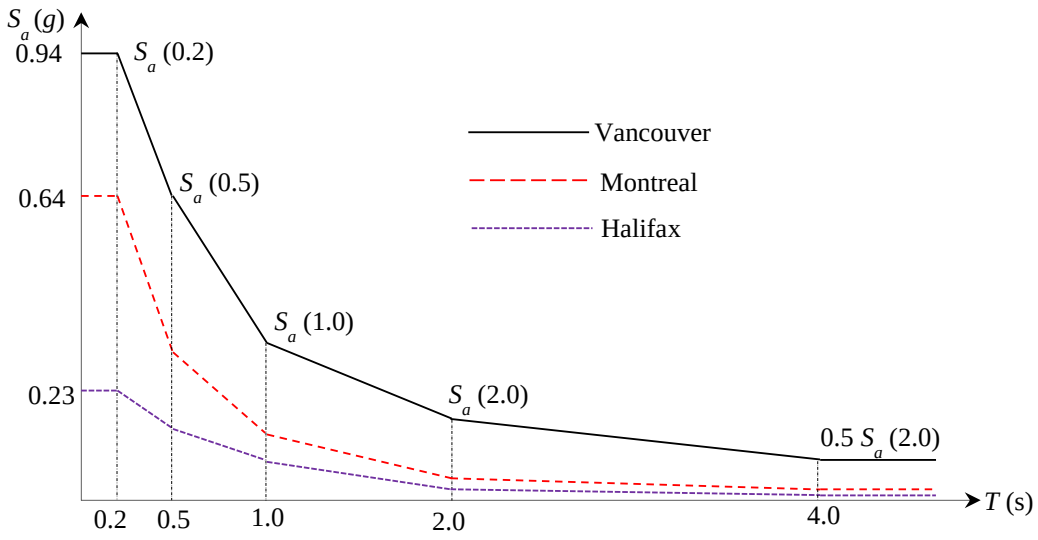

(a) design spectra for Vancouver, Montreal and Halifax

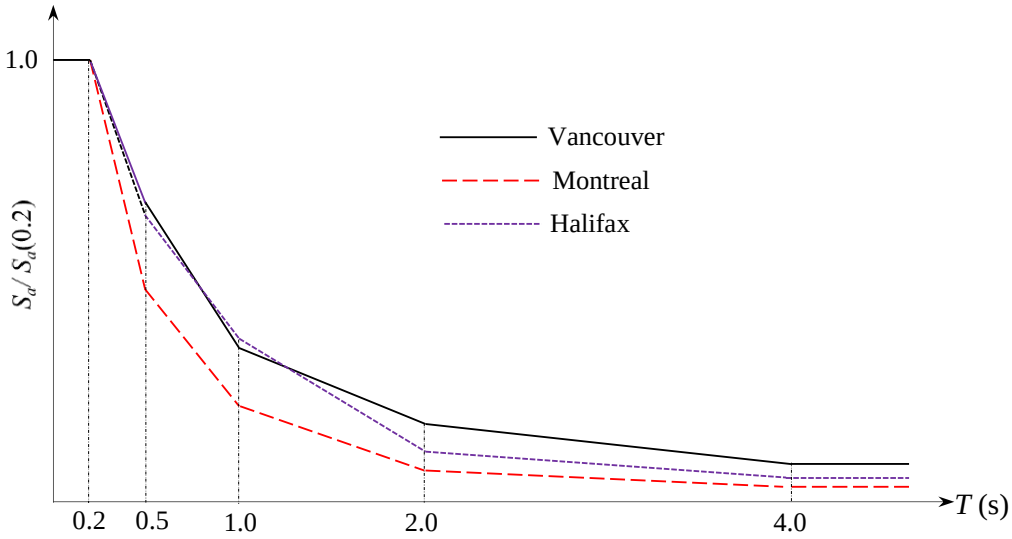

(b) design spectra normalized with respect to $S_a(0.2)$

Figure 5.2: NBCC 2010 design spectrum (NBCC, 2010)

construct the spectrum that closely matches the shape of UHS (Adams & Atkinson, 2003). With the four spectral values, the design spectral accelerations $S_a(T)$ are determined as shown in Figure 5.2 (a): (a) $S_a(T)=S_a(0.2)$ for $T\leq 0.2$ second; (b) $S_a(T)=S_a(2.0)/2$ for $T\geq 4.0$ second; and (c) using linear interpolation to determine $S_a(T)$ for the intermediate values of T.

By comparing the ASCE 7 design spectrum shown in Figure 1.4 to the Canadian spectrum shown in Figure 5.2 (a), it is seen that the primary differences of the design spectrum between the two standards are as follows:

(1) Although both the NBCC 2010 and ASCE 7 spectra have a constant acceleration segment, the period range associated with the constant acceleration is different. In the ASCE 7, the constant acceleration range starts from T_0 and ends with T_S, with T_0=0.2 T_S, as shown in Figure 1.4. For each location across USA, the transition period T_S is provided and the value of the transition period T_S is greatly dependent on the building site location. For example, the transition period T_S in Washington D.C. is 0.26 second but in Los Angeles it is 0.35 second (USGS, 2014). However, in the NBCC 2010, the constant acceleration starts from T=0 second and ends with T=0.2 second regardless of the location of the building, as shown in Figure 5.2 (a).

(2) Right after the constant acceleration segment, as shown in Figure 1.4, the ASCE 7 design spectrum starts a constant velocity segment, in which the spectral acceleration is proportional to the reciprocal of the period 1/T. However, the NBCC 2010 adopts a more site-specific spectral shape rather than the "reciprocal of the period" spectral shape. The shape of the Canadian spectrum is dependent on the relative values of spectral accelerations at periods 0.2, 0.5, 1.0 and 2.0 seconds. With different relative spectral accelerations at periods 0.2, 0.5, 1.0 and 2.0 seconds, the spectral shape may be quite different for different cities in Canada. Take cities of Vancouver, Montreal and Halifax as example. For better comparison, normalize the response spectrum accelerations with respect to the peak response spectrum acceleration $S_a(0.2)$. As shown in Figure 5.2 (b), the spectral shapes of Vancouver, Montreal and Halifax are quite different from each other. This further indicates the Canadian spectrum is more site-specific and the differences in spectral shapes across the country are reflected directly.

(3) On the right of the constant velocity segment, as shown in Figure 1.4, the ASCE 7 design spectrum starts a constant displacement segment. Meanwhile, on the left of the constant acceleration segment, the response acceleration increases rapidly from the effective peak ground acceleration for infinite stiff structures to the constant response acceleration S_{DS}. However, the buildings' periods investigated in this study is not less than T_0, as specified in section 1.3.2. In addition, from the provided ASCE 7 seismic map, the long-period transition period T_{long} for most cities are greater than 4.0 second. Therefore, the buildings' periods are usually not located in these two segments. The differences of the design spectra between the two standards in these two ranges (T <0.2 s and T> 4.0 s) are not significant and will not be accounted for in the following discussion.

5.3 Stiffness evaluations of lower and upper structures based on NBCC 2010

A simplified approach for evaluating the feasible lateral stiffness distributions of lower and upper structures based on the NBCC 2010 spectrum and the pre-determined mass distribution is presented in this section. To distinguish the approach based on ASCE 7 (ASCE, 2010) presented in Chapter 3,

the approach presented in this section is referred as the Canadian approach. The Canadian approach is obtained by modifying the USA approach with the consideration of differences between the two standards discussed in section 5.2.

5.3.1 Formulation of design equation: design criterion

Recall Eq.(3.4), which is the governing design equation established based on the ASCE 7 (ASCE, 2010) to obtain the feasible stiffness distributions of the lower and upper structures. As discussed in section 5.2.1, by substituting both R and C_d in Eq. (3.4) with R_dR_0, the governing design equation for evaluating the lateral stiffnesses of the lower and upper structures for the Canadian application is as follows:

$$\alpha_U \le \frac{k_U \Delta_{U\lim}}{m_U N_U S_a(T_U)} \tag{5.1}$$

Compared to Eq. (3.4), Eq. (5.1) is not related to the seismic performance factors R_d, R_0 or C_d. This is resulted primarily from the fact that the NBCC 2010 adopts the Newmark's "equal displacement rule" to determine the relationship between R_dR_0 and C_d. Newmark's "equal displacement rule" states that the anticipated inelastic displacement is approximately equivalent to the elastic displacement calculated under the design ground motions. Therefore, seismic performance factors related to the inelastic behavior of the structure, i.e., R_d, R_0 or C_d, are eliminated in Eq.(5.1).

5.3.2 Formulation of design equation II: analytical study on factor α_U

The proposed equations to evaluate the shear-force-amplification factor of the upper structure α_U based on the ASCE 7 design spectrum were discussed in detail in section 3.3.3. Considering the NBCC 2010 (NBCC, 2010) and ASCE 7 (ASCE, 2010) adopt different design spectra as discussed in section 5.2.2, several modifications are made on the equations proposed in section 3.3.3 to ensure they are compatible with the NBCC 2010 spectrum.

Values of α_{U1} and $\alpha_{U\max}$

As discussed in Appendix B.3, the shear-force-amplification factor of the upper structure α_U is affected by the spectral acceleration ratio $S_a(T_1)/S_a(T_U)$, where T_1 and T_U are the first mode periods of the simplified 2DOF model and the upper structure, respectively. In the proposed approach, the effect of the spectral acceleration ratio $S_a(T_1)/S_a(T_U)$ on the factor α_U is resulted from its influence on the values of α_{U1} and $\alpha_{U\max}$, as demonstrated in Eqs. (3.15) and (3.17). In the case that the ASCE 7 design spectrum is adopted, the spectral acceleration ratio $S_a(T_1)/S_a(T_U)$ can be determined by the period ratio T_U/T_S, as shown in Eq. (A.19) of Appendix A. Therefore, the effect of the spectral acceleration ratio

$S_a(T_1)/S_a(T_U)$ on values of α_{U1} and $\alpha_{U\max}$ are both represented by the effect of the period ratio T_U/T_S when the ASCE 7 design spectrum is adopted, as shown in Eqs. (3.15) and (3.17).

To provide equations to evaluate values of α_{U1} and $\alpha_{U\max}$ based on the NBCC 2010 spectrum, a relationship between the value of α_{U1} ($\alpha_{U\max}$) and the spectral acceleration ratio $S_a(T_1)/S_a(T_U)$ needs to be investigated at first. By setting $T_1=[(N_U+N_L)/(N_U+0.12N_L)]^{0.5}T_U$ and $T_1=1.30(R_m)^{-0.059}T_U$ in Eqs.(3.15) and (3.17), respectively, and then by substituting Eq. (A.19) of Appendix A into Eqs. (3.15) and (3.17), respectively, the relationship between the value of α_{U1} ($\alpha_{U\max}$) and the spectral acceleration ratio $S_a(T_1)/S_a(T_U)$ can be obtained as follows:

$$\alpha_{U1}=\begin{cases}\alpha_{U11} & \text{if } \dfrac{S_a\left[\sqrt{\dfrac{N_U+N_L}{N_U+0.12N_L}}T_U\right]}{S_a(T_U)}=\sqrt{\dfrac{N_U+0.12N_L}{N_U+N_L}}\\ \alpha_{U12}\left\{\dfrac{S_a\left[\sqrt{\dfrac{N_U+N_L}{N_U+0.12N_L}}T_U\right]}{S_a(T_U)}\right\}^{-x_3} & \text{if } \sqrt{\dfrac{N_U+0.12N_L}{N_U+N_L}}<\dfrac{S_a\left[\sqrt{\dfrac{N_U+N_L}{N_U+0.12N_L}}T_U\right]}{S_a(T_U)}<1\\ \alpha_{U12} & \text{if } \dfrac{S_a\left[\sqrt{\dfrac{N_U+N_L}{N_U+0.12N_L}}T_U\right]}{S_a(T_U)}=1\end{cases} \quad (5.2)$$

$$\alpha_{U\max}=\begin{cases}\alpha_{U\max 1} & \text{if } \dfrac{S_a\left[1.30\left(R_m\right)^{-0.059}T_U\right]}{S_a(T_U)}=0.769\left(R_m\right)^{0.059}\\ \alpha_{U\max 2}\left\{\dfrac{S_a\left[1.30\left(R_m\right)^{-0.059}T_U\right]}{S_a(T_U)}\right\}^{-x_4} & \text{if } 0.769\left(R_m\right)^{0.059}<\dfrac{S_a\left[1.30\left(R_m\right)^{-0.059}T_U\right]}{S_a(T_U)}<1\\ \alpha_{U\max 2} & \text{if } \dfrac{S_a\left[1.30\left(R_m\right)^{-0.059}T_U\right]}{S_a(T_U)}=1\end{cases} \quad (5.3)$$

As shown in Eqs. (5.2) and (5.3), values of α_{U1} and $\alpha_{U\max}$ proposed based on the ASCE 7 design spectrum only consider the cases that the spectral acceleration $S_a(T_1)/S_a(T_U)$ lies between the value of the ratio T_U/T_1 and unity, where $T_1=[(N_U+N_L)/(N_U+0.12N_L)]^{0.5}T_U$ and $T_1=1.30(R_m)^{-0.059}T_U$ in Eqs. (5.2) and (5.3), respectively. However, the spectral acceleration ratio $S_a(T_1)/S_a(T_U)$ evaluated based on the NBCC 2010 site-specific spectrum is much different from that based on the ASCE 7 design spectrum. Take cities of Vancouver, Montreal and Halifax as examples, and let the period ratio T_1/T_U=1.5. From Figure 5.3, it is found for given values of T_1/T_U, the spectral acceleration ratio $S_a(T_1)/S_a(T_U)$ evaluated based on the ASCE 7 design spectrum lies between the value of the ratio T_U/T_1 (0.67 for this case)

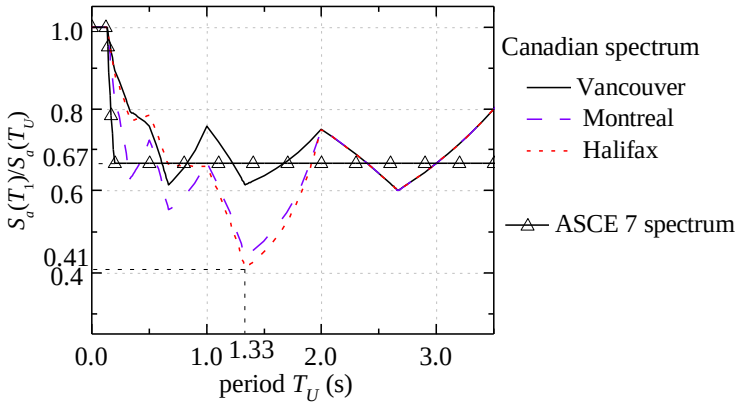

Figure 5.3: Comparison of spectral acceleration ratio $S_a(T_1)/S_a(T_U)$ by using different design spectra (T_1/T_U=1.5)

and unity. For the reason of comparison, set the transition period T_S to be 0.2 second to ensure the ASCE 7 and NBCC 2010 spectra have the same constant acceleration segment, as shown in Figures 1.4 and 5.2 (a). Nevertheless, when the NBCC 2010 spectrum is adopted, the value of spectral acceleration ratio $S_a(T_1)/S_a(T_U)$ is dependent not only on the period of the upper structure T_U but also on the shape of the site-specific spectrum. Since shapes of the spectra associated with different cities are different, the spectral ratios $S_a(T_1)/S_a(T_U)$ for different cities are consequently different. The ratio $S_a(T_1)/S_a(T_U)$ may be much smaller than T_U/T_1 (0.67 for this case). For example, when adopting the spectrum of Halifax, the ratio $S_a(T_1)/S_a(T_U)$ can be as low as 0.41 when the period T_U=1.33 second, as shown in Figure 5.3.

The difference of the spectrum acceleration ratio $S_a(T_1)/S_a(T_U)$ between the two standards is resulted primarily from the difference between the constant velocity range in the ASCE 7 design spectrum and the linear interpolation range in the NBCC 2010 spectrum. In the ASCE 7 design spectrum, the spectral acceleration ratio $S_a(T_1)/S_a(T_U)$ reaches the minimum value when both periods T_1 and T_U are located in the constant velocity range, as shown in Figure 1.4. Since the spectral acceleration is proportional to the reciprocal of the period in the constant velocity range, the minimum spectral acceleration ratio $S_a(T_1)/S_a(T_U)$ is equal to the reciprocal of T_1/T_U, i.e., $S_a(T_1)/S_a(T_U)=T_U/T_1$, as shown in Figure 5.3. However, the spectral acceleration of the NBCC 2010 spectrum is linearly interpolated by the value of the period rather than proportional to the reciprocal of the period when the period is greater than 0.2 second, as shown in Figure 5.2 (a). Therefore, the fluctuation of the spectral acceleration ratio $S_a(T_1)/S_a(T_U)$ with the period T_U can be significant, and the magnitude of ratio $S_a(T_1)/S_a(T_U)$ may even be less than that of T_U/T_1, as shown in Figure 5.3.

Since the spectral acceleration ratio $S_a(T_1)/S_a(T_U)$ evaluated based on the NBCC 2010 spectrum can be less than the ratio T_U/T_1, Eqs. (5.2) and (5.3) may not be applicable since the ratio $S_a(T_1)/S_a(T_U)$ in these two equations is limited between T_U/T_1 and unity. In this study, the power functions used in Eqs.(5.2) and (5.3) are still used for the cases where the magnitude of the $S_a(T_1)/S_a(T_U)$ is less than the value of period ratio T_U/T_1. The validity of using the power function for such cases can be demonstrated by the following example. Take the combined framing systems with N_L=5, N_U=3 and r_m=2, which results in the simplified 2DOF model having the overall mass ratio R_m=3.3 and the minimum overall stiffness ratio R_{kU1}=2.32 based on Eqs. (3.6) and (3.22), respectively. In accordance with Eq. (A.8) of Appendix A, it is calculated that the period ratio T_1/T_U=1.5 for the simplified 2DOF model with R_m=3.3 and R_k=R_{kU1}=2.32. By adopting the spectrum of Halifax shown in Figure 5.2 (a) and assigning different values for the period T_U, the calculated spectral ratio $S_a(T_1)/S_a(T_U)$ can be as low as 0.41, which is considerably less than the value of T_U/T_1 (0.67 for this case) , as shown in Figure 5.3. Meanwhile, the shear-force-amplification factor of the upper structure α_U associated with this 2DOF model can be derived from the elastic modal response spectrum analysis (Chopra, 2007). Shown in Figure 5.4 are the relationships between the calculated spectral ratio $S_a(T_1)/S_a(T_U)$ and the factor α_U evaluated based on the elastic modal response spectrum analysis (marked as "MRS" in Figure 5.4) and Eq. (5.2). Values of α_{U11} and α_{U12} and the exponent x_3 of the power function in Eq.(5.2) are determined from the values of factors α_{U1} at $S_a(T_1)/S_a(T_U)$=T_U/T_1=0.67 and $S_a(T_1)/S_a(T_U)$=1. As shown in Figure 5.4, although the power function in Eq. (5.2) is derived based on $T_U/T_1 \le S_a(T_1)/S_a(T_U) \le 1$, the power function is applicable for the case where $S_a(T_1)/S_a(T_U) < T_U/T_1$. The fact that the power function in Eq.(5.2) or (5.3) is applicable for the case where $S_a(T_1)/S_a(T_U)$)$<T_U/T_1$ is further justified in section 5.3.5, in which errors of the shear-force-amplification factor of the upper structure α_U obtained from the proposed method with use of Eqs. (5.2) and (5.3) are discussed.

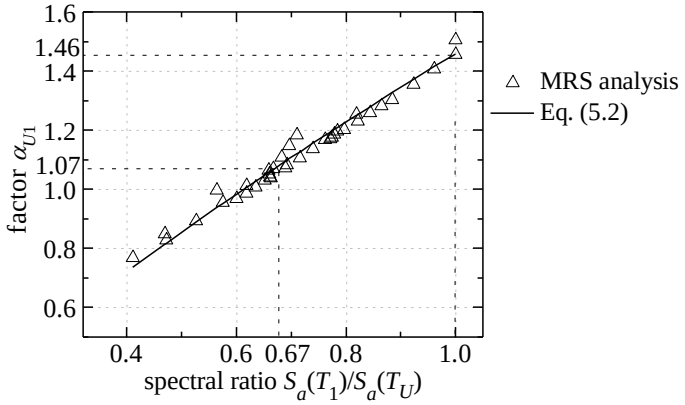

Figure 5.4: Effect of spectral acceleration ratio $S_a(T_1)/S_a(T_U)$ on the factor α_U (T_1/T_U=1.5)

With the justification of that the power functions in Eq. (5.2) or (5.3) can be applied for the case where the spectral acceleration $S_a(T_1)/S_a(T_U)<T_U/T_1$, set $T_1=[(N_U+N_L)/(N_U+0.12N_L)]^{0.5}T_U$ and $T_1=1.30(R_m)^{-0.059}T_U$ in Eqs. (5.2) and (5.3), respectively. Then, considering that $S_a(T_1)/S_a(T_U)=1$ when the period T_1 is not greater than 0.2 second, Eqs. (5.2) and (5.3) can be rewritten as Eqs. (5.4) and (5.5), respectively:

$$\alpha_{U1}=\begin{cases}\alpha_{U12}\left\{\dfrac{S_a\left[\sqrt{\dfrac{N_U+N_L}{N_U+0.12N_L}}T_U\right]}{S_a(T_U)}\right\}^{-x_3} & \text{if } \sqrt{\dfrac{N_U+N_L}{N_U+0.12N_L}}T_U>0.2\text{ s}\\ \alpha_{U12} & \text{if } \sqrt{\dfrac{N_U+N_L}{N_U+0.12N_L}}T_U\le 0.2\text{ s}\end{cases} \tag{5.4}$$

$$\alpha_{U\max}=\begin{cases}\alpha_{U\max 2}\left\{\dfrac{S_a\left[1.30\left(R_m\right)^{-0.059}T_U\right]}{S_a(T_U)}\right\}^{-x_4} & \text{if } 1.30\left(R_m\right)^{-0.059}T_U>0.2\text{ s}\\ \alpha_{U\max 2} & \text{if } 1.30\left(R_m\right)^{-0.059}T_U\le 0.2\text{ s}\end{cases} \tag{5.5}$$

Eqs. (5.4) and (5.5) calculate α_{U1} and $\alpha_{U\max}$ based on the NBCC 2010 spectrum. The expressions of α_{U12} and the exponent x_3 of the power function in Eq. (5.4) are the same as those based on the ASCE 7. In addition, minor modifications are made for evaluating $\alpha_{U\max1}$ and $\alpha_{U\max2}$, which further determines the exponent x_4 of the power function by Eq. (3.18). Recall that in the proposed approach based on the ASCE 7 design spectrum, equations to calculate $\alpha_{U\max1}$ and $\alpha_{U\max2}$ are Eqs.(3.19) and (3.20) of section 3.3.3, respectively. However, Eqs. (3.19) and (3.20) are not applicable if the NBCC 2010 design spectrum if adopted. In such case, values of $\alpha_{U\max1}$ and $\alpha_{U\max2}$ to be used in Eq. (5.5) can be obtained from Table 5.1 rather than from Eqs. (3.19) and (3.20). The values of $\alpha_{U\max1}$ and $\alpha_{U\max2}$ listed in Table 5.1 are calculated based on the elastic modal response spectrum analysis of the MDOF model.

In the proposed approach based on the ASCE 7 design spectrum, Eqs. (3.19) and (3.20) are empirically obtained based on the elastic modal response spectrum analysis of the simplified 2DOF model. As discussed in section 3.3.4 and Appendix D.1, the simplified 2DOF model yields to an overestimation of values of $\alpha_{U\max}$, which subsequently results in an overestimation, i.e., positive error, on the factor α_U. Such positive error may be acceptable because it is conservative when the ASCE 7 design spectrum is adopted. However, if the NBCC site-specific spectrum is used, the overestimation on $\alpha_{U\max}$ associated with the simplified 2DOF model can be substantial, as discussed in Appendix E.1.

Table 5.1: Values of $\alpha_{U\max1}$ and $\alpha_{U\max2}$ for NBCC 2010 design spectrum

N_L	N_U	r_m=1		r_m =2		r_m =3	
		$\alpha_{U\max1}$	$\alpha_{U\max2}$	$\alpha_{U\max1}$	$\alpha_{U\max2}$	$\alpha_{U\max1}$	$\alpha_{U\max2}$
1	1	1.070	1.270	1.240	1.479	1.410	1.688
1	2	1.015	1.135	1.070	1.270	1.155	1.375
1	3	1.010	1.100	1.040	1.193	1.080	1.270
1	4	1.008	1.100	1.015	1.135	1.060	1.230
1	5	1.006	1.100	1.012	1.100	1.018	1.170
1	6	1.005	1.100	1.010	1.100	1.015	1.135
1	7	1.004	1.100	1.009	1.100	1.013	1.110
1	8	1.004	1.100	1.008	1.100	1.011	1.100
1	9	1.003	1.100	1.007	1.100	1.010	1.100
2	1	1.240	1.479	1.580	1.897	1.870	2.180
2	2	1.070	1.270	1.240	1.479	1.410	1.688
2	3	1.020	1.193	1.127	1.340	1.240	1.479
2	4	1.015	1.135	1.070	1.270	1.155	1.375
2	5	1.012	1.100	1.036	1.228	1.104	1.312
2	6	1.010	1.100	1.020	1.193	1.070	1.270
2	7	1.009	1.100	1.017	1.140	1.046	1.160
2	8	0.900	1.000	1.015	1.080	1.028	1.130
3	1	1.410	1.688	1.870	2.180	2.215	2.503
3	2	1.155	1.375	1.410	1.688	1.665	2.002
3	3	1.020	1.180	1.240	1.479	1.410	1.688
3	4	0.990	1.127	1.155	1.375	1.283	1.531
3	5	0.965	1.080	1.050	1.198	1.123	1.291
3	6	1.015	1.135	1.070	1.270	1.155	1.375
3	7	0.900	1.030	1.046	1.180	1.119	1.330
4	1	1.580	1.897	2.110	2.400	2.470	2.780
4	2	1.240	1.479	1.580	1.897	1.870	2.180
4	3	1.050	1.280	1.353	1.618	1.580	1.897
4	4	1.010	1.240	1.151	1.350	1.410	1.688
4	5	0.990	1.240	1.142	1.395	1.232	1.520
4	6	0.940	1.100	1.043	1.230	1.141	1.479
5	1	1.735	2.063	2.310	2.600	2.635	3.013
5	2	1.325	1.584	1.735	2.063	2.054	2.347
5	3	1.082	1.274	1.467	1.758	1.735	2.063
5	4	1.040	1.285	1.224	1.436	1.538	1.845
5	5	1.000	1.220	1.198	1.479	1.293	1.550
6	1	1.870	2.180	2.470	2.780	2.764	3.200
6	2	1.410	1.688	1.870	2.180	2.215	2.503
6	3	1.102	1.320	1.580	1.897	1.870	2.180

Note: Values of $\alpha_{U\max1}$ and $\alpha_{U\max2}$ not listed can be obtained from linear interpolation by the magnitude of r_m.

Table 5.1: Values of $\alpha_{U\max1}$ and $\alpha_{U\max2}$ for NBCC 2010 design spectrum (continued)

N_L	N_U	r_m=1		r_m =2		r_m =3	
		$\alpha_{U\max1}$	$\alpha_{U\max2}$	$\alpha_{U\max1}$	$\alpha_{U\max2}$	$\alpha_{U\max1}$	$\alpha_{U\max2}$
6	4	1.050	1.260	1.295	1.540	1.665	2.002
7	1	1.995	2.293	2.590	2.940	2.905	3.343
7	2	1.495	1.793	1.995	2.293	2.354	2.647
7	3	1.152	1.365	1.688	2.022	1.995	2.293
8	1	2.110	2.400	2.670	3.080	3.046	3.443
8	2	1.580	1.897	2.110	2.400	2.470	2.780
9	1	2.215	2.503	2.764	3.200	3.187	3.544

Note: Values of $\alpha_{U\max1}$ and $\alpha_{U\max2}$ not listed can be obtained from linear interpolation by the magnitude of r_m.

From Tables E.1 ~ E.6 in Appendix E.1 and Table D.1 in Appendix D.1, it is seen the errors induced by the simplified 2DOF model are related to the shape of the design spectrum. For example, when N_L=4 and N_U=6, the overestimation of $\alpha_{U\max}$ associated with the simplified 2DOF model can be as large as 35.0% if the spectrum of Halifax shown in Figure 5.2 (a) is selected; however, the overestimation is 21.6% if the ASCE 7 design spectrum shown in Figure 1.4 is adopted. Therefore, it is recommended values of $\alpha_{U\max1}$ and $\alpha_{U\max2}$ in Eq. (5.5) be obtained from the MDOF model rather than the simplified 2DOF model. It is noted that if the ASCE 7 design spectrum is adopted, values of $\alpha_{U\max1}$ and $\alpha_{U\max2}$ provided in Table 5.1 can result in a more accurate value of α_U as well. Consequently, as an alternative of Eqs. (3.19) and (3.20), Table 5.1 can be used to determine $\alpha_{U\max1}$ and $\alpha_{U\max2}$ in (3.17) and it will result in a more accurate value of α_U compared to Eqs. (3.19) and (3.20).

Considering that the NBCC 2010 specifies various spectral shapes for different cities in Canada, it would be cumbersome and impractical to compute $\alpha_{U\max1}$ and $\alpha_{U\max2}$ for all possible different spectral shapes. In fact, values of $\alpha_{U\max1}$ and $\alpha_{U\max2}$ shown in Table 5.1 are calculated based on the ASCE 7 design spectrum. By setting T_U/T_S=1 and T_U/T_S=0.769$(R_m)^{0.059}$, the maximum values of α_U for $r_{kU2}\leq r_k\leq r_{kU3}$ computed based on the elastic modal response spectrum analysis of the MDOF model, are set to be $\alpha_{U\max1}$ and $\alpha_{U\max2}$, respectively, as shown in Table 5.1. The effects of the different spectral shapes on values of $\alpha_{U\max}$ are accounted for in Eq. (5.5).

Note that not all the values of $\alpha_{U\max1}$ and $\alpha_{U\max2}$ listed in Table 5.1 are obtained directly from the elastic modal response spectrum of the MODF model. Adjustments have made on the results from the elastic modal response spectrum analysis of the MDOF model to ensure errors of the factor α_U are within an acceptable limit, which is discussed in section 5.3.5.

Overall two-stage stiffness ratio of the upper structure R_{kU2stg}

When the NBCC 2010 site-specific spectrum is to be used, modifications are needed on the overall two-stage stiffness ratio of the upper structure R_{kU2stg}. In such case, the ratio R_{kU2stg} can be determined by the following equation rather than Eq. (3.9):

$$R_{kU2stg} = \begin{cases} 0.907R_m + 9.78 & R_m \le 1.213 \\ 11.029R_m - 2.5 & R_m > 1.213 \end{cases} \tag{5.6}$$

Compared to Eq. (3.9), the value of the ratio R_{kU2stg} determined by Eq.(5.6) is increased for the case of which the overall mass ratio R_m is less than 1.213. Such increase is resulted from the modification of the determination of the ratio R_{kU2stg}. Ideally, the ratio R_{kU2stg} should be determined based on the requirement that the first mode period of the simplified 2DOF model T_1 is equivalent to the period of the upper structure T_U, i.e., $T_1 = T_U$. Considering the fact that the period ratio T_1/T_U is always greater than unity, as discussed in Appendix B.1.3, the ratio R_{kU2stg} of Eq. (3.9) is determined based on the requirement that the period ratio $T_1/T_U \le 1.1$, as discussed in Appendix C.2. The requirement $T_1/T_U \le 1.1$ is the approximation to the requirement $T_1 = T_U$ and it is appropriate if the ASCE 7 design spectrum is adopted. This is due to the fact the requirement $T_1/T_U \le 1.1$ results in the spectral acceleration ratio $S_a(T_1)/S_a(T_U)$ lies in the range between 0.91 and unity if the ASCE 7 design spectrum is adopted, which is quite close to unity. However, when the NBCC 2010 site-specific spectrum is adopted, the resulted ratio $S_a(T_1)/S_a(T_U)$ may not be close to unity. For example, by setting T_U=1.818 second and T_1/T_U=1.1, it is calculated that $S_a(T_1)$=0.027 g and $S_a(T_U)$=0.0376 g if the spectrum of Halifax is adopted, which then results in the spectrum ratio $S_a(T_1)/S_a(T_U)$ be as low as 0.719. Therefore, to account for such great variation of the spectrum acceleration $S_a(T_1)/S_a(T_U)$, the requirement on the period ratio T_1/T_U needs to be more stringent if the NBCC 2010 spectrum is adopted. As discussed in detail Appendix E.2, it is selected that $T_1/T_U \le 1.05$ to be the condition to be satisfied to determine the overall two-stage stiffness ratio of the upper structure R_{kU2stg}. Consequently, the equation to determine the R_{kU2stg} that is compatible with the NBCC 2010 spectrum is presented in Eq. (5.6).

5.3.3 Formulation of design equation III: stiffness evaluation

In accordance with the NBCC 2010 spectrum shown in Figure 5.2 (a), the spectral acceleration is evaluated as follows:

$$S_a(T)=\begin{cases} S_a(0.2) & T \le 0.2 \text{ s} \\ S_a(0.2)+\dfrac{S_a(0.5)-S_a(0.2)}{0.3}(T-0.2) & 0.2 \text{ s} < T \le 0.5 \text{ s} \\ S_a(0.5)+\dfrac{S_a(1.0)-S_a(0.5)}{0.5}(T-0.5) & 0.5 \text{ s} < T \le 1.0 \text{ s} \\ S_a(1.0)+\left[S_a(2.0)-S_a(1.0)\right](T-1.0) & 1.0 \text{ s} < T \le 2.0 \text{ s} \\ S_a(2.0)-0.25S_a(2.0)(T-2.0) & 2.0 \text{ s} < T \le 4.0 \text{ s} \\ 0.5S_a(2.0) & T > 4.0 \text{ s} \end{cases} \tag{5.7}$$

where $S_a(0.2)$, $S_a(0.5)$, $S_a(1.0)$ and $S_a(2.0)$ denote the spectral values of 0.2, 0.5, 1.0 and 2.0 seconds, respectively. Having the spectral values shown in Eqs. (5.1), (5.4) and (5.5) evaluated from Eq.(5.7) and following the same procedure discussed in section 3.4, it is anticipated that the analytical solutions corresponding to the critical storey-stiffnesses of the upper structure $k_{\alpha U1}$, $k_{\alpha U\max}$ and $k_{\alpha U2stg}$ can be derived from Eq. (5.1). If the ASCE 7 design spectrum is adopted and the spectral values are evaluated from (3.24), the analytical solutions of $k_{\alpha U1}$, $k_{\alpha U\max}$ and $k_{\alpha U2stg}$ can be derived from the governing design equation (Eq.(3.4)), as presented in Eqs. (3.33) ~ (3.35), respectively. However, because the NBCC 2010 specifies a linear relationship between the spectral acceleration $S_a(T)$ and the period T as shown in Eq.(5.7), the analytical solutions of $k_{\alpha U1}$, $k_{\alpha U\max}$ and $k_{\alpha U2stg}$ cannot be obtained directly from the governing design equation, i.e., Eq. (5.1). The reason of that is discussed in Appendix E.3.

To facilitate that the analytical solution of $k_{\alpha U1}$, $k_{\alpha U\max}$ and $k_{\alpha U2stg}$ can be derived from Eq.(5.1), the spectral acceleration $S_a(T)$ needs to be expressed by either a power or an exponential function of the period T. If the power function is adopted to approximate the linear segments of the NBCC 2010 spectrum, the spectral acceleration $S_a(T)$ is expressed as

$$S_a(T)=\begin{cases} S_a(0.2) & T \le T_S' \\ A_1(T)^{\tau_1} & T_S' < T \le 0.5 \text{ s} \\ A_2(T)^{\tau_2} & 0.5 \text{ s} < T \le 1.0 \text{ s} \\ A_3(T)^{\tau_3} & 1.0 \text{ s} < T \le 2.0 \text{ s} \\ A_4(T)^{\tau_4} & 2.0 \text{ s} < T \le 4.0 \text{ s} \end{cases} \tag{5.8}$$

where T_S', A_i and τ_i are curve fitting parameters. For the case that the exponential function is adopted, the corresponding spectral acceleration $S_a(T)$ is then expressed as

$$S_a(T) = \begin{cases} S_a(0.2) & T \le T_S' \\ A_1 \exp(\tau_1 T) & T_S' < T \le 0.5 \text{ s} \\ A_2 \exp(\tau_2 T) & 0.5 \text{ s} < T \le 1.0 \text{ s} \\ A_3 \exp(\tau_3 T) & 1.0 \text{ s} < T \le 2.0 \text{ s} \\ A_4 \exp(\tau_4 T) & 2.0 \text{ s} < T \le 4.0 \text{ s} \end{cases} \quad (5.9)$$

where exp(.) represents the exponential function, and T_S', A_i and τ_i are curve fitting parameters. Considering that the maximum single storey-period of the upper structure T_{singU} is 0.31 second and the maximum number of storey of the upper structure N_U=9, as stated in section 1.3.2, the resulted maximum period of the upper structure T_U=0.31/0.165=1.88 second. In addition, since the maximum period ratio T_1/T_U is less than 2.0 as discussed in Appendix E.3.1, the corresponding maximum period T_1 is less than 3.76 second (1.88×2=3.76). Therefore, the spectrum approximation is needed for the case that the period is less than 4.0 second, as shown in Eqs. (5.8) and (5.9).

With adopting either the power or exponential function to approximate the NBCC 2010 spectrum, analytical solutions corresponding to the critical storey-stiffnesses $k_{\alpha U1}$, $k_{\alpha U\max}$ and $k_{\alpha U2stg}$ can be derived. If the power function shown in Eq. (5.8) is adopted, the solutions are presented in Eqs.(E.8) ~ (E.10) of Appendix E.3.1. For the case that the exponential function shown in Eq. (5.9) is adopted, the corresponding solutions are shown in Eqs. (E.15) ~ (E.17) of Appendix E.3.2. However, errors associated with the values of the spectrum will be resulted from the approximation of the NBCC 2010 spectrum with either the power or exponential function, which will consequently result in errors on the critical storey-stiffnesses $k_{\alpha U1}$, $k_{\alpha U\max}$ and $k_{\alpha U2stg}$. To ensure the errors of the critical storey-stiffnesses are within an acceptable limit, it is critical to select an appropriate approximate function and curve fitting technique to simulate the linear segments of the NBCC 2010 spectrum in the specified region. For the power and exponential functions shown in Eqs. (5.8) and (5.9), respectively, two different techniques were provided in this study to determine the curving fitting parameters T_S', A_i and τ_i, which are discussed in Appendix E.4. Therefore, as shown in Table E.9 of Appendix E.4, a total of four types of curve fitting schemes are available. As to which curve fitting scheme to be selected, engineers can make the decision based on the acceptable limit of the errors of the critical storey-stiffnesses associated with each scheme. Errors of the critical storey-stiffnesses associated with each curve fitting scheme are discussed in section 5.3.5.

Finally, considering that the single storey-periods T_{singU} and T_{singL} are not greater than 0.31 second as discussed in section 1.3.2, the corresponding k_U and k_L should satisfy following requirements:

$$k_U \ge 41.62\pi^2 m_U \quad (5.10)$$

$$k_L \geq 41.62\pi^2 m_U \tag{5.11}$$

5.3.4 Design procedure

Similar to that discussed in section 3.5, the spectral acceleration specified in the NBCC 2010 (NBCC, 2010) should also be scaled up by the factor C_{NE}, as shown in Eq. (3.42), to satisfy the 90% NE probability. The scaled up factor C_{NE} is still taken as 2.61. With such adjusted spectral acceleration and considering the modifications that have been made in sections 5.3.1 ~ 5.3.3, the procedure to evaluate feasible storey-stiffnesses k_U and k_L based on the NBCC 2010 can be carried out as follows:

Step 1: Evaluate the effective seismic weight distribution (m_L and m_U); calculate the storey-mass ratio r_m (r_m=m_L /m_U) and the overall mass ratio R_m as per Eq.(3.6).

Step 2: Determine critical overall stiffness ratios R_{kU1}, R_{kU2}, R_{kU3} and R_{kU2stg} according to Eqs.(3.22), (3.10), (3.23) and (5.6), respectively.

Step 3: Compute values of α_{U11} and α_{U12} based on Table 3.1 and the exponent x_3 in accordance with Eq. (3.16) if R_{kU1}<R_{kU2}; calculate values of $\alpha_{U\max 1}$ and $\alpha_{U\max 2}$ in accordance with Table 5.1 and evaluate the exponent x_4 in accordance with Eq. (3.18); and evaluate the value of α_{U2stg} by Eq.(3.21).

Step 4: Select either the power or exponential function to approximate the NBCC 2010 spectrum; if the power function is selected, calculate the critical storey-stiffnesses $k_{\alpha U1}$, $k_{\alpha Umax}$ and $k_{\alpha U2stg}$ based on Eqs. (E.8) ~ (E.10), respectively, or if the exponential function is selected, calculate $k_{\alpha U1}$, $k_{\alpha Umax}$ and $k_{\alpha U2stg}$ as per Eqs. (E.15) ~ (E.17), respectively. Then, evaluate the critical storey-stiffnesses k_{Umax} and k_{Umin} based on Eqs. (3.31) and (3.32), respectively. Note that if R_{kU1}≥R_{kU2}, k_{Umax} and k_{Umin} are determined only based on $k_{\alpha U\max}$ and $k_{\alpha U2stg}$, as shown in Eqs. (3.31) and (3.32); therefore, $k_{\alpha U1}$, and α_{U11} and α_{U12} that are used to compute $k_{\alpha U1}$ based on Eq. (E.8) or (E.15) are not required to be calculated.

Step 5: Select the feasible storey-stiffness of upper structure k_U based on the value of k_{Umin} computed in step 4. Note that the value of k_U also needs to satisfy Eq. (5.10) .

Step 6: With the value of k_U selected in step 5, calculate the period of the upper structures T_U from Eq.(3.8); then, compute values of α_{U1} and $\alpha_{U\max}$ based on Eqs. (5.4) and (5.5), respectively; finally, the corresponding value of the storey-stiffness of the lower structure k_L can be selected to satisfy Eqs. (3.26) ~ (3.29) and as well as Eqs. (5.11) and (3.41). Note that α_{U1}, which is the value of α_U when R_k=R_{kU1}, is required to be calculated only if R_{kU1}<R_{kU2}. If R_{kU1}≥R_{kU2}, the value of α_U when R_k=R_{kU1} should be computed in accordance with the magnitude of R_{kU1} through Eqs. (3.12) (b) ~ (d). In addition, when computing values of α_{U1} and α_{Umax}, the spectral values in Eqs. (5.4) and (5.5) are

suggested directly be determined from the NBCC 2010 spectrum rather than the one approximated by either the power or exponential function for the reason of accuracy.

5.3.5 Error analysis

Errors associated with the proposed procedure to evaluate the storey-stiffnesses of the lower and upper structures for the Canadian application are resulted from the following two aspects: (a) the proposed equations of evaluating the factor α_U; and (b) the approximation of the NBCC 2010 spectrum with either the power or exponential function. In general, the design procedure provided in section 5.3.4 can be categorized into two phases. Phase I includes Step 1 to Step 5 in which the feasible range of the storey-stiffness of the upper structure k_U is determined. A critical step in Phase I is to determine the critical storey-stiffnesses $k_{\alpha U1}$, $k_{\alpha Umax}$ and $k_{\alpha U2stg}$ from either Eqs. (E.8) ~ (E.10) or Eqs. (E.15) ~ (E.17) depending on whether the power or exponential function is selected to approximate the NBCC 2010 spectrum. By observing Eq. (5.1), which is the governing equation from which Eqs. (E.8) ~ (E.10) or Eqs. (E.15) ~ (E.17) are obtained, it is found that errors of the critical storey-stiffnesses can be characterized by the error associated with the product of the factor α_U and the spectrum value $S_a(T_U)$, i.e., $\alpha_U S_a(T_U)$. Therefore, the error associated with $\alpha_U S_a(T_U)$ is the primary concern of Phase I as it is influenced by both errors of computing the shear-force-amplification factor α_U and approximation of NBCC 2010 spectrum.

Phase II of the design procedure, stated as Step 6 in section 5.3.4, is to determine the required storey-stiffness of the lower structure k_L based on the given storey-stiffness of the upper structure k_U. With the given storey-stiffness of the upper structure k_U, the period of the upper structure T_U can be uniquely determined, and the spectrum values in Eqs.(5.4) and (5.5) can be obtained directly from the NBCC 2010 spectrum, i.e., by Eq.(5.7), without approximation. Thus, errors associated with Phase II are induced only by the procedure of computing the factor α_U.

Error associated with the procedure of computing shear-force-amplification factor α_U

The results of shear-force-amplification factor α_U computed by the Eq. (3.12) with use of the modifications discussed in section 5.3.2 are compared to that obtained from the elastic modal response spectrum analysis of the MDOF model with CQC rule of combining the peak modal responses (Chopra, 2007). By considering all possible combinations of r_m, r_k, T_{singU} and T_{singL} that are presented in section 1.3.2, the maximum and minimum errors of the shear-force-amplification factor obtained from Eq. (3.12) are listed in Table 5.2 and Table 5.3, respectively. The positive and negative errors signify that the proposed approach overestimates and underestimates the shear-force-amplification factor α_U, respectively. From Table 5.2 and Table 5.3, it is seen errors associated with

the proposed approach of computing the factor α_U based on the NBCC 2010 spectrum are in the range of -2.8% to 33.5%, which are comparable to errors of the proposed approach based on the ASCE 7 spectrum as discussed in section 3.3.4.

It is found that errors of proposed approach of computing the factor α_U are related not only to values of design parameters r_m, r_k, T_{singU} and T_{singL}, but also to the design spectral shape. Since the ASCE 7 (ASCE, 2010) adopts the Newmark spectrum, the effect of the spectral shape is characterized by the ratio T_{singU}/T_S, as discussed in section 3.3.4. However, considering the NBCC 2010 (NBCC, 2010) specifies different spectral shapes for different cities in Canada, as shown in Figure 5.2 (b), the errors of the factor α_U computed by the proposed approach may be different for different cities. The spectral shapes of Vancouver, Montreal and Halifax, which are representative seismic cities in Canada, are selected to check the error of the factor α_U computed by the proposed approach. The

Table 5.2: Maximum errors of the proposed method on factor α_U (NBCC 2010 spectrum)

N_L \ N_U	1	2	3	4	5	6	7	8	9
1	13.7%	15.7%	20.7%	23.6%	24.4%	25.7%	28.2%	27.9%	28.3%
2	17.0%	30.4%	24.0%	27.3%	26.7%	29.4%	31.8%	28.5%	N/A
3	18.9%	29.6%	27.8%	28.4%	28.7%	32.9%	25.7%	N/A	N/A
4	19.5%	27.4%	25.2%	31.6%	34.1%	24.6%	N/A	N/A	N/A
5	20.6%	25.5%	26.1%	29.7%	33.5%	N/A	N/A	N/A	N/A
6	19.7%	24.4%	25.7%	28.4%	N/A	N/A	N/A	N/A	N/A
7	10.9%	23.8%	27.2%	N/A	N/A	N/A	N/A	N/A	N/A
8	10.2%	23.7%	N/A	N/A	N/A	N/A	N/A	N/A	N/A
9	10.5%	N/A	N/A	N/A	N/A	N/A	N/A	N/A	N/A

Note: N/A denotes the proposed approach is not applicable for the combination of the lower and upper structures.

Table 5.3: Minimum errors of the proposed method on factor α_U (NBCC 2010 spectrum)

N_L \ N_U	1	2	3	4	5	6	7	8	9
1	-0.4%	2.7%	5.7%	6.6%	5.6%	11.4%	9.6%	11.8%	13.1%
2	6.7%	2.1%	4.6%	3.6%	2.0%	3.2%	3.3%	4.9%	N/A
3	5.7%	2.6%	0.5%	0.7%	0.1%	4.0%	-2.8%	N/A	N/A
4	5.4%	8.6%	2.5%	2.2%	-1.6%	-0.9%	N/A	N/A	N/A
5	5.5%	8.8%	0.0%	3.6%	-1.5%	N/A	N/A	N/A	N/A
6	5.6%	7.7%	0.0%	1.6%	N/A	N/A	N/A	N/A	N/A
7	-1.0%	7.9%	0.0%	N/A	N/A	N/A	N/A	N/A	N/A
8	-1.0%	7.5%	N/A	N/A	N/A	N/A	N/A	N/A	N/A
9	-0.9%	N/A	N/A	N/A	N/A	N/A	N/A	N/A	N/A

Note: N/A denotes the proposed approach is not applicable for the combination of the lower and upper structures.

maximum and minimum errors listed in Table 5.2 and Table 5.3 are determined based on the three representative seismic cities. The errors of the factor α_U for each of these three cities are also provided in Tables E.10 ~ E.15 in Appendix E.5.

Finally note the maximum single-storey periods T_{singU} and T_{singL} for the storey combinations of lower and upper structures listed in Table 5.2 and Table 5.3 are limited to be not greater than 0.22 second, which is less than the 0.31 second that is specified by the NBCC 2010 (NBCC, 2010), as discussed in section 1.3.2. The maximum single-storey periods T_{singU} and T_{singL} are extended to be 0.31 second for storey combinations listed in Tables E.10~ E.15 in Appendix E.5. As demonstrated in those tables, a relative large magnitude of negative error may occur for certain storey combinations. For example, when N_L=4 and N_U=5, r_m=3, and T_{singU}=0.3 second, the negative error associated with the factor α_U obtained from the proposed approach can be as low as -5.8% if the spectrum of Montreal is selected, as shown in Table E.13. However, such flexible structures are rare in practices. For most structures, the single-storey periods T_{singU} and T_{singL} are not likely be greater than 0.22 second. In accordance with ASCE 7 (ASCE, 2010), T_{singU} and T_{singL} for most structures are not greater than $1.1T_S$, as discussed in section 1.3.2. By comparing the ASCE 7 and NBCC 2010 spectra shown in Figure 1.4 and Figure 5.2, respectively, it is found the corresponding T_S of the NBCC 2010 spectrum can be set as 0.2 second, i.e. T_S=0.2 s. Consequently, it is reasonable to derive that T_{singU} and T_{singL} for most structure are not likely be greater than 0.22 second based on the NBCC 2010 spectrum, where $0.22=1.1T_S=1.1\times0.2$. As long as that T_{singU} and T_{singL} are not less than 0.22 second, the corresponding errors associated with the proposed approach based on the NBCC 2010 spectrum are considered as acceptable, as shown in Table 5.2 and Table 5.3.

Error associated with $\alpha_U S_a(T_U)$

Computed values of product $\alpha_U S_a(T_U)$ based on proposed approach are compared to corresponding accurate values. When computing the values of the factor α_U and the resulted product $\alpha_U S_a(T_U)$ based on the proposed approach, the spectrum value $S_a(T_U)$ is determined based on the approximation of NBCC 2010 spectrum. On the other hand, for the so-called accurate value of $\alpha_U S_a(T_U)$, the spectral value $S_a(T_U)$ is determined from the NBCC 2010 spectrum rather than the approximation, and the factor α_U is computed based on the modal response spectrum analysis of the MDOF model with the CQC rule of combining the peak modal responses (Chopra, 2007). Apparently, errors of $\alpha_U S_a(T_U)$ evaluated based on the proposed approach is affected by the approximation of the NBCC 2010 spectrum. As to all approximations listed in Table E.9 of Appendix E.4, the maximum and minimum errors of the estimated $\alpha_U S_a(T_U)$ for the three Canadian representative seismic cities, i.e., Vancouver, Montreal and Halifax, are listed in Tables E.16 ~ E.39 of Appendix E.6. The pros and cons for each

approximation are also discussed in Appendix E.6. From such discussion, it is suggested that approximation "EXP-2" listed in Table E.9 provides the most reasonable values of $\alpha_U S_a(T_U)$ from a general aspect.

As to the approximation "EXP-2", the possible maximum and minimum errors of the evalauted $\alpha_U S_a(T_U)$ are listed in Table 5.4 and Table 5.5. For the three Canadian representative seismic cities, the maximum and minimum errors listed in these tables are obtained by considering all possible combinations of r_m, r_k, T_{singU} and T_{singL} as presented in section 1.3.2. It is found that errors associated with the approximation "EXP-2" listed in Table E.9 are in the range of -1.0% and 36.5%, which is comparable to errors of the factor α_U obtained from the proposed approach. Note that the range of -1.0% and 36.5% are obtained based on that the maximum single-storey periods T_{singU} and T_{singL} are not greater than 0.22 second. Considering that 0.31 second is the limit for the maximum single-storey period specified in the NBCC 2010 (NBCC, 2010), errors associated with the single periods to be 0.22 to 0.31 second are listed in Tables E.16 ~ E.39 of Appendix E.6.

Table 5.4: Maximum errors of the estimated $\alpha_U S_a(T_U)$ (NBCC 2010 spectrum, EXP-2)

N_L \ N_U	1	2	3	4	5	6	7	8	9
1	16.5%	18.1%	28.0%	28.6%	32.2%	33.1%	35.5%	34.8%	36.5%
2	18.9%	34.0%	28.7%	30.7%	31.3%	31.9%	34.2%	33.7%	N/A
3	20.8%	32.8%	31.0%	30.7%	31.8%	35.1%	32.8%	N/A	N/A
4	21.8%	30.2%	28.6%	34.9%	37.3%	29.5%	N/A	N/A	N/A
5	23.5%	28.2%	28.7%	32.8%	36.0%	N/A	N/A	N/A	N/A
6	23.2%	27.5%	28.3%	29.7%	N/A	N/A	N/A	N/A	N/A
7	13.4%	26.2%	30.3%	N/A	N/A	N/A	N/A	N/A	N/A
8	13.7%	27.3%	N/A	N/A	N/A	N/A	N/A	N/A	N/A
9	14.8%	N/A	N/A	N/A	N/A	N/A	N/A	N/A	N/A

Note: N/A denotes the proposed approach is not applicable for the combination of the lower and upper structures.

Table 5.5: Minimum errors of the estimated $\alpha_U S_a(T_U)$ (NBCC 2010 spectrum, EXP-2)

N_L \ N_U	1	2	3	4	5	6	7	8	9
1	-0.4%	3.2%	7.8%	8.1%	7.4%	12.5%	16.0%	15.5%	14.3%
2	6.9%	2.1%	4.6%	6.1%	6.2%	6.9%	8.4%	7.1%	N/A
3	6.7%	3.4%	0.5%	0.7%	0.1%	5.0%	0.5%	N/A	N/A
4	6.0%	9.2%	3.5%	2.2%	3.1%	0.7%	0.0%	N/A	N/A
5	5.9%	9.0%	0.0%	3.6%	2.5%	N/A	N/A	N/A	N/A
6	5.8%	8.9%	0.0%	1.6%	N/A	N/A	N/A	N/A	N/A
7	-1.0%	8.8%	0.0%	N/A	N/A	N/A	N/A	N/A	N/A
8	-1.0%	8.7%	N/A	N/A	N/A	N/A	N/A	N/A	N/A
9	-0.9%	N/A	N/A	N/A	N/A	N/A	N/A	N/A	N/A

Note: N/A denotes the proposed approach is not applicable for the combination of the lower and upper structures.

5.4 Seismic loading based on NBCC 2010

5.4.1 Modified ELF procedure

The applicable requirement of the modified ELF procedure to be applied in "appendage-style" building based on NBCC 2010 is the same as that based on ASCE 7 discussed in Chapter 4. However, as the seismic load distribution of the ELF procedure based on NBCC 2010 is different from that based on ASCE 7, a modified ELF procedure for seismic loading of the appendage-style building based on NBCC 2010 is provided in the following.

Seismic load distribution of lower structure

When adopting the ELF procedure to evaluate seismic load of "regular" structures, the NBCC 2010 (NBCC, 2010) specifies a higher mode factor to account for the possible effect of the higher mode on the base shear force obtained from the first mode of vibration. The applicable requirement of the modified ELF procedure in below is proposed based on that the effective mass of the entire building associated with the first mode is not less than 90% of the total mass. Therefore, the higher mode effect on the base shear force is not significant, and the higher mode factor specified in the NBCC 2010 is no need to be accounted for when evaluating the base shear force of the lower structure V_{Lb}. Thus, the base shear force of the lower structure can be calculated based on Eq. (4.1).

Different from that of ASCE 7 (ASCE, 2010), the lateral seismic force distribution along the height of the building specified in the NBCC 2010 (NBCC, 2010), *i.e.*, the lateral seismic force associated with the *i*th-storey F_i, is calculated as

$$F_i = \frac{m_i h_i}{\sum_{j=1}^{N} m_j h_j}\left(V_{Lb} - F_{t,ELF}\right) \tag{5.12}$$

where $F_{t,\,ELF}$ is the specified top storey loading, which is calculated as follows:

$$F_{t,ELF} = \begin{cases} 0 & T_1 \le 0.7\ s \\ 0.07 T_1 V_{Lb} & 0.7\ s < T_1 < 3.6\ s \\ 0.25 V_{Lb} & T_1 \ge 3.6\ s \end{cases} \tag{5.13}$$

where T_1 is still the first mode period of the entire building, which is approximated by Eq.(A.5) of Appendix A.

By comparing Eq. (4.4) to Eq. (5.12), it is seen that ASCE 7 adopts the exponent κ to account for the higher mode effect on the top storey shear force, while NBCC 2010 specifies a top storey loading $F_{t,ELF}$ to account for such effect.

Seismic load distribution of upper appendage

The base shear force of the upper "appendage" can be calculated by Eq. (4.7). However, when Eq.(3.12) was employed to determine the factor α_U, modifications discussed in section 5.3.2 should be considered. The modifications include: (1) values of α_{U1} and $\alpha_{U\max}$ should be calculated through Eqs.(5.4) and (5.5), respectively; (2) values of $\alpha_{U\max 1}$ and $\alpha_{U\max 2}$, which are used to determine the exponent x_4 in Eq. (5.5) from Eq. (3.18), should be obtained from Table 5.1; and (3) the overall two-stage storey stiffness ratio of the upper structure is to be calculated by Eq. (5.6).

5.4.2 Proposed two-stage analysis procedure

The applicable requirement and seismic load distribution of the proposed two-stage analysis procedure based on the NBCC 2010 are the same as those developed based on ASCE 7 and presented in section 4.3 except the empirical equations to determine the top storey loading F_t based on the NBCC 2010 are different. As shown in Eqs. (4.17) and (4.18), the top storey loading is computed based on the proposed parameters γ_{reg} and γ_{intr}. Therefore, modifications based on the NBCC 2010 can be directly made on parameters γ_{reg} and γ_{intr}.

Determination of γ_{reg}

Recall Eq. (4.20), which is the equation to determine the value of γ_{reg} for "regular" structures based on the modal response spectrum analysis. Since ASCE 7 adopts the Newmark design spectrum, the spectral ratio $S_a(T_i)/S_a(T_1)$ can be determined by $T_{\text{sing}U}/T_S$ for an N-storey regular structure. However, the spectral shape specified by NBCC 2010 varies for different locations, as shown in Figure 5.2 (b). The spectral ratio $S_a(T_i)/S_a(T_1)$ cannot be calculated in the way similar to that of ASCE 7. It is suggested that the γ_{reg} be directly computed based on modal response spectrum analysis. Since the "regular" structure usually has well separated natural frequencies, the CQC combination rule in Eq.(4.20) can be replaced by the SRSS combination rule. By adopting such simplification, the γ_{reg} for an N_U-storey "regular" structure can be determined as follows:

$$\gamma_{\text{reg}} = \frac{\sqrt{\sum_{i=1}^{N_U}\left[M_{Ni}S_a\left(T_i\right)/N/S_a\left(T_1\right)\right]^2} - \left(mh_N\right)/\left(\sum_{i=1}^{N_U} mh_i\right)}{1-\left(mh_N\right)/\left(\sum_{i=1}^{N_U} mh_i\right)} \tag{5.14}$$

where M_{Ni} and T_i are the normalized effective modal mass of the top storey and the period associated with the ith-mode, respectively. Numerical values of M_{Ni} for an N_U-storey "regular" structure are provided in Table 5.6. The period T_i is calculated as follows:

$$T_i = \frac{2\pi}{\bar{\omega}_i}\sqrt{\frac{m_U}{k_U}} \tag{5.15}$$

where $\bar{\omega}_i$ is the normalized natural frequency associated with the *i*th-mode for an N_U-storey "regular" structure. Numerical values of $\bar{\omega}_i$ are listed in Table 5.7.

Determination of γ_{intr}

Recall Eq. (4.21), which is the equation to determine the value of γ_{intr} through the proposed η_{intr}. As discussed in Appendix D.2.1, the proposed η_{intr} is related to the spectral ratio $S_a(T_L)/S_a(T_U)$, where T_L and T_U are first mode periods of the lower and upper structures, respectively. If Newmark spectrum is adopted as that did in ASCE 7, the spectral ratio $S_a(T_L)/S_a(T_U)$ can be determined by ratios T_L/T_U and T_U/T_S. Therefore, the effect of the spectral ratio $S_a(T_L)/S_a(T_U)$ on the proposed η_{intr} is represented by

Table 5.6: Normalized effective modal masses of top storey for uniform structures

N_U \ mode number	1	2	3	4	5	6	7	8	9
2	1.171	-0.171	N/A	N/A	N/A	N/A	N/A	N/A	N/A
3	1.220	-0.280	0.060	N/A	N/A	N/A	N/A	N/A	N/A
4	1.241	-0.333	0.120	-0.028	N/A	N/A	N/A	N/A	N/A
5	1.25	-0.36	0.16	-0.06	0.02	N/A	N/A	N/A	N/A
6	1.258	-0.379	0.183	-0.090	0.038	-0.009	N/A	N/A	N/A
7	1.262	-0.390	0.200	-0.110	0.057	-0.024	0.006	N/A	N/A
8	1.264	-0.398	0.211	-0.124	0.072	-0.038	0.016	-0.004	N/A
9	1.266	-0.403	0.220	-0.135	0.084	-0.050	0.027	-0.012	0.003

Table 5.7: Normalized natural frequencies of uniform structures

N_U \ mode number	1	2	3	4	5	6	7	8	9
2	0.618	1.618	N/A	N/A	N/A	N/A	N/A	N/A	N/A
3	0.445	1.247	1.802	N/A	N/A	N/A	N/A	N/A	N/A
4	0.347	1.000	1.532	1.879	N/A	N/A	N/A	N/A	N/A
5	0.285	0.831	1.310	1.683	1.919	N/A	N/A	N/A	N/A
6	0.241	0.709	1.136	1.497	1.771	1.942	N/A	N/A	N/A
7	0.209	0.618	1.000	1.338	1.618	1.827	1.956	N/A	N/A
8	0.185	0.547	0.891	1.205	1.478	1.700	1.865	1.966	N/A
9	0.149	0.445	0.731	1.000	1.247	1.466	1.652	1.802	1.911

the effect of T_U/T_S if ASCE 7 design spectrum is adopted, as shown in Eq. (4.22). However, as NBCC 2010 specifies different spectral shapes, a relationship between the value of η_{intr} and the spectral ratio $S_a(T_L)/S_a(T_U)$ is directly established. By combining Eqs. (4.22) and (D.2), it is obtained that

$$\eta_{\text{intr}} = \begin{cases} 1 & \dfrac{S_a(T_L)}{S_a(T_U)} \le \left(T_U / T_S\right)_{CRT} \\ \eta_{\min}\left[\dfrac{S_a(T_L)/S_a(T_U)}{T_U/T_L}\right]^{x_5} & \left(T_U / T_S\right)_{CRT} < \dfrac{S_a(T_L)}{S_a(T_U)} < T_U/T_L \\ \eta_{\min} & \dfrac{S_a(T_L)}{S_a(T_U)} = T_U/T_L \end{cases} \tag{5.16}$$

The spectral ratio $S_a(T_L)/S_a(T_U)$ in Eq. (5.16), which is calculated based on ASCE 7 design spectrum, is limited between unity and the ratio T_U/T_L. However, similar to the spectral ratio $S_a(T_1)/S_a(T_U)$ in Eqs.(5.2) and (5.3), the spectral ratio $S_a(T_L)/S_a(T_U)$ may be greater than the ratio T_U/T_L if NBCC 2010 spectrum is adopted. Therefore, Eq. (5.16) may not be applicable since the ratio $S_a(T_L)/S_a(T_U)$ in this equation is limited between unity than T_U/T_L. In this study, the power function used in Eq. (5.16) is still used for the cases where the magnitude of the ratio $S_a(T_L)/S_a(T_U)$ is greater than the ratio T_U/T_L. The validity of using the power function for such cases can be demonstrated by the following example. Take the combined framing systems with N_L=3, N_U=7, r_m=2 and r_k=10, which results in the period ratio between the lower and upper structures T_U/T_L=4.76. In accordance with Table 4.2, the critical storey-stiffness ratio associated with the two-stage analysis procedure for this building r_{k2stg}=5.40. Since $r_k > r_{k2stg}$, the two-stage analysis procedure consequently can be used to analyze the building. By adopting the spectrum of Montreal shown in Figure 5.2 (a) and assigning different values for the period of the upper structure T_U, the spectral ratio $S_a(T_L)/S_a(T_U)$ can be evaluated. In addition, the value of η_{intr}, which is related to the top storey loading associated with the interaction of the first mode of the lower structure and other higher vibration modes of the upper structure, can be calculated based on the elastic modal response spectrum analysis of the MDOF model. Shown in Figure 5.5 are the relationships between the calculated spectral ratio $S_a(T_L)/S_a(T_U)$ and values of η_{intr} evaluated based on the elastic modal response spectrum analysis (marked as "MRS" in Figure 5.5) and Eq.(5.16). Values of $\eta_{\min}$ and the exponent x_5 of the power function in Eq. (5.16) are determined from the values of η_{intr} at $S_a(T_L)/S_a(T_U)=T_U/T_L$=4.76 and $S_a(T_L)/S_a(T_U)=(T_U/T_S)_{CRT}$=1.43. As shown in Figure 5.5, although the power function in Eq. (5.16) is derived based on $(T_U/T_S)_{CRT} \le S_a(T_L)/S_a(T_U) \le T_U/T_L$, the power function is applicable for the case where $S_a(T_L)/S_a(T_U) > T_U/T_L$. The fact that the power function in Eq. (5.16) is applicable for the case where $S_a(T_L)/S_a(T_U) > T_U/T_L$ is further justified in section 5.4.3, in which errors of the shear force distribution obtained from the proposed two-stage analysis procedure with use of Eq. (5.16) are discussed.

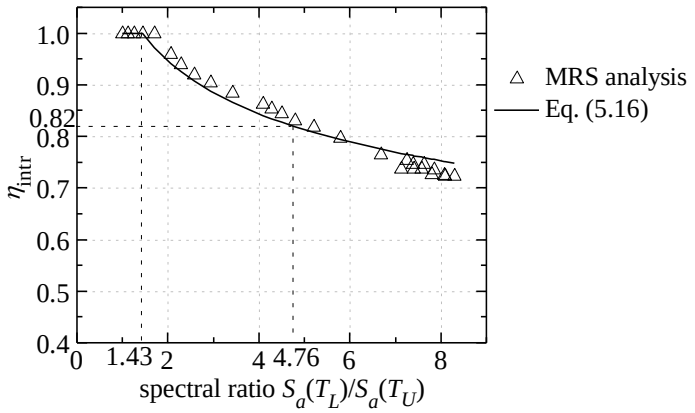

Figure 5.5: Effect of spectral acceleration ratio $S_a(T_L)/S_a(T_U)$ on the proposed η_{intr} (N_L=3, N_U=7, r_m=2 and r_k=10)

With the justification of that the power function in Eq. (5.16) can be applicable if the spectral ratio $S_a(T_L)/S_a(T_U)$ is greater than the ratio T_U/T_L, the value of η_{intr} can be determined as follows:

$$\eta_{intr} = \begin{cases} 1 & \dfrac{S_a(T_L)}{S_a(T_U)} \le \left(T_U / T_S\right)_{CRT} \\ \eta_{\min}\left[\dfrac{S_a(T_L)/S_a(T_U)}{T_U/T_L}\right]^{x_5} & \dfrac{S_a(T_L)}{S_a(T_U)} > \left(T_U / T_S\right)_{CRT} \end{cases} \tag{5.17}$$

5.4.3 Error analysis

Shear forces for each storey of the combined framing systems obtained from the modified ELF and proposed two-stage analysis procedures based on the NBCC 2010 are compared with those from the elastic modal response spectrum analysis of the MDOF model with CQC rule to combine the peak modal responses (Chopra, 2007). The maximum and minimum errors associated with the modified ELF and proposed two-stage analysis procedures, as shown in Table 5.8 and Table 5.9, respectively, are obtained based on all the possible combinations of r_m, r_k, T_{singU} and T_{singL} as stated in section 1.3.2. All the three representative seismic cities in Canada, i.e., Vancouver, Montreal and Halifax, are also considered in the error analysis. The maximum and minimum errors for each of the three cities are also listed in Tables E.40 ~E.45 in Appendices E.7 and E.8.

From Table 5.8, it is seen errors induced by the modified ELF procedure for the lower and upper structures are in the range 10.8% ~ 39.0% and -1.0% ~ 20.5%, respectively. Such errors are comparable to those of the modified ELF procedure based on ASCE 7, as discussed in section 4.2.5. In addition, errors of the shear forces for the upper and lower structures induced by the proposed two-stage analysis procedure based on NBCC 2010, as shown in Table 5.9, are also comparable to those associated with the proposed procedure of ASCE 7, as discussed in section 4.3.5.

Table 5.8: Errors associated with modified ELF procedure (NBCC 2010 spectrum)

N_L	N_U	lower structure		upper structure	
		maximum	minimum	maximum	minimum
2	1	23.6%	11.2%	18.7%	6.4%
3	1	28.1%	12.4%	20.0%	4.7%
4	1	31.7%	13.0%	19.9%	4.1%
5	1	33.7%	13.4%	19.4%	4.1%
6	1	35.3%	13.7%	20.5%	5.4%
7	1	36.4%	10.8%	14.9%	-1.0%
8	1	35.6%	11.7%	14.9%	-1.0%
9	1	39.0%	11.4%	12.4%	-0.9%

Table 5.9: Errors associated with proposed two-stage procedure (NBCC 2010 spectrum)

N_L	N_U	upper structure		lower structure	
		maximum	minimum	maximum	maximum
1	3	27.7%	8.1%	35.2%	13.6%
2	3	28.3%	5.0%	50.3%	13.2%
3	3	29.0%	5.0%	55.6%	11.4%
4	3	25.0%	5.9%	58.4%	10.5%
1	4	34.9%	10.3%	38.9%	13.3%
2	4	33.9%	3.6%	53.4%	14.7%
3	4	31.8%	4.9%	62.0%	12.5%
4	4	35.4%	4.9%	65.8%	10.6%
5	4	26.1%	6.5%	67.8%	9.4%
1	5	37.6%	6.0%	43.5%	13.8%
2	5	36.9%	4.1%	57.3%	16.6%
3	5	34.4%	3.7%	63.8%	14.5%
4	5	36.3%	4.5%	68.9%	12.6%
5	5	36.6%	3.9%	71.6%	11.2%
1	6	37.4%	5.0%	50.5%	13.7%
2	6	36.7%	1.0%	65.6%	20.6%
3	6	39.6%	-0.4%	72.5%	18.9%
4	6	38.1%	-0.9%	78.0%	17.0%
1	7	37.9%	3.5%	51.9%	18.3%
2	7	37.5%	-3.3%	66.9%	22.0%
3	7	36.5%	-4.7%	74.5%	20.8%
1	8	38.4%	4.1%	52.5%	15.8%
2	8	40.0%	-0.3%	68.7%	23.2%
1	9	38.1%	2.4%	55.0%	19.8%

The errors shown in Table 5.9 do not account for the case that F_t=0 and the case that the single storey period either T_{singU} or T_{singL} lies between 0.22 and 0.31 seconds. The errors associated with these two cases are accounted for in errors listed in Tables E.43 ~ E.45 of Appendix E.8 and it is found that the shear force of the upper structure may be overestimated considerably for certain storey combinations. From the investigation, there are eight storey combinations that may result in the maximum errors being greater than 40.0% and they are (N_L=1, N_U=6), (N_L=2, N_U=6), (N_L=1, N_U=7), (N_L=2, N_U=7), (N_L=3, N_U=7), (N_L=1, N_U=8), (N_L=2, N_U=8), and (N_L=1, N_U=9). For the eight storey combinations, such a large overestimation of shear forces occurs at the top storey of the upper structure when F_t shown in Figure 4.4 (b) is zero. Usually, F_t =0 when the single storey period of the upper structure, i.e., T_{singU}, is considerably small which signifies a very stiff upper structure as discussed in Appendix D.2.1. Therefore, it is concluded that shear forces for the top storey of the upper structure may be overestimated when the single storey period T_{singU} is small. For example, for buildings with N_L=1, N_U=9 and r_m=1, the maximum overestimation of the shear force is 46.6%, as shown in Table E.43, which occurs when T_{singU}=0.03 second and T_{singL}=0.007 second. However, such stiff lower and upper structures are rarely used in practices. For the eight storey combinations, if the values of T_{singU} are not small, i.e. F_t≠0, then errors associated with the shear forces of the upper structures are acceptable as shown in Table 5.9.

The shear forces of the upper structure may be underestimated by more than 5.0% if the single storey period either T_{singU} or T_{singL} lies between 0.22 and 0.31 seconds. For example, when N_L=4 and N_U=6, the underestimation of the shear force can be as large as 6.4% if T_{singU} lies between 0.22 and 0.31 seconds, as shown in Table E.44. However, such flexible structures are rare in practices. For most structures in practice, the single-storey period T_{singU} and T_{singL} are less than 0.22 second. From this aspect, the underestimation of the shear forces for the upper structure associated with the proposed two-stage analysis is likely not exceed 5%, as that shown in Table 5.9.

5.5 Examples

The two buildings investigated in sections 3.6.1 and 3.6.2 are selected to illustrate the proposed approach for evaluating the required storey-stiffnesses of the lower and upper structures based on the NBCC 2010 (NBCC, 2010). In addition, the two examples investigated in sections 4.6.1 and 4.6.2 are selected to illustrate the modified ELF and the proposed two-stage analysis procedures based on NBCC 2010. The only difference is that the buildings in Examples 5-1, 5-2, 5-3 and 5-4 are located in Vancouver rather than in California. Based on the site classification of the NBCC 2010, the soil condition for the site is assumed as Class C. The building importance category is set as “Normal”.

In accordance with NBCC 2010 (NBCC, 2010), the permissible storey drift is limited to $0.025h_n$ for buildings with "Normal Importance Category", where h_n is the storey height. However, as the permissible storey drift specified in Examples 3-1 and 3-2 is $0.02h_n$, the permissible storey drift for buildings in Examples 5-1 and 5-2 is also taken as $0.02h_n$ for the reason of comparison.

5.5.1 Example 5-1

The storey and floor layouts, storey masses and lateral stiffness of the nine-storey building are taken as the same as those shown in Example 3-1 and the permissible storey drift of the CFS shear wall is also 61.2 mm. In accordance with the NBCC 2010 (NBCC, 2010), the spectral values of Vancouver at periods of 0.2, 0.5, 1.0 and 2.0 seconds are respectively $S_a(0.2)$=0.94 g, $S_a(0.5)$=0.64 g, $S_a(1.0)$=0.33 g and $S_a(2.0)$=0.17 g, and the corresponding factored design spectral values are $\bar{S}_a(0.2) = 2.61 \times 0.94 = 2.45$ g , $\bar{S}_a(0.5) = 2.61 \times 0.64 = 1.67$g, $\bar{S}_a(1.0) = 2.61 \times 0.33 = 0.86$ g and $\bar{S}_a(2.0) = 2.61 \times 0.17 = 0.44$ g.

By following Steps 1 ~ 4 described in section 5.3.4, it is obtained that $k_{\alpha U1}$=1.21×10^5 kN/m, $k_{\alpha U\max}$=1.79×10^5 kN/m and $k_{\alpha U2\text{stg}}$=9.14×10^4 kN/m, which then results in $k_{U\max}$=1.79×10^5 kN/m and $k_{U\min}$=9.14×10^4 kN/m. When computing the critical storey-stiffnesses $k_{\alpha U1}$, $k_{\alpha U\max}$ and $k_{\alpha U2\text{stg}}$, the approximation"EXP-2", as shown in Table E.9 of Appendix E.4, is selected to simulate the factored spectrum of Vancouver spectrum. The curve fitting parameters associated with Eq.(5.9) for the factored spectrum of Vancouver are listed in Table 5.10. Based on Step 5, it is obtained that the feasible storey-stiffness of the upper structure k_U should not be less than 9.14×10^4 kN/m, and corresponding requirement on the lateral stiffness of the lower structure k_L can then be computed in accordance with Step 6. By converting the obtained feasible storey-stiffnesses k_U and k_L in terms of the required length of CFS shear wall and number of columns in the RC moment frame, respectively, the domain of feasible SFRS designs of lower and upper structures can be obtained. Additionally, the number of columns in the RC moment frame and the CFS shear wall length in this example are limited to 16 and 73.2 m, respectively (Figure 3.8). The ranges of stiffness combinations of the lower and upper structure for the combined framing systems investigated in this example are shown in Figure 5.6 (a).

Elastic-analysis-based modal response spectrum analysis (Chopra, 2007) is carried out for the building as a MDOF model, as shown in Figure 1.3 (a), with the corresponding effective storey-masses and storey-stiffnesses evaluated previously. For all combinations of the CFS shear wall length and the number of columns in the RC moment frame shown in the shaded areas of Figure 5.6 (a), storey drifts of the first storey of CFS shear walls calculated from the elastic-analysis-based modal

Table 5.10: Curve fitting parameters of approximation "EXP-2" for factored spectrum of Vancouver

parameter	A_1 (g)	τ_1	A_2 (g)	τ_2	A_3 (g)	τ_3	A_4 (g)	τ_4	T_S'
value	3.211	-1.266	3.095	-1.192	1.949	-0.729	0.840	-0.309	0.213

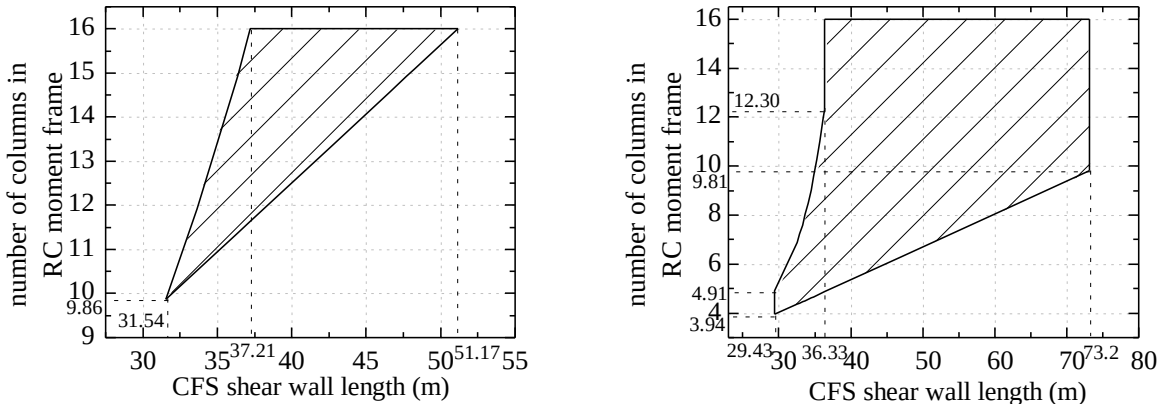

(a) Example 5-1 (b) Example 5-2

Figure 5.6: Feasible SFRS designs of lower and upper structures of Examples 5-1 and 5-2

response spectrum analyses are less than 1.8% of the storey height. The maximum storey drifts for the derived feasible designs of this example is the same as that of Example 3-1, as discussed in section 3.6.3. Since the specified storey-drift limit for the building is 2% of the storey height, all combinations the CFS shear wall length and the number of columns in the RC moment frame obtained from the proposed procedure are conservative.

5.5.2 Example 5-2

The eight-storey building investigated herein are identical to that in Example 3-2 excepted the location is in Vancouver. With the factored design spectral values being the same as that shown in Example 5-1, by following Steps 1~6 of section 5.3.4, the domain of feasible SFRS designs of lower and upper structures can be obtained and is illustrated as the shaded area in Figure 5.6 (b). The curve fitting parameters of Scheme "EXP-2" are listed in Table 5.10. Note that the factored spectrm of Vancouver is still fitted by the fitting "EXP-2" and the obtained curve fitting parameters are listed in Table 5.10.

Elastic-analysis-based modal response spectrum analysis (Chopra, 2007) is carried out for the building as a MDOF model, as shown in Figure 1.3 (a), with the values of corresponding effective storey-masses and storey-stiffnesses being evaluated previously. For all combinations of the CFS shear wall length and the number of columns in the RC moment frame shown in the shaded areas of Figure 5.6 (b), storey drifts of the first storey of CFS shear walls calculated from the elastic-analysis-

based modal response spectrum analyses are less than 1.9% of the storey height. The maximum storey drifts for the derived feasible designs of this example is almost equal to that of Example 3-2, which is 1.8% as discussed in section 3.6.3. Therefore, the required stiffnesses for the upper and lower structures obtained from the proposed procedure are conservative.

5.5.3 Example 5-3

The storey and floor layouts, storey masses and lateral stiffness of the nine-storey building are taken as the same as those shown in Example 4-1. As discussed in section 4.6.1, the modified ELF procedure can be used to distribute the lateral load and then estimate the resulted shear force of the combined framing systems. Shear forces of the combined framing system calculated by the modified ELF procedure are shown in Figure 5.7. Also shown in this figure are results evaluated from the ELF procedure prescribed NBCC 2010 (NBCC, 2010). The accurate results shown in the figure are calculated based on the elastic modal response spectrum analysis (Chopra, 2007). As shown in the figure, the modified ELF procedure provides a good approximation for the shear forces of both the lower structure and upper "appendage". The ELF procedure prescribed in NBCC 2010 (NBCC, 2010) yields a good estimation for the shear force of the lower structure only and the shear force of the upper "appendage" is underestimated by 6.1%.

5.5.4 Example 5-4

The eight-storey building investigated in Example 4-2 are re-examined by the proposed two-stage analysis based on NBCC 2010. As discussed in section 4.6.2, the proposed two-stage analysis procedure can be used to estimate the shear forces of the combined framing systems. The calculated additional top storey loading based the proposed two-stage analysis is obtained as F_t=0.07V_{Ub}. Shear forces for each storey of the combined framing system calculated by the proposed two-stage analysis methods are shown in Figure 5.8. The accurate results shown in the figure are also calculated based on the elastic modal response spectrum analysis (Chopra, 2007). From the figure, it is seen the proposed two-stage analysis procedure based on NBCC 2010 provides good approximations for the shear forces of both the lower and upper structures.

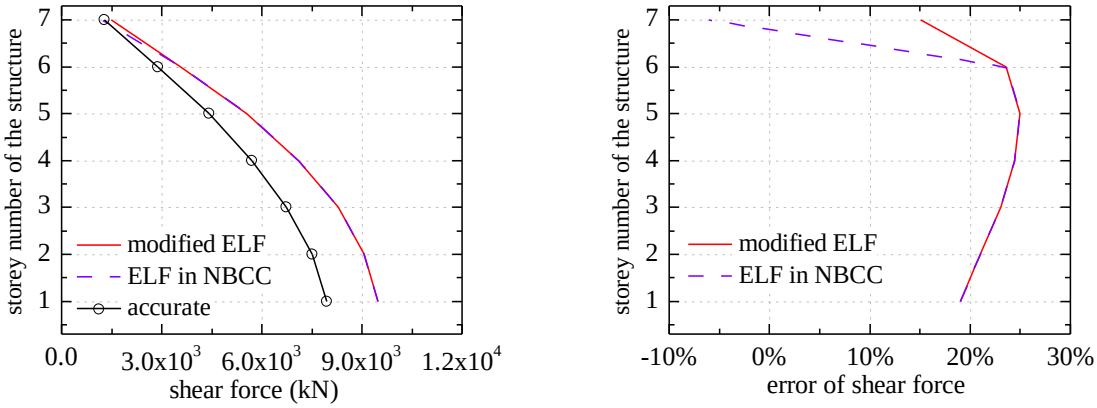

Figure 5.7: Results comparison of Example 5-3

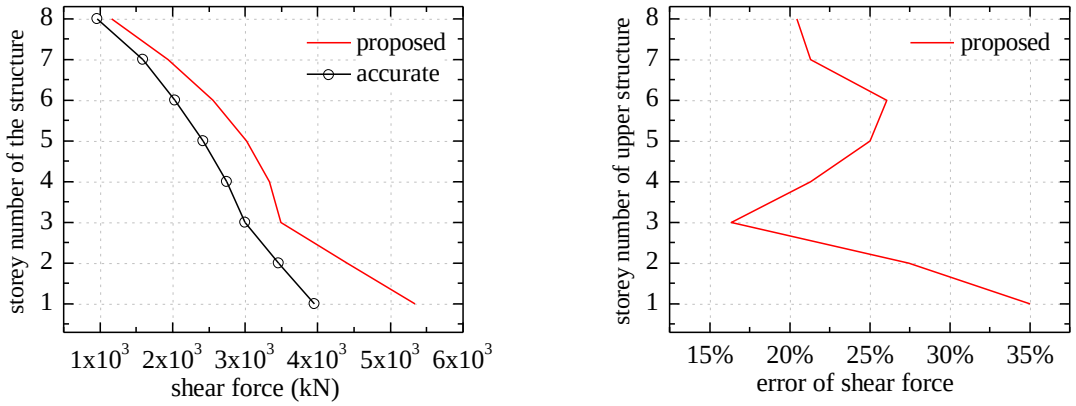

Figure 5.8: Results comparison of Example 5-4

5.6 Nonlinear time history analysis discussion

The evaluation of feasible lateral storey-stiffness for the lower and upper structures based on the pre-determined mass distribution and specified storey drift needs to consider the nonlinear structural behavior of the combined framing systems. In the proposed approach, the nonlinear seismic response of the structural system is approximated by the linear elastic analysis together with the adoption of seismic performance factors, i.e., elastic-analysis-based modal response spectrum analysis, rather than nonlinear time history analysis. The structural nonlinear seismic responses approximated by the elastic-analysis-based modal response spectrum analysis in previous examples need to be compared to that of the nonlinear time history analyses.

The feasible stiffness combinations obtained from the proposed approach in terms of the length of CFS shear wall and the number of columns in the RC moment frame for the two buildings in Examples 5-1 and 5-2 are shown in Figures 5.6 (a) and (b), respectively. From the figures, as shown in Table 5.11, two different SFRS designs of lower and upper structure are selected for each building. to be investigated with nonlinear time history analysis. The earthquake ground motions and the

Table 5.11: Selected buildings for nonlinear time history analyses

building ID	Examples	CFS shear wall length (m)	No. of columns in RC moment frame
1	Example 5-1	39.04	16
2	Example 5-1	51.24	16
3	Example 5-2	34.16	6
4	Example 5-2	51.24	10

hysteretic models of the CFS shear wall and the RC moment frame are presented in sections 5.6.1 and 5.6.2, respectively. The results of the nonlinear time history analyses are discussed in sections 5.6.3 and 5.6.4.

5.6.1 Ground motion record set: selection and scaling

FEMA P695 (FEMA, 2009) provides twenty-two "Far-Field" earthquake records to evaluate the collapse probability of the buildings. With each earthquake record including two horizontal components, in total of forty-four lateral grounds motions (twenty-two pairs) are provided. In thisstudy, twenty-one pairs out of the twenty-two pairs of the "Far-Field" ground motions are selected, as shown in Table 5.12. All the ground motions for the earthquake records listed in Table 5.12 are downloaded from the NGA-West2 ground motion database (PEER, 2015). The unselected pair out of the twenty-two pairs that are provided in Table A4-C of FEMA P695 (FEMA, 2009) is the earthquake record with the record sequence number (RSN) being 829. It was unselected since the earthquake record with RSN being 829 was not found in the NGA-West2 database.

The procedure of scaling of earthquake records consists of the processes of normalization and scaling in according to FEMA P695 (FEMA, 2009). The normalization process is carried out with respect to the peak ground velocity (PGV) as follows:

$$NM_i = \text{median}\left[(PGV)_i\right] / \left(PGV\right)_i \tag{5.18}$$

where NM_i is the normalization factor of both horizontal components of the ith-record, $(\text{PGV})_i$ is the PGV of the ith-record, and median$[(\text{PGV})_i]$ is the median of $(\text{PGV})_i$ values of the twenty-one records. The normalization factor of each earthquake record for the selected twenty-one records is listed in Table 5.12. Once the normalization factors are obtained from Eq (5.18) , the two horizontal components of the ith-record can then be normalized as follows:

$$NTH_{1,i} = NM_i \times TH_{1,i} \tag{5.19 a}$$

$$NTH_{2,i} = NM_i \times TH_{2,i} \tag{5.19 b}$$

Table 5.12: Summary of earthquake records and corresponding normalization factors for the selected earthquake record set (PEER, 2015)

ID No.	RSN	Earthquake					normalization
		magnitude	year	Name	PGA[1](g)	PGV[1] (cm/s)	factor (NM)
1	953	6.7	1994	Northridge	0.47	62.90	0.64
2	960	6.7	1994	Northridge	0.44	42.72	0.94
3	1602	7.1	1999	Duzce, Turkey	0.77	60.70	0.66
4	1787	7.1	1999	Hector Mine	0.30	34.15	1.17
5	169	6.5	1979	Imperial	0.29	29.48	1.36
6	174	6.5	1979	Imperial	0.37	40.08	1.00
7	1111	6.9	1995	Kobe, Japan	0.47	42.32	0.95
8	1116	6.9	1995	Kobe, Japan	0.23	26.14	1.53
9	1158	7.5	1999	Kocaeli, Turkey	0.34	57.23	0.70
10	1148	7.5	1999	Kocaeli, Turkey	0.17	23.65	1.69
11	900	7.3	1992	Landers	0.19	38.52	1.04
12	848	7.3	1992	Landers	0.34	34.63	1.16
13	752	6.9	1989	Loma	0.47	33.57	1.19
14	767	6.9	1989	Loma	0.45	40.61	0.99
15	1633	7.4	1990	Manjil, Iran	0.51	46.52	0.86
16	721	6.5	1987	Superstition	0.30	44.82	0.89
17	725	6.5	1987	Superstition	0.37	34.57	1.16
18	1244	7.6	1999	Chi-Chi	0.37	84.25	0.48
19	1485	7.6	1999	Chi-Chi	0.49	48.19	0.83
20	68	6.6	1971	San	0.21	19.16	2.09
21	125	6.5	1976	Friuli	0.34	26.41	1.52

Note: 1. PGA (peak ground acceleration) and PGV (peak ground velocity) listed in the table are the geometric mean of the two horizontal components.

where $TH_{1,i}$ and $TH_{2,i}$ are the horizontal components 1 and 2 of the record *i*, respectively. The normalization process eliminates the unwarranted variability between records due to the inherent differences in the event magnitude, distance to source, source type and site conditions but preserves the inherent aleatory (i.e., record-to-record variability) necessary for accurately predicting the collapse probability.

Following the process of normalization, the normalized ground motions are to be scaled to the code-specified design response spectrum. The unscaled response spectra for all the normalized earthquake records listed in Table 5.12 are calculated and the corresponding median is shown in Figure 5.9. The median spectrum is then scaled to match the spectrum of Vancouver at the periods of the dominating modes of the building until an acceptable match between the median and design

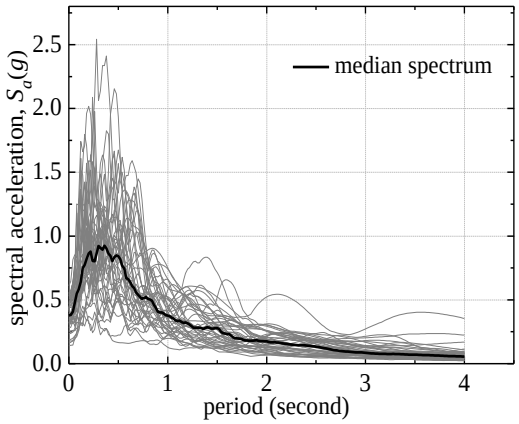

Figure 5.9: Response spectra for the forty-two normalized ground motions and their median spectrum

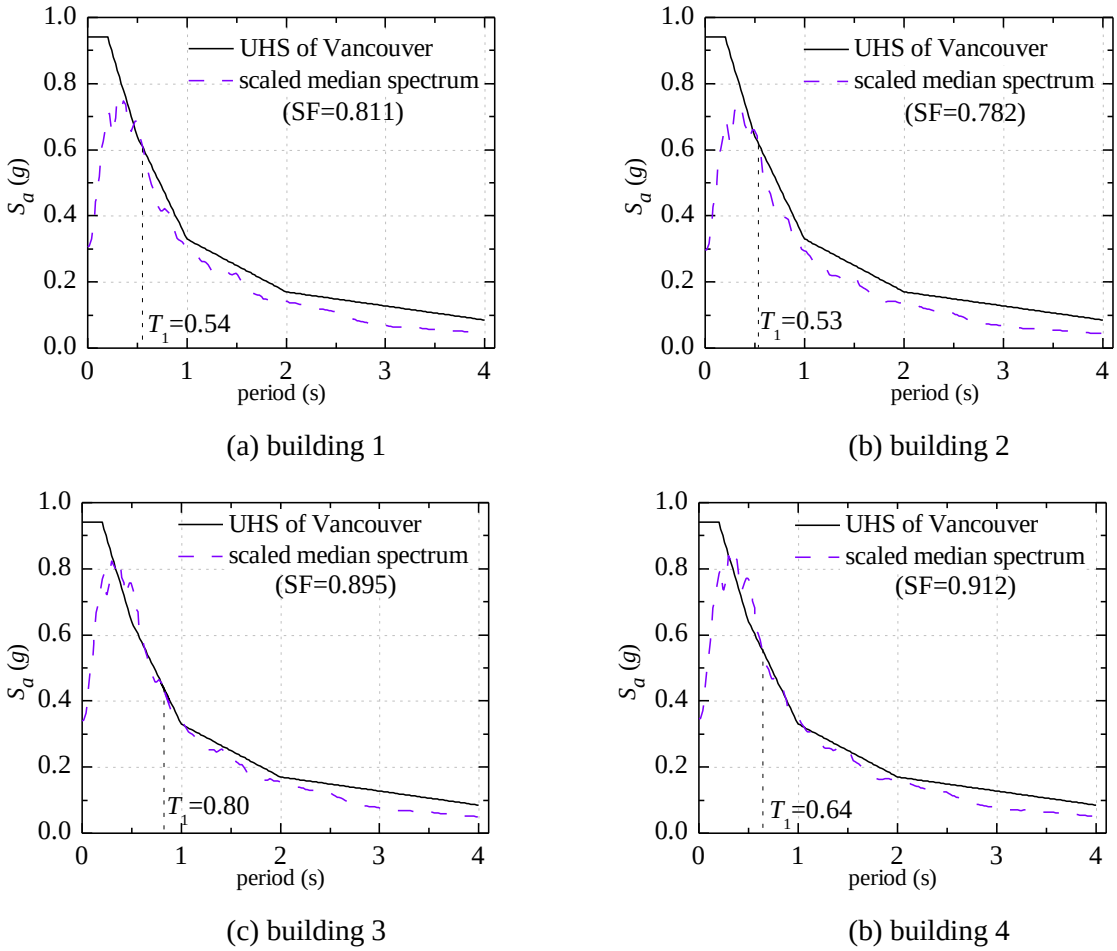

Figure 5.10: Matching the median and design spectra at periods of the dominating modes of the building

response spectrum is observed. Since the lateral displacements of the selected four buildings are dominated by the first mode of vibration, the median spectrum is scaled to the match the spectrum of Vancouver at the first mode period of the building. The comparison between the spectrum of Van-

couver and the scaled median spectrum for the selected four buildings listed in Table 5.15 are shown in Figure 5.10. The corresponding scaled factors (SF) are also shown in the figure.

5.6.2 Modelling CFS and RC framing

The OpenSees software (OpenSees, 2014) is utilized to analyze the nonlinear behaviour of the combined framing systems. The building with combined framing systems is idealized as a stick model as shown in Figure 1.3 (a). By adopting this idealized stick model, the nonlinear behavior of each floor is simulated by an 1-D truss element subjected to axial deformation and loading. The floor mass is attached to the end of the truss element, as shown in Figure 5.11. In addition, the earthquake ground motions are applied in the axial direction of the truss element. Since the P-Δ effect and the gravity load are not considered in the stick model, the finite element model shown in Figure 5.11 can be used to represent the seismic behavior of the stick model shown in Figure 1.3 (a). By setting the axial stiffness of each truss element be equal to the lateral storey-stiffness of the corresponding floor, the calculated lateral deformation of each floor in the stick model shown in Figure 1.3 (a) is numerically equal to the calculated axial deformation of each truss element in the finite element model shown in Figure 5.11.

The Rayleigh damping is adopted to characterize the damping properties of the combined framing systems. By selecting two vibration modes and assigning the specified damping ratio, i.e., 5% in this study, to the two vibration modes, the mass and stiffness proportional coefficients of the Rayleigh damping can be determined. The two vibration modes should be carefully chosen to ensure that all the modes contributing significantly to the response have the damping ratio being 5%. For all the four buildings listed in Table 5.11, the selected two vibration modes that are used to determine the mass and stiffness proportional coefficients are the first and third vibration modes.

In addition to the damping model, it is of great significance to select appropriate hysteretic models for the truss elements that are used to represent the CFS shear wall and the special RC moment frame, respectively, to capture the nonlinear behavior combined framing systems. The primary hysteretic characteristics of the CFS shear wall include pinching, strength deterioration, and unloading and reloading stiffness deteriorations. To capture these features, the Pinching4 material is utilized to simulate the nonlinear behavior of the wood-sheathed CFS shear wall, as recommend by Shamim (2012). In addition, as suggested by Haselton et.al (2008), the modified Ibarra-Medina-Krawinkler deterioration model with peak-oriented hysteretic response (Ibarra et.al, 2005) is selected to capture the nonlinear hysteretic behavior of the special RC moment frame.

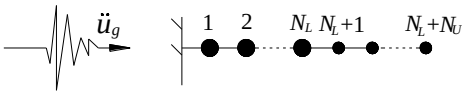

Figure 5.11: Finite element model of mid-rise building with vertical combination of framing systems

5.6.2.1 Hysteretic model of CFS frame

The Pinching4 material was originally proposed by Lowes et.al (2003) to characterize the pinching behavior of the reinforced concrete beam-column joints subjected to cyclic loading. Shamim (2012) employed the Pinching4 material for the hysteretic behavior of the CFS framing with wood-sheathed shear walls. The total of 38 parameters that are required to identify the Pinching4 material are as shown in Figure 5.12. The backbone curve is decided by the parameters (Pd_1, Pf_1), (Pd_2, Pf_2), (Pd_3, Pf_3), (Pd_4, Pf_4), (Nd_1, Nf_1), (Nd_2, Nf_2), (Nd_3, Nf_3) and (Nd_4, Nf_4), where Pd_i and Nd_i are the positive and negative deformations, respectively, and Pf_i and Nf_i are the corresponding shear forces. The parameters (rDisP, rForceP) and (rDisN, rForceN) signify the starting point of the reloading curve, and the parameters uForceP and uForceN determine the force at the ending point of the unloading curve, as shown in Figure 5.12. In addition, (gK_1, gK_2, gK_3, gK_4, gKLim), (gF_1, gF_2, gF_3, gF_4, gFLim) and (gD_1, gD_2, gD_3, gD_4, gDLim) are introduced to account for the deterioration associated with unloading stiffness (unloading stiffness degradation), strength achieved at the previously unachieved deformation demands (envelope strength degradation), and strength developed in the vicinity of the maximum and minimum deformation demands (reloading strength degradation), respectively. With these parameters, the damage indices are calculated as follows:

$$\delta k_i = \left[gK_1 \left(\tilde{d}_{\max} \right)^{gK_3} + gK_2 \left(\frac{E_i}{gE \cdot E_{\text{monotonic}}} \right)^{gK_4} \right] \leq gKLim \tag{5.20}$$

$$\delta d_i = \left[gD_1 \left(\tilde{d}_{\max} \right)^{gD_3} + gD_2 \left(\frac{E_i}{gE \cdot E_{\text{monotonic}}} \right)^{gD_4} \right] \leq gDLim \tag{5.21}$$

$$\delta f_i = \left[gF_1 \left(\tilde{d}_{\max} \right)^{gF_3} + gF_2 \left(\frac{E_i}{gE \cdot E_{\text{monotonic}}} \right)^{gF_4} \right] \leq gFLim \tag{5.22}$$

where

$$\tilde{d}_{\max} = \max \left[\frac{(d_{\max})_i}{def_{\max}}, \frac{(d_{\min})_i}{def_{\min}} \right] \tag{5.23}$$

$$E_i = \int_{\text{load history}} dE \tag{5.24}$$

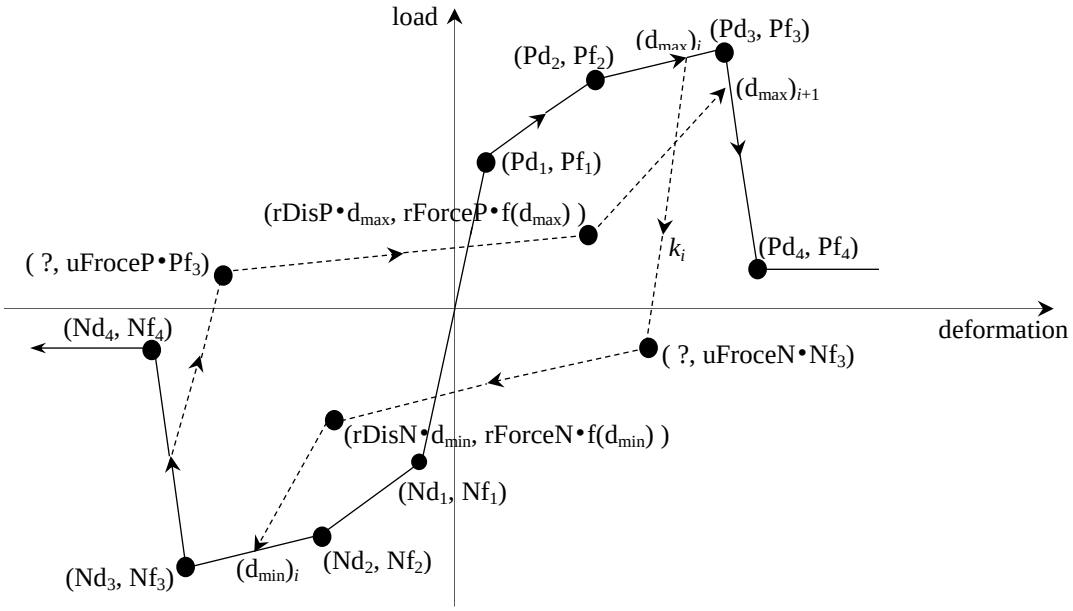

Figure 5.12: Definition of Pinching4 material

In Eqs.(5.20) ~ (5.24), δk_i, δd_i and δf_i are the current values of the stiffness, reloading strength and strength damage indices, respectively. (gK_1, gK_2, gK_3, gK_4), (gD_1, gD_2, gD_3, gD_4) and (gF_1, gF_2, gF_3, gF_4) are the parameters that control the cyclic degradation of unloading stiffness, reloading strength and strength, respectively; and g*KLim*, g*DLim*, and g*FLim* are limited values associated with the damage indices δk_i, δd_i and δf_i, respectively. E_i is the hysteretic energy; $E_{\text{monotonic}}$ is the energy required to achieve the deformation that defines the failure; and *gE* is used to define the maximum energy dissipation capacity under cyclic loading. $def_{\max}$ and $def_{\min}$ are the positive and negative deformations that define the failure, respectively; and $(d_{\max})_i$ and $(d_{\min})_i$ are the maximum and minimum historic deformation demands, respectively. Then, once the damage indices being calculated, the following equations are used to determine the deteriorations associated with the unloading stiffness, reloading strength and envelope strength:

$$k_i = k_0(1-\delta k_i) \tag{5.25}$$

$$(d_{\max})_{i+1} = (d_{\max})_i(1+\delta d_i) \tag{5.26}$$

$$(f_{\max})_i = (f_{\max})_0(1-\delta f_i) \tag{5.27}$$

where k_i , $(d_{max})_{i+1}$ and $(f_{max})_i$ are the current unloading stiffness, deformation that defines the end of the reloading cycle, and envelop maximum strength, respectively, and k_0, $(d_{max})_i$ and $(f_{max})_0$ are the initial unloading stiffness, maximum historic deformation demand and initial envelope maximum strength, respectively.

The Pinching4 material was calibrated with the test results of the CFS shear wall under the cyclic or earthquake loading. Since the hysteretic response of the tested walls is almost symmetric (Shamim, 2012), the same backbone curve was used for both the positive and negative response excursions in the study. Therefore, it is obtained that Pd_i=Nd_i=d_i, Pf_i=Nf_i=f_i, rForceP=rForceN=rForce, rDispP=rDispN=rDisp, and uForceP= uForceN=uForce. Values of f_i and d_i are directly calibrated from the backbone curve of the cyclic test results. The CFS shear walls used in Examples 5-1 and 5-2 are sheathed with double-sided 11mm OSB panel. The spacing of the screw that connects the stud and the OSB sheathing is 100 mm for the chord stud and 300 mm for the intermediate stud. The dimensions of the C-shape stud are 92.1×41.3×12.7×1.12 mm and the stud spacing is 600 mm. In accordance with the cyclic test results carried out at McGill University (Branston, 2004; Chen, 2004; & Boudreault, 2005), values of f_i and d_i that are calibrated from the test results are listed in Table 5.13. It is noted that values of f_i provided in Table 5.13 are the unit shear capacity per meter of CFS shear walls. The shear capacity of the CFS framing at each floor of the upper structure is based on the total length of the CFS shear wall. It is also noted that the negative tangent stiffness is not considered in the finite element model. The stiffness from the point (d_3, f_3) to (d_4, f_4) is set to be zero rather than the tested negative value from the test, as shown in Figure 5.13.

Table 5.13: Suggested model parameters for the OSB-sheathed CFS shear wall

parameter	d (mm)				f (kN/m)			
	d_1	d_2	d_3	d_4	f_1	f_2	f_3	f_4
value	3.552	16.640	30.829	50.968	13.627	30.162	34.068	34.068
parameter	gK_1	gK_2	gK_3	gK_4	gD_1	gD_2	gD_3	gD_4
value	0.2	0.2	1.5	1.5	0.2	0.2	1.5	1.5
parameter	*gK*Lim	*gD*Lim	*gF*Lim	*gE*	rForce	uForce	rDisp	
value	0.5	0.5	0	3.58	0.18	-0.1	0.4	

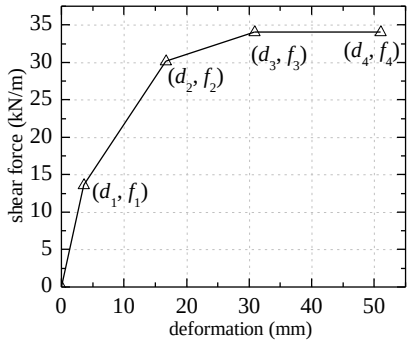

Figure 5.13: Adopted backbone curve of the CFS shear walls

Besides f_i and d_i, other hysteretic degradation parameters for the OSB-sheathed CFS shear wall are also shown in Table 5.12. The hysteretic degradation parameters listed in Table 5.12 were originally calibrated from the test results of the CSP- (Canadian softwood plywood) and DFP- (Dogulas fir plywood) sheathed CFS shear walls by Shamim (2012). The calibrated results from Shamim show regardless of the CSP- or DFP-sheathed CFS shear walls, the hysteretic degradation parameters are almost the same. Considering the similarity of the mechanical behavior between the OSB-sheathed and CSP- or DFP-sheathed CFS shear walls, hysteretic degradation parameters suggested by Shamim (2012) are directly adopted in this study to characterize the hysteretic behavior of the OSB-sheathed CFS shear walls, as shown in Table 5.12.

5.6.2.2 Hysteretic model of RC frame

Shown in Figure 5.14 is the backbone curve of the modified Ibarra-Medina-Krawinkler model (Ibarra et.al, 2005) which consists of three portions: the elastic branch, the strain hardening branch and the post-peak strain softening branch. As to the hysteretic behavior, the modified Ibarra-Medina-Krawinkler model captures the deterioration by the following four modes: (a) strength deterioration of the inelastic strain hardening branch, (b) strength deterioration of the post-peak strain softening branch, (c) accelerated reloading stiffness deterioration, and (d) unloading stiffness deterioration. For each one of these four modes, an energy index (λ) and an exponent term (c) are adopted to describe how the rate of hysteretic deterioration changes with the accumulation of damage (Ibarra et.al, 2005). Therefore, four pairs of (λ, *c*) are required to completely identify the deteriorations of all the four modes. However, similar to the RC frame model recommend by FEMA P695 (FEMA, 2009), the accelerated reloading and unloading stiffness deteriorations are neglected in this study. Furthermore,

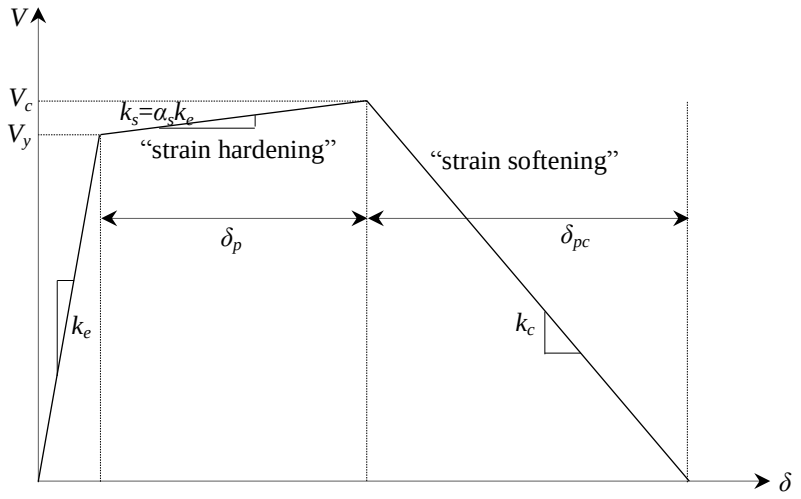

Figure 5.14: Backbone curves of the modified Ibarra-Medina-Krawinkler model (Ibarra et.al, 2005)

Table 5.14: Suggested model parameters for the RC column of the moment frame

k_e (kN/m)	V_y (kN)	δ_p (m)	δ_{pc} (m)	α_s	λ	c
5.41×10^4	316.02	0.1445	0.1650	0.0053	87.93	1.0

the deterioration rate λ is set to be equal for the strain hardening branch and the post-peak strain softening branch. Only one pair of (λ, c) is needed to describe the cyclic deterioration rule. Consequently, seven parameters required to construct the modified Ibarra-Medina-Krawinkler model are: k_e, V_y, α_s, δ_p, δ_{pc}, λ and c, where k_e, V_y, α_s, δ_p and δ_{pc} are used to define the backbone curve as shown in Figure 5.14, and (λ, c) are used to determine the hysteretic deterioration of both the strain hardening and post-peak strain softening branches.

The seven parameters of the modified Ibarra-Medina-Krawinkler model associated with the RC columns had been carefully calibrated with 255 experimental tests of the RC columns (Haselton et.al, 2007), and the corresponding empirical equations were developed to establish relationships between the design parameters and the modelling parameters. The process of evaluating the seven modelling parameters from the empirical equations is discussed in Appendix E.9 and the resulted modal parameters are listed in Table 5.14. Note that values of k_e and V_y provided in Table 5.14 are the initial stiffness and yield shear force for a single column of the moment frame, respectively. The initial stiffness of each storey is obtained by multiplying the number of the columns of the storey to the value of k_e listed in Table 5.14. Similarly, the yield shear force of each storey is equal to the product of the number of the columns and the value of V_y listed in Table 5.14.

5.6.3 Results of nonlinear time history analysis

Presented in Figures 5.15 (a) ~ (d) are the maximum displacements and storey-drift ratios obtained from the nonlinear time history analysis of the four selected buildings listed in Table 5.11 subject to the forty-two ground motions. The median values of the maximum displacements and storey-drift ratios under the forty-two ground motions are also shown in the figures. As clearly demonstrated in the figures, the maximum storey-drift ratios obtained from the nonlinear time history analysis are always located at the first storey of the upper structure, which is consistent with the assumption made in section 1.3.2. Recall the discussion in section 1.3.2. To ensure that the maximum storey-drift ratio to be located at the first storey of the upper structure, it is required the storey-stiffness ratio r_k to be not less than the minimum storey-stiffness ratio r_{kU1}, i.e., $r_k \geq r_{kU1}$. Note that such requirement is derived based on the elastic modal response spectrum analysis, in which the nonlinear behavior is not considered. The results obtained from the nonlinear time history analyses ratify the assumption: if the

first storey drift of the upper structure satisfies the specified limit, the drifts of the rest storey of the combined framing systems should be within the specified limit.

In accordance with FEMA P695 (FEMA, 2009), the collapse probability of the designed buildings should not be greater than 10% under the designed earthquake ground motions. The permissible storey-drift ratio for buildings in Examples 5-1 and 5-2 is 2.0%. Therefore, to ensure the collapse probability be not greater than 10%, the maximum storey-drift ratio associated with the first storey of the upper structure corresponding to the 90% non-exceedance (NE) probability should not be greater than 2.0%. Considering the selected forty-two earthquake ground motions, the non-exceedance probability distribution of the maximum storey-drift ratio for the selected four buildings is shown in Figures 5.16 (a) ~ (d). As demonstrated in Figures 5.16 (a) and (c), the nonlinear maximum storey-drift ratios corresponding to the 90% NE probability associated with building 1 and building 3 are 2.6% and 2.3%, respectively. The permissible storey-drift ratio, i.e., 2.0%, is violated for these two buildings. However, as discussed in sections 5.5.1 and 5.5.2, if the elastic-analysis-based modal response spectrum analysis is adopted to verify all the designs shown in shaded areas of Figures 5.6 (a) and (b), the maximum storey-drift ratios for buildings in Example 5-1 and 5-2 are less than 1.8% and 1.9%, respectively. The results from the elastic-analysis-based modal response spectrum analysis are not consistent with the results from the nonlinear time history analyses.

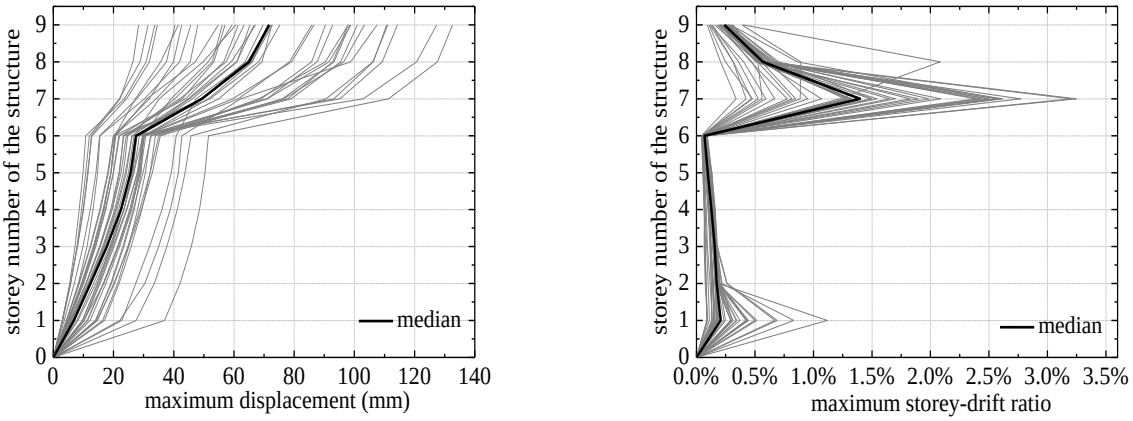

(a) building 1

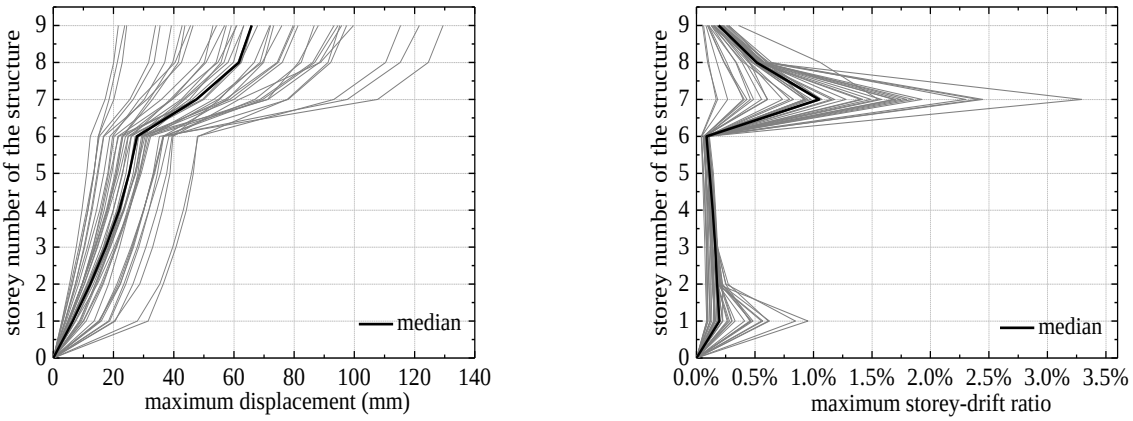

(b) building 2

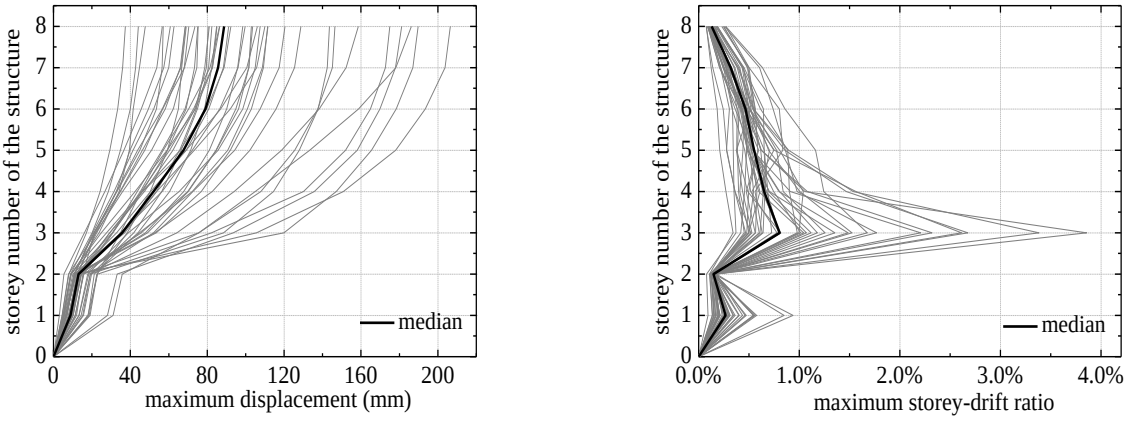

(c) building 3

Figure 5.15: Maximum displacement and storey-drift ratio of the four selected buildings under nonlinear time history analyses

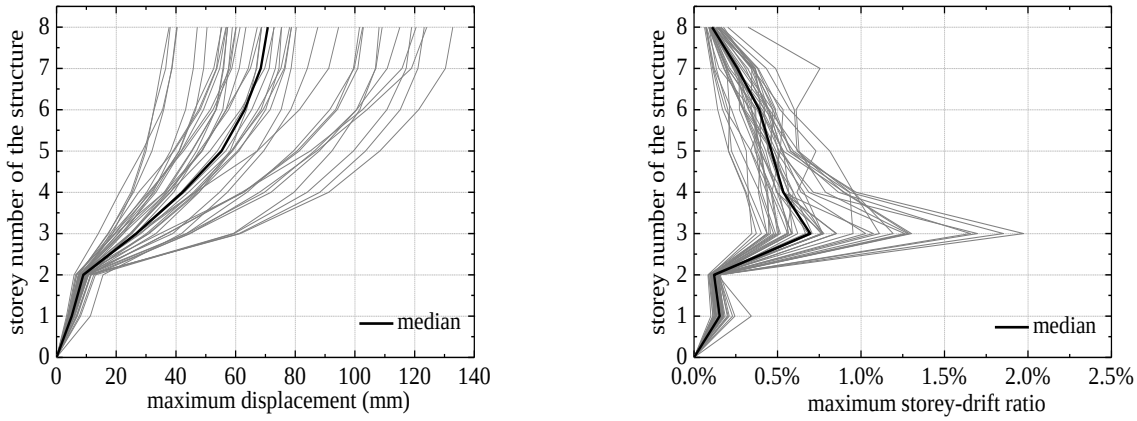

(d) building 4

Figure 5.15: Maximum displacement and storey-drift ratio of the four selected buildings under nonlinear time history analyses (continued)

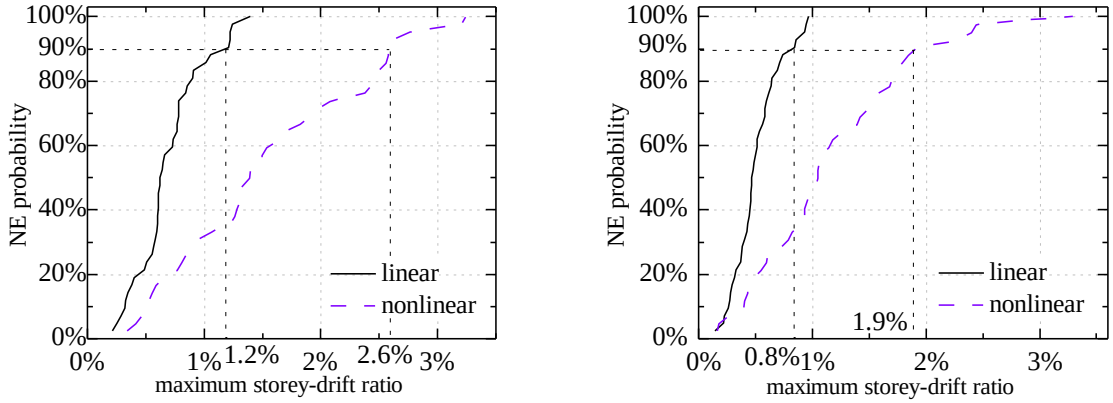

(a) building 1

(a) building

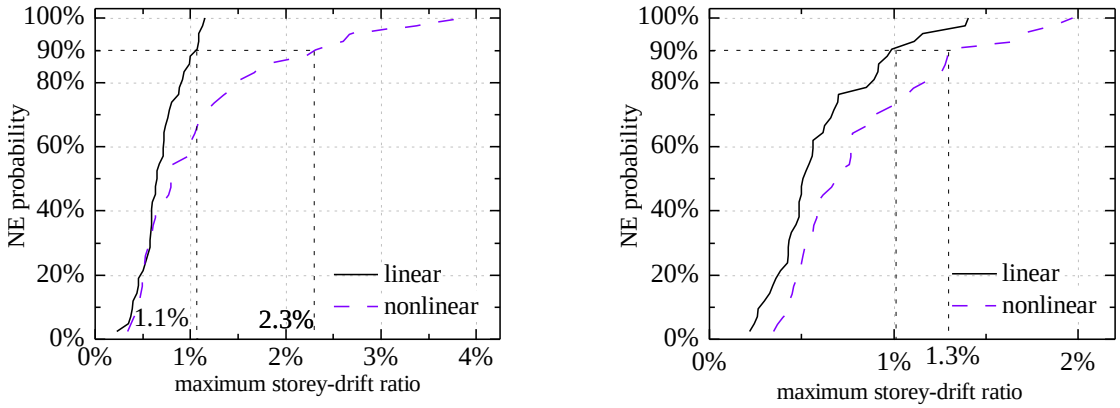

(c) building 3

(d) building 4

Figure 5.16: Non-exceedance probability distribution of the maximum storey-drift ratio for the selected four buildings

Table 5.15: Comparison of maximum storey-drift ratios associated with the first storey of the upper structure

building ID	elastic-analysis-based MRS[1]			linear time history		nonlinear linear history	
	median	90th percentile		median	90th percentile	median	90th percentile
		C_{NE}=2.61	C_{NE}=1.67				
1	0.6%	1.7%	1.1%	0.6%	1.2%	1.4%	2.6%
2	0.5%	1.2%	0.8%	0.5%	0.8%	1.0%	1.9%
3	0.7%	1.8%	1.1%	0.6%	1.1%	0.8%	2.3%
4	0.5%	1.4%	0.9%	0.5%	1.0%	0.7%	1.3%

Note: 1. MRS=model response spectrum

To investigate the inconsistency between the results obtained from the elastic-analysis-based modal response spectrum analysis and nonlinear time history analysis, a comparison is made on the maximum storey-drift ratios at the first storey of the upper structure associated with elastic-analysis-based modal response spectrum analysis, linear time history and nonlinear time history analyses. The comparison is presented in Table 5.15. Note that the elastic-analysis-based modal response spectrum analysis is different from the elastic model response analysis. The elastic model response analysis considers the linear behavior of the system only. The elastic-analysis-based modal response spectrum analysis evalauted the maximum storey-drift ratio for the first storey of the upper structure based on Eq. (3.1). The shear force V_{Ub} in Eq.(3.1) is calculated by the elastic modal response spectrum analysis, and $C_d=R=R_dR_0$ based on NBCC 2010 (NBCC, 2010). The median value is computed based the design response spectrum and the 90th percentile value is computed based on the factored design response spectrum, as shown in Eq. (3.42). In addition, the median and 90th percentile values for the linear and nonlinear time history analyses are determined from the maximum storey-drift distribution curves shown in Figures 5.16 (a) ~ (d). As demonstrated in Table 5.15, the following are observed:

(1) The median values of the maximum storey-drift ratios for the first storey of the upper structure computed from the elastic-analysis-based modal response spectrum analysis are very close to that computed from the linear time history analysis. Nevertheless, the 90th percentile value computed from the elastic-analysis-based modal response spectrum analysis by setting C_{NE}=2.61 is greater than that computed from the linear time history analysis. The scale factor C_{NE} determines the magnitude of the factored design response spectrum, as shown in Eq. (3.42). By considering the uncertainty of the ground motion as well as the uncertainty associated with the design procedure, the logarithmic standard deviation β_R is set as 0.75 and the corresponding C_{NE} is set as 2.61, as discussed in section 3.5. However, the linear time history analysis carried out herein only accounts for the uncertainty associated with ground motion but the uncertainty associated with the design procedure is not involved. If only the uncertainty associated with the ground motion is considered, the logarithmic

standard deviation β_R is 0.4 (Pang et.al, 2011), and the scale factor $C_{NE}=\exp[\Phi^{-1}(0.9)\times 0.4+\ln(1)]=1.67$. As shown in Table 5.15, the calculated 90th percentile value agrees well with that of the linear time history analyses if $C_{NE}=1.67$. Consequently, it is concluded that the results from elastic-analysis-based modal response spectrum can well represent the linear behavior of the combined framing systems.

(2) Compared to the results obtained from the linear analyses, the maximum storey-drift ratios at the first storey of the upper structure, both the median and the 90th percentile values, increase considerably but the results associated with the lower structure decrease if the nonlinear structural behavior is considered, as demonstrated in Table 5.15 and Figures 5.17 (a) ~ (d). This is a result of the fact that under the earthquake loading, the first storey of the upper structure reaches the maximum strength at first, as shown in Figures 5.18 (a) and (b). The storey drift corresponds to the maximum shear force of the OSB-sheathed shear wall is 30.83 mm, which can be seen from Table 5.13 and Figure 5.13. When the building 1 is subjected to the Northridge earthquake ground motion, the first time that the storey drift for the first storey of the upper structure is greater than 30.83 mm is marked by point "A" in Figures 5.18 (a) and (b). Once the upper structure reaches its maximum strength, the stiffness turns to be zero based on the hysteretic model of CFS shear wall, as shown in Figure 5.13. With a large storey drift located at the first storey of the upper structure the earthquake energy dissipation then is primarily concentrated at the first storey of the upper structure which deviates the lower structure from experiencing large deformations. Therefore, the maximum storey-drift ratio associated with the lower structure of building 1 decreases if the nonlinear structural behavior is accounted for, as shown in Figure 5.17 (a).

In addition, the maximum lateral displacement of each storey obtained from the nonlinear analyses decreases as the result of decrease of the maximum storey-drift ratio associated with the lower structure. An interesting point observed from of the results of the nonlinear analysis is that although the maximum storey-drift ratio at the first storey of the upper structure increases considerably, the lateral displacements of other storeys of the upper structures decrease as shown in Figures 5.17 (a) ~ (d). This is due to the decrease of the maximum storey-drift ratio in the lower structure. With the concentrated deformation at the first storey of the upper structure, the maximum storey-drift ratio and lateral displacement of the lower structures decreases. The, the decrease of the maximum lateral displacement in the lower structure consequently results in the decrease of the lateral displacement of the upper structure.

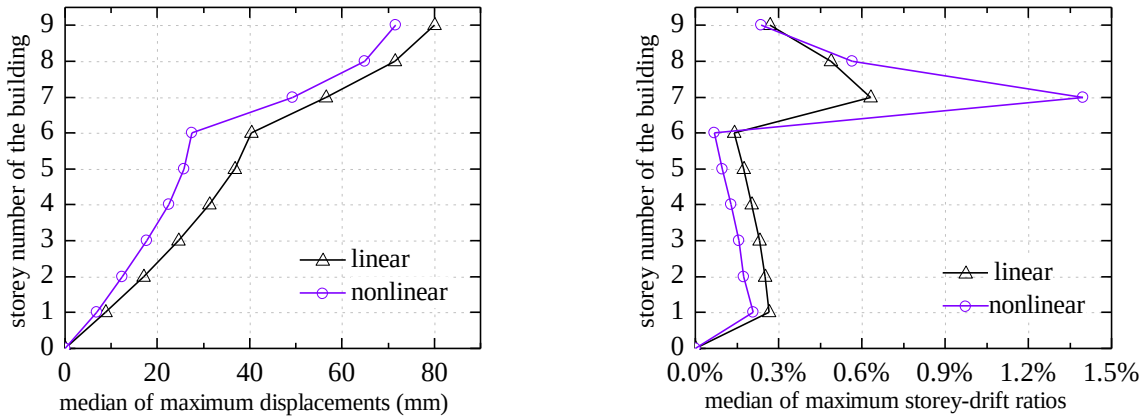

(a) building 1

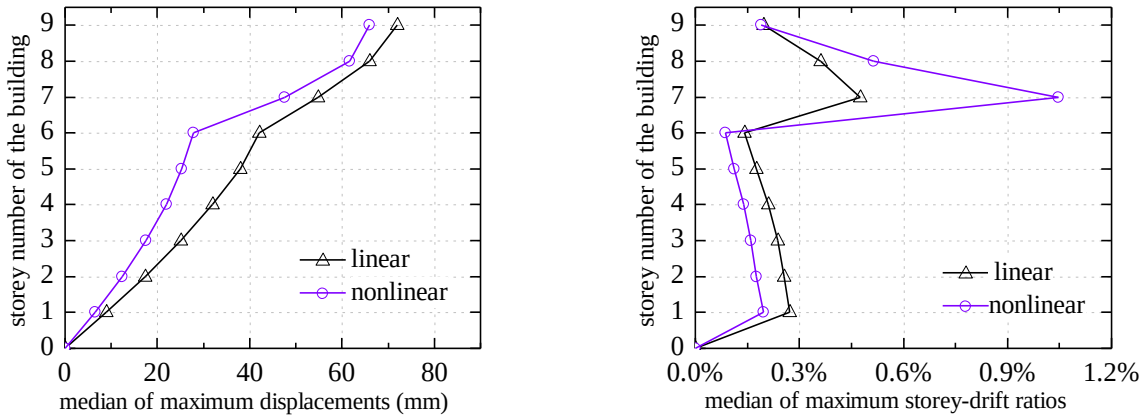

(b) building 2

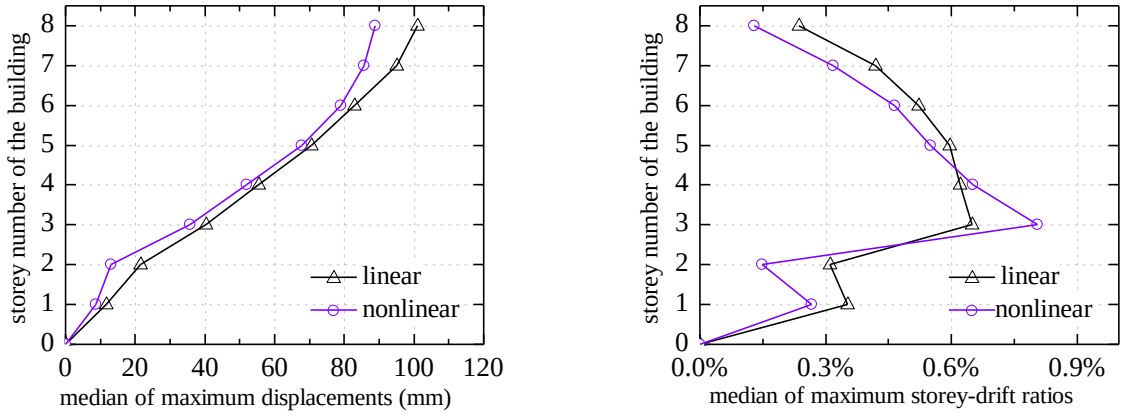

(c) building 3

Figure 5.17: Comparison of linear and nonlinear time history results

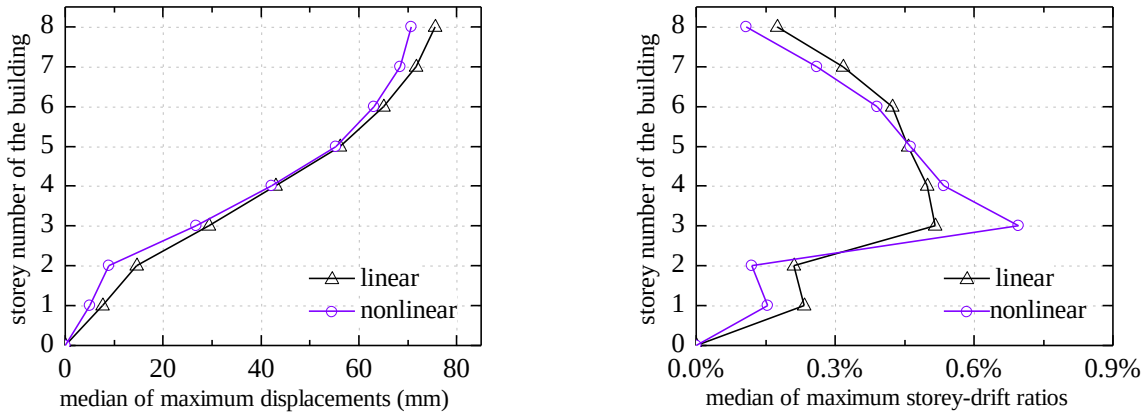

(d) building 4

Figure 5.17: Comparison of linear and nonlinear time history results (continued)

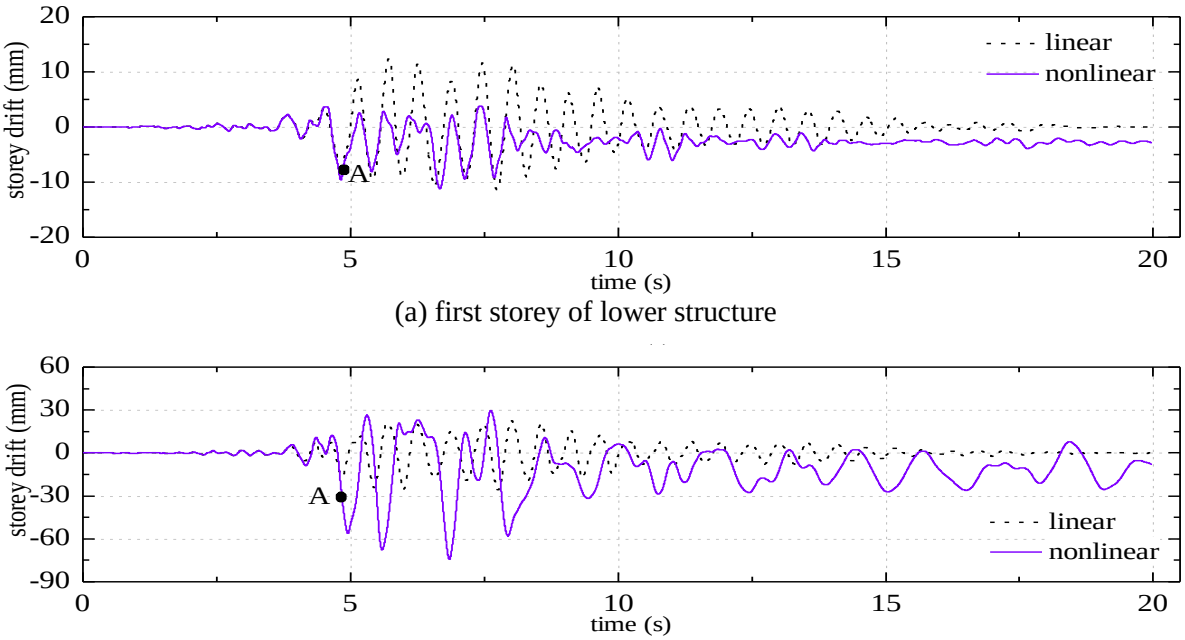

(a) first storey of lower structure

(b) first storey of upper structure

Figure 5.18: Seismic response of building 1 under one ground motion of the Northridge earthquake

Upon the foregoing discussion, it is seen the inconsistency between the elastic-analysis-based modal response spectrum analysis and the nonlinear time history analysis is not resulted from the proposed approaches to evaluate the shear-force-amplification factor α_U. The primary reason of the inconsistency is associated with use the Newmark's "equal displacement rule" to compute the inelastic displacement, which may not be appropriate. By adopting the Newmark's "equal displacement rule", the inelastic maximum storey-drift ratio calculated from Eq.(3.1), i.e., elastic-analysis-based modal response spectrum analysis, is equal to the elastic maximum storey-drift ratio.

However, the nonlinear maximum storey-drift ratio at the first storey of the upper structure in fact is greater than the elastic result, as shown in Figures 5.17 (a) ~ (d). In other words, the maximum storey-drift ratio may be underestimated by conducting the linear analysis such as that for buildings 1 and 3 listed in Table 5.15. To ensure that the elastic-analysis-based modal response spectrum analysis can well represent the nonlinear behavior of the combined framing systems, a more appropriate value of C_d should be selected in Eq. (3.1). However, to investigate how to determine the appropriate value of the C_d for a SFRS is complex and out of the scope of this study. In this study, a few suggestions on the determination values of C_d are discussed in the following section. The issue of selection C_d is going to be carried out in the future study.

5.6.4 Discussion on C_d factor

In fact, the Newmark's "equal displacement rule" is only valid for the buildings with long period (Chopra, 2007). For buildings in practice, the "equal energy rule" may be more appropriate. The initial values of the ductility-related force modification factor R_d for the CFS shear walls specified in NBCC 2010 are determined by the Newmark's "equal energy rule" (Balh & Rogers, 2011). By adopting the "equal energy rule", the deflection amplification factor C_d has the following relationship with the response modification factor R:

$$C_d = \frac{R^2 + 1}{2} \tag{5.28}$$

where $R=R_dR_0$ based on NBCC 2010. Then, by substituting C_d , as shown in Eq. (5.28), and $R=R_dR_0$ into Eq.(3.1), the following equation can be derived:

$$\Delta_U = \frac{V_{Ub}}{k_U} \frac{\left(R_d R_0\right)^2 + 1}{2R_d R_0} \tag{5.29}$$

Based on Eq. (5.29), it is seen that the maximum storey-drift ratio is closely related with the seismic response modification factor R (R_dR_0). The larger the value of the factor $R(R_dR_0)$, the greater magnitude of storey-drift ratio Δ_U. Therefore, appropriate values of R (R_dR_0) should be selected for the CFS shear wall systems. For the four selected buildings shown in Table 5.15, the elastic base shear force for the first storey of the upper structure can be evaluated by the elastic modal response spectrum analysis (Chopra, 2007). On the other hand, the yield shear force of the OSB-sheathed CFS shear wall can be evaluated based on the experimental results shown in Table 5.13. The yield shear force V_y for the double-sided OSB-sheathed CFS shear walls is 30.16 kN per meter. Then, the response modification factor R can be determined by the definition as follows:

Table 5.16: Comparison of adjusted elastic-analysis-based modal response spectrum analysis and nonlinear time history analysis

building ID	R ($R_d R_0$)	C_d	Eq.(5.29)		nonlinear time history	
			median	90th percentile	median	90th percentile
1	2.49	3.59	0.9%	2.4%	1.4%	2.6%
2	1.85	2.22	0.6%	1.5%	1.0%	1.9%
3	2.61	3.91	1.0%	2.6%	0.8%	2.3%
4	2.08	2.67	0.7%	1.8%	0.7%	1.3%

$$R = R_d R_0 = \frac{V_{Ub}}{V_y} \tag{5.30}$$

The calculated values of $R_d R_0$ for the selected four buildings are listed in Table 5.16. With the values of $R_d R_0$ computed, the nonlinear maximum storey-drift ratio for the first storey of the CFS frames can then be estimated by Eq. (5.29). By comping Table 5.16 to Table 5.15, it is seen that the resulted maximum storey-drift ratio with the 90% NE probability computed by the elastic-analysis-based modal response spectrum analysis with the adoption of Eq.(5.29) has better accuracy than that obtained based on the "equal displacement rule". Therefore, it is recommended that the value of deflection amplification C_d be determined by (5.28) rather than C_d=$R_d R_0$. However, such recommendation needs to be further investigated in the future study.

In addition to the selection of C_d, it is also noted that the proposed approach considers the requirement on the lateral stiffness of the design only while the requirement on the lateral strength has not been accounted for. However, the lateral strength of the structure may also significantly influence the nonlinear structural behaviour. According to the current code requirement (ASCE, 2010; NBCC, 2010), the yield shear force of the SFRS should not be less than the calculated elastic shear force divided by the code -specified R ($R_d R_0$) value. Therefore, for all the feasible lateral designs yielded from the proposed approach of this study, such strength requirement needs to be further checked. Only those lateral designs that satisfy both the stiffness requirement and the strength requirement can be used in the buildings with combined framing systems.

5.7 Conclusions

Presented in this chapter is the development of simplified approaches for evaluating feasible stiffness distributions and seismic loads of the mid-rise buildings with vertical combination of framing systems for the Canadian application. The Canadian approaches are developed by modifying the USA approaches that are presented in Chapters 3 and 4 with the consideration of the differences between the ASCE 7 (ASCE, 2010) and the NBCC 2010 (NBCC, 2010). In addition, since the proposed

simplified approaches for evaluating the required stiffness distributions of lower and upper structures involves the nonlinear structural behavior of the combined framing systems, nonlinear time history analysis are also carried to verify the stiffness obtained from the proposed simplified approaches. The following conclusions are obtained from this study:

(1) The proposed simplified approaches are highly related to the seismic performance factors and the design response spectrum specified in the seismic design provisions. Because of the differences between the ASCE 7 and NBCC 2010 in the foregoing two aspects, the proposed simplified approaches are country specific.

(2) The ASCE 7 (ASCE, 2010) directly specifies the value of the seismic response modification factor (R) for each commonly used SFRS, while NBCC 2010 (NBCC, 2010) attempts to quantify the relative contribution of the overstrength (R_0) and the inelastic behavior (R_d). Furthermore, NBCC 2010 assumes that the deflection amplification factor C_d is equal to the response modification factor R, i.e., $C_d=R=R_dR_0$, but in ASCE 7 (ASCE, 2010), the provided value of C_d is usually not equal to the response modification factor R, i.e., $C_d \neq R$.

(3) The NBCC 2010 and ASCE 7 adopt different approaches to construct the design response spectrum. The ASCE 7 design spectrum is established based on the spectral shape proposed by Newmark and Hall (FEMA, 1997). However, the NBCC 2010 (NBCC, 2010) selects the uniform hazard spectrum (UHS) rather than the Newmark and Hall spectrum. The Canadian UHS spectrum provides more site-specific descriptions of the earthquake spectrum and the shape of the UHS spectra for different cities in Canada are different.

(4) The accuracy of the modified ELF and proposed two-stage analysis procedures for seismic load estimation developed based on NBCC 2010 is comparable to the similar procedures developed in Chapters 3 and 4 based on ASCE 7.

(5) The stiffness distributions of the lower and upper structures obtained from the proposed simplified approach based on NBCC 2010 are verified by the code-specified elastic-analysis-based modal response spectrum, which calculates the seismic response by the elastic modal response spectrum analysis together with the adoption of seismic performance factors. The results of code-specified elastic-analysis-based modal response spectrum show that the proposed simplified approach for evaluating required stiffness distributions of lower and upper structures based on NBCC 2010 yields a conservative design.

(6) Results from the nonlinear time history analysis confirmed that the maximum storey-drift ratio was located at the first storey of the upper structure, which is the key assumption in the development

of proposed simplified approaches. However, it is found that the elastic-analysis-based modal response spectrum analysis based on NBCC 2010 with the assumption that the deflection amplification factor is equal to the response modification factor (C_d=R=$R_d R_0$) could not provide satisfactory estimation on the nonlinear storey-drift ratio at the first storey of the upper structure. A future study on the determination of appropriate value of the deflection amplification factor C_d is recommended.

Chapter 6 Analytical approximation of equivalent modal damping ratio for buildings with vertical combination of framing systems

6.1 Introduction

This chapter presents an analytical method to approximate the equivalent modal damping ratio for buildings with vertical combination of framing systems. The conventional modal analysis for a classically damped system is briefly reviewed first. By assuming that the structures have classical damping, equations to approximate equivalent modal damping ratios are then derived. However, as the combined framing system in fact is a non-classically damped system, such approximation may induce significant error in certain cases. Therefore, errors resulted from the classical damping approximation are quantitatively analyzed. Finally, the proposed equivalent modal damping ratio together with the error quantification is validated by two examples. The examples demonstrate that the proposed approximation of equivalent modal damping ratios is applicable for most of mid-rise buildings with vertical combination of framing systems in current practice.

6.2 Conventional modal analysis of classically damped system

The equation of motion for a MDOF model, as shown in Figure 3.1 (a), under an earthquake ground motion is (Chopra, 2007)

$$\mathbf{M}\ddot{\mathbf{x}} + \mathbf{C}\dot{\mathbf{x}} + \mathbf{K}\mathbf{x} = -\mathbf{M}\boldsymbol{\tau}\ddot{x}_g \tag{6.1}$$

where **M**, **C**, **K** are mass, damping and stiffness matrices of the entire combined framing system, respectively; **x**, $\dot{\mathbf{x}}$ and $\ddot{\mathbf{x}}$ are the displacement, velocity and acceleration vector, respectively; $\ddot{x}_g$ is the earthquake ground motion acceleration; and $\boldsymbol{\tau}$ is the influence vector. The un-damped eigenvalues and eigenvectors associated with Eq.(6.1) can be solved for by the following equation:

$$\mathbf{K}\boldsymbol{\varphi} = \mathbf{M}\boldsymbol{\varphi}\boldsymbol{\Omega}^2 \tag{6.2}$$

where the matrix $\boldsymbol{\varphi}$ is the un-damped mode shape normalized with respect to the mass matrix **M**, and $\boldsymbol{\Omega}^2$ is a diagonal matrix as follows:

$$\boldsymbol{\Omega}^2 = \begin{bmatrix} \omega_1^2 & 0 & \cdots & 0 \\ 0 & \omega_2^2 & \cdots & 0 \\ \vdots & \vdots & \ddots & \vdots \\ 0 & 0 & 0 & \omega_N^2 \end{bmatrix} \tag{6.3}$$

In Eq.(6.3), ω_i is the natural frequency associated with the *i*th-mode. Having the mode shape, the displacement vector **x** can be expressed as

$$\mathbf{x} = \boldsymbol{\varphi}\mathbf{q} = \sum_{i=1}^{N} \boldsymbol{\varphi}_i q_i \tag{6.4}$$

where $\mathbf{q}$ is the modal coordinate vector with $\mathbf{q} = [q_1 \quad q_2 \quad \cdots \quad q_N]^T$. By substituting the vector $\mathbf{x}$ in Eq.(6.1) with Eq.(6.4), and then pre-multiplying both sides of Eq.(6.1) by $\boldsymbol{\varphi}^{\mathrm{T}}$, the following equation is obtained:

$$\ddot{\mathbf{q}} + \boldsymbol{\Xi}'\dot{\mathbf{q}} + \boldsymbol{\Omega}^2\mathbf{q} = -\boldsymbol{\Gamma}\ddot{x}_g \tag{6.5}$$

where

$$\boldsymbol{\Gamma} = \boldsymbol{\varphi}^T\mathbf{M}\boldsymbol{\tau} = \begin{bmatrix}\Gamma_1 & \Gamma_2 & \cdots & \Gamma_N\end{bmatrix}^T \tag{6.6}$$

$$\boldsymbol{\Xi}' = \boldsymbol{\varphi}^T\mathbf{C}\boldsymbol{\varphi} = \begin{bmatrix} \Xi'_{11} & \Xi'_{12} & \cdots & \Xi'_{1N} \\ \Xi'_{21} & \Xi'_{22} & \cdots & \Xi'_{2N} \\ \vdots & \vdots & \ddots & \vdots \\ \Xi'_{N1} & \Xi'_{N2} & \cdots & \Xi'_{NN} \end{bmatrix} \tag{6.7}$$

Let

$$\mathbf{q} = \mathrm{diag}(\Gamma_i)\mathbf{D} \tag{6.8}$$

where the operation diag(Γ_i) represents that the matrix is a diagonal one with the diagonal term being Γ_i . The substitution of the vector $\mathbf{q}$, as represented in Eq.(6.8), into Eq.(6.5) leads to

$$\ddot{\mathbf{D}} + \boldsymbol{\Xi}\dot{\mathbf{D}} + \boldsymbol{\Omega}^2\mathbf{D} = -\boldsymbol{\tau}\ddot{x}_g \tag{6.9}$$

where

$$\boldsymbol{\Xi} = \mathrm{diag}(1/\Gamma_i)\boldsymbol{\Xi}'\mathrm{diag}(\Gamma_i) = \begin{bmatrix} \Xi'_{11} & \Xi'_{12}\dfrac{\Gamma_2}{\Gamma_1} & \cdots & \Xi'_{1N}\dfrac{\Gamma_N}{\Gamma_1} \\ \Xi'_{21}\dfrac{\Gamma_1}{\Gamma_2} & \Xi'_{22} & \cdots & \Xi'_{2N}\dfrac{\Gamma_N}{\Gamma_2} \\ \vdots & \vdots & \ddots & \vdots \\ \Xi'_{N1}\dfrac{\Gamma_1}{\Gamma_N} & \Xi'_{N2}\dfrac{\Gamma_2}{\Gamma_N} & \cdots & \Xi'_{NN} \end{bmatrix} \tag{6.10}$$

For the classically damped system, the un-damped mode shape is orthogonal with respect to the damping matrix $\mathbf{C}$, i.e., the off-diagonal terms of the modal damping matrix Ξ are zero. Therefore, Eq.(6.9) can be decoupled into *N* following independent equations

$$\ddot{D}_i + 2\varsigma_i\omega_i\dot{D}_i + \omega_i^2 D_i = -\ddot{x}_g \tag{6.11}$$

where

$$\varsigma_i = \frac{\Xi_{ii}}{2\omega_i} \tag{6.12}$$

It is seen that Eq.(6.11) can be considered as the equation of motion for a single-degree-of-freedom (SDOF) system having the natural frequency ω_i and the damping ratio ζ_i. The displacement vector **x** can be determined by solving *N* independent equations as shown in Eq.(6.11), rather than by solving the *N* coupled equations as shown in Eq. (6.1). Such conventional modal analysis is widely used in current practice for regular buildings.

6.3 Approximation of equivalent modal damping ratio

6.3.1 Damping model of combined framing system

The damping matrix of the combined framing systems **C** is assembled from the corresponding damping matrices of the lower and upper structures as follows:

$$\mathbf{C} = \mathbf{C}_L + \mathbf{C}_U \tag{6.13}$$

where $\mathbf{C}_L$ and $\mathbf{C}_U$ represent the damping matrices associated with the lower and upper structures, respectively. In this study, the damping matrix of the lower structure $\mathbf{C}_L$ is constructed by the superposition of modal damping matrices (Chopra, 2007) via one of the following:

(1) stiffness proportional damping

$$\mathbf{C}_L = 2\varsigma_L \mathbf{K}\left[\sum_{i=1}^{N} \frac{\boldsymbol{\varphi}_i \boldsymbol{\varphi}_i^T}{(\omega_i)^3}\right]\mathbf{K}_L \tag{6.14 a}$$

(2) mass proportional damping

$$\mathbf{C}_L = 2\varsigma_L \mathbf{M}\left[\sum_{i=1}^{N}\left(\omega_i \boldsymbol{\varphi}_i \boldsymbol{\varphi}_i^T\right)\right]\mathbf{M}_L \tag{6.14 b}$$

(3) mass-stiffness proportional damping

$$\mathbf{C}_L = 2a\varsigma_L \mathbf{K}\left[\sum_{i=1}^{N} \frac{\boldsymbol{\varphi}_i \boldsymbol{\varphi}_i^T}{(\omega_i)^3}\right]\mathbf{K}_L + 2b\varsigma_L \mathbf{M}\left[\sum_{i=1}^{N}\left(\omega_i \boldsymbol{\varphi}_i \boldsymbol{\varphi}_i^T\right)\right]\mathbf{M}_L \tag{6.14 c}$$

where ς_L is the damping ratio of the lower structure. **K** and **M** are stiffness and mass matrices of the entire building and ω_i is the un-damped natural frequency associated with the *i*th-mode as shown in Eq.(6.3); $\mathbf{K}_L$ and $\mathbf{M}_L$ are stiffness and mass matrices which assume that both the storey-mass and lateral storey-stiffness of the upper structure are zero. Coefficients *a* and *b* are mass- and stiffness-proportional coefficients of the lower structure, respectively, with $a+b=1$.

The method to establish the damping matrix of the upper structure $\mathbf{C}_U$ is similar to that of the lower structure $\mathbf{C}_L$. By replacing ζ_L, $\mathbf{K}_L$ and $\mathbf{M}_L$ with ζ_U, $\mathbf{K}_U$ and $\mathbf{M}_U$, respectively, $\mathbf{C}_L$ is constructed as follows:

(1) stiffness proportional damping

$$\mathbf{C}_U = 2\varsigma_U \mathbf{K}\left[\sum_{i=1}^{N}\frac{\boldsymbol{\varphi}_i\boldsymbol{\varphi}_i^T}{\left(\omega_i\right)^3}\right]\mathbf{K}_U \tag{6.15 a}$$

(2) mass proportional damping

$$\mathbf{C}_U = 2\varsigma_U \mathbf{M}\left[\sum_{i=1}^{N}\left(\omega_i\boldsymbol{\varphi}_i\boldsymbol{\varphi}_i^T\right)\right]\mathbf{M}_U \tag{6.15 b}$$

(3) mass-stiffness proportional damping

$$\mathbf{C}_U = 2a\varsigma_U \mathbf{K}\left[\sum_{i=1}^{N}\frac{\boldsymbol{\varphi}_i\boldsymbol{\varphi}_i^T}{\left(\omega_i\right)^3}\right]\mathbf{K}_U + 2b\varsigma_U \mathbf{M}\left[\sum_{i=1}^{N}\left(\omega_i\boldsymbol{\varphi}_i\boldsymbol{\varphi}_i^T\right)\right]\mathbf{M}_U \tag{6.15 c}$$

Theoretically, the mass- and stiffness-proportional coefficients (*a* and *b*) associated with the lower structure can be different from those associated with the upper structure. In this study, it is assumed that values of *a* and *b* of the lower structure are the same as those of the upper one.

6.3.2 Approximation of equivalent modal damping ratio

Assume that the structure is classically damped. At first, substitute the damping matrices $\boldsymbol{C}_L$ and $\boldsymbol{C}_U$ in Eq.(6.13) with Eqs.(6.14 a) ~ （6.14 c）and Eqs. (6.15 a) ~ （6.15 c）in pairs, respectively. Then, substitute the damping matrix **C** in Eq. (6.7) with Eq.(6.13). Finally, with the substitution of Eq. (6.7) into Eqs. (6.10) and (6.12), the corresponding equivalent modal damping ratio associated with the *i*th-mode, ς_{eqi}, can be calculated as follows:

(1) stiffness proportional damping

$$\varsigma_{eqi} = \frac{\varsigma_U\boldsymbol{\varphi}_i^T\mathbf{K}_U\boldsymbol{\varphi}_i + \varsigma_L\boldsymbol{\varphi}_i^T\mathbf{K}_L\boldsymbol{\varphi}_i}{\left(\omega_i\right)^2} \tag{6.16 a}$$

(2) mass proportional damping

$$\varsigma_{eqi} = \varsigma_U\boldsymbol{\varphi}_i^T\mathbf{M}_U\boldsymbol{\varphi}_i + \varsigma_L\boldsymbol{\varphi}_i^T\mathbf{M}_L\boldsymbol{\varphi}_i \tag{6.16 b}$$

(3) mass-stiffness proportional damping

$$\varsigma_{eqi} = a\frac{\varsigma_U\boldsymbol{\varphi}_i^T\mathbf{K}_U\boldsymbol{\varphi}_i + \varsigma_L\boldsymbol{\varphi}_i^T\mathbf{K}_L\boldsymbol{\varphi}_i}{\left(\omega_i\right)^2} + b\left(\varsigma_U\boldsymbol{\varphi}_i^T\mathbf{M}_U\boldsymbol{\varphi}_i + \varsigma_L\boldsymbol{\varphi}_i^T\mathbf{M}_L\boldsymbol{\varphi}_i\right) \tag{6.16 c}$$

It can be seen the equivalent modal damping ratios shown in Eqs. (6.16 a) ~ (6.16 c) are dependent on how the damping matrix is constructed. To calculate the equivalent modal damping ratio, firstly reasonable damping matrices for the lower and upper structures should be selected from Eqs. (6.14 a)

~ （6.14 c）and (6.15 a) ~ （6.15 c）, respectively. Note Eq. (6.16 a) is the same as the composite damping rule method (Raggett, 1975), which is currently integrated into the commercial software Midas/Gen (MIDAS/Gen Program, 2000). Therefore, it can be concluded that the composite damping rule method was obtained based on the classical damping approximation with the assumption that the damping matrix is proportional to the stiffenss.

6.4 Error estimation of the approximation

The proposed equivalent modal damping ratios presented in section 6.3 are obtained based on the assumption that the buildings with vertical combination of framing system are classically damped. However, by: (1) taking Eqs. (6.14 a) ~ （6.14 c）and (6.15 a) ~ （6.15 c）in pairs into Eq.(6.13), respectively, (2) substituting Eq. (6.13) into (6.7) , and (3) further substituting Eq. (6.7) into Eq.(6.10), the off-diagonal terms of the corresponding modal damping matrices are obtained as follows:

(1) stiffness proportional damping

$$\Xi_{ij} = 2\left(\varsigma_L - \varsigma_U\right)\frac{\boldsymbol{\varphi}_i^T \mathbf{K}_L \boldsymbol{\varphi}_j}{\omega_i}\frac{\Gamma_j}{\Gamma_i} \tag{6.17 a}$$

(2) mass proportional damping

$$\Xi_{ij} = 2\left(\varsigma_L - \varsigma_U\right)\omega_i \boldsymbol{\varphi}_i^T \mathbf{M}_L \boldsymbol{\varphi}_j \frac{\Gamma_j}{\Gamma_i} \tag{6.17 b}$$

(3) mass-stiffness proportional damping

$$\Xi_{ij} = 2a\left(\varsigma_L - \varsigma_U\right)\frac{\boldsymbol{\varphi}_i^T \mathbf{K}_L \boldsymbol{\varphi}_j}{\omega_i}\frac{\Gamma_j}{\Gamma_i} + 2b\left(\varsigma_L - \varsigma_U\right)\omega_i \boldsymbol{\varphi}_i^T \mathbf{M}_L \boldsymbol{\varphi}_j \frac{\Gamma_j}{\Gamma_i} \tag{6.17 c}$$

As demonstrated in Eqs. (6.17 a) ~ (6.17 c), if the damping ratio of the lower structure is not equal to that of the upper one, i.e., $\varsigma_L \neq \varsigma_U$, the off-diagonal term Ξ_{ij} will not be zero. In this case, the structure is non-classically damped. Therefore, using the proposed equivalent modal damping ratio to evaluate the seismic response may result in errors, since the proposed equivalent modal damping ratio is based on the assumption of classical damping. In order to determine whether the proposed equivalent modal damping ratio is acceptable for design practice, the error induced by the classical damping assumption needs to be investigated.

6.4.1 Theory of error estimation

Recall the modal analysis discussed in section 6.2. Based on Eqs.(6.4) and (6.8), the response for any quantity of interest *r* can be can be calculated as follows(Chopra, 2007):

$$r = \sum_{i=1}^{N} r_i = \sum_{i=1}^{N} \mathbf{l}^T \boldsymbol{\varphi}_i \Gamma_i D_i \tag{6.18}$$

where $\mathbf{l}^T$ is the transform vector between the response quantity r and the displacement vector $\mathbf{x}$, and D_i is the response of following equation:

$$\ddot{D}_i + \sum_{i=1}^{N} \Xi_{ij} \dot{D}_j + \omega_i^2 D = -\ddot{x}_g \tag{6.19}$$

Note Eq. (6.19), which is different from Eq.(6.11), contains off-diagonal terms of the modal damping matrix $\boldsymbol{\Xi}$. Then, based on Eq.(6.18), the mean square for the quantity r can be computed as

$$E\left(r^2\right) = \sum_{i=1}^{N}\sum_{j=1}^{N} E\left(r_i r_j\right) = \sum_{i=1}^{N}\sum_{j=1}^{N} \left(\mathbf{l}^T \boldsymbol{\varphi}_i \Gamma_i\right)\left(\mathbf{l}^T \boldsymbol{\varphi}_j \Gamma_j\right) E\left(D_i D_j\right) \tag{6.20}$$

where $E(\cdot)$ represents the expected value. In addition, the correlation coefficient ρ_{ij} is defined as follows:

$$\rho_{ij} = \frac{E\left(D_i D_j\right)}{\sqrt{E\left(D_i^2\right)}\sqrt{E\left(D_j^2\right)}} \tag{6.21}$$

Assume: (1) the earthquake ground motion is a white noise process with a constant power spectral density being S_0; and (2) the earthquake ground motion has a constant peak factor p, which is defined as

$$p = \frac{D_{\max,i}}{\sqrt{E\left(D_i^2\right)}} \tag{6.22}$$

where $D_{max,i}$ represents the maximum displacement response of D_i associated with Eq.(6.19). Finally, in accordance with Eqs. (6.20) ~ (6.22), the maximum value of the response quantity r can be calculated as

$$\begin{aligned} r_{\max} &= p\sqrt{E\left(r^2\right)} = p\sqrt{\sum_{i=1}^{N}\sum_{j=1}^{N} \rho_{ij}\left(\mathbf{l}^T \boldsymbol{\varphi}_i \Gamma_i\right)\left(\mathbf{l}^T \boldsymbol{\varphi}_j \Gamma_j\right)\frac{D_{\max,i}}{p}\frac{D_{\max,j}}{p}} \\ &= \sqrt{\sum_{i=1}^{N}\sum_{j=1}^{N} \rho_{ij} r_{\max,i} r_{\max,j}} \end{aligned} \tag{6.23}$$

where $r_{max,i}$ is the maximum response of r associated with the ith-mode calculated as follows:

$$r_{\max,i} = \mathbf{l}^T \boldsymbol{\varphi}_i \Gamma_i D_{\max,i} \tag{6.24}$$

Eq. (6.23) represents the typical modal response spectrum analysis that adopts the CQC combination rule to combine the peak modal responses based on the un-damped modal properties. If the building structure is classically damped, the modal damping matrix $\boldsymbol{\Xi}$ is a diagonal one. The seismic response

of D_i can be determined from the SDOF system with the natural frequency ω_i and the damping ratio ς_i, as shown in Eq. (6.11). The maximum displacement response $D_{max,i}$ can be directly determined from the code-specified response acceleration spectrum (ASCE, 2010) as follows

$$D_{\max,i} = \frac{S_a(\omega_i, \varsigma_i)}{\omega_i^2} \tag{6.25}$$

where $S_a(\omega_i, \varsigma_i)$ is the code-specified response acceleration (Figure 1.4). In addition, if the buildings are classically damped, the correlation coefficient ρ_{ij} in (6.23) can be theoretically solved based on Eq.(6.21), as presented in Eq. (F.41) in Appendix F.2.

However, when the building structures are non-classically damped, the modal damping matrix is not a diagonal one. The maximum response of D_i, as shown in Eq.(6.19), is related not only to the natural frequency ω_i and the diagonal damping ratio ς_i (Ξ_{ii}), but also to the off-diagonal term of the modal damping matrix Ξ_{ij}. Therefore, the maximum displacement response $D_{max,i}$ cannot be directly determined by Eq.(6.25). As well, the analytical solution of the correlation coefficient ρ_{ij} for the non-classically damped system also cannot be determined based on Eq.(F.41) in Appendix F. The correlation coefficient ρ_{ij} for the non-classically damped system can be solved for only by a numerical approach based on Eq.(6.21) (Falsone & Muscolino, 1999).

6.4.2 Formula to estimate modal errors

The proposed equivalent modal damping ratio is obtained by neglecting the off-diagonal terms of the modal damping matrix $\boldsymbol{\Xi}$; consequently, Eq.(6.19) becomes

$$\ddot{D}_{0i} + 2\varsigma_{eqi}\omega_i\dot{D}_{0i} + \omega_i^2 D_{0i} = -\ddot{x}_g \tag{6.26}$$

In order to distinguish the accurate and approximate response, the subscript "0" denotes the approximate response. Therefore, In Eq.(6.26), D_{0i} represents the approximation of D_i. Let δ_i be the error of the maximum response associated with the ith-mode, the relationship between the accurate and approximate response is

$$r_{\max,i} = r_{0\max,i}(1-\delta_i) \tag{6.27}$$

From Eqs. (6.22) and (6.24), δ_i can be evaluated as

$$\delta_i = 1 - \sqrt{1+\varepsilon_i} \tag{6.28}$$

where ε_i is defined as

$$E\left(D_i^2\right) = E\left(D_{0,i}^2\right)\left(1+\varepsilon_i\right) \tag{6.29}$$

As discussed in Appendix F.1, the estimation of ε_i can be approximated as

$$\varepsilon_i = -\sum_{j=1, j\neq i}^{N} \rho_{ij} \frac{\Xi_{ij}}{\sqrt{\Xi_{ii}\Xi_{jj}}} \tag{6.30}$$

where ρ_{ij} is the correlation coefficient between the *i*th- and *j*th-modes for the classically damped system, as presented in Eq.(F.41) in Appendix F.2. From Eqs. (6.28) and (6.30), it can be seen that the error is related not only to the conventional non-proportional damping index $\frac{\Xi_{ij}}{\sqrt{\Xi_{ii}\Xi_{jj}}}$ (Falsone & Muscolino, 1999), but also to the correlation coefficient ρ_{ij}. Since the correlation coefficient ρ_{ij} may become significant if the natural frequencies of two different modes are close to each other, as discussed in Appendix F.2, large values of ε_i and δ_i may occur if the *j*th-mode natural frequency is close to the *i*th-mode natural frequency.

6.4.3 Error of seismic response

Based on the CQC modal combination rule shown in Eq.(6.23), it is noted that the error of the final seismic response r_{max} is dominated primarily by vibration modes that contributes significantly to the seismic quantity *r*. For modes that do not dominate the seismic response, the modal error has almost no effect on the structure response. Therefore, to limit the error of the seismic quantity *r* to be within an acceptable range, it is required that only the modal errors associated with the dominating modes of the structure are within a certain range. Use δ_r to define the error of r_{max} induced by the proposed equivalent modal damping ratio as follows:

$$r_{\max} = r_{0\max}(1-\delta_r) \tag{6.31}$$

From Eq.(6.23), it is seen the maximum seismic response r_{max} is related not only to the modal seismic response $r_{max,i}$, but also to the correlation between the *i*th- and *j*th-modes, i.e., $\rho_{ij} r_{\max,i} r_{\max,j}$. In general, the correlation coefficient ρ_{ij} is limited to the range between zero and unity and for most cases $\rho_{ij} \approx 0$, as discussed in Appendix F.2. Therefore, although the correlation term $\rho_{ij} r_{\max,i} r_{\max,j}$ has certain influence on the error of the seismic response *r*, such influence can be neglected when estimating the error of the seismic quantity *r*. Accordingly, the CQC combination rule shown in Eq.(6.23) is reduced to the following SRSS combination rule when estimating the error δ_r:

$$r_{\max} = \sqrt{\sum_{i=1}^{N} \left(r_{\max,i}\right)^2} \tag{6.32}$$

Based on Eqs. (6.27) and (6.31) ~ (6.32), it can be concluded that

$$\delta_{r,\min} \approx 1 - \sqrt{1 + \max\left[\left(1-\delta_i\right)^2 - 1\right]} \tag{6.33 a}$$

$$\delta_{r,\max} \approx 1 - \sqrt{1 + \min\left[\left(1-\delta_i\right)^2 - 1\right]} \tag{6.33 b}$$

where $\delta_{r,\min}$ and $\delta_{r,\max}$ represent the minimum and maximum error of the seismic quantity r associated with the proposed equivalent modal damping ratio, respectively, and the subscript i refers to the dominating modes of the structure. It is noted that the dominating modes for different seismic quantities r are different. For example, the base shear force of a regular building is dominated primarily by the first mode, but the shear force of the top storey may be dominated also by higher vibration modes other than the first mode. Nevertheless, all the seismic response qualities r are calculated in accordance with $\boldsymbol{\varphi}_i\Gamma_i$ as shown in Eq. (6.24). Therefore, the dominating modes can be determined based on the quantities $\boldsymbol{\varphi}_i\Gamma_i$. In accordance with the modal expansion theory (Chopra, 2007),

$$\sum_{i=1}^{n}\varphi_{ij}\Gamma_i = 1 \tag{6.34}$$

where the subscripts i and j represent the ith-mode and jth-DOF, respectively. The ith-vibration mode that has a significant $\varphi_{ij}\Gamma_i$ value is the dominating mode of the jth-DOF.

6.5 Examples

The suggested equivalent modal damping ratios are applied to the two hypothetical buildings discussed in sections 3.6.

6.5.1 Example 6-1

The building is the same as that discussed in section 3.6.1. The damping ratios of the lower RC and upper CFS frames, ς_L and ς_U, are set as 5% and 2%, respectively. In accordance with the obtained feasible lateral designs for the lower RC and upper CFS structures shown in Figure 3.9 (b), all columns shown in Figure 3.8 are selected as the columns in the RC moment frame and the corresponding CFS shear wall length is 43.2 m. The basic mass, stiffness and damping properties of the combined framing systems are summarized in Table 6.1.

Equivalent modal damping ratio

With the effective storey-masses and storey-stiffnesses presented in Table 6.1, the conventional modal response spectrum analysis (Chopra, 2007) is carried out for the nine-storey building by adopting the MDOF model as shown in Figure 3.1 (a). The calculated natural frequencies of the nine-storey combined framing system are listed in Table 6.2. Assume both the lower and upper structures have stiffness proportional damping. The proposed equivalent modal damping ratio associated with the ith-mode can be calculated based on Eq.(6.16 a). As indicated in Table 6.3, the equivalent modal damping ratios associated with the eighth- and ninth-modes are equal to the damping ratio of the

lower structure ς_L. This can be explained by the un-damped mode shapes of the eighth- and ninth-modes. As shown in Figure 6.1, the three-storey upper structure keeps almost still and the vibration occurs primarily at the lower structure for the eighth- and ninth-modes. Therefore, the earthquake energy is dissipated primarily by the lower structure. The equivalent damping ratios associated with the eighth- and ninth-modes are equal to the damping ratio of the lower structure ς_L. For other vibration modes, both the lower and upper structures deform and the earthquake energy is dissipated by both of them. Consequently, based on Eq. (6.16 a), the modal damping ratios lie between ς_L and ς_U. If most of the earthquake energy is dissipated by the lower structure, the damping ratio is close to that of the lower one ς_L, such as the first-, third-, fifth- and seventh-modes. Otherwise, the damping ratio is close to that of the upper one ς_U, such as the second-, fourth- and sixth-modes.

Table 6.1: Structural properties of Example 6-1

	storey number	storey-mass (kg)	SFRSs	storey-stiffness (kN/m)	damping ratio
lower structure	6	96,113	RC moment frame, 16 columns in moment frame	8.66×10^5	0.05
upper structure	3	219,352	CFS shear wall, with the wall length being 43.2 m	1.66×10^5	0.02

Table 6.2: Natural frequencies of Example 6-1

mode number	1	2	3	4	5	6	7	8	9
natural frequency (Hz)	11.68	22.54	43.94	54.06	71.62	76.49	94.95	111.66	122.18
period (s)	0.54	0.28	0.14	0.12	0.09	0.08	0.07	0.06	0.05

Table 6.3: Approximated equivalent modal damping ratio and modal error of Example 6-1

mode number	1	2	3	4	5	6	7	8	9
equivalent damping ratio ς_{eqi}	0.044	0.029	0.043	0.027	0.041	0.028	0.049	0.050	0.050
modal error δ_i	0.1%	0.4%	0.8%	3.4%	6.0%	17.4%	0.3%	0.2%	0.1%

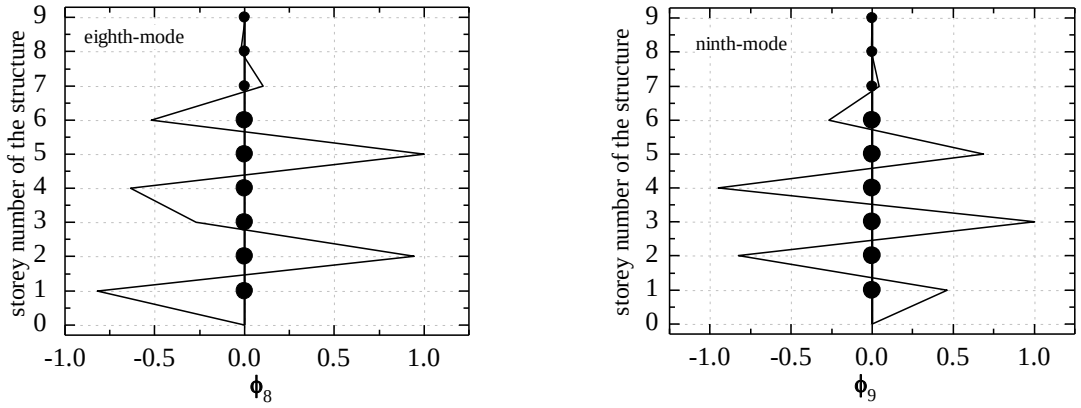

Figure 6.1: Eighth and ninth mode shapes of Example 6-1

Table 6.4: Correlation coefficients ρ_{ij} of Example 6-1

*i*th-mode \ *j*th-mode	1	2	3	4	5	6	7	8	9
1	1.000	0.010	0.003	0.001	0.001	0.001	0.001	0.001	0.001
2	0.010	1.000	0.011	0.003	0.003	0.002	0.002	0.002	0.001
3	0.003	0.011	1.000	0.096	0.027	0.014	0.013	0.008	0.007
4	0.001	0.003	0.096	1.000	0.054	0.024	0.017	0.010	0.008
5	0.001	0.003	0.027	0.054	1.000	0.508	0.091	0.039	0.027
6	0.001	0.002	0.014	0.024	0.508	1.000	0.111	0.040	0.026
7	0.001	0.002	0.013	0.017	0.091	0.111	1.000	0.270	0.132
8	0.001	0.002	0.008	0.010	0.039	0.040	0.270	1.000	0.550
9	0.001	0.001	0.007	0.008	0.027	0.026	0.132	0.550	1.000

Table 6.5: Conventional non-classical modal damping index $\frac{\Xi_{ij}}{\sqrt{\Xi_{ii}\Xi_{jj}}}$ of Example 6-1

*i*th-mode \ *j*th-mode	1	2	3	4	5	6	7	8	9
1	0.00	0.19	-0.04	-0.02	0.01	0.01	-0.01	0.00	0.00
2	0.54	0.00	0.17	0.02	-0.05	-0.02	0.03	-0.01	0.00
3	-0.13	0.21	0.00	0.15	-0.01	-0.02	0.01	0.00	0.00
4	-0.23	0.09	0.57	0.00	0.22	0.06	-0.08	0.03	-0.01
5	0.11	-0.14	-0.02	0.14	0.00	0.22	-0.01	0.00	0.00
6	0.20	-0.16	-0.15	0.11	0.60	0.00	0.12	-0.03	0.01
7	-0.10	0.11	0.03	-0.07	-0.02	0.06	0.00	0.01	0.00
8	0.09	-0.10	-0.02	0.06	0.01	-0.04	0.01	0.00	0.00
9	-0.09	0.10	0.02	-0.06	0.00	0.04	-0.01	0.00	0.00

Table 6.6: Values of $\varphi_{ij}\Gamma_i$ of Example 6-1

*j*th-DOF \ *i*th-mode	1	2	3	4	5	6	7	8	9	dominating modes
1	0.19	0.13	0.20	0.07	0.14	0.06	0.13	0.06	0.02	1, 2, 3, 5, 7
2	0.38	0.24	0.31	0.09	0.10	0.03	-0.04	-0.07	-0.03	1, 2, 3
3	0.55	0.32	0.26	0.04	-0.07	-0.04	-0.12	0.02	0.04	1,2,3
4	0.71	0.36	0.09	-0.04	-0.15	-0.05	0.07	0.05	-0.03	1,2
5	0.84	0.35	-0.13	-0.08	-0.03	0.01	0.10	-0.08	0.03	1, 2, 3
6	0.94	0.30	-0.28	-0.07	0.13	0.06	-0.10	0.04	-0.01	1, 2, 3
7	1.29	-0.17	-0.37	0.27	0.11	-0.16	0.03	-0.01	0.00	1, 2, 3, 4
8	1.55	-0.59	-0.04	0.15	-0.23	0.17	-0.01	0.00	0.00	1, 2, 4, 5
9	1.68	-0.84	0.33	-0.22	0.12	-0.07	0.00	0.00	0.00	1, 2, 3, 4

Modal error estimation

The modal error δ_i associated with the proposed equivalent modal damping ratio is estimated by Eq.(6.27), as shown in Table 6.3. Note that from the definition of the modal error δ_i as presented in Eq. (6.27), positive value signifies that the proposed equivalent modal damping ratio overestimates the response while negative value denotes that the proposed equivalent damping ratio underestimates the response. Table 6.3 shows that the modal error has following features:

(1) A large magnitude of δ_i occurs when natural frequencies of two vibration modes are close to each other. For example, the natural frequency of the fifth-mode is close to that of the sixth-mode, as shown in Table 6.2. Based on Eq. (F.41) in Appendix F.2, the correlation coefficient between these two modes, i.e., ρ_{65}, has a significant value, i.e., 0.508, as shown in Table 6.4. In addition, based on Eq.(6.17 a), the off-diagonal term Ξ_{65} also has a significant value and so does the conventional non-proportional modal damping index $\frac{\Xi_{65}}{\sqrt{\Xi_{66}\Xi_{55}}}$, i.e., 0.60, as shown in Table 6.5. Therefore, based on Eqs. (6.27) ~ (6.30), ε_6 has a significant value and so does the modal error δ_6, i.e., 17.4%, as demonstrated in Table 6.3.

The conventional non-proportional modal damping index $\frac{\Xi_{ij}}{\sqrt{\Xi_{ii}\Xi_{jj}}}$ is widely used to characterize the extent of the non-proportional damping. However, by comparing Table 6.3 and Table 6.5, it is seen that the conventional non-proportional damping index $\frac{\Xi_{65}}{\sqrt{\Xi_{55}\Xi_{66}}}$ (Falsone & Muscolino, 1999) cannot accurately represent the extent of the non-proportional damping in certain cases. For example, the conventional non-proportional damping index between the second- and first-modes $\frac{\Xi_{21}}{\sqrt{\Xi_{11}\Xi_{22}}}$ is 0.54,

which is quite close to that between the sixth and fifth-modes $\frac{\Xi_{65}}{\sqrt{\Xi_{55}\Xi_{66}}}$, i.e., 0.6, as shown in Table 6.5. The modal error of the second mode δ_2 should be comparable to that of the sixth mode δ_6 if the conventional non-proportional damping index can accurately represent the extent of the non-proportional damping. However, the modal error of the second mode δ_2, i.e., 0.4%, in fact is much smaller than that of the sixth mode δ_6, i.e., 17.4%, as shown in Table 6.3. This is a result of the fact that the extent of the non-proportional damping is related not only to the conventional non-proportional modal damping index, but also to the correlation coefficient. Since the un-damped first and second modes have well separated natural frequencies, as shown in Table 6.2, the correlation coefficient ρ_{12} is negligible, being 0.010 as shown in Table 6.4. Therefore, the error of the second mode δ_2 is negligible due to the smaller value of ρ_{12}, as shown in Table 6.3. Accordingly, $\rho_{ij}\frac{\Xi_{ij}}{\sqrt{\Xi_{ii}\Xi_{jj}}}$ is a better index to characterize the extent of the non-proportional damping compared to the conventional non-proportional damping index $\frac{\Xi_{ij}}{\sqrt{\Xi_{ii}\Xi_{jj}}}$, and should be used as the index of the non-proportional damping.

(2) By using the proposed equivalent modal damping ratio, the modal seismic response is always overestimated for this example, as shown in Table 6.3. This is a primary result of the fact that the damping ratio of the lower structure is larger than that of the upper one. Usually, the large magnitude of modal error δ_i occurs when two modes have close natural frequencies. For the case where the natural frequencies of two modes are close to each other and $\varsigma_L > \varsigma_U$, the off-diagonal terms Ξ_{ij} are positive and ε_i is therefore negative, based on Eqs. (6.17 a) and (6.30), respectively. Furthermore, the modal error δ_i is positive based on Eq. (6.28), which indicates the proposed equivalent modal damping ratio will result in an overestimated seismic response associated with the *i*th-mode. On the other hand, if the damping ratio of the lower structure is less than that of the upper one, i.e., $\varsigma_L < \varsigma_U$, the proposed equivalent modal damping ratio will lead to an underestimation of the seismic response associated with the *i*th-mode.

Error of seismic response

The calculated values $\varphi_{ij}\Gamma_i$ for the nine-story combined framing system are presnted in Table 6.6. Also shown in the table are the dominating modes for each degree-of-freedom (DOF). For example, from Table 6.6, it is seen the dominating modes for the 1st-DOF are first, second, third, fifth and seventh modes. By considering all the DOFs in the MDOF model, it can be seen the entire builing is domianted by the first to fifth and seventh modes, as shown in Table 6.6. The error of the seismic response is related only to these dominating modes. Then, by substituting the modal errors δ_i

associated with these dominating modes that are shown in Table 6.3 into Eqs.(6.33 a) ~ (6.33 b), it is obtained that the error for all the seismic response quantities induced by the proposed equivalent modal damping ratios are limited to the range between 0.1% and 6%. The seismic response approximated from the proposed equivaelnt modal damping ratio is almost the same as that of the accurate one. Althought the modal error associated with the sixth mode is 17.4% as shown in Table 6.3, such error has almost no effect on the seismic response, since the sixth mode is not the dominating mode of the structure.

As indicated in the foregoing discussion, a large modal error δ_i occurs when natural frequencies of two vibration modes are close to each other. On the other hand, the error of seismic response associated with the proposed equivalent modal damping ratio is influenced primarily by the dominating modes that make a significant contribution to the seismic response. Therefore, it is concluded that the large error of seismic response induced by the proposed equivalent modal damping ratio usually occurs when the dominating modes of the structures have closely spaced natural frequencies. As for this example, since the dominating modes of the structures, i.e., first- to fifth- and seventh modes, have well separated natural frequencies, as shown in Table 6.2, the error of the seismic response associated with the proposed equivalent modal damping ratio is acceptable. The proposed equivalent modal damping ratio can be used for this nine-storey building with combined framing systems.

Method validation

In order to verify the conclusion made in the previous discussions that the proposed equivalent modal damping ratio is acceptable, the lateral seismic force and shear force of the nine-storey building calculated by the proposed method are compared with the accurate results, as shown in Figure 6.2. The accurate results shown in the figures are computed in accordance with the conventional modal response spectrum analysis based on Eqs.(6.23) ~ (6.25). However, the correlation coefficients ρ_{ij} and damping ratio ς_i associated with the accurate results are different from those of the classically damped structures. The correlation coefficient ρ_{ij} and damping ratio ς_i prospsed by Falsone and Muscolino (1999), which are speicfically for the non-classically damped structure, are adopted in this study to compute the accurate response. As seen in Figures 6.2 (a) ~ (b), the errors of the lateral seismic force and shear force that are evaluated by the proposed equivalent modal damping ratio are limited to the range -0.3% ~ 0.8% and -0.3% ~ 0.1%, respectively. These errors are basically located in the previous estimated error range, i.e., 0.1% ~6%. Although the error -0.3% is not located in the previously estimated error range, such a violation is basically acceptable. Consequently, it is

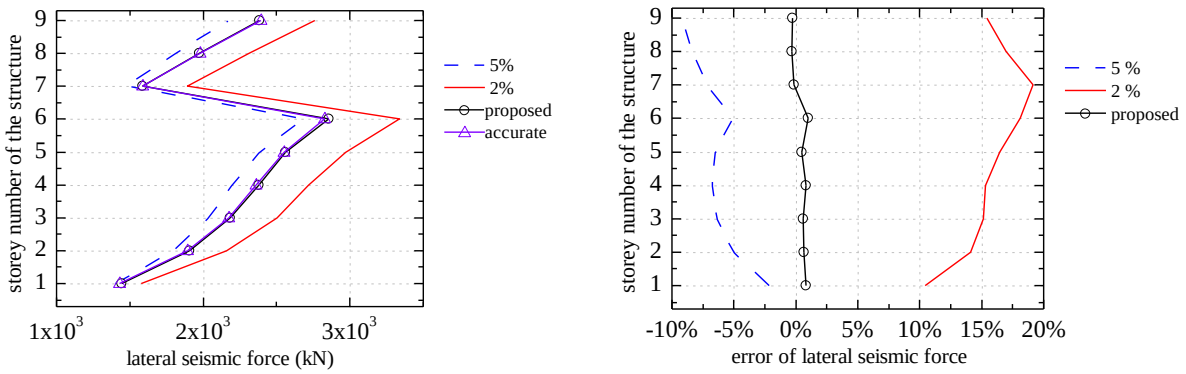

(a) lateral seismic force

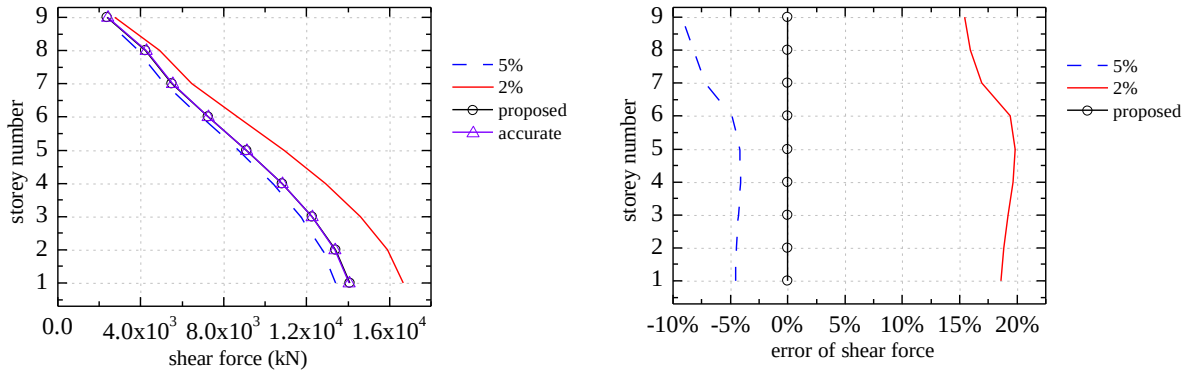

(b) shear force

Figure 6.2: Results comparison of Example 6-1

concluded that both the proposed equivalent modal damping ratio and the error estimation method are acceptable.

The lateral seismic force and shear force calculated by assuming the modal damping ratios of the combined framing systems are equal to that of the lower structure (5%) and that of the upper structure (2%), respectively, are also shown in Figures 6.2 (a) ~ (b). It can be seen that using the 2% damping ratio overestimates the seismic response while using the 5% damping ratio underestimates the seismic response. The proposed equivalent modal damping ratio provides more accurate results.

6.5.2 Example 6-2

The eight-storey building investigated in this example is the same as the one discussed in section 3.6.2. The damping ratios of the lower RC and upper CFS frames, ς_L and ς_U, are still set as 5% and 2%, respectively. In accordance with the obtained feasible lateral designs for the lower RC and upper CFS structures shown in Figure 3.10 (b), all columns shown in Figure 3.8 are selected as the columns in the moment frame and the CFS shear wall length is still 43.2 m. The selected designs of the

stiffnesses for both the lower and upper structures are the same as those of the building investigated in section 4.6.2. The basic mass, stiffness and damping properties of the combined framing systems are summarized in Table 6.7.

Still assume both the lower and upper structures have stiffness proportional damping. The calculated equivalent modal damping ratios ς_{eqi} together with the modal errors δ_i are presented in Table 6.8. Meanwhile, Table 6.9 shows that the eight-storey combined framing system is dominated by the first- to fifth- and eight-modes. Therefore, in accordance with the proposed Eqs. (6.33 a) and (6.33b), the error of all seismic quantities is limited to the range between 0.0% to 1.7%. Using the proposed equivalent modal damping ratio to estimate the seismic response of the eight-storey combined framing system is acceptable.

The lateral seismic force and shear force of the eighth-storey building calculated by the proposed equivalent modal damping ratio are compared with the accurate results, as shown in Figure 6.3. As indicated in Figures 6.3 (a) ~ (b), the errors of the lateral seismic force and shear force that are evaluated by the proposed equivalent modal damping ratio are limited to the range -0.4% ~ 1.3% and -0.4% ~ 0.3%, respectively. These errors are basically located in the previous estimated error range, i.e., 0.0% ~1.7%. Although the error -0.4% is not located in the previously estimated error range, such a violation is basically acceptable. Therefore, the previously estimated error range, i.e., 0.0% ~ 1.7%, is acceptable. The proposed equivalent modal damping ratio and the proposed error estimation method are both acceptable.

Table 6.7: Structural properties of Example 6-2

	storey number	storey-mass (kg)	SFRSs	storey-stiffness (kN/m)	damping ratio
Lower structure	2	96,113	RC moment frame, 16 columns in moment frame	8.66×10^5	0.05
Upper structure	6	219,352	CFS shear wall, with the wall length being 43.2 m	1.66×10^5	0.02

Table 6.8: Approximated equivalent modal damping ratio and modal error of Example 6-2

mode number	1	2	3	4	5	6	7	8
equivalent damping ratio	0.024	0.026	0.034	0.026	0.021	0.020	0.020	0.049
modal error δ_i	0.0%	0.6%	0.9%	1.7%	1.1%	1.2%	2.0%	0.1%

Table 6.9: Values of $\varphi_{ij}\Gamma_i$ of Example 6-2

*j*th-DOF \ *i*th-mode	1	2	3	4	5	6	7	8	dominating modes
1	0.06	0.13	0.35	0.16	0.04	0.01	0.00	0.25	2, 3, 4, 8
2	0.12	0.24	0.55	0.22	0.03	0.01	0.00	-0.17	1, 2, 3, 4, 8
3	0.42	0.56	0.44	-0.22	-0.15	-0.06	-0.02	0.04	1, 2, 3, 4, 5
4	0.69	0.64	-0.09	-0.34	0.01	0.07	0.03	-0.01	1, 2, 3, 4
5	0.93	0.45	-0.53	0.05	0.15	-0.01	-0.03	0.00	1, 2, 3, 5
6	1.12	0.06	-0.47	0.36	-0.06	-0.05	0.03	0.00	1, 3, 4
7	1.26	-0.35	0.03	0.14	-0.13	0.07	-0.02	0.00	1, 2, 4, 5
8	1.33	-0.61	0.50	-0.29	0.10	-0.03	0.01	0.00	1, 2, 3, 4

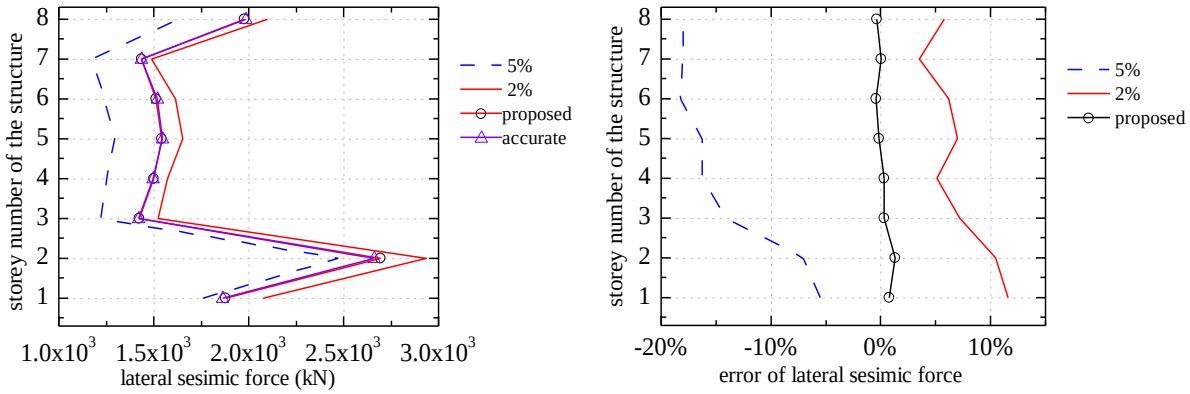

(a) lateral seismic force

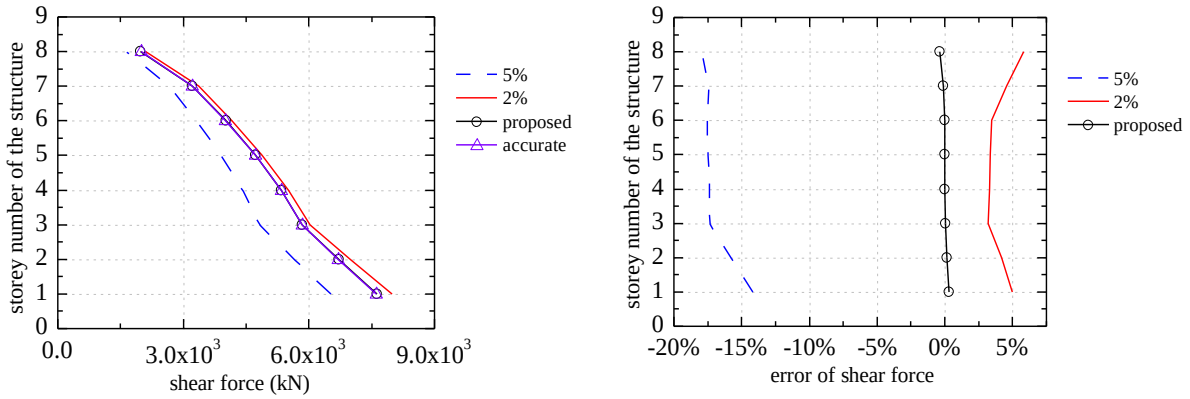

(b) shear force

Figure 6.3: Results comparison of Example 6-2

Based on Table 6.7, it is calculated that the storey-mass ratio r_m and the storey-stiffness ratio r_k are 2.28 and 5.22 for this eight-storey building, respectively. Then, in accordance with Table 4.2, the two-stage analysis procedure can be used to approximate the seismic load. The seismic loads of the upper and lower structures can be calculated independently by the ELF procedure. Since the damping

ratio of the upper structure is 2%, the accurate lateral seismic force and shear force for the upper structure are closer to those evaluated by assuming the damping ratio is 2%, as shown in Figures 6.3 (a) and (b). However, for the lower structure, the obtained accurate lateral force is not always close to that calculated by assuming the damping ratio is 5%. In fact, as shown in Figure 6.3 (a), the lateral seismic force for the first storey of the lower structure is closer to the result that is evaluated by assuming the damping ratio is 2% rather than 5%. Therefore, once the applicable requirement of the two-stage analysis procedure is satisfied, the seismic load of the upper structure can be evaluated by the ELF procedure by setting the damping ratio equal to the damping ratio of the upper structure. However, when using the ELF procedure to compute the seismic load of the lower structure, to be conservative, it is suggested that the damping ratio be equal to the smaller one of the damping ratio values associated with lower and upper structures.

6.6 Conclusion

This chapter has presented an analytical method to approximate the equivalent modal damping ratio for buildings with vertical combination of framing systems. In addition, a simplified method to quantity the error of the seismic response induced by the proposed equivalent modal damping ratio was also proposed. Two examples were investigated to demonstrate the validity and efficiency of the proposed method. These results lead to the following conclusions:

(1) If the damping ratios of the lower and upper structures are not equal, i.e., $\varsigma_L \neq \varsigma_U$, the combined framing system is non-classically damped. Therefore, the seismic response of the combined framing system theoretically cannot be computed by the conventional modal response spectrum analysis.

(2) The conventional non-proportional modal damping index $\frac{\Xi_{ij}}{\sqrt{\Xi_{ii}\Xi_{jj}}}$ could not accurately represent the extent of the non-proportional damping. It is suggested that $\rho_{ij}\frac{\Xi_{ij}}{\sqrt{\Xi_{ii}\Xi_{jj}}}$ be used as the index of the non-proportional damping, where ρ_{ij} is the correlation coefficient between the *i*th- and *j*th- vibraton mode, and $\boldsymbol{\Xi}$ is the modal damping matrix.

(3) A large error of the seismic response induced by the proposed equivalent modal damping ratio usually occurs when the dominating modes of the structures have closely spaced natural frequencies. The proposed equivalent modal damping ratio will overestimate the structural modal response if the damping ratio of the lower structure is greater than that of the upper one, and vice versa. However, for most practical combined framing systems, the dominating modes have well separated natural frequencies. The proposed equivalent modal damping ratio can be adopted to evaluate the seismic responses.

Chapter 7 Conclusions and recommendations

7.1 Summary and conclusions

The mid-rise buildings with vertical combination of framing systems are characterised by different SFRSs for the lower and upper structures. Challenges for the seismic design of such buildings primarily arise from: (a) vertical irregularities on mass and stiffness associated with different intended occupancies and SFRSs between lower and upper structures; and (b) damping irregularity induced by the different damping ratios associated with different construction materials and framing systems of the lower and upper structures. Presented in this thesis is research with aiming to solve for the challenges arising from the foregoing two aspects in relatively simple and practical ways.

7.1.1 Vertical irregularities on mass, stiffness and strength

Due to the mass irregularity in the vertical direction, the required stiffness arrangement for the lower and upper structures in the combined framing system based on the specified storey drift limit may be quite different from that in "regular" buildings. In this study, a simplified seismic design approach is proposed for the determination of the required storey-stiffness arrangement of such buildings based on the pre-determined mass distribution and specified storey drift limit. In addition, by considering both the mass and stiffness irregularities, two simplified seismic loading methods to evaluate the seismic loads of the mid-rise building with vertical combination of framing systems, i.e., modified ELF and two-stage analysis procedures, are proposed. The proposed simplified approaches to evaluate the feasible stiffness distributions and seismic loads are affected by the design standards. Since certain difference in seismic design provisions exists between the US standard ASCE 7 (ASCE, 2010) and the Canadian code NBCC 2010 (NBCC, 2010), simplified approaches that can be used together with each standard are developed, respectively. The difference in seismic design provisions between the US standard and the Canadian code, which has certain effect on the proposed simplified approaches, is also discussed in this thesis. Main contributions from this research include:

(1) The effects of the interaction between the lower and upper structures in terms of mass and stiffness on the seismic load are investigated. In order to quantify effects of such interaction on the base shear force of the upper structure, a shear-force-amplification factor α_U is proposed to account for the effect of the shear force amplification contributed by the lower structure to the upper one. It is found: (a) when the lower structure is much stiffener than the upper one, $\alpha_U \approx 1$, which indicates the lower structure has no influence on the upper one, and the upper structure behaves as it is fixed to the ground base; however, (b) when periods of the lower and upper structures are close to each other, e.g., $T_U \approx T_L$, a large amount of the mass of the lower structure will contribute to the shear force associated

with the upper structure and the factor α_U is usually greater than the unity; and (c) when T_U is far more less than T_L, the lower structure may act similar to a damper to dissipate the energy generated by earthquakes, which results in α_U<1. Applicable equations to evaluate the shear-force-amplification factor α_U are proposed based on ASCE 7 and NBCC 2010, respectively. Errors of the proposed equations based on ASCE 7 are limited to the range between -0.9% and 35.8%, which is comparable with the conventional ELF procedure that is applicable for "regular" structures in current design practice. Errors of proposed equations based on NBCC 2010 are comparable to those based on ASCE 7.

(2) The relative seismic weight between the lower and upper structures has a significant influence on the determination of required lateral stiffnesses of the lower and upper structures. In general, when the number of the storey and total seismic weight associated with the lower structure are much greater than that of the upper structure, the required stiffness of the upper structure will be significantly influenced by the interaction between lower and upper structures in terms of mass and stiffness. On the other hand, if the number of the storey and total seismic weight associated with the lower structure are less than that of the upper structure, such interaction has less effect on the required stiffness of the upper structure. In such case, the determination of the lateral stiffness of the upper structure is primarily based on the characteristics of the upper structure.

(3) When there is only one-storey upper structure in the combined framing system, if the storey-stiffness ratio between lower and upper structures r_k is less than the proposed r_{kb1}, the one-storey upper structure almost has no effect on the effective mass distribution of the lower structure. The behaviour of the lower structure is dominated by the first mode and the modified ELF procedure is applicable to approximate the seismic load of the lower structure. However, the upper one-storey structure may still be dominated higher vibration modes of the combined framing system. It is suggested that the shear force of the one-storey upper structure be calculated by the proposed shear-force-amplification factor α_U.

(4) When the lower structure is much stiffer than the upper one, the interaction between lower and upper structures in terms of mass and stiffness can be ignored, and the lower and upper structure can be analyzed by the ELF procedure separately. This is the two-stage analysis procedure prescribed in ASCE 7 (ASCE, 2006; 2010). In this study, new applicable requirements and seismic load distributions of the two-stage analysis procedures are proposed based on ASCE 7. It is found the stiffness requirement of ASCE two-stage analysis procedure may be over-relaxed. Consequently, the procedure may underestimate the seismic load of the upper structure in certain cases. Furthermore, it is found even when the applicable requirement of the proposed two-stage analysis procedure is

satisfied, the shear force of the top storey of the upper structure, which is calculated by the assumption that the upper structure is fixed to the ground base, may still be underestimated. Thus, an additional top shear force is proposed to be applied to the top of the upper structure. Equations to compute the additional top shear force are provided based on ASCE 7. In general, the accuracy of the proposed two-stage analysis procedure is greatly improved compared to that prescribed in ASCE 7 (ASCE, 2006; 2010).

The Canadian code NBCC 2010 (NBCC, 2010) does not specify any simplified method similar to the two-stage analysis procedure to analyze the building with vertical combination of framing systems. By considering the difference in seismic design provisions between the ASCE 7 and the NBCC 2010, several modifications are made on the ASCE 7 two-stage analysis procedure for its Canadian application. The accuracy of the proposed two-stage analysis procedure based on NBCC 2010 is comparable to that based on ASCE 7.

(5) The proposed simplified approach for evaluating the required stiffness distributions of lower and upper structures involves the nonlinear behavior of the combined framing systems. Therefore, nonlinear time history analyses are also carried to verify the stiffness designs. Results from the nonlinear time history analysis show that the maximum storey-drift ratio occurs at the first storey of the upper structure, which is the same as the results of the linear analysis. However, the elastic-analysis-based modal response spectrum analysis based on NBCC 2010 cannot well estimate the nonlinear storey-drift ratio for the first storey of the upper structure. A more appropriate value of the deflection amplification factor C_d is required.

7.1.2 Damping irregularity

An analytical method is proposed to approximate the equivalent modal damping ratio for the case where lower and upper structures have different damping ratios. The proposed equivalent modal damping ratio can be used directly in the conventional modal analysis. Meanwhile, a simplified method to quantity the error of the seismic response induced by the proposed equivalent modal damping ratio is also proposed. Main contributions from this investigation include:

(1) Different from the mass and stiffness matrices, the damping matrix for structures in practice cannot be directly assembled from the damping properties of the structural members (Chopra, 2007). Different methods to construct the damping matrix of the combined framing system based on the damping ratios of lower and upper structures are proposed in this study. In accordance with the established damping matrix, it is found when the damping ratios of the lower and upper structures are not equal, i.e., $\varsigma_L \neq \varsigma_U$, the combined framing system is non-classically damped. Therefore, the

conventional modal analysis is theoretically not applicable to compute the seismic response of the system.

(2) The conventional non-proportional modal damping index $\frac{\Xi_{ij}}{\sqrt{\Xi_{ii}\Xi_{jj}}}$ could not well represent the extent of non-proportional damping. It is suggested using $\rho_{ij}\frac{\Xi_{ij}}{\sqrt{\Xi_{ii}\Xi_{jj}}}$ as the index of non-proportional damping, where ρ_{ij} is the correlation coefficient between the *i*th- and *j*th- vibraton mode, and $\boldsymbol{\Xi}$ is the modal damping matrix.

(3) It is found that a considerable error of seismic response associated with the proposed equivalent modal damping ratios may occur when the dominating modes of the structures have closely spaced natural frequencies. In such case, the proposed equivalent modal damping ratios will overestimate the structural modal response if the damping ratio of the lower structure is greater than that of the upper one, and vice versa. However, for most combined framing systems in practice, the dominating modes have well separated natural frequencies, the proposed equivalent modal damping ratios can be adopted to evaluate the seismic response.

7.2 Recommendations for future research

Concerning to the mid-rise buildings with vertical combination of framing systems, it is recommended that following future research be carried out:

- Investigate how to determine the seismic response modification coefficient *R* of the combined framing system if lower and upper structures have different *R* values. The seismic response modification coefficient *R* is introduced in current standards to account for the earthquake energy that will be dissipated by the non-linear behavior of the structure. In accordance with article 12.2.3.1 of ASCE 7 (ASCE, 2010), the modification coefficient *R* for the vertical combined building can be determined as follows: (a) if the upper structure has a larger value of *R*, the lower and upper structures should be designed using their own value of *R*; (b) if the upper structure has a smaller value *R*, the smaller value of *R* should be used for the both upper and lower structures. However, this code-approved *R* is largely based on engineering judgement and is somewhat arbitrarily assigned (FEMA, 2009). The code approved method to determine the *R* value needs further verification. Nevertheless, the method prescribed in FEMA P695 (FEMA, 2009) to justify whether the *R* value is acceptable or not is only applicable for "regular" structures, the seismic behavior of which is primarily dominated by the first mode. For the structures with vertical combined framing systems, especially for the structures that are influenced by the higher vibration modes other than the first mode, there is no method currently available to justify how

to determine the appropriate *R* value. A method on how to justify the appropriate values of *R* for the structures with combined framing system needs to be investigated or developed.

- A structure is often considered to be "regular" if it has uniform structural properties or a uniform variation in structural properties (ASCE, 2010; NBCC, 2010). As to the "regular" lower and upper structures investigated in this study, the storey-masses and lateral storey-stiffness of the lower and upper structures are assumed to be uniformly distributed. However, in practice, the lower and upper structures are more likely to have a uniform variation in structural properties rather than uniform structural properties. Therefore, it is necessary to investigate how the results obtained in this study will be affected if the lower and upper structures have a uniform variation in mass and stiffness distributions rather than uniform mass and stiffness distributions.
- The total number of storey for the combined framing system is limited to ten in this study. However, the applicability of the proposed methods on buildings with the combined framing system having more than ten storeys is not investigated. It is desirable to extend the current research into the buildings with more stories such as the building shown Figure 1.1.
- The effects of damping irregularity and the effects of mass and stiffness irregularities on the seismic behavior of the combined framing system are investigated separately in this study. However, these irregularities usually coexist in the mid-rise building with vertical combination of framing system. The effects of coupled mass-stiffness-damping irregularity on the seismic behavior needs to be further explored.
- Two simplified methods for evaluating the seismic load of the combined framing system, i.e., modified ELF and two-stage analysis procedures, are investigated in this study. The modified ELF procedure is applicable for the combined framing system which has only one-storey upper structure. The proposed two-stage analysis procedure is applied to the combined framing system when the lower structure is much stiffer than the upper one. However, in practice the mid-rise buildings with vertical combination of framing systems cannot always satisfy the applicable requirements associated with these two simplified methods. When these two simplified methods are not applicable, the combined framing system can be analyzed only by dynamic analysis (Chopra, 2007). Therefore, it is necessary to develop a simplified method to evaluate the seismic load of the mid-rise buildings with vertical combination of framing systems when the modified ELF and two-stage analysis procedures are not applicable.
- Since the NBCC 2010 (NBCC, 2010) adopts the piecewise linear function to describe the relationship between the period and the spectral acceleration, the proposed equations to evaluate the required stiffnesses of the lower and upper structure are quite complicated. A future study on

simplifying the proposed complicated equations so that they can be widely accepted in practices is recommended.

- Results from the nonlinear time history analysis show that the deflection amplification factor C_d specified in NBCC 2010 (NBCC, 2010) cannot provide satisfactory approximation on the nonlinear deformation of the combined framing systems. A future study on the determination of appropriate value of the deflection amplification factor C_d is recommended.

Bibliography

Adams, J., & Atkinson, G. (2003). Development of seismic hazard maps for the proposed 2005 edition of the National Building Code of Canada. *Can. J. Civ. Eng., 30*(2), pp. 255-271.

Al-Ali, A. K. (1998). *Effects of vertical irregularities on seismic behavior of building structures.* Doctor Dissertation, Standford Unviersity, Department of Civil and Environmental Engineering, Standford, California.

Allen, M., Chung, N., Tran, A., & Zepeda, D. (2013). Two stage analysis: implementation challenges. *Structures Congress 2013* (pp. 2192-2202). Pittsburgh: ASCE.

American Society of Civil Engineers (ASCE). (2006). *Minimum design loads for buildings and other structures.* Reston,Virginia: American Society of Civil Engineers.

American Society of Civil Engineers (ASCE). (2010). *Minimum design loads for buildings and other structures.* Reston,Virginia: American Society of Civil Engineers.

Applied Technology Council (ATC). (1978). *Tentative provisions for the development of seismic regulartions for buildings.* Washington, D.C: Applied Technology Council.

Athanassiadou, C. J. (2008). Seismic Response of R/C plane frames irregular in elevation. *Engineering Structures, 30*(5), pp. 1250-1261.

Balh, N., & Rogers, C. (2011). *Development of Canadian seismic design provisions for steel shearthed shear walls.* McGill University, Department of Civil Engineering and Applied Mechanics. Montreal, QC: American Iron and Steel Institute (AISI).

Bhaskar, A. (1994). Estimates of errors in the frequency response of non-classically damped systems. *Journal of Sound and Vibration, 184*(1), 59-72.

Boudreault, F. (2005). *Seismic analysis of steel frame/wood panel shear walls.* Thesis, McGill University, Department of Civil Engineering and Applied Mechanics, Montreal, QC.

Branston, A. E. (2004). *Development of a design methodology for steel/wood panel shear walls.* Thesis, McGill University, Montreal,QC.

Caughey, T. K., & O'Kelly, M. J. (1965). Classical normal modes in damped linear dynamic systems. *Journal of Applied Mechanics*, pp. 583-588.

CEN. (2004). *Eurocdoe 8: Design of structures for earthquake resistance-Part I: general rules, sesimic actions and rules for buildings.* Brussels.

Chen, C. (2004). *Testing and performance of steel frame/wood panel shear walls.* Thesis, McGill University, Department of Civil Engineering and Applied Mechancis.

Chen, Z. Y., Chui, Y. H., & Ni, C. (2013). Seismic performance of mid-rise hybrid light wood frame buildings and influence of diaphragm flexibility. *Structures Congress 2013* (pp. 1229-1241). Pittsburgh: ASCE.

Chen, Z., Chui, Y., Ni, C., & Xu, J. (2013). Seismic response of midrise light wood-frame buildings with portal frames. *Journal of Structural Engineering, 140*(special issue: computational simulation in structural engineering), 1-10.

Chopra, A. K. (2007). *Dynamics of structures:theory and applications to earthquake engineering* (3rd ed.). Upper Saddle River, New Jersey: Prentice Hall.

Cuesta, I., Mark, A., & Fajfar, P. (2003). Seismic R-factor relationships for strong ground motions. *Earthquake spectra, 19*(1), 25-45.

Falsone, G., & Muscolino, G. (1999). Cross-correlation coefficients and modal combination rules for non-classically damped systems. *Earthquake Engineering and Structural Dynamics, 28*(12), pp. 1669-1684.

Falsone, G., & Muscolino, G. (2004). New real-value modal combination rules for non-classically damped structures. *Earthquake Enigneering and Structural Dynamics, 33*(12), pp. 1187-1209.

Federal Emergency Management. (1997). *NEHRP recommended provisions for seismic regulartions for new buildings and other structures part 2: commentary.* Washington D.C.: Building Seismic Safety Council.

Federal Emergency Management Agency (FEMA). (2000). *Prestandard and commentary for the seismic rehabitation of buildings.* Reston, Virginia: American Society of Civil Engineers.

Federal Emergency Management Agency. (2004). *NEHRP recommended provisions for seismic regulations for buildings and other structures part 2:commentary.* Washington, D.C.: Building Seismic Safety Council.

Federal Emergency Management Agency. (2009). *NEHRP recommended seismic design provisions for new buildings and other structures (FEMA P-750).* Washington D.C.: Building Seismic Safety Council.

Federal Emergeny Management Agency (FEMA). (2009). *Quantification of building seismic performance factors.* Reston,Virginia: American Society of Civil Engineers.

Haselton, C., Liel, A., Lange, S., & Deierlein, G. (2008). *Beam-column element model calibrated for predicting flexural reponse leading to global collapse of RC frame buildings.* Pacific Earthquake Engineering Research Center.

Hasselman, T. (1976). Modal copuling in lightly damped structures. *AIAA Journal, 14*(11), 1627-1628.

Huang, B., Leung, A., Lam, K., & Cheung, Y. (1996). Analytical determination of equivalent modal damping ratios of a composite tower in wind-induced vibrations. *Computers & Structures, 59*(2), 311-316.

Humar, J. L. (1977). Earthquake response of steel-frame multi-storey buildings with set-backs. *Earthquake Engineering & Structural Dynamics, 5*(1), pp. 15-39.

Ibarra, L., Medina, R., & Krawinkler, H. (2005). Hysteretic models that incorporate strength and sitffness deterioration. *Earthquake Engineering and Structural Dynamics, 34*(12), 1489-1511.

International Code Council (ICC). (2011). *2012 International builidng code.* Country Club Hills, Illinois: International Code Council.

International Conference of Building Officials. (1988). *Uniform Building Code.* Pasedena, California: Internatioinal Conference of Building Officials.

Key, D. (1988). *Earthquake design practice for buildings.* Heron Quay, London: Thomas Telford Limited.

Liu, H. Y., van de Lindt, J. W., & Pryor, S. (2008). Seismic performance assessment of a seven-storey wood-steel hybrid buildings. *The 14th World Conference on Earthquake Engineering.* Beijing, China.

Lowes, L., & Altoontash, A. (2003). Modelling reinforced-concrete baeam-column joints subjected to cyclic loading. *Journal of Structural Engineering, 12,* 1686-1697.

Luco , N., Ellingwood, B., Hamburger, R., Hooper, J., & Kimball, J. (2007). Risk-targted versus current sesimic design maps for the conterminous United States. *SEAOC 2007 convention proceddings,* (pp. 1-13).

MIDAS/Gen Program. (2000). *MIDAS/Gen-General structure design system.MIDAS/Gen Ver.5.7.1 analysis and design manual.* MIDAS Information Technology, Co., Ltd.

Mitchell, D., Paultre, P., Tinawi, R., Saatcioglu, M., Tremblay, M., Elwood, K., . . . Devall, R. (2010). Evaluation of seismic design provisions in the National Builidng Code of Canada. *Canadian J.Civ.Eng., 37*(9), pp. 1157-1170.

Morzfeld , M., Ajavakom, N., & Ma, F. (2009). Diagonal dominance of damping and the decoupling approximation in linear vibratory system. *Journal of Sound and Vibration, 320*(1-2), 406-420.

National Building Code of Canada. (2011). *User's guide-NBC 2010 structural commentaries (part 4 of Division B).* Ottawa, ON: National Reserach Council of Canada .

National Research Council of Canada (NRCC). (2005). *National Building Code of Canada 2005.* Ottawa: Canadian Commission on Building and Fire Codes, National Research Council of Canada.

National Research Council of Canada (NRCC). (2010). *National building code of Canada 2010.* Ottawa: Canadian Commission on Building and Fire Codes, National Reserach Council of Canada.

Pacific Earthquake Engineering Research Center. (2015). *PEER ground motion database: NGA-West2*. Retrieved from http://ngawest2.berkeley.edu/spectras/8454/searches/new

Panagiotakos, T., & Fardis, M. (2001). Deformations of reinforced concrete members at yielding and ultimate. *ACI Structural Journal, 98*(2), 135-148.

Pang, W. C., Rosowsky, D. V., Pei, S. L., & van de Lindt, J. W. (2011). Simplified direct displacement design of six-storey woodframe building and pretest seismic performance assessment. *Journal of Structural Engineering, 136*(7), pp. 813-825.

Papageorgiou, A. V., & Gantes, C. J. (2010). Equivalent modal damping ratios for concrete/steel mixed structures. *Computers & Structures, 88*(19), pp. 1124-1136.

Papageorgiou, A. V., & Gantes, C. J. (2011). Equivalent uniform damping ratios for linear irregularly damped concrete/steel mixed structures. *Soil Dynamics and Earthquake Engineering, 31*(3), pp. 418-430.

Penzien, J., & Chopra, A. K. (1965). Earthquake response of appendage on multistorey buildings. *Proceedings of the 3rd Word Conference of Earthquake Engineering.* New Zealand.

Perotti, F. (1994). Analytical and numerical techniques for the dynamic analysis of non-classically damped system. *Soil Dynamics and Earthquake Engineering, 13*(3), 197-212.

Raggett, J. (1975). Estimating damping of real structures. *Earthquake Engineering and Structure Dynamics, 101*(9), 1823-1835.

SEAOC. (1973). *Recommended lateral force requirements and commentary.* San Franciso, California: Structural Engineers Association of California.

Shahrooz, B. M., & Moehle, J. P. (1990). Evaluation of performance of reinforced concrete frames. *Jounral of Structural Engineering, 116*(5), 1403-1422.

Shahrooz, B. M., & Moehle, J. P. (1990). Seismic response and design of setback buildings. *Journal of Structural Engineering, 116*(5), 1423-1439.

Shamim, I. (2012). *Seismic design of lateral-force-resisting cold-formed steel (CFS) structures.* Doctor Dissertation, McGill University, Department of Civil Engineering and Mechanics, Montreal, Canada.

Sinha, R., & Igusa, T. (1995). CQC and SRSS methods for non-classically damped structures. *Earthquake Engineringa and Structural Dyanmics, 24*(4), pp. 615-619.

Tena-Colunga, A. (2004). Evaluation of the seismic response of slender, setback RC moment-resisting frame buildings designed according to the seismic guidelines of a modern building code. *13th Word Conference on Earthquake Engineering.* Vancouver, B.C.

Tremblay, R., & Poncet, L. (2005). Seismic performance of concentrically braced steel frames in multi-storey builidngs with mass irregularity. *Journal of Structural Engineering, 131*(9), pp. 1363-1375.

Tso, W. K., & Yao, S. (1994). Seismic load distribution in buildings with eccentric setback. *Canadian Journal of Civil Engineering, 21*(1), pp. 50-62.

United States Geological Survey (USGS). (2014). *Seismic Design Maps and Tools*. Retrieved from http://earthquake.usgs.gov/hazards/designmaps/

Warburton, G., & Soni, S. (1977). Errors in response calculations for non-classically damped structures. *Earthquake Engineering and Structural Dynamics, 5*(4), 365-376.

Wong, C. M., & Tso, W. K. (1994). Seismic loading for buildings with setbacks. *Canadian Journal of Civil Engineering, 21*(5), 863-871.

Wood, S. L. (1985). *Experiments to study the earthquake response of reinforced concrete frame with setbacks.* Doctor Dissertation, University of Illinois at Urban-Champaign, Illinois, United States.

Wood, S. L. (1992). Seismic response of R/C frames with irregular profiles. *Jounral of Structural Engineering, 118*(2), 545-566.

Xiong, H. B., & Jia, G. C. (2008). Research on sesimic behavior of wood-concrete hybrid structure. *Proceedings of the 10th World Conference on Timber Engineering.* Miyazaki, Japan.

Xiong, H. B., Ni, C., Lv, X. L., & Jia, G. C. (2008). Shake table tests on 3-storey wood hybrid structures. *Proceedings of the 10th World Conference on Timber Engineering.* Miyazaki, Japan.

Xu, L., & Yuan, X. (2015). A simplified seismic design approach for mid-rise buildings with vertical combination of framing systems. *Engineering Structures, 99,* 568-581.

Appendix A Modal response spectrum analysis to evaluate α_U

The eigenvalue equation (Chopra, 2007) for the simplified 2DOF model shown in Figure 3.1 (b) is as follows:

$$\mathbf{K\Phi} = \omega^2 \mathbf{M\Phi} \tag{A.1}$$

where ω is the natural frequency, $\mathbf{\Phi}$ is the mode shape, and $\mathbf{K}$ and $\mathbf{M}$ are the stiffness and mass matrices of the 2DOF model, respectively, with

$$\mathbf{K} = \begin{bmatrix} K_L + K_U & -K_U \\ -K_U & K_U \end{bmatrix} \tag{A.2}$$

$$\mathbf{M} = \begin{bmatrix} M_L & 0 \\ 0 & M_U \end{bmatrix} \tag{A.3}$$

By substituting $\mathbf{K}$ and $\mathbf{M}$ evaluated respectively based on Eqs.(A.2) and (A.3) into Eq.(A.1), it is obtained that

$$\left(K_L + K_U - \omega^2 M_U\right)\left(K_U - \omega^2 M_U\right) - \left(K_U\right)^2 = 0 \tag{A.4}$$

By solving for Eq.(A.4), the natural frequencies (ω_1 and ω_2) and modal periods (T_1 and T_2) of the 2DOF model, as shown in Figure A.1, can be obtained. The modal periods are calculated as follows:

$$T_1 = \sqrt{\frac{8\pi^2 R_m}{R_k + R_m + 1 - \sqrt{\left(R_m - R_k - 1\right)^2 + 4R_m}} \frac{M_U}{K_U}} \tag{A.5}$$

$$T_2 = \sqrt{\frac{8\pi^2 R_m}{R_k + R_m + 1 + \sqrt{\left(R_m - R_k - 1\right)^2 + 4R_m}} \frac{M_U}{K_U}} \tag{A.6}$$

where R_m and R_k are overall mass and stiffness ratios of the simplified 2DOF model as defined in Eqs.(3.6) and (3.7), respectively. Then, based on Eqs.(A.5) and (A.6), the associated two mode shapes, as shown in Figure A.1, can be obtained as follows:

$$\mathbf{\Phi}_1 = \begin{Bmatrix} \varphi_{L1} \\ \varphi_{U1} \end{Bmatrix} = \begin{Bmatrix} \frac{1}{2}\frac{R_m - R_k - 1 + \sqrt{\left(R_m - R_k - 1\right)^2 + 4R_m}}{R_m} \\ 1 \end{Bmatrix} \tag{A.7}$$

$$\varphi_{L1} = 1 - \left(\frac{T_U}{T_1}\right)^2 \tag{A.8}$$

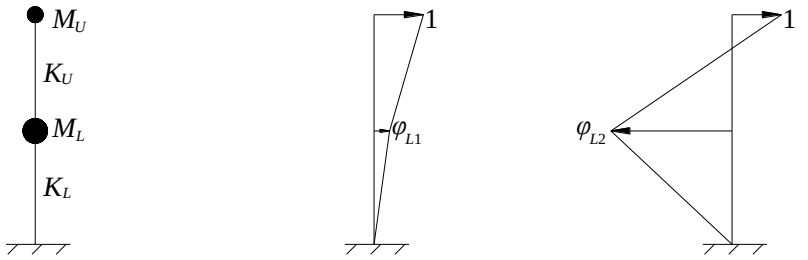

(a) 2DOF model (b) first mode (T_1) (c) second mode (T_2)

Figure A.1: Natural modes of vibration for simplified 2DOF model

$$\mathbf{\Phi}_2 = \begin{Bmatrix} \varphi_{L2} \\ \varphi_{U2} \end{Bmatrix} = \begin{Bmatrix} \frac{1}{2}\frac{R_m - R_k - 1 - \sqrt{\left(R_m - R_k - 1\right)^2 + 4R_m}}{R_m} \\ 1 \end{Bmatrix} \tag{A.9}$$

$$\varphi_{L2} = 1 - \left(\frac{T_U}{T_2}\right)^2 \tag{A.10}$$

In accordance with the modal expansion theory, the effective modal masses of the upper structure associated with the first and second modes can be evaluated based on the mode shapes as follows:

$$M_{U1}^* = \frac{R_m\varphi_{L1} + 1}{R_m\varphi_{L1}^2 + 1} M_U \tag{A.11}$$

$$M_{U2}^* = M_U - M_{U1}^* \tag{A.12}$$

With the evaluated periods T_1 and T_2, and effective modal masses M_{U1}^* and M_{U2}^* , the elastic shear force V_{Ub} of the 2DOF model shown in Figure 3.1 (b) can be calculated through the modal response spectrum analysis (Chopra, 2007) as follows:

$$V_{Ub} = \sqrt{\left(M_{U1}^*\right)^2\left[S_a\left(T_1\right)\right]^2 + \left(M_{U2}^*\right)^2\left[S_a\left(T_2\right)\right]^2 + 2\rho M_{U1}^* M_{U2}^* S_a\left(T_1\right)S_a\left(T_2\right)} \tag{A.13}$$

where $S_a(T_1)$ and $S_a(T_2)$ are design spectral response accelerations associated with the first and second modes, and ρ is the correlation coefficient between the first and second modes (Chopra, 2007) , which is evaluated as

$$\rho = \frac{8\varsigma^2\left(1+\beta\right)\beta^{3/2}}{\left(1-\beta^2\right)^2 + 4\varsigma^2\beta\left(1+\beta\right)^2} \tag{A.14}$$

In Eq.(A.14), ζ is the damping ratio of the structure which is assumed 5% for the simplified 2DOF model, and β is the period ratio between the first and second modes defined as $\beta=T_2/T_1$. In accordance with Eqs.(A.5) and (A.6), the period ratio β is expressed as

$$\beta = \frac{T_2}{T_1} = \sqrt{\frac{1-\varphi_{L1}}{1+\dfrac{1}{R_m \varphi_{L1}}}} \tag{A.15}$$

Finally, by substituting V_{Ub} in Eq.(3.2) with that of Eq.(A.13), it is obtained that the factor α_U for the simplified 2DOF model can be computed as

$$\alpha_U = \sqrt{\left(M_{U1}\right)^2 \left[\frac{S_a\left(T_1\right)}{S_a\left(T_U\right)}\right]^2 + \left(M_{U2}\right)^2 \left[\frac{S_a\left(T_2\right)}{S_a\left(T_U\right)}\right]^2 + 2\rho M_{U1} M_{U2} \frac{S_a\left(T_1\right)}{S_a\left(T_U\right)} \frac{S_a\left(T_2\right)}{S_a\left(T_U\right)}} \tag{A.16}$$

where M_{Uj} is the normalized effective modal mass of the jth-mode of the upper structure defined as

$$M_{U1} = \frac{M_{U1}^*}{M_U} = \frac{R_m \varphi_{L1} + 1}{R_m \varphi_{L1}^2 + 1} \tag{A.17}$$

$$M_{U2} = \frac{M_{U2}^*}{M_U} = 1 - M_{U1} \tag{A.18}$$

As analyzed subsequently in Appendix B, $T_1/T_U>1$ and $0<T_2/T_U<1$. Therefore, in accordance with the design spectrum shown in Figure 1.4, spectrum ratios $S_a(T_1)/S_a(T_U)$ and $S_a(T_2)/S_a(T_U)$ can be further expressed as

$$\frac{S_a(T_1)}{S_a(T_U)} = \begin{cases} 1 & T_U / T_S \le T_U / T_1 \\ T_S / T_1 & T_U / T_1 < T_U / T_S < 1 \\ T_U / T_1 & T_U / T_S \ge 1 \end{cases} \tag{A.19}$$

$$\frac{S_a(T_2)}{S_a(T_U)} = \begin{cases} 0.4 + 3T_2 / T_S & T_U / T_S \le \min(1, 0.2T_U / T_2) \\ 1 & 0.2T_U / T_2 \le T_U / T_S \le 1 \\ \left(0.4 + 3T_2 / T_S\right) T_U / T_S & 1 \le T_U / T_S \le 0.2T_U / T_2 \\ T_U / T_S & \max(1, 0.2T_U / T_2) \le T_U / T_S \le T_U / T_2 \\ T_U / T_2 & T_U / T_S \ge \max(1, T_U / T_2) \end{cases} \tag{A.20}$$

From Eqs.(A.7), (A.9), (A.17) , (A.18), (A.14) and (A.15), it is seen the magnitudes of M_{U1}, M_{U2} and ρ are determined by the overall mass ratio R_m and overall stiffness ratio R_k. Meanwhile, based on Eqs. (A.7) ~ (A.10) and Eqs.(A.19) and (A.20), it is seen spectrum ratios $S_a(T_1)/ S_a(T_U)$ and $S_a(T_2)/S_a(T_U)$ are not only related with R_m and R_k, but also related with the period ratio T_U/T_S, where T_S is the period at which the horizontal and descending curve of the response spectrum intersects, as shown in Figure 1.4. Consequently, in accordance with Eq.(A.16), the shear-force-amplification-factor α_U is related with the overall mass ratio R_m, overall stiffness ratio R_k and the period ratio T_U/T_S.

Note as discussed in Appendix B.1.4, the maximum correlation coefficient ρ in Eq.(A.16) is 0.22. The effects of R_m, R_k and T_U/T_S on the factor α_U is primarily resulted from their incfluences on M_{U1}, M_{U2}, $S_a(T_1)/ S_a(T_U)$ and $S_a(T_2)/S_a(T_U)$. Therefore, when qualitatively analyzing how the factor α_U is affected by ratios R_m, R_k and T_U/T_S, the correlation term in Eq.(A.16) may be neglected for the reason of simplicity. The CQC rule in Eq.(A.16) can be reduced to the SRSS (square-root-of-sum-of-squares) rule as follows:

$$\alpha_U = \sqrt{\left(M_{U1}\right)^2 \left[\frac{S_a\left(T_1\right)}{S_a\left(T_U\right)}\right]^2 + \left(M_{U2}\right)^2 \left[\frac{S_a\left(T_2\right)}{S_a\left(T_U\right)}\right]^2} \tag{A.21}$$

However, for the evaluating of the factor α_U, Eq.(A.16) is adopted.

Appendix B Analytical study on factor α_U

B.1 Effects of overall stiffness ratio R_k on α_U

As shown in Eq.(A.21), in order to find out how the factor α_U is influenced by the stiffness ratio R_k, an analysis is first carried out on how R_k affects M_{U1}, M_{U2}, $S_a(T_1)/ S_a(T_U)$ and $S_a(T_2)/S_a(T_U)$.

B.1.1 Effects of overall stiffness ratio R_k on φ_{L1}

According to Eq. (A.7), the derivative of the first mode shape of the lower structure φ_{L1} with respect to the stiffness ratio R_k is

$$\frac{d\varphi_{L1}}{dR_k} = \frac{-\sqrt{\left(R_m - R_k - 1\right)^2 + 4R_m} - \left(R_m - R_k - 1\right)}{2R_m\sqrt{\left(R_m - R_k - 1\right)^2 + 4R_m}} < 0 \tag{B.1}$$

Therefore, for a given overall mass ratio R_m, φ_{L1} decreases as the increase of overall stiffness ratio R_k. φ_{L1} gradually decreases from unity to zero as R_k increases from zero to infinity.

B.1.2 Effects of overall stiffness ratio R_k on M_{U1} and M_{U2}

Based on Eq.(A.17) , the derivative of the first mode normalized effective modal mass of the upper structure, M_{U1}, with respect to stiffness ratio φ_{L1} is

$$\frac{dM_{U1}}{d\varphi_{L1}} = \frac{-R_m}{\left(R_m\varphi_{L1}^2 + 1\right)^2}\left(R_m\varphi_{L1}^2 + 2\varphi_{L1} - 1\right) \tag{B.2}$$

Based on Eqs.(B.2), (B.1) and (A.7), it is observed that, as shown in Figure B.1 (a), as the increase of the stiffness ratio R_k, M_{U1} first increases from unity to its maximum value at $R_k = R_m+1$. Then, as further increase of R_k, M_{U1} gradually decreases to unity. When $R_k=R_m+1$, the maximum value of M_{U1} is

$$M_{U1\max} = \frac{R_m\sqrt{1+R_m}}{\left(\sqrt{1+R_m} - 1\right)^2 + R_m} \tag{B.3}$$

Meanwhile, based on (A.18), M_{U2} is always negative and the variation for the magnitude of M_{U2} is the same as that of M_{U1}, as shown in Fig.B.1 (a).

B.1.3 Effects of overall stiffness ratio R_k on spectrum ratios $S_a(T_1)/ S_a(T_U)$ and $S_a(T_2)/S_a(T_U)$

Based on Eqs. (A.8), (A.10), (B.1), (A.19) and (A.20), it is concluded that for a given overall mass ratio R_m, as the increase of the overall stiffness ratio R_k : (1) the period ratio T_1/T_U gradually decreases

from infinity to unity, and the period ratio T_2/T_U gradually decreases from $[R_m/(R_m+1)]^{0.5}$ to zero, as shown in Figure B.1 (b); (2) the spectrum ratio $S_a(T_1)/S_a(T_U)$ gradually increases from zero to unity, as shown Figure B.1 (c); and (3) the effect of R_k on spectrum ratio $S_a(T_2)/S_a(T_U)$ is greatly affected by the magnitude of the period ratio T_U/T_S, as shown in Figure B.1 (d). For example, when T_U/T_S=0.2, the spectrum ratio $S_a(T_2)/S_a(T_U)$ gradually decreases as the ratio R_k increases; however, when T_U/T_S =4, the spectrum ratio $S_a(T_2)/S_a(T_U)$ gradually increases as the ratio R_k increases.

B.1.4 Effects of overall stiffness ratio R_k on T_2/T_1 and ρ

From Eq.(A.15), it is obtained that the derivative of $(T_2/T_1)^2$ with respect to φ_{L1} is

$$\frac{d\left(T_2/T_1\right)^2}{d\varphi_{L1}} = -\frac{R_m\varphi_{L1}^2 + 2\varphi_{L1} - 1}{\left(R_m\varphi_{L1}+1\right)^2} \tag{B.4}$$

Based on Eqs.(B.4), (B.1) and (A.15) and Figure B.1 (e), it is observed that as the increase of the stiffness ratio R_k, the period ratio T_2/T_1 first increases from zero to its maximum value at $R_k = R_m+1$, and then as R_k further increases, the ratio T_2/T_1 gradually decreases to zero. When $R_k=R_m+1$, the maximum value of T_2/T_1 is:

$$\left|T_2/T_1\right|_{\max} = \sqrt{\frac{\left(\sqrt{1+R_m}-1\right)\left(R_m+1-\sqrt{1+R_m}\right)}{R_m\sqrt{1+R_m}}} \tag{B.5}$$

For the mid-rise buildings which are within the limitation presented in section 1.3.2, the maximum overall mass ratio R_m occurs when r_m=3, N_L=9 and N_U=1. The minimum ratio R_m occurs when r_m=1, N_L=1 and N_U=9. Therefore, based on Eq.(3.6), it is obtained that the ratio R_m is limited to the range between 0.11 and 27. Then, by letting R_m=27 in Eq.(B.5), the calculated maximum T_2/T_1 is 0.826. Finally, by setting β in Eq. (A.14) be 0.826, it is obtained that the corresponding maximum correlation coefficient ρ is 0.22.

B.1.5 Effects of overall stiffness ratio R_k on factor α_U

Through Eq.(A.21) and Figures B.1 (a) ~ (d), it is obtained that:

(1) When $R_k \to 0$, $M_{U1} \to 1$ and $M_{U2} \to 0$ as shown in Figure B.1 (a) and $(T_1/T_U) \to \infty$ as shown in Figure B.1 (b). Consequently, based on Eq.(A.21), it is concluded that $\alpha_U \to 0$.

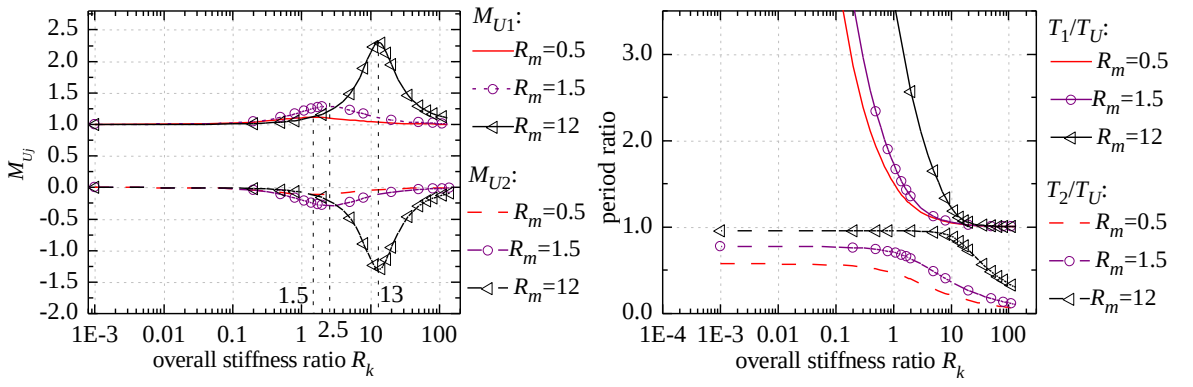

(a) M_{U1} and M_{U2} (b) T_1/T_U and T_2/T_U

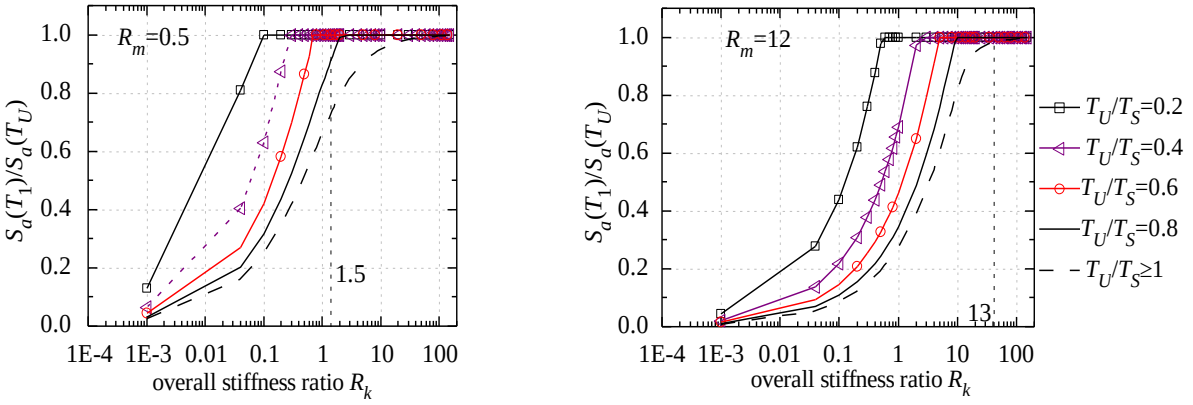

(c) $S_a(T_1)/S_a(T_U)$

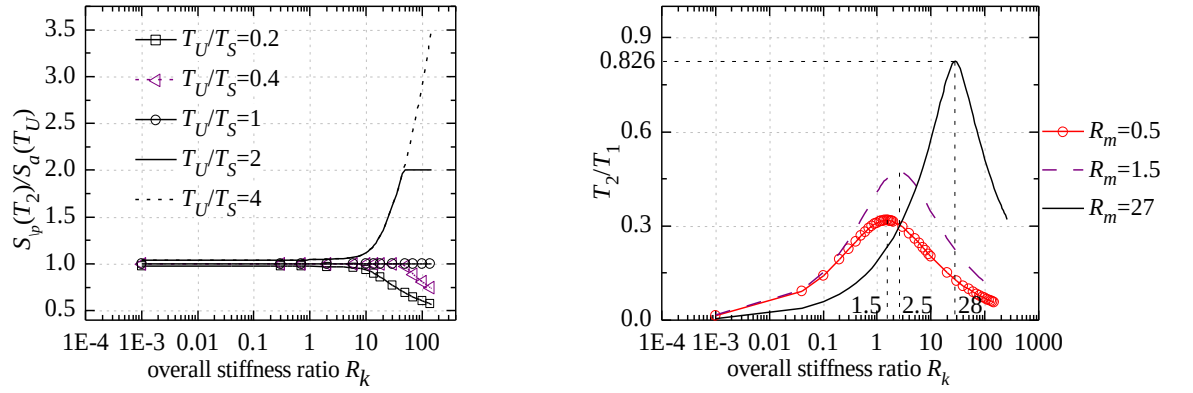

(d) $S_a(T_2)/S_a(T_U)$ (e) T_2/T_1

Figure B.1: Variation of dynamic parameters with respect to ratios R_m and R_k

(2) When $R_k \to \infty$, $M_{U1} \to 1$ and $M_{U2} \to 0$ as shown in Figure B.1 (a) and $(T_1/T_U) \to 1$ as shown in Figure B.1 (b). Consequently, based on Eq.(A.21), it is concluded that $\alpha_U \to 1$

(3) By comparing Figures B.1 (a) ~ (d) and Figures 3.3 (a) ~ (c), it is found the variation of amplification factor α_U with respect to the overall stiffness ratio R_k is primarily affected by M_{U1}, M_{U2} and $S_a(T_1)/S_a(T_U)$, while the spectrum ratio $S_a(T_2)/S_a(T_U)$ has the least influence on the factor α_U. The initial increase of factor α_U is associated with the increases of $|M_{U1}|$, $|M_{U2}|$ and the spectrum ratio $S_a(T_1)/S_a(T_U)$, and the later decrease of the factor α_U is resulted from the decrease of $|M_{U1}|$ and $|M_{U2}|$ after α_U reaches the maximum value.

B.2 Effects of overall mass ratio R_m on factor α_U

From Figure B.1 (a), it is observed that M_{U1} is always greater than or equal to unity regardless of values of R_m and R_k, which indicates the first mode effective modal mass of the upper structure is greater than or equal to the total mass of the upper structure. The increasing portion is due to the dynamic interaction between lower and upper structures. Furthermore, for each given value of R_m, as shown in Figure B.1 (a): (a) the maximum value of M_{U1} increases as the increase of ratio R_m, and (b) based on M_{U2}=1-M_{U1}, the maximum magnitude of M_{U2} also increases as the increase of ratio R_m. Consequently, in accordance with Eq.(A.21), the maximum α_U for given values of R_m and T_U/T_S increases as the increase of the ratio R_m.

B.3 Effects of period ratio T_U/T_s on factor α_U

Based on Eqs.(A.21), (A.19) and (A.20), it is found the influence of T_U/T_S on the amplification factor α_U is resulted from its effect on spectrum ratios $S_a(T_1)/S_a(T_U)$ and $S_a(T_2)/S_a(T_U)$. However, by comparing Figures B.1 (c) ~ (d) to Figures 3.3 (a) ~ (c), it is found although the ratio T_U/T_S has a considerable influence on the spectrum ratio $S_a(T_2)/S_a(T_U)$, but such influence has resulted in little effect on the value of the factor α_U. The influence of T_U/T_S on the factor α_U is primarily resulted from its effect on $S_a(T_1)/S_a(T_U)$:

(1) As shown in Eq.(A.19) and Figures B.1 (b) ~ (c), when $(T_U/T_S)\leq(T_U/T_1)$ or $(T_U/T_S)\geq 1$, the ratio T_U/T_S has no influence on the spectrum ratio $S_a(T_1)/S_a(T_U)$, whereas the spectrum ratio $S_a(T_1)/S_a(T_U)$ decreases as the increase of T_U/T_S when $(T_U/T_1)<(T_U/T_S)<1$. Then, based on Eq.(A.21), it can be seen that the effect of the ratio T_U/T_S on factor α_U is the same as the effect of the ratio T_U/T_S on the spectrum ratio $S_a(T_1)/S_a(T_U)$.

(2) As shown in Figure B.1 (c), for given values of R_m and T_U/T_S, the overall stiffness ratio R_k at which the spectrum ratio $S_a(T_1)/S_a(T_U)$ reaches unity increases as the increase of the ratio T_U/T_S if $T_U/T_S\leq 1$. Therefore, in accordance with Eq.(A.21), for given values of R_m, the overall stiffness ratio at which the factor α_U reaches the maximum value also generally increases as the increase of the ratio T_U/T_s when $(T_U/T_s)\leq 1$.

Appendix C Determination of critical stiffness ratios

C.1 Minimum overall stiffness ratio R_{kU1}

The minimum overall stiffness ratio R_{kU1} can be solved by setting

$$\varphi_{L1} = \frac{0.88N_L}{N_L + N_U} \tag{C.1}$$

Based on Eq.(A.7), φ_{L1} can be expressed as

$$\varphi_{L1} = \frac{R_m - R_{kU1} - 1 + \sqrt{(R_m - R_{kU1} - 1)^2 + 4R_m}}{2R_m} \tag{C.2}$$

By combing Eqs.(C.1) and (C.2), R_{kU1} can be solved for, and the obtained expression for R_{kU1} is shown in Eq.(3.22). Then, based on Eq.(3.7), the corresponding r_{kU1} can be obtained, as shown in Eq.(1.1) in Chapter 1.

C.2 Overall two-stage stiffness ratio of the upper structure R_{kU2stg}

Based on Eq.(A.21) and Figures B.1 (a) ~ (b), it is reasonable to assume α_U=1 if the following two requirements are satisfied simultaneously:

$$\begin{cases} M_{U1} \le 1.1 \\ T_1 / T_U \le 1.1 \end{cases} \tag{C.3}$$

In accordance with Eq.(A.17), the theoretical solution for M_{U1}≤1.1 is:

$$\begin{cases} \forall R_k & R_m \le 0.44 \\ R_k \le \dfrac{q_1(2R_m - 2 - q_1) + 4R_m}{2q_1} \quad \text{or } R_k \ge \max[R_m - 1 - q_2, \dfrac{q_2(2R_m - 2 - q_2) + 4R_m}{2q_2}] & R_m \ge 0.44 \end{cases} \tag{C.4}$$

where q_1 and q_2 are expressed as

$$q_1 = \frac{R_m + \sqrt{R_m^2 + 4.4R_m - 4.84R_m}}{1.1} \tag{C.5}$$

$$q_2 = \frac{R_m - \sqrt{R_m^2 + 4.4R_m - 4.84R_m}}{1.1} \tag{C.6}$$

Meanwhile, based on Eq.(A.8), the theoretical solution for T_1/T_U ≤1.1 is

$$R_k \ge 0.826R_m + 4.76 \tag{C.7}$$

By combining Eqs. (C.4) and (C.7), R_{kU2stg} is finally determined as presented in Eq.(3.9), where R_{kU2stg}=11.029R_m-2.5 (R_m>0.71) is obtained by curve fitting of Eq.(C.4), as shown in Figure.C.1 (a) with logarithmic scale on both horizontal and vertical axes.

C.3 Overall two-stage stiffness ratio R_{k2stg}

In accordance with the modal expansion theory (Chopra, 2007), the effective modal masses of the lower structure associated with the first and second modes, designated as M_{L1}^* and M_{L2}^*, respectively, can be evaluated based on the mode shapes shown in Figures A.1 (b) and (c) as follows :

$$M_{L1}^* = \frac{R_m\varphi_{L1}^2 + \varphi_{L1}}{R_m\varphi_{L1}^2 + 1} M_L \tag{C.8}$$

$$M_{L2}^* = M_L - M_{L1}^* \tag{C.9}$$

Similar to that of the upper structure, define normalized effective modal mass of the *j*th-mode of the lower structure M_{Lj} as

$$M_{L1} = \frac{R_m\varphi_{L1}^2 + \varphi_{L1}}{R_m\varphi_{L1}^2 + 1} \tag{C.10}$$

$$M_{L2} = 1 - M_{L1} \tag{C.11}$$

C.3.1 Effects of R_k on M_{L1} and M_{L2}

Based on Eq.(C.10), the derivative of the first mode normalized effective modal mass of the lower structure, M_{L1}, with respect to φ_{L1} is

$$\frac{dM_{L1}}{d\varphi_{L1}} = \frac{-R_m\varphi_{L1}^2 + 2\varphi_{L1} + 1}{\left(R_m\varphi_{L1}^2 + 1\right)^2} \tag{C.12}$$

By examing on Eqs.(C.12), (C.10), (B.1) and (A.7), it is observed that, as shown in Figure C.2 (a), M_{L1} gradually decreases from unity to zero as the stiffness ratio R_k increases from zero to infinity. On the other hand, based on Eq.(C.11), M_{L2} gradually increases from zero to unity as the stiffness ratio R_k increases from zero to infinity. It is also observed from Figure C.2 (a), M_{L1}=M_{L2}=0.5 if R_k=R_m+1.

C.3.2 Effects of R_k on T_1/T_L and T_2/T_L

Based on Eqs.(A.5) and (A.6), the following relationship among the periods can be derived:

$$T_1 T_2 = T_U T_L \tag{C.13}$$

Therefore, variations of T_1/T_L and T_2/T_L with respect to R_k are just opposite to variations of T_2/T_U and T_1/T_U with respect to R_k, respectively.

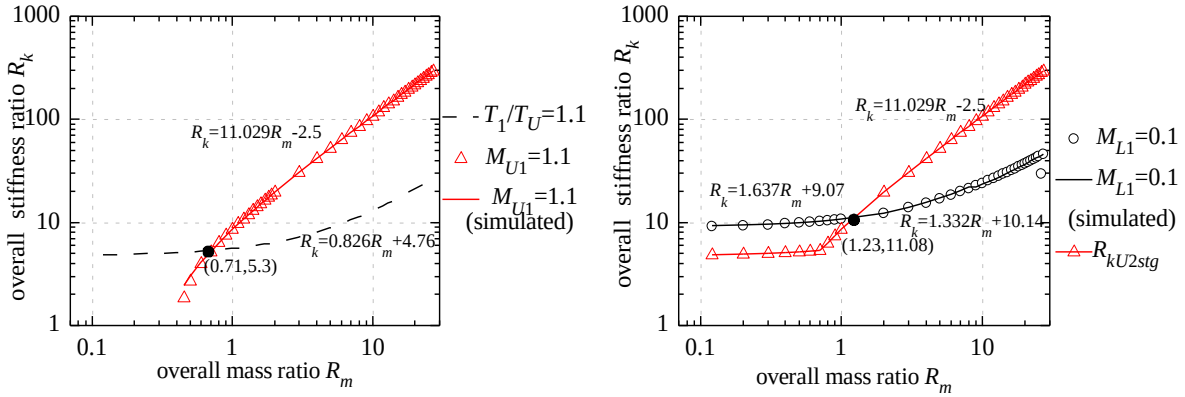

(a) R_{kU2stg} (b) R_{k2stg}

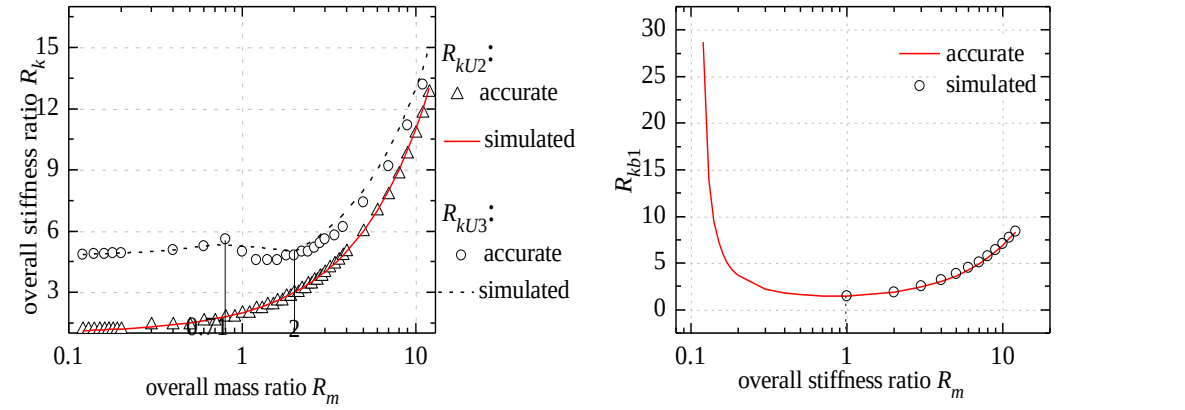

(c) R_{kU2} and R_{kU3} (d) R_{kb1}

Figure C.1: Determination of critical stiffness ratios

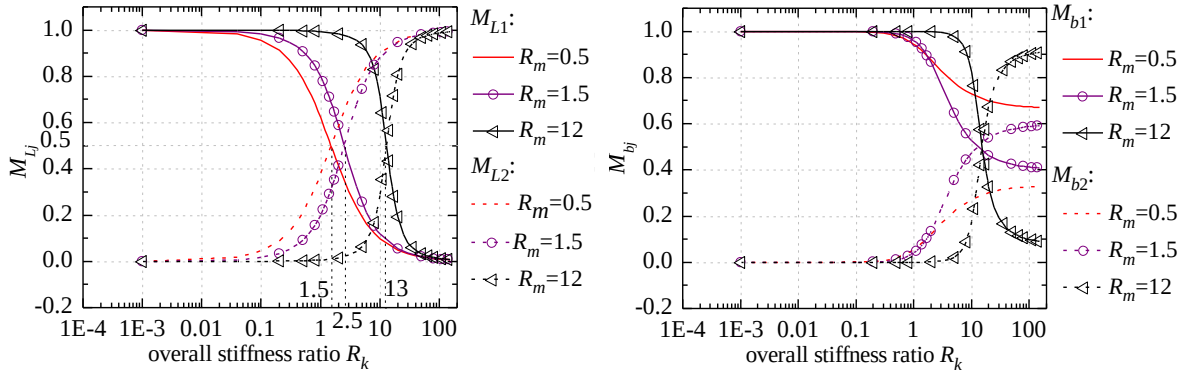

(a) M_{L1} and M_{L2} (b) M_{b1} and M_{b2}

Figure C.2: Variation of normalized effective mass distribution with respect to R_m and R_k

C.3.3 Overall two-stage stiffness ratio R_{k2stg}

Based on Figures C.2 (a) and B.1(b) and Eq.(C.13), it is reasonable to assume that Eq.(4.9) is satisfied if the following two requirements are satisfied simultaneously:

$$\begin{cases} M_{L1} \le 0.1 \\ T_1 / T_U \le 1.1 \end{cases} \tag{C.14}$$

The solution of $M_{L1} \le 0.1$ can be obtained numerically as follows:

$$\begin{cases} R_k \ge 1.637 R_m + 9.07 & R_m \le 3.5 \\ R_k \ge 1.332 R_m + 10.14 & R_m \le 3.5 \end{cases} \tag{C.15}$$

By combining Eqs.(C.15), (C.7) and (3.9), R_{k2stg} is finally determined as presented in Eq.(4.10), as shown in Figure C.1(b).

C.4 Overall two-stage stiffness ratio $R_{k2stg\text{-}ASCE}$ prescribed in ASCE 7

The two applicable requirements associated with the two-stage analysis procedure of ASCE 7 (ASCE, 2006) are: (a) the stiffness of the lower structure is at least 10 times the stiffness of the upper structure; and (b) the period of the entire structure is not greater than 1.1 times the period of the upper structure considered as a separate structure fixed at the base. These two applicable requirements can be expressed as

$$\begin{cases} R_k \ge 10 \\ T_1 / T_U \le 1.1 \end{cases} \tag{C.16}$$

By combining Eqs.(C.16) and (C.7), $R_{k2stg\text{-}ASCE}$ can be finally expressed by Eq.(4.27).

C.5 R_{kU2} and R_{kU3}

Parametric studies are carried out to determine the appropriate values of R_{kU2} and R_{kU3}. When T_U/T_S=0.2, $S_a(T_1)/S_a(T_U)$ is always unity when $R_k \ge R_m+1$ as shown in Figure B.1 (c). Therefore, in accordance with Eq.(A.21), R_{kU2} is set to be equal to R_m+1, as shown in Figure C.1 (c).

However, as presented in Eq.(3.11) and Figure C.1 (c), the value of R_{kU3} is highly dependent on the overall mass ratio R_m: (a) when the overall stiffness ratio R_m is less than 0.71, the shear-force-amplification factor of the upper structure always increases as the increase of the overall stiffness ratio R_k if $T_U/T_S \ge 1$, which results in that R_{kU3} is identical to R_{kU2stg}; (b) when R_m is greater than 2, period ratio T_U/T_S has little influence on the factor α_U, and R_{kU2} and R_{kU3} are located close to each other; by curving fitting, R_{kU3} can be fitted as $R_{kU3}=R_m+3$; and (c) when the overall mass ratio R_m is in the range $0.71<R_m<2$, R_{kU3} gradually decreases as the increase of overall mass ratio R_m and R_{kU3} can be approximated as $R_{kU3}=-0.26R_m+5.52$.

C.6 R_{kb1}

The effective masses of the entire building associated with the first and second modes, designated as M_{b1}^* and M_{b2}^*, are defined as

$$M_{b1}^* = M_{L1}^* + M_{U1}^* \tag{C.17}$$

$$M_{b2}^* = M_{L2}^* + M_{U2}^* \tag{C.18}$$

Similar to that of the upper structure, define the normalized effective modal mass of the *j*th-mode of the entire building M_{bj} as

$$M_{b1} = \frac{M_{L1}^* + M_{U1}^*}{M_L + M_U} = \frac{\left(R_m\varphi_{L1}^2 + \varphi_{L1}\right)R_m + R_m\varphi_{L1} + 1}{\left(R_m + 1\right)\left(R_m\varphi_{L1}^2 + 1\right)} \tag{C.19}$$

$$M_{b2} = 1 - M_{b1} \tag{C.20}$$

C.6.1 Effects of R_k on M_{b1} and M_{b2}

Based on Eq.(C.19), the derivative of the normalized effective modal mass of the first mode of the entire building, M_{b1}, with respect to φ_{L1} is

$$\frac{dM_{b1}}{d\varphi_{L1}} = \frac{-2R_m}{\left(R_m\varphi_{L1}^2 + 1\right)^2}\left[R_m\varphi_{L1}^2 - \left(R_m - 1\right)\varphi_{L1} - 1\right] \tag{C.21}$$

In accordance with Eqs.(C.21), (C.19), (B.1) and (A.7), it is observed that, as shown in Figure C.2.(b), as the stiffness ratio R_k increases from zero to infinity, M_{b1} gradually decreases from unity to the following minimum value:

$$\left|M_{b1}\right|_{\min} = \frac{1}{R_m + 1} \tag{C.22}$$

On the other hand, based on Eq.(C.20), it is obtained that, as shown in Figure C.2.(b), as the stiffness ratio R_k increases from zero to infinity, M_{b2} gradually increases from zero to the following maximum value:

$$\left|M_{b1}\right|_{\max} = \frac{R_m}{R_m + 1} \tag{C.23}$$

C.6.2 R_{kb1}

The applicable requirement of the modified ELF procedure presented in section 4.2.2 is that the effective mass of the entire building associated with the first mode is not less than 90% of the total mass, i.e., $M_{b1}\geq 0.9$. In accordance with Eqs.(C.19) and (A.7) , the theoretical solution for $M_{b1}\geq 0.9$ is

$$\begin{cases} \forall R_k & R_m \le 1/9 \quad \text{(a)} \\ R_k \le R_m - 1 - \dfrac{d}{2} + \dfrac{2R_m}{d} \quad \text{where } d = \dfrac{2\left[-10R_m + 3\sqrt{R_m}(R_m+1)\right]}{R_m - 9} & R_m > 1/9 \ \ (R_m \ne 9) \quad \text{(b)} \\ R_k \le \dfrac{25}{4} & R_m = 9 \quad \text{(c)} \end{cases} \tag{C.24}$$

Based on Eq.(C.24), the calculated R_{kb1} is shown in Figure C.1 (d). As to the practical "appendage-style" buildings, the overall mass ratio R_m is usually greater than unity. For simplicity, the calculated R_{kb1} is fitted by Eq. (4.2) by curve fitting when $R_m \ge 1$.

Appendix D Validation of simplified 2DOF model

In order to investigate how the interaction of lower and upper structures in terms of mass and stiffness affects the seismic response of the combined framing system, a simplified 2DOF model, as shown in Figure 3.1 (b), is proposed to approximate the seismic response of the MDOF model. However, such simplification is an empirical process. The accuracy of such simplification needs to be validated.

D.1 Errors of amplification factor α_U

The amplification factor α_U based on MDOF modal response spectrum analysis with CQC rule to combined the peak modal response (Chopra, 2007) can be computed as

$$\alpha_U = \sum_{i=1}^{N}\sum_{j=1}^{N}\sqrt{\rho_{ij}\frac{M_{Ui}S_a(T_i)}{S_a(T_U)}\frac{M_{Uj}S_a(T_j)}{S_a(T_U)}} \tag{D.1}$$

where N is the number of the storey of the combined framing system; T_i and M_{Ui}, are periods and normalized effective modal mass of the upper structure associated with the ith-mode, respectively; and ρ_{ij} is the correlation coefficient between the ith- and jth-modes. Modal parameters T_i, M_{Ui} and ρ_{ij} can be obtained in a similar way as that of the simplified 2DOF model, as discussed in Appendix A. However, as to the MDOF model, the eigenvalue analysis can be carried out only with the numerical analysis and no analytical expression concerning the modal parameters are available. To illustrate the error of the factor α_U associated with the simplified 2DOF model, buildings with N_L=8, N_U=2 and r_m=3 are selected as examples for the purpose of demonstration. For the reason of better illustration, the storey-stiffness ratio r_k in Figure D.1 is set to be between 0.1 and 500, which exceeds the limitation specified in section 1.3.2.

By comparing Figures.D.1 (c) and (d), it can be seen the error of factor α_U is primarily induced by the error of M_{Ui} associated with the simplified 2DOF:

(1) When $r_k<r_{kU2}$, the negative error of α_U is primarily induced by the smaller M_{U1} associated with the simplified 2DOF model. The smaller M_{U1} associated with the simplified 2DOF model is inherited from the empirical model simplification process. Possible improvement on M_{U1} may require to model the multi-storey building in a simplified model more than 2DOF.

(2) When $r_k>r_{kU3}$, the negative error of α_U is primarily associated with the fact that only the interaction of the first modes of the lower and upper structures is considered in the simplified 2DOF model. However, in the MDOF model, the interaction of vibration modes other than the first ones between the lower and upper structures, especially the interaction of the first mode of the lower structure and the second mode of the upper structure, may not be ignored.

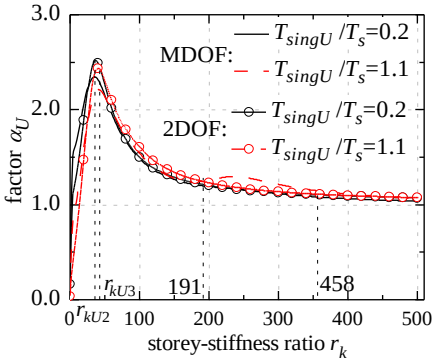

(a) comparison of factor α_U

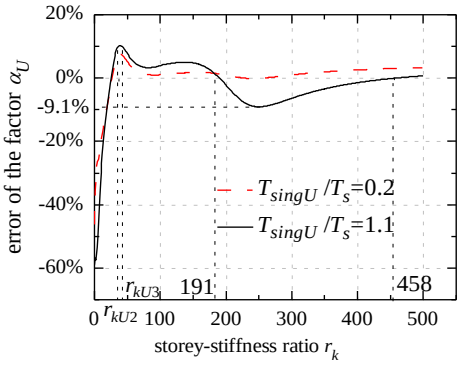

(b) error of simplified 2DOF model

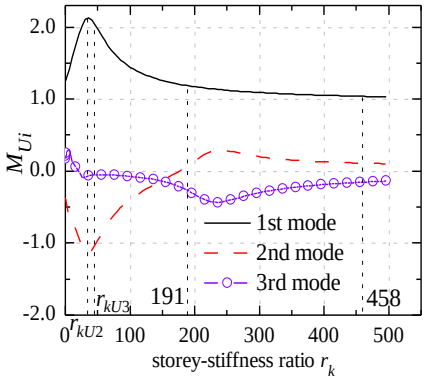

(c) M_{Ui} in the MDOF model

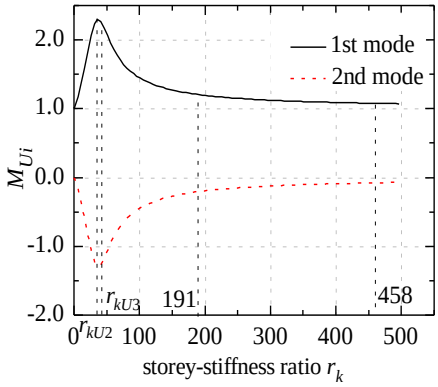

(d) M_{Ui} in simplified 2DOF model

Figure D.1: Comparison of factor α_U between MDOF and simplified 2DOF models (N_L=8, N_U=2 and r_m=3)

When 191≤r_k≤458, the calculated ratio between the first period of the lower structure and the second period of the upper structure ranges between 0.71 and 1.10, which is close to unity. As discussed in section 3.3.1, when periods of the lower and upper structures are close to each other, the shear-force-amplification effect of the lower structure on the upper one can be significant. Consequently, as the result of the interaction of the first mode of the lower structure and the second mode of the upper structure, there are local maxima of normalized modal masses of the upper structure M_{U2} and M_{U3} when 191≤r_k≤458, as shown in Figure.D.1 (c). Although the magnitudes of M_{U2} and M_{U3} are much less than that of M_{U1}, if the storey-period of the upper structure T_{singU} is relatively large, say T_{singU}/T_s=1.1, it will result in large spectrum ratio $S_a(T_2)/S_a(T_1)$, say $S_a(T_2)/S_a(T_1)$=1.81. Therefore, the contribution of M_{U2} and M_{U3} cannot be neglected. In such case, the simplified 2DOF model leads to smaller α_U, with the maximum negative error being -9.1%, as shown in Figures.D.1 (a) and (b). However, when the period of the upper structure is short, for example, T_{singU}/T_s=0.2, $S_a(T_2)/S_a(T_1)$ is small, say $S_a(T_2)/S_a(T_1)$=(0.79~0.81); as the result, the contribution of

M_{U2} and M_{U3} can be ignored and the factor α_U evaluated from the simplified 2DOF model is larger than that from the MDOF model.

(3) When $r_{kU2} \leq r_k \leq r_{kU3}$, the dominating modes of the MDOF model, which are first and second vibration modes, can be well represented by the simplified 2DOF model, as shown in Figures.D.1 (c) ~ (d).

Errors of the factor α_U induced by the simplified 2DOF model for the case where $r_{kU2} \leq r_k \leq r_{kU3}$ are further justified. By considering all possible combinations of r_m, T_{singU}/T_S and T_{singL}/T_S as stated in section 1.3.2 and letting $r_{kU2} \leq r_k \leq r_{kU3}$, the maximum and minimum errors induced by the simplified 2DOF model for the building with an N_L-storey lower structure and an N_U-storey upper structure are listed in Tables D.1 and D.2. It is seen errors of the factor α_U associated with the simplified 2DOF model for the case where $r_{kU2} \leq r_k \leq r_{kU3}$ are acceptable.

Table D.1: Maximum errors of factor α_U induced by the simplified 2DOF model when $r_{kU2} \leq r_k \leq r_{kU3}$ (ASCE 7 spectrum)

N_L \ N_U	1	2	3	4	5	6	7	8	9
1	0.0%	6.1%	9.1%	N/A	N/A	N/A	N/A	N/A	N/A
2	8.0%	12.4%	14.3%	15.3%	16.1%	15.4%	13.3%	N/A	N/A
3	10.1%	15.0%	17.7%	18.8%	19.0%	19.4%	19.2%	N/A	N/A
4	11.0%	15.9%	19.0%	20.7%	21.5%	21.6%	N/A	N/A	N/A
5	11.3%	16.3%	19.5%	21.5%	22.4%	N/A	N/A	N/A	N/A
6	N/A	16.4%	19.8%	22.0%	N/A	N/A	N/A	N/A	N/A
7	N/A	16.4%	19.9%	N/A	N/A	N/A	N/A	N/A	N/A
8	N/A	16.3%	N/A	N/A	N/A	N/A	N/A	N/A	N/A
9	N/A	N/A	N/A	N/A	N/A	N/A	N/A	N/A	N/A

Note: N/A denotes the storey combination of the lower and upper structures, or the storey-stiffness ratio r_k that lies between r_{kU2} and r_{kU3} for that storey combination, is out of the scope of this study.

Table D.2: Minimum errors of factor α_U induced by the simplified 2DOF model when $\boldsymbol{r_{kU2} \leq r_k \leq r_{kU3}}$ (ASCE 7 spectrum)

N_L \ N_U	1	2	3	4	5	6	7	8	9
1	0.0%	2.0%	3.7%	N/A	N/A	N/A	N/A	N/A	N/A
2	0.7%	2.8%	3.6%	5.3%	6.0%	6.7%	9.9%	N/A	N/A
3	1.7%	3.8%	4.1%	5.7%	6.0%	7.4%	11.0%	N/A	N/A
4	2.6%	5.3%	6.6%	11.8%	7.0%	11.6%	N/A	N/A	N/A
5	4.3%	6.6%	12.9%	14.3%	13.1%	N/A	N/A	N/A	N/A
6	N/A	10.8%	12.9%	14.2%	N/A	N/A	N/A	N/A	N/A
7	N/A	11.7%	12.8%	N/A	N/A	N/A	N/A	N/A	N/A
8	N/A	13.0%	N/A	N/A	N/A	N/A	N/A	N/A	N/A
9	N/A	N/A	N/A	N/A	N/A	N/A	N/A	N/A	N/A

Note: N/A denotes the storey combination of the lower and upper structures, or the storey-stiffness ratio r_k that lies between r_{kU2} and r_{kU3} for that storey combination , is out of the scope of this study.

D.2 Errors of shear force associated with the proposed two-stage analysis procedure

D.2.1 Upper structure

Seismic loads of the upper structure that are calculated by the proposed two-stage analysis procedure with the assumption that $\gamma_{intr}=0$ are compared with the accurate results. In this study, seismic loads calculated by the modal response spectrum analysis (Chopra, 2007) based on the MODF model shown in Figure 3.1 (a) are considered as the accurate results. In order to illustrate such comparison, take buildings with $N_L=2$, $N_U=8$ and $r_m=3$ as example. The storey-mass of the upper structure is $m_U=1000$ kg. The site spectrum are $S_S=2.447$ g, $S_1=0.858$ g, and the long transition period $T_{Long}=8$ second. The selected storey-stiffness ratio r_k for this building ranges between 3.67 and 60, where 3.67 is the two-stage storey-stiffness ratio of the selected combined framing system, as shown in Table 4.2. Note for the reason of better illustration, the range of the selected storey-stiffness ratios exceeds the limitation specified in section 1.3.2. The comparison is shown in Figures D.2 (a) ~ (d).

The results marked by "$\gamma_{intr}=0$" in Figures D.2 (a) ~ (d) are calculated by the proposed two-stage analysis procedure with the assumption that $\gamma_{intr}=0$. Negative and positive errors shown in the figure signify the proposed two-stage analysis procedure with the assumption that $\gamma_{intr}=0$ underestimates and overestimates the seismic load, respectively. From Figures D.2 (a) ~ (d), it is seen although the base shear force of the upper structure can be well approximated by setting $\gamma_{intr}=0$, the shear force of the top storey of the upper structure may be considerably underestimated. For example, when $T_{singU}/T_S=1.1$ and $r_k=10$, as shown in Figure D.2 (d), the proposed two-stage analysis procedure with the assumption that $\gamma_{intr}=0$ underestimates the shear force of the top storey by 40.0%. In fact, from Figures D.2 (a) ~ (d), it is observed that all the largest negative error occurs at the top storey of the upper structure. Therefore, the error of seismic load associated with the top storey of the upper structure needs to be further investigated.

From Figures D.2 (a) ~ (d), it is seen the underestimation of seismic load associated with top storey is significantly affected by the storey-stiffness ratio r_k and the single storey-period of the upper structure T_{singU}/T_S:

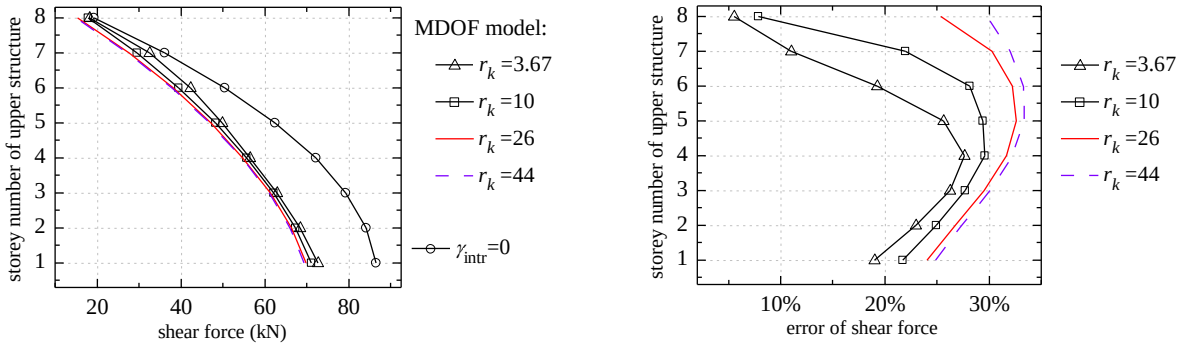

(a) comparison of shear force (T_{singU}/T_S=0.3)

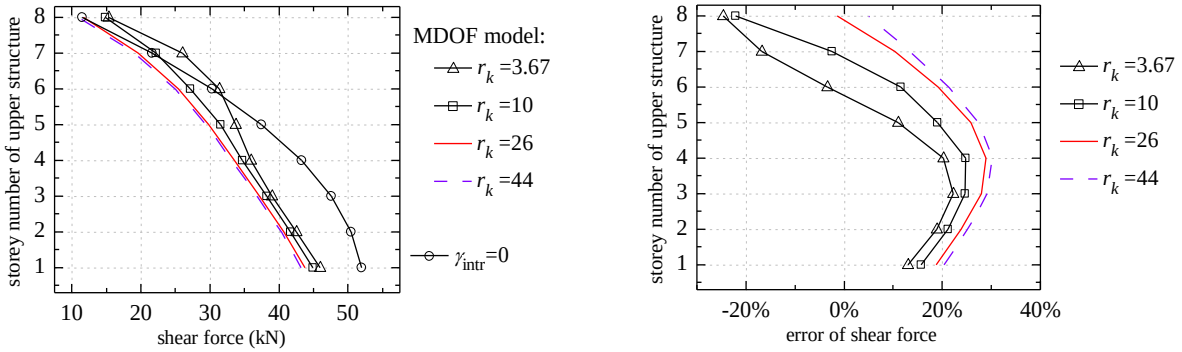

(b) comparison of shear force (T_{singU}/T_S=0.5)

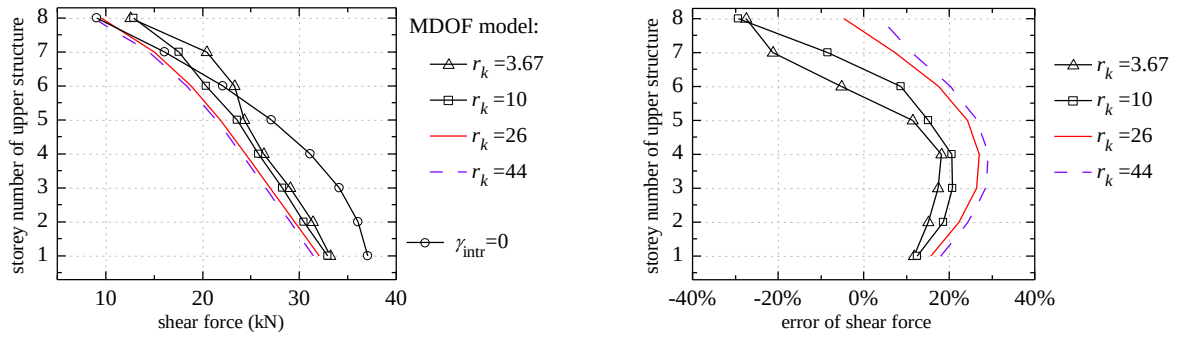

(c) comparison of shear force (T_{singU}/T_S=0.7)

Figure D.2: Errors of shear force for upper structure associated with proposed two-stage analysis procedure with the assumption γ_{intr}=0 (N_L=2, N_U=8 and r_m=3)

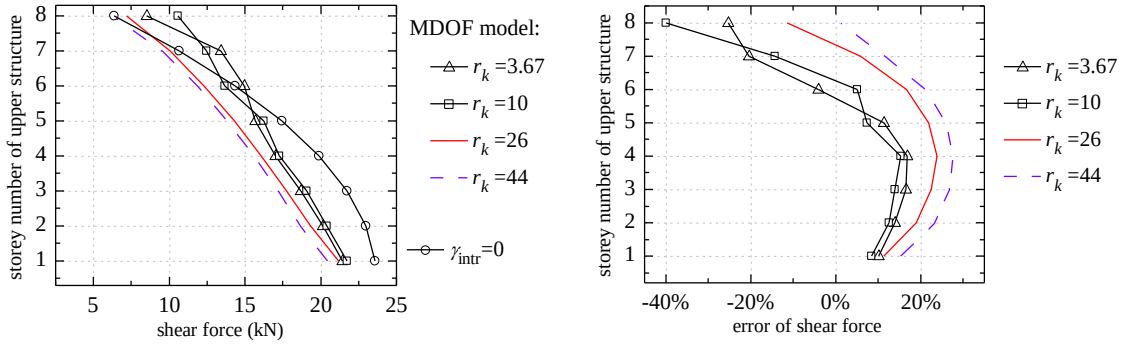

(d) comparison of shear force (T_{singU}/T_S=1.1)

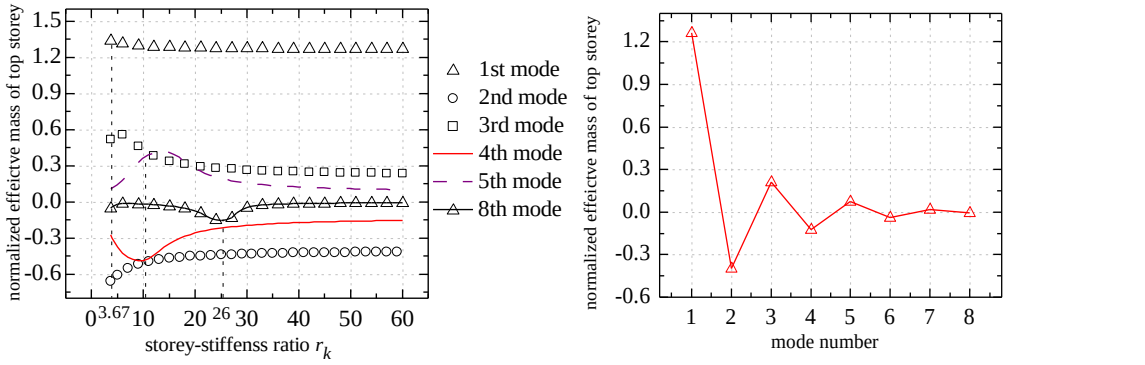

(e) normalized effective mass of top storey in combined framing MDOF model

(f) normalized effective mass of top storey in separate upper structure MDOF model

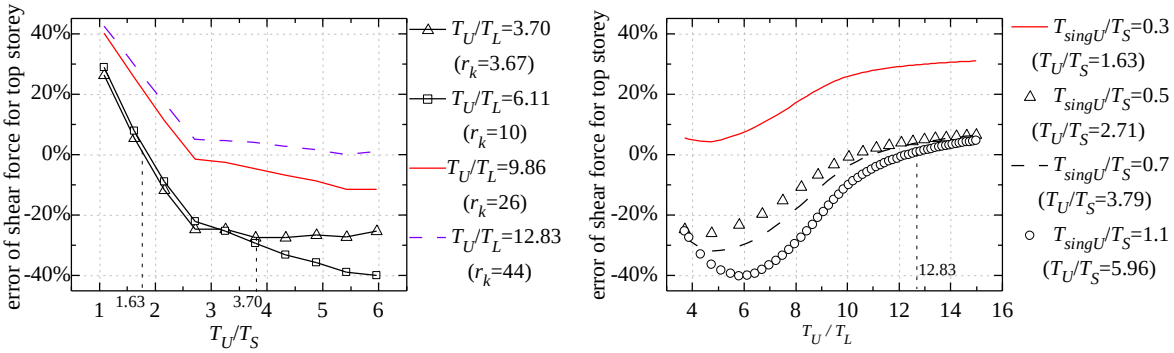

(g) effects of T_U/T_S on the error of top storey shear force

(h) effects of T_U/T_L on the error of top storey shear force

Figure D.2: Errors of shear force for upper structure associated with proposed two-stage analysis procedure with the assumption γ_{intr}=0 (N_L=2, N_U=8 and r_m=3) (continued)

(1) When the storey-stiffness ratio r_k=3.67, the calculated period ratio between the lower and upper structures, T_U/T_L, is 3.70. Meanwhile, concerning the eight-storey upper structure, its second and third mode periods are 2.97 and 4.83 times the period of the first mode, respectively. Therefore, for the case r_k=3.67, the first mode period of the lower structure lies between the second and third mode

periods of the upper structure. Owing to the interaction of these vibration modes, the normalized effective masses of the top storey associated with the second to fourth modes of the combined framing system, as shown in Figure D.2 (e), are much larger than those calculated by setting the upper structure as a separate fixed-base MDOF model, as shown in Figure D.2 (f). Although magnitudes of the normalized effective masses associated with those modes are still less than that of the first mode, if the storey-period of the upper structure T_{singU} is relatively large, say T_{singU}/T_s=1.1, it will result in large spectrum ratios, say $S_a(T_2)/S_a(T_1)$=2.87, $S_a(T_3)/S_a(T_1)$=4.19, and $S_a(T_4)/S_a(T_1)$=5.46. Therefore, the contribution of these modes cannot be neglected. In such case, the assumption γ_{intr}=0 leads to an underestimation of the shear force of the top storey by 25.3%, as shown in Figure D.2 (d). However, when the period of the upper structure is short, for example, T_{singU}/T_s=0.3, corresponding spectrum ratios are relatively small, say $S_a(T_2)/S_a(T_1)$=$S_a(T_3)/S_a(T_1)$=$S_a(T_4)/S_a(T_1)$=1.73. For this case, the assumption γ_{intr}=0 can well approximate the shear force for the top storey of the upper structure with the error of shear force being 5.5%, as shown in Figure D.2 (a).

(2) As the increase of the storey-stiffness ratio r_k, the magnitude of the negative error associated with the assumption γ_{intr}=0 may further increase. For example, when r_k=10, the first mode period of the lower structure is close to the fourth mode period of the upper structure. Therefore, the interaction of the first mode of the lower structure and the fourth mode of the upper structure becomes significant. The normalized effective masses of the top storey associated with the fourth and fifth modes have the local maximum values, as shown in Figure D.2 (e). Meanwhile, the corresponding spectrum ratios can be quite large when T_{singU}/T_s=1.1, say $S_a(T_4)/S_a(T_1)$=$S_a(T_5)/S_a(T_1)$=6.10. Therefore, due to the increase of the spectrum ratios, the magnitude of the negative error of the top shear force associated with the assumption γ_{intr}=0 will further increase. In this case, the assumption γ_{intr}=0 results in an underestimation of the shear force of the top storey by 40.0%, as shown in Figure D.2 (d). However, when T_{singU}/T_s=0.3, the assumption γ_{intr}=0 can still well approximate the shear force for the top storey of the upper structure, with the error of top storey shear force being 7.9%, as shown in Figure D.2 (a).

(3) As the further increase of r_k, the magnitude of negative error associated with the top storey gradually decreases. For example, the error is only -11.5% when r_k=26 and T_{singU}/T_s=1.1. For the case where r_k=26, the first mode period of the lower structure is close to the eighth mode period of the upper structure. The interaction of these two vibration modes results in that the normalized effective mass of the top storey associated with the eighth mode has a local maximum value, as shown in Figure D.2 (e). However, compared to the normalized effective mass of the first mode, the local maximum normalized effective mass associated with the eighth mode is so small that it has little influence on the seismic load. Therefore, the interaction of the first mode of the lower structure and

eighth mode of the upper structure does not introduce a significant negative error for the seismic load of the top storey.

(4) Finally, when r_k further increases as it is not less than 44, the first mode period of the lower structure is much greater than the eighth mode period of the upper structure. The lower structure has no effect on the upper one. The upper structure now can be truly treated it is fixed to the ground base. The assumption γ_{intr}=0 can well approximate the shear force of the top storey regardless values of the T_{singU}/T_S, as shown in Figures D.2 (a) ~ (d).

Upon the foregoing discussions, it is seen the underestimation of the shear force associated with the top storey is primarily resulted from the fact that the assumption γ_{intr}=0 ignores the interaction of the first mode of the lower structure and other higher vibration modes of the upper structure. This is also the primary reason for the underestimation of the amplification factor α_U associated with the simplified 2DOF model when $r_k > r_{kU3}$, as discussed in Appendix D.1. The only difference is that the amplification associated with these interactions is far more significant on the shear force of the top storey than on the base shear force of the upper structure. Therefore, an additional top shear force should be added to account for the "extra" amplification effect contributed by the interaction of the first mode of the lower structure and other higher vibration modes of the upper structure on the shear force of the top storey. The value of γ_{intr} shown in Eq.(4.18) cannot be zero in certain cases.

The foregoing discussions also show that the error of the shear force for the top storey associated with the assumption γ_{intr}=0 is primarily affected by the period ratio of the upper structure T_U/T_S and period ratio between lower and upper structures T_U/T_L.

Effects of T_U/T_S

The effect of T_U/T_S on the error of the shear force of the top storey associated with the assumption γ_{intr}=0 is illustrated in Figure D.2 (g). From the figure, it is seen the error is positive when the period ratio of the upper structure T_U/T_S is small. Then, as the increase of T_U/T_S, the effect of the "*i*th-interacted vibration modes" becomes more significant due to the increase the spectrum ratio $S_a(T_i)/S_a(T_1)$; therefore, the error turns to be negative and the magnitude of the negative error gradually increases. Finally, when the period ratio T_U/T_S is approximately equal to the period ratio between the lower and upper structures, i.e, $T_U/T_S=T_U/T_L$, the negative error reaches the minimum value and remains invariant as the further increase of T_U/T_S. For example, when r_k=3.67, which results in T_U/T_L=3.70, the error is positive if $T_U/T_S \leq 1.63$; then as T_U/T_S increases from 1.63 to 3.70, the error decreases from 0% to -27%; and finally, the error remains the minimum value -27% when the period ratio T_U/T_S increases from 3.70 to 5.96, as shown in Figure D.2 (g).

The effect of the T_U/T_S on the error of the top shear force is primarily resulted from its effect on the spectrum ratio between the "*i*th-interacted vibration modes" and the first mode, i.e., $S_a(T_i)/S_a(T_1)$. The spectrum ratio $S_a(T_i)/S_a(T_1)$ is not only related with the period ratio T_i/T_1, but also related with T_1/T_S, as shown in the response spectrum curve shown in Figure 1.4. Meanwhile, when the proposed two-stage analysis procedure is applicable for the combined framing system, it is seen $T_1 \approx T_U$ as shown in Figure 4.3 (b). Furthermore, upon the foregoing discussion, it is seen the period of the "*i*th-interacted vibration mode" is approximately equivalent to the period of the lower structure T_L. Therefore, the spectrum ratio between the "*i*th-interacted vibration modes" and the first mode, i.e., $S_a(T_i)/S_a(T_1)$, can be approximately evaluated by T_L/T_U and T_U/T_S as follows :

$$\frac{S_a(T_i)}{S_a(T_U)} \approx \frac{S_a(T_L)}{S_a(T_U)} = \begin{cases} 1 & T_U / T_S \le 1 \\ T_U / T_S & 1 < T_U / T_S < T_U / T_L \\ T_U / T_L & T_U / T_S \ge T_U / T_L \end{cases} \quad \text{(D.2)}$$

Based on Eq.(D.2), it is seen when $(T_U/T_S) \geq (T_U/T_L)$, the ratio T_U/T_S has no influence on the spectrum ratio $S_a(T_i)/S_a(T_1)$. Therefore, when $T_U/T_S \geq (T_U/T_L)$, the error of the top storey shear force associated with the assumption $\gamma_{intr}=0$ remains as the constant being the minimum value.

Effects of T_U/T_L

As shown in Figure D.2 (h), with a given period ratio of the upper structure T_U/T_S, the magnitude of the negative error firstly increases and then decreases as the increase of the period ratio T_U/T_L. When the first mode period of the lower structure is greater than the period of the highest mode the upper structure, the interaction between the lower and upper structures in terms of mass and stiffness can be completely ignored and the negative error of the top storey shear force completely vanishes. For example, when r_k=44, which results in T_U/T_L=12.83, the first mode period of the lower structure is greater than the eighth mode period of the upper structure, and the proposed two-stage analysis procedure with the assumption $\gamma_{intr}=0$ can well approximate the shear force, as shown in Figures D.2 (a) ~ (d).

D.2.2 Lower structure

The seismic load of the lower structure evaluated by the proposed two-stage analysis procedure may be much greater than that calculated from the MDOF model. To illustrate how the error occurs, take buildings with N_L=4, N_U=6 and r_m=1.2 as example. The storey-mass of the upper structure and the site spectrum of the combined framing system are identical to those of the combined framing system discussed in Appendix D.2.1. The selected storey-stiffness ratio r_k for the building ranges between 7.50 and 80, with 7.50, which is calculated based on Eq.(4.11), being the two-stage storey-stiffness

ratio of the selected combined framing system. Note for the reason of better illustration, the range of the selected storey-stiffness ratio r_k exceeds the limitation specified in section 1.3.2. The comparison is shown in Figures D.3 (a) ~ (d).

The results marked by "proposed" in Figures D.3 (a) ~ (d) are calculated by the proposed two-stage analysis procedure, and the results marked by "ASCE 7" are calculated by the two-stage analysis procedure prescribed in ASCE 7 (ASCE, 2006). Negative and positive errors shown in the figures signify the two-stage analysis procedure underestimates and overestimates the seismic load, respectively. From Figures D.3 (a) ~ (d), it is seen the proposed two-stage analysis procedure may considerably overestimate the shear forces of the lower structure. However, compared to the overestimation of shear forces of the lower structure associated with the two-stage analysis procedure prescribed in ASCE 7 (ASCE, 2006), the accuracy of the proposed two-stage analysis procedure is greatly improved. For example, when T_{singU}/T_S=1.1 and r_k=12, the proposed two-stage analysis procedure overestimates the shear force for the second storey of the lower structure by 87.1%, while such overestimation associated with ASCE 7 is 133.4%, as shown in Figure D.3 (b). The primary reason for the improved accuracy associated with the proposed two-stage analysis procedure is discussed in section 4.5.2.1. The proposed two-stage analysis procedure adopts the SRSS rule to combine the peak modal responses while the two-stage analysis procedure in ASCE 7 (ASCE, 2006) selected the ABSSUM rule to combine the peak modal response. Usually, using the ABSSUM rule to combine the peak modal response will lead to much larger results (Chopra, 2007).

As to the proposed two-stage analysis procedure, the primary reason for the overestimation of the shear forces of the lower structure is similar to that for the underestimation of the top storey shear force of the upper structure discussed in Appendix D.2.1. The proposed two-stage analysis procedure is established based on the simplified 2DOF model and does not account for the interaction of the first mode of the lower structure and higher vibration modes of the upper structure. To illustrate how such interaction affects the error of shear forces of the lower structure associated with the proposed two-stage analysis procedure, the base shear force of the lower structure, i.e., the shear force for the first storey of the lower structure, is selected as the example to be further investigated.

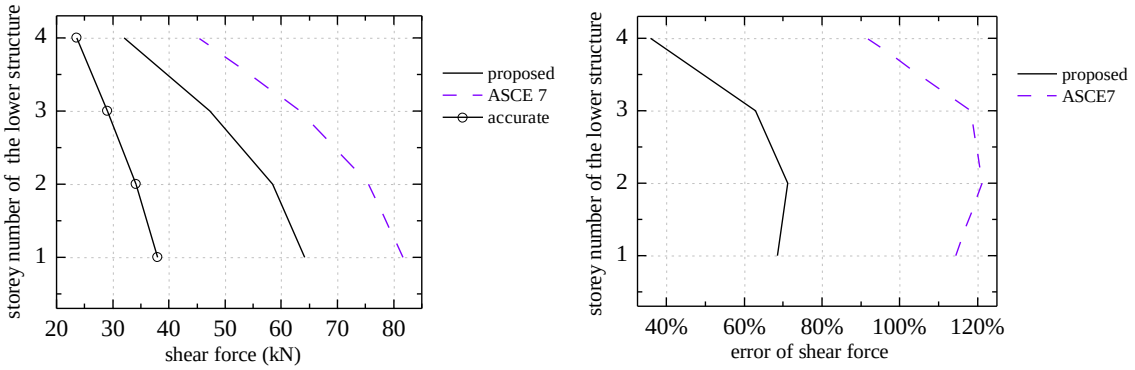

(a) comparison of shear force (r_k=7.5)

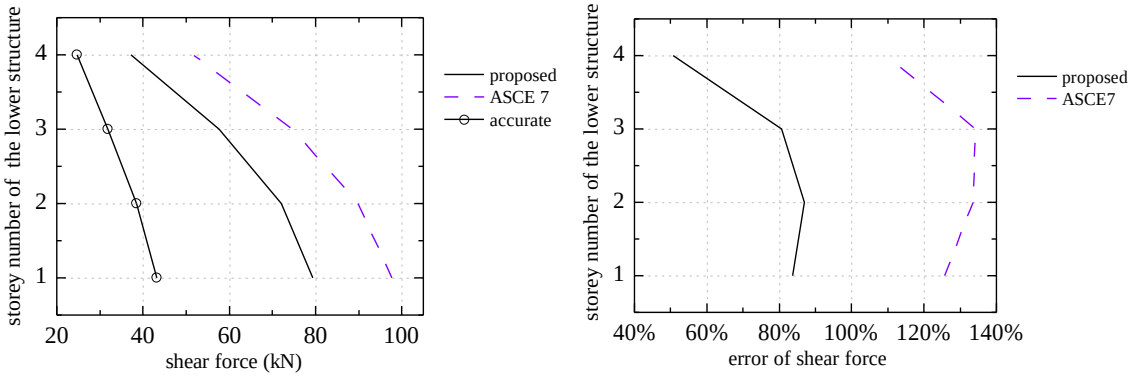

(b) comparison of shear force (r_k=12)

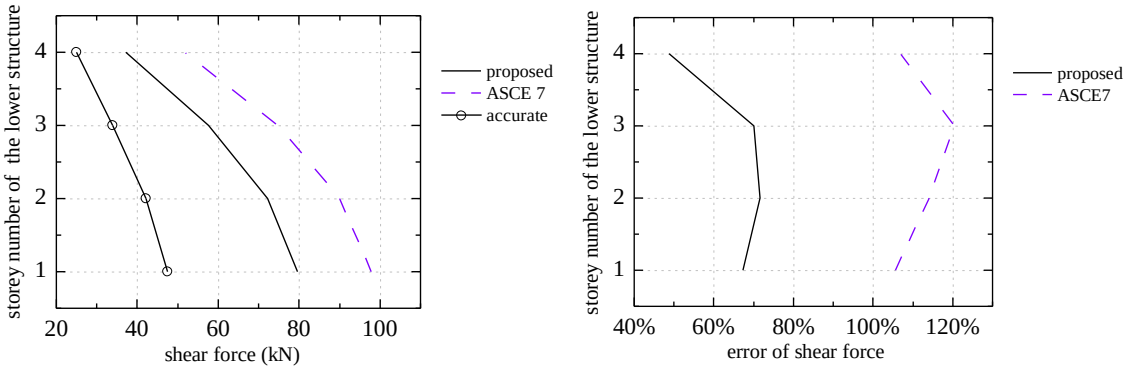

(c) comparison of shear force (r_k=21)

Figure D.3: Errors of shear force for lower structure associated with two-stage analysis procedure (N_L=4, N_U=6 ,r_m=1.2 and T_{singU}/T_S=1.1)

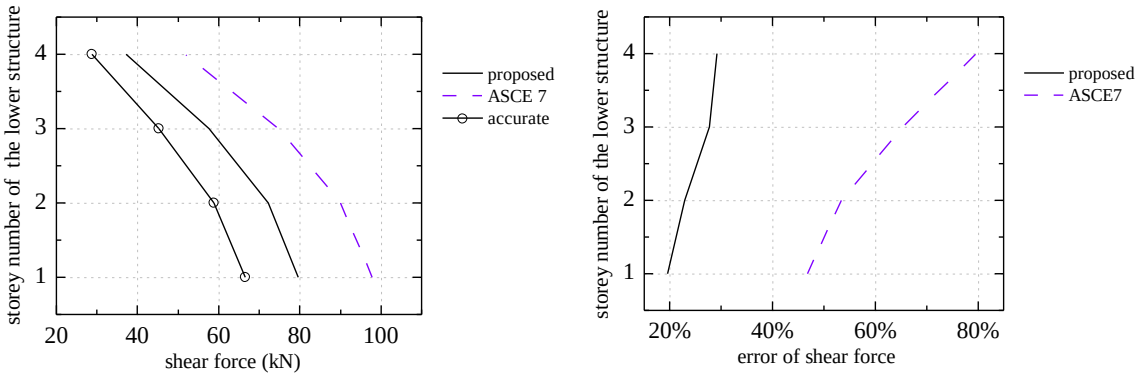

(d) comparison of shear force (r_k=80)

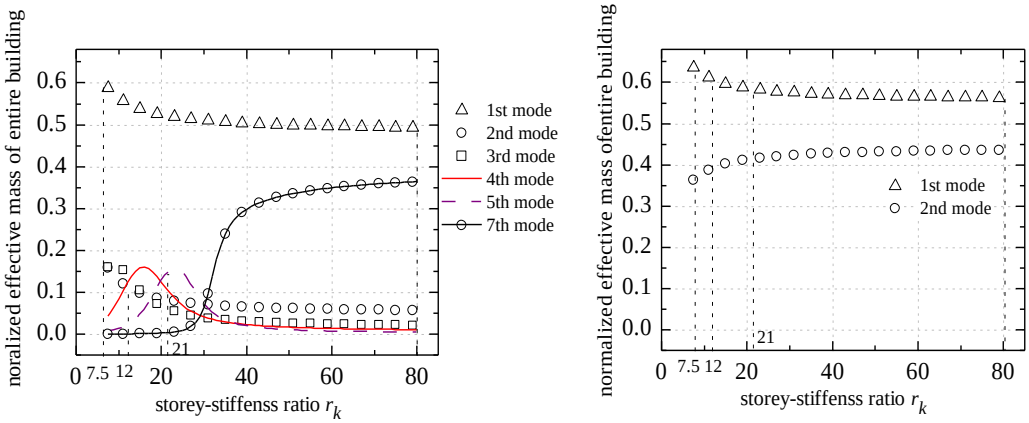

(e) normalized effective mass of entire building in combined framing MDOF model

(f) normalized effective mass of entire building in simplified 2DOF model

Figure D.3: Errors of shear force for lower structure associated with two-stage analysis procedure (N_L=4, N_U=6 ,r_m=1.2 and T_{singU}/T_S=1.1) (continued)

From Figures D.3 (a) ~ (d), it is seen when T_{singU}/T_S=1.1, the error of the base shear forces of the lower structure is greatly dependent on the storey-stiffness ratio r_k. The following is observed:

(1) When the storey-stiffness ratio r_k=7.50, the normalized first mode effective modal mass of entire building for both the MDOF model and the simplified 2DOF model are close to each other, i.e., 0.59 vs. 0.64, as shown in Figures D.3 (e) and (f), respectively. Note since the proposed two-stage analysis procedure is established based on the simplified 2DOF model, the normalized effective modal mass distribution associated with the simplified 2DOF model represents the normalized effective modal distribution associated with the proposed two-stage analysis procedure. On the other hand, the calculated period ratio between lower and upper structures, T_U/T_L, is 3.60. Concerning the six-storey upper structure, its second and third mode periods are 2.94 and 4.71 times its first mode period, respectively. Therefore, for the case where r_k=7.50, the first mode period of the lower

structure lies between the second and third mode periods of the upper structure. Owing to the interaction of these vibration modes, the rest of the normalized effective modal mass of the entire building other than that of the first mode, i.e., 0.41 in the MDOF model, is primarily distributed in the second and third vibration modes, as shown in Figure D.3 (e). However, in the simplified 2DOF model, the remaining normalized effective modal mass of the entire building other than that of the first mode, i.e., 0.36, is "lumped" in the second mode, as shown in Figure D.3 (f). Since the normalized effective modal mass of the entire building for each mode in both the MDOF and 2DOF modes lies between zero and unity, according to the CQC rule, the simplified 2DOF model will lead to larger base shear force of the lower structure, with the error being 60.6% as shown in Figure D.3 (a).

(2) As the increase of the storey-stiffness ratio r_k, the normalized effective modal mass of the entire building associated with the first mode in the MDOF model does not change a lot. However, the remaining normalized effective modal mass of the entire building other than that of the first mode changes. The normalized effective modal mass of the entire building associated with the second mode decreases while that associated with the fourth mode increases, as shown in Figure D.3 (e). For example, when r_k=12, T_U/T_L= 4.55. The first mode period of the lower structure is more close to the third mode period of the upper structure, the interaction of the first mode of the lower structure and the third mode of the upper structure is more significant. Such interaction results in that the normalized effective modal masses of the entire building associated with the fourth mode increases while that associated with the second mode decreases. In general, the remaining normalized effective modal mass of the entire building other than that of the first mode is distributed in three modes: the second to fourth modes in the MDOF model, as shown in Figure D.3 (e). Therefore, the "lumped" mass effect associated with the second mode of the simplified 2DOF model becomes more significant. The error of the base shear force of the lower structure associated with the proposed two-stage analysis procedure increases, with the error being 83.7% if r_k=12 as shown in Figure D.3 (b).

(3) As the further increase of r_k, the error of the base shear force of the lower structure associated with the proposed two-stage analysis procedure gradually decreases. For example, the error is 67.3% when r_k=21, as shown in Figure D.3 (c). For the case where r_k=21, T_U/T_L= 6.02. The first mode period of the lower structure is close to the fourth mode period of the upper structure, and the interaction occurs between the first mode of the lower structure and fourth mode of the upper structure. Such interaction then results in that the remaining normalized effective modal masses of the entire building other than that of the first mode is primarily distributed in two vibration modes of the MDOF model,

i.e., fourth and fifth modes, as shown in Figure D.3 (e). The "lumped" mass effect associated with the second mode of the simplified 2DOF model slightly decreases.

(4) With the continuing increase of r_k, the error of the base shear force of the lower structure associated with the proposed two-stage analysis procedure continues decreasing. Finally, the base shear force of the lower structure in the MDOF model is only dominated by two modes: the first and seventh modes. For example at r_k=80, the first period of the lower structure is approximately 1.45 times the last (sixth) period of the upper structure, the interaction of the first mode of the lower structure and other higher vibration modes of the upper structure can be ignored. The base shear force of the lower structure in the MDOF model is dominated by the first and (N_U+1) modes, with the corresponding normalized effective modal masses of the entire building being 0.49 and 0.36, respectively, as shown in Figure D.3 (e). On the other hand, the normalized effective modal masses of the entire building in the simplified 2DOF model for the first and second modes are 0.56 and 0.44, respectively, as shown in Figure D.3 (f). It is seen the simplified 2DOF model can represent the MDOF structure well when =80. Therefore, as shown in Figure D.3 (d), the error of the base shear force of the lower structure associated with the proposed two-stage analysis procedure turns to be acceptable for this case.

Upon the foregoing discussions, it is seen one significant reason for the underestimation of the base shear force of the lower structure associated with the proposed two-stage analysis procedure is that the normalized effective modal mass of the entire building for each mode lies between zero and unity, as shown in Figure D.3 (e). In addition, the interaction of the higher vibration modes distributes the normalized effective modal masses of the entire building into several "interacted vibration modes". The simplified 2DOF model associated with the proposed two-stage analysis procedure ignores such interaction and lumps the normalized effective modal masses of the entire building in two or three "interacted vibration modes" of the MDOF model in one mode, i.e., the second mode of the simplified 2DOF model. Therefore, based on the CQC combination rule, the proposed two-stage analysis procedure leads to very conservative results for the shear forces of the lower structure. However, as to the upper structure, since the normalized effective modal masses associated with the first mode is greater than unity, as shown in both Figures D.1 (c) ~ (d) and Figures D.2 (e) ~ (f), such interaction will lead to larger shear force of the upper structure.

The two-stage analysis procedure prescribed in ASCE 7 (ASCE, 2006; 2010) also does not account for the effect of the interaction of the first mode of the lower structure and higher vibration modes of the upper structure. In addition, ASCE 7 selects the ABSSUM rule to combine the peak modal response. Therefore, the two-stage analysis procedure prescribed in ASCE 7 often leads to overly

conservative results associated with the shear forces of the lower structures, as shown in Figures D.3 (a) ~ (d).

Appendix E Development of Canadian simplified approaches

E.1 Error of the simplified 2DOF model

With the adoption of the NBCC 2010 spectrum, the factor α_U evaluated by the simplified 2DOF model (Eq.(A.16)) is compared with that evaluated based on the MDOF model (Eq.(D.1)). By limiting the storey-stiffness ratio r_k be in the range between r_{kU2} and r_{kU3}, the maximum and minimum errors of the factor α_U induced by the simplified 2DOF model for the three representative seismic cities, i.e., Vancouver, Montreal and Halifax, are listed in Tables E.1 to E.6. The positive and negative errors in the tables represent the simplified 2DOF model overestimate and underestimate the factor α_U, respectively.

Table E.1: Maximum errors of factor α_U induced by the simplified 2DOF model when $r_{kU2} \leq r_k \leq r_{kU3}$ (Vancouver spectrum)

N_L \ N_U	1	2	3	4	5	6	7	8	9
1	0.0%	4.8%	6.4%	N/A	N/A	N/A	N/A	N/A	N/A
2	4.9%	9.7%	15.2%	16.9%	16.0%	16.3%	15.1%	N/A	N/A
3	6.4%	12.1%	22.8%	22.6%	22.6%	21.5%	21.2%	N/A	N/A
4	7.1%	12.9%	25.3%	26.6%	26.7%	26.2%	N/A	N/A	N/A
5	7.4%	13.1%	25.3%	27.6%	27.3%	N/A	N/A	N/A	N/A
6	N/A	13.2%	24.6%	28.4%	N/A	N/A	N/A	N/A	N/A
7	N/A	13.4%	23.8%	N/A	N/A	N/A	N/A	N/A	N/A
8	N/A	13.5%	N/A	N/A	N/A	N/A	N/A	N/A	N/A
9	N/A	N/A	N/A	N/A	N/A	N/A	N/A	N/A	N/A

Note: N/A denotes the storey combination of the lower and upper structures, or the storey-stiffness ratio r_k that lies between r_{kU2} and r_{kU3} for that storey combination , is out of the scope of this study.

Table E.2: Minimum errors of factor α_U induced by the simplified 2DOF model when $r_{kU2} \leq r_k \leq r_{kU3}$ (Vancouver spectrum)

N_L \ N_U	1	2	3	4	5	6	7	8	9
1	0.0%	2.2%	4.0%	N/A	N/A	N/A	N/A	N/A	N/A
2	0.7%	2.8%	3.6%	4.4%	5.4%	6.5%	7.5%	N/A	N/A
3	1.7%	3.6%	4.1%	4.3%	4.7%	5.1%	5.7%	N/A	N/A
4	2.6%	4.7%	5.0%	4.8%	4.8%	5.0%	N/A	N/A	N/A
5	3.2%	5.3%	5.8%	5.5%	5.2%	N/A	N/A	N/A	N/A
6	N/A	5.8%	6.4%	6.2%	N/A	N/A	N/A	N/A	N/A
7	N/A	6.3%	7.0%	N/A	N/A	N/A	N/A	N/A	N/A
8	N/A	6.7%	N/A	N/A	N/A	N/A	N/A	N/A	N/A
9	N/A	N/A	N/A	N/A	N/A	N/A	N/A	N/A	N/A

Note: N/A denotes the storey combination of the lower and upper structures, or the storey-stiffness ratio r_k that lies between r_{kU2} and r_{kU3} for that storey combination , is out of the scope of this study.

Table E.3: Maximum errors of factor α_U induced by the simplified 2DOF model when $r_{kU2} \leq r_k \leq r_{kU3}$ (Montreal spectrum)

N_L \ N_U	1	2	3	4	5	6	7	8	9
1	0.0%	6.5%	8.1%	N/A	N/A	N/A	N/A	N/A	N/A
2	7.7%	16.2%	18.8%	21.4%	19.7%	20.0%	17.6%	N/A	N/A
3	9.3%	20.0%	27.8%	28.1%	28.3%	26.3%	30.2%	N/A	N/A
4	9.8%	20.5%	29.7%	31.9%	33.3%	32.6%	N/A	N/A	N/A
5	9.8%	20.1%	28.8%	33.0%	31.9%	N/A	N/A	N/A	N/A
6	N/A	19.8%	27.4%	33.1%	N/A	N/A	N/A	N/A	N/A
7	N/A	20.1%	25.9%	N/A	N/A	N/A	N/A	N/A	N/A
8	N/A	19.7%	N/A	N/A	N/A	N/A	N/A	N/A	N/A
9	N/A	N/A	N/A	N/A	N/A	N/A	N/A	N/A	N/A

Note: N/A denotes the storey combination of the lower and upper structures, or the storey-stiffness ratio r_k that lies between r_{kU2} and r_{kU3} for that storey combination , is out of the scope of this study.

Table E.4: Minimum errors of factor α_U induced by the simplified 2DOF model when $r_{kU2} \leq r_k \leq r_{kU3}$ (Montreal spectrum)

N_L \ N_U	1	2	3	4	5	6	7	8	9
1	0.0%	1.9%	3.7%	N/A	N/A	N/A	N/A	N/A	N/A
2	0.7%	2.8%	3.6%	4.4%	5.4%	6.5%	7.5%	N/A	N/A
3	1.7%	3.6%	4.1%	4.3%	4.7%	5.1%	5.7%	N/A	N/A
4	2.6%	4.7%	5.0%	4.8%	4.8%	5.0%	N/A	N/A	N/A
5	3.2%	5.3%	5.8%	5.5%	5.2%	N/A	N/A	N/A	N/A
6	N/A	5.8%	6.4%	6.2%	N/A	N/A	N/A	N/A	N/A
7	N/A	6.3%	7.0%	N/A	N/A	N/A	N/A	N/A	N/A
8	N/A	6.7%	N/A	N/A	N/A	N/A	N/A	N/A	N/A
9	N/A	N/A	N/A	N/A	N/A	N/A	N/A	N/A	N/A

Note: N/A denotes the storey combination of the lower and upper structures, or the storey-stiffness ratio r_k that lies between r_{kU2} and r_{kU3} for that storey combination , is out of the scope of this study.

Table E.5: Maximum errors of factor α_U induced by DOF model when $r_{kU2} \leq r_k \leq r_{kU3}$ (Halifax spectrum)

N_L \ N_U	1	2	3	4	5	6	7	8	9
1	0.0%	5.0%	6.5%	N/A	N/A	N/A	N/A	N/A	N/A
2	5.2%	9.7%	13.5%	15.0%	14.6%	16.0%	16.7%	N/A	N/A
3	6.7%	12.4%	19.8%	19.5%	20.0%	25.1%	32.4%	N/A	N/A
4	7.4%	13.2%	21.8%	22.9%	26.6%	35.0%	N/A	N/A	N/A
5	7.7%	13.6%	22.0%	24.0%	30.2%	N/A	N/A	N/A	N/A
6	N/A	13.9%	21.6%	24.6%	N/A	N/A	N/A	N/A	N/A
7	N/A	14.2%	21.0%	N/A	N/A	N/A	N/A	N/A	N/A
8	N/A	14.2%	N/A	N/A	N/A	N/A	N/A	N/A	N/A
9	N/A	N/A	N/A	N/A	N/A	N/A	N/A	N/A	N/A

Note: N/A denotes the storey combination of the lower and upper structures, or the storey-stiffness ratio r_k that lies between r_{kU2} and r_{kU3} for that storey combination , is out of the scope of this study.

Table E.6: Minimum errors of factor α_U induced by the simplified 2DOF model when $r_{kU2} \le r_k \le r_{kU3}$ (Halifax spectrum)

N_L \ N_U	1	2	3	4	5	6	7	8	9
1	0.0%	2.2%	4.2%	N/A	N/A	N/A	N/A	N/A	N/A
2	0.7%	2.8%	3.6%	4.4%	5.4%	6.5%	7.5%	N/A	N/A
3	1.7%	3.6%	4.1%	4.3%	4.7%	5.1%	5.7%	N/A	N/A
4	2.6%	4.7%	5.0%	4.8%	4.8%	5.0%	N/A	N/A	N/A
5	3.2%	5.3%	5.8%	5.5%	5.2%	N/A	N/A	N/A	N/A
6	N/A	5.8%	6.4%	6.2%	N/A	N/A	N/A	N/A	N/A
7	N/A	6.3%	7.0%	N/A	N/A	N/A	N/A	N/A	N/A
8	N/A	6.7%	N/A	N/A	N/A	N/A	N/A	N/A	N/A
9	N/A	N/A	N/A	N/A	N/A	N/A	N/A	N/A	N/A

Note: N/A denotes the storey combination of the lower and upper structures, or the storey-stiffness ratio r_k that lies between r_{kU2} and r_{kU3} for that storey combination , is out of the scope of this study.

E.2 Determination of R_{kU2stg}

As the NBCC 2010 specifies different spectral shapes for different cities in Canada, the limits of the period ratio T_1/T_U that ensure the spectral ratio $S_a(T_1)/S_a(T_U)$ be close to unity are different for different cities. Take cities of Vancouver, Montreal and Halifax as example. To ensure that the spectral ratio $S_a(T_1)/S_a(T_U)$ is not less than 0.91, it is required that T_1/T_U is not greater than 1.063 if the Vancouver spectrum is selected; however, if the Montreal and Halifax spectra are selected, it is required that T_1/T_U is not greater than 1.026, as shown in Figures E.1 (a) ~ (b).

While the period requirement $T_1/T_U \le 1.1$, which is the requirement used in the ASCE 7 spectrum, is over-relaxed for the Montreal and Halifax spectra, the period requirement $T_1/T_U \le 1.026$ is too stringent for the Vancouver spectrum. The question arises as what is the appropriate threshold value for the period ratio T_1/T_U when determining the ratio R_{kU2stg} based on the NBCC 2010 spectra. The selection in this study is based on the spectral shapes of Vancouver, Montreal and Halifax. As a compromise, the value 1.05 is selected as the threshold limit for the period ratio T_1/T_U that is used to determine the ratio R_{kU2stg}. As shown in Figure E.1 (c), when $T_1/T_U=1.05$, the minimum spectral ratio $S_a(T_1)/S_a(T_U)$ is 0.83, and for most ranges of periods T_U, the ratio $S_a(T_1)/S_a(T_U)$ is greater than 0.90. Therefore, the compromise value 1.05 is appropriate. Such selection can be further justified by the acceptable error of the proposed factor α_U discussed in section 5.3.5.

Then, similar to Eq.(C.3) of Appendix C.2, the overall two-stage stiffness ratio of the upper structure R_{kU2stg} can be determined based on the following two requirements:

$$\begin{cases} M_{U1} \le 1.1 \\ T_1 / T_U \le 1.05 \end{cases} \tag{E.1}$$

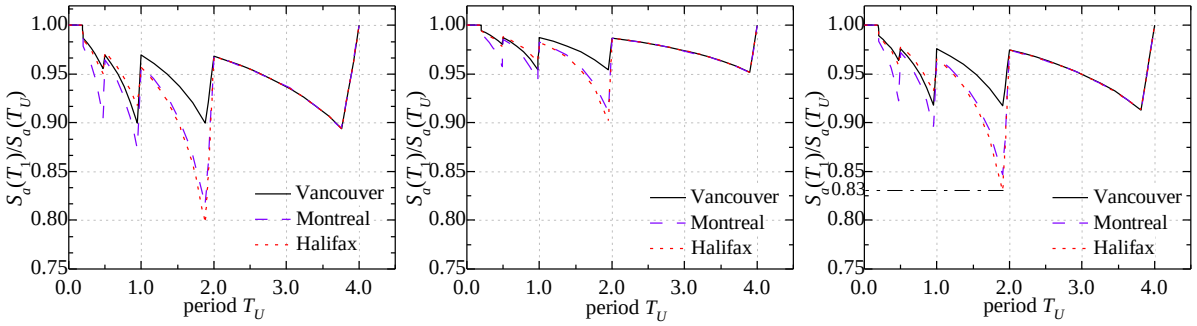

(a) T_1/T_U=1.063 (b) T_1/T_U =1.026 (c) T_1/T_U =1.05

Figure E.1: Effect of spectral shape on spectral acceleration ratio $S_a(T_1)/S_a(T_U)$

Based on Eq.(A.8), the theoretical solution for $T_1/T_U \leq 1.05$ is

$$R_k \geq 0.907R_m + 9.78 \tag{E.2}$$

By combining Eqs. (C.4) and (E.2), R_{kU2stg} is finally determined as presented in Eq.(5.6), where R_{kU2stg}=11.029R_m-2.5 (R_m>0.71) is still obtained by curve fitting of Eq.(C.4), as shown in Figure.C.1 (a) with logarithmic scale on both horizontal and vertical axes.

E.3 Analytical solution of critical storey-stiffensses

Take the critical storey-stiffness $k_{\alpha U\max}$ as example to illustrate why solutions of the critical storey-stiffensses cannot be analytically derived from Eq.(5.1) if the spectral acceleration is expressed by Eq.(5.7). In accordance with Eq. (3.8), express the storey-stiffness of the upper structure k_U in terms of the period T_U as follows:

$$k_U = m_U \left(\frac{2\pi}{\bar{\omega}_{1U} T_U} \right)^2 \tag{E.3}$$

The critical storey-stiffness $k_{\alpha U\max}$ corresponds to the minimum required storey-stiffness of the upper structure when the storey-stiffness ratio r_k lies between r_{kU2} and r_{kU3}. The condition $r_{kU2} \leq r_k \leq r_{kU3}$ in terms of the MDOF model corresponds to the condition $R_{kU2} \leq R_k \leq R_{kU3}$ in terms of the simplified 2DOF model. Therefore, based on Eq. (3.12), it is obtained that the factor α_U in the governing design equation, i.e. Eq. (5.1), is equal to $\alpha_{U\max}$ since $R_{kU2} \leq R_k \leq R_{kU3}$. By assuming T_1=1.30$(R_m)^{-0.059}T_U \geq$0.2second, the substitution of k_U and $\alpha_{U\max}$ in Eq. (5.1) with Eqs. (E.3) and (5.5), respectively, leads to

$$\alpha_{U\max 2} \left\{ \frac{S_a\left[1.30\left(R_m\right)^{-0.059} T_U\right]}{S_a(T_U)} \right\}^{-x_4} \leq \left(\frac{2\pi}{\bar{\omega}_{1U} T_U} \right)^2 \frac{\Delta_{U\lim}}{N_U S_a(T_U)} \tag{E.4}$$

If the spectral acceleration $S_a(T)$ is expressed by Eq. (5.7), it is obvious that the period T_U that corresponds to $k_{\alpha U\max}$ cannot be analytical derived from Eq. (E.4). To ensure that the period T_U and the corresponding $k_{\alpha U\max}$ be analytically solved, the spectral value $S_a(T)$ should be either a power or an exponential function of the period T.

E.3.1 Power function

If each linear segment of the NBCC 2010 spectrum is approximated by a power function as shown in Eq. (5.8), the spectral ratio $S_a(T_1)/S_a(T_U)$ can be evaluated as follows:

$$\frac{S_a(T_1)}{S_a(T_U)}=\begin{cases}1 & T_U \le T_S^{'}\left(T_U/T_1\right)\ \text{s} \quad \text{(a)}\\ \dfrac{A_1}{S_a(0.2)}\left(\dfrac{T_1}{T_U}\right)^{\tau_1}\left(T_U\right)^{\tau_1} & T_S^{'}\left(T_U/T_1\right)<T_U \le T_S^{'} \quad \text{(b)}\\ \left(\dfrac{T_1}{T_U}\right)^{\tau_1} & T_S^{'}<T_U \le 0.5\left(T_U/T_1\right)\ \text{s} \quad \text{(c)}\\ \dfrac{A_2}{A_1}\left(\dfrac{T_1}{T_U}\right)^{\tau_2}\left(T_U\right)^{\tau_2-\tau_1} & 0.5\left(T_U/T_1\right)\ \text{s}<T_U \le 0.5\ \text{s} \quad \text{(d)}\\ \left(\dfrac{T_1}{T_U}\right)^{\tau_2} & 0.5\ \text{s}<T_U \le 1.0\left(T_U/T_1\right)\ \text{s} \quad \text{(e)}\\ \dfrac{A_3}{A_2}\left(\dfrac{T_1}{T_U}\right)^{\tau_3}\left(T_U\right)^{\tau_3-\tau_2} & 1.0\left(T_U/T_1\right)\ \text{s}<T_U \le 1.0\ \text{s} \quad \text{(f)}\\ \left(\dfrac{T_1}{T_U}\right)^{\tau_3} & 1.0\ \text{s}<T_U \le 2.0\left(T_U/T_1\right)\ \text{s} \quad \text{(g)}\\ \dfrac{A_4}{A_3}\left(\dfrac{T_1}{T_U}\right)^{\tau_4}\left(T_U\right)^{\tau_4-\tau_3} & 2.0\left(T_U/T_1\right)\ \text{s}<T_U \le 2.0\ \text{s} \quad \text{(h)}\end{cases} \tag{E.5}$$

When determining the spectral ratio $S_a(T_1)/S_a(T_U)$ based on Eq. (5.8), it is assumed that periods T_U and T_1 in Eq. (E.5) are located either in the same linear segment or in the adjacent linear segments of the NBCC 2010 spectrum. For example, if the period T_U lies between 0.5 and 1.0(T_U/T_1) second, the period T_1 is in the range between 0.5 and 1.0 second; therefore, periods T_U and T_1 are in the same linear segment and the spectral ratio is as shown in Eq. (E.5 e). If T_U lies between 1.0(T_U/T_1) and 1.0 second, the period T_1 is in the range between 1.0 and 2.0 second; therefore, periods T_U and T_1 are in the adjacent linear segments and the spectral ratio is as shown in Eq. (E.5 f). It is impossible that the period T_U is in the range between 0.5 and 1.0 second, and the period T_1 is in the range between 2.0 and 4.0 second. Considering that $T_1=[(N_U+N_L)/(N_U+0.12N_L)]^{0.5}T_U$ and $T_1=1.30(R_m)^{-0.059}T_U$ in Eqs. (5.4) and (5.5), respectively, the assumption that T_U and T_1 are either in the same linear segment or in the adjacent linear segments can be justified as follows:

Table E.7: Maximum period ratio T_1/T_U

N_L \ N_U	1	2	3	4	5	6	7	8	9
1	1.34	1.19	1.13	1.10	1.08	1.07	1.06	1.05	1.05
2	1.56	1.34	1.24	1.19	1.16	1.13	1.11	1.10	N/A
3	1.71	1.46	1.34	1.27	1.22	1.19	1.17	N/A	N/A
4	1.84	1.56	1.42	1.34	1.28	1.24	N/A	N/A	N/A
5	1.94	1.64	1.49	1.40	1.34	N/A	N/A	N/A	N/A
6	2.02	1.71	1.56	1.46	N/A	N/A	N/A	N/A	N/A
7	2.09	1.78	1.61	N/A	N/A	N/A	N/A	N/A	N/A
8	2.14	1.84	N/A	N/A	N/A	N/A	N/A	N/A	N/A
9	2.19	N/A	N/A	N/A	N/A	N/A	N/A	N/A	N/A

Note: N/A denotes the proposed approach is not applicable for the combination of the lower and upper structures.

(1) The period ratio T_1/T_U by setting $T_1=[(N_U+N_L)/(N_U+0.12N_L)]^{0.5}T_U$ for each storey combination of the lower and upper structures is shown in Table E.7. From the table, it is see that for most storeycombinations, the maximum period ratio T_1/T_U is not greater than 2.0. Compared to the characteristics of the NBCC 2010 spectrum shown in Figure 5.2 (a), it is obvious that periods T_U and T_1 either locate in the same linear segment or in the adjacent linear segments. The possible storey combinations that may result in the calculated period ratio being greater than 2.0 are N_L=6, 7, 8, or 9 and N_U=1, with the maximum value being 2.19. However, since the maximum period T_U is not greater than 0.31 second if N_U=1, as discussed in section 1.3.2, the maximum period T_1=0.3×2.19=0.66 second, which is less than the 1.0 second of Figure 5.2 (a). Periods T_U and T_1 still locate in the adjacent linear segments.

(2) On the other hand, the maximum period ratio T_1/T_U by setting $T_1=1.30(R_m)^{-0.059}T_U$ occurs when R_m reaches the minimum value. Considering the scope of the investigated building stated in section 1.3.2, the minimum R_m=0.11 which occurs when N_L=1, N_U=9 and r_m=1. Consequently, the maximum period ratio T_1/T_U by setting $T_1=1.30(R_m)^{-0.059}T_U$ is $T_1/T_U=1.30\times(0.11)^{-0.059}=1.48$, which is less than 2.0. Periods T_U and T_1 still locate in the same linear segment or adjacent linear segments of the NBCC 2010 spectrum.

By comparing Eq. (5.8) to Eq. (5.7), it is found the difference in the flat portion exists between the approximated spectrum and the NBCC 2010 spectrum. The flat portion of the NBCC 2010 spectrum starts with T=0 second and ends with T=0.2 second, as shown in Figure 5.2 (a). However, the ending point for the flat portion of the approximated spectrum is dependent on the curve fitting parameter T_S', as shown in Figures E.2 (a) ~ (b). Such difference between the approximated and the NBCC 2010 spectra results in the difference in the condition for $S_a(T_1)/S_a(T_U)=1$. By using the NBCC 2010 spectrum, the condition for $S_a(T_1)/S_a(T_U)=1$ is $T_1\leq 0.2$ second, but by using the approximated spectrum,

the condition turns to be $T_1 \leq T_S'$. Considering such difference, Eqs. (5.4) and (5.5) turn to be the following two equations, respectively, if the approximated spectrum is adopted:

$$\alpha_{U1} = \begin{cases} \alpha_{U12} \left\{ \dfrac{S_a\left[\sqrt{\dfrac{N_U + N_L}{N_U + 0.12N_L}} T_U\right]}{S_a(T_U)} \right\}^{-x_3} & \text{if } \sqrt{\dfrac{N_U + N_L}{N_U + 0.12N_L}} T_U > T_S' \\ \alpha_{U12} & \text{if } \sqrt{\dfrac{N_U + N_L}{N_U + 0.12N_L}} T_U \leq T_S' \end{cases} \tag{E.6}$$

$$\alpha_{U\max} = \begin{cases} \alpha_{U\max 2} \left\{ \dfrac{S_a\left[1.30\left(R_m\right)^{-0.059} T_U\right]}{S_a(T_U)} \right\}^{-x_4} & \text{if } 1.30\left(R_m\right)^{-0.059} T_U > T_S' \\ \alpha_{U\max 2} & \text{if } 1.30\left(R_m\right)^{-0.059} T_U \leq T_S' \end{cases} \tag{E.7}$$

Then, by: (1) using Eq. (5.8) to express $S_a(T_U)$ and Eq. (E.5) to express $S_a(T_1)/S_a(T_U)$, (2) using Eq.(E.6) to express α_{U1} and Eq. (E.7) to express $\alpha_{U\max}$, and (3) following the same procedure discussed in section 3.4, analytical solutions for the critical storey-stiffnesses $k_{\alpha U}$, $k_{\alpha U\max}$ and $k_{\alpha U2\text{stg}}$ can be derived from Eq. (5.1) as follows:

$$k_{\alpha U1} = \begin{cases} \alpha_{U12} m_U N_U \dfrac{S_a(0.2)}{\Delta_{U\lim}} & k_{\alpha U1} \geq k_{U03} \\ m_U \left(\dfrac{2\pi}{\bar{\omega}_{1U}}\right)^{2+\frac{4}{\tau_1-2}} \left\{ \alpha_{U12} N_U \left[\dfrac{S_a(0.2)}{A_1}\right]^{x_3} \left(\dfrac{N_U + 0.12N_L}{N_U + N_L}\right)^{0.5\tau_1 x_3} \dfrac{S_a(0.2)}{\Delta_{U\lim}} \right\}^{\frac{-2}{\tau_1-2}} & k_{U01} \leq k_{\alpha U1} < k_{U03} \\ m_U \left(\dfrac{2\pi}{\bar{\omega}_{1U}}\right)^{2-\frac{4}{\tau_1+2}} \left\{ \alpha_{U12} N_U \left[\dfrac{S_a(0.2)}{A_1}\right]^{x_3} \left(\dfrac{N_U + 0.12N_L}{N_U + N_L}\right)^{0.5\tau_1 x_3} \dfrac{A_1}{\Delta_{U\lim}} \right\}^{\frac{2}{\tau_1+2}} & \dfrac{k_{U03}\left(T_S'\right)^2}{0.25} \leq k_{\alpha U1} < k_{U01} \\ m_U \left(\dfrac{2\pi}{\bar{\omega}_{1U}}\right)^{2-\frac{4}{x_3(\tau_1-\tau_2)+\tau_1+2}} \left\{ \alpha_{U12} N_U \left(\dfrac{A_1}{A_2}\right)^{x_3} \left(\dfrac{N_U + 0.12N_L}{N_U + N_L}\right)^{0.5\tau_2 x_3} \dfrac{A_1}{\Delta_{U\lim}} \right\}^{\frac{2}{x_3(\tau_1-\tau_2)+\tau_1+2}} & \dfrac{k_{U01}\left(T_S'\right)^2}{0.25} \leq k_{\alpha U1} < \dfrac{k_{U03}\left(T_S'\right)^2}{0.25} \\ m_U \left(\dfrac{2\pi}{\bar{\omega}_{1U}}\right)^{2-\frac{4}{\tau_2+2}} \left\{ \alpha_{U12} N_U \left[\dfrac{S_a(0.2)}{A_1}\right]^{x_3} \left(\dfrac{N_U + 0.12N_L}{N_U + N_L}\right)^{0.5\tau_2 x_3} \dfrac{A_2}{\Delta_{U\lim}} \right\}^{\frac{2}{\tau_2+2}} & k_{U03}\left(T_S'\right)^2 \leq k_{\alpha U1} < \dfrac{k_{U01}\left(T_S'\right)^2}{0.25} \\ m_U \left(\dfrac{2\pi}{\bar{\omega}_{1U}}\right)^{2-\frac{4}{x_3(\tau_2-\tau_3)+\tau_2+2}} \left\{ \alpha_{U12} N_U \left(\dfrac{A_2}{A_3}\right)^{x_3} \left(\dfrac{N_U + 0.12N_L}{N_U + N_L}\right)^{0.5\tau_3 x_3} \dfrac{A_2}{\Delta_{U\lim}} \right\}^{\frac{2}{x_3(\tau_2-\tau_3)+\tau_2+2}} & k_{U01}\left(T_S'\right)^2 \leq k_{\alpha U1} < k_{U03}\left(T_S'\right)^2 \\ m_U \left(\dfrac{2\pi}{\bar{\omega}_{1U}}\right)^{2-\frac{4}{\tau_3+2}} \left\{ \alpha_{U12} N_U \left[\dfrac{S_a(0.2)}{A_1}\right]^{x_3} \left(\dfrac{N_U + 0.12N_L}{N_U + N_L}\right)^{0.5\tau_3 x_3} \dfrac{A_3}{\Delta_{U\lim}} \right\}^{\frac{2}{\tau_3+2}} & \dfrac{k_{U03}\left(T_S'\right)^2}{4} \leq k_{\alpha U1} < k_{U01}\left(T_S'\right)^2 \\ m_U \left(\dfrac{2\pi}{\bar{\omega}_{1U}}\right)^{2-\frac{4}{x_3(\tau_3-\tau_4)+\tau_3+2}} \left\{ \alpha_{U12} N_U \left(\dfrac{A_3}{A_4}\right)^{x_3} \left(\dfrac{N_U + 0.12N_L}{N_U + N_L}\right)^{0.5\tau_3 x_3} \dfrac{A_3}{\Delta_{U\lim}} \right\}^{\frac{2}{x_3(\tau_3-\tau_4)+\tau_3+2}} & \dfrac{k_{U01}\left(T_S'\right)^2}{4} \leq k_{\alpha U1} < \dfrac{k_{U03}\left(T_S'\right)^2}{4} \end{cases} \quad \text{(E.8)}$$

$$k_{\alpha U\max}=\begin{cases}\alpha_{U\max 2}m_U N_U\dfrac{S_a(0.2)}{\Delta_{U\lim}} & k_{\alpha U\max}\ge k_{U02}\\ m_U\left(\dfrac{2\pi}{\bar{\omega}_{1U}}\right)^{2+\frac{4}{\tau_1-2}}\left\{\alpha_{U\max 2}N_U\left[\dfrac{S_a(0.2)}{A_1}\right]^{x_4}\left(0.769R_m^{0.059}\right)^{\tau_1x_4}\dfrac{S_a(0.2)}{\Delta_{U\lim}}\right\}^{\frac{-2}{\tau_1-2}} & k_{U01}\le k_{\alpha U\max}<k_{U02}\\ m_U\left(\dfrac{2\pi}{\bar{\omega}_{1U}}\right)^{2-\frac{4}{\tau_1+2}}\left\{\alpha_{U\max 2}N_U\left[\dfrac{S_a(0.2)}{A_1}\right]^{x_4}\left(0.769R_m^{0.059}\right)^{\tau_1x_4}\dfrac{A_1}{\Delta_{U\lim}}\right\}^{\frac{2}{\tau_1+2}} & \dfrac{k_{U02}\left(T_S^{'}\right)^2}{0.25}\le k_{\alpha U\max}<k_{U01}\\ m_U\left(\dfrac{2\pi}{\bar{\omega}_{1U}}\right)^{2-\frac{4}{x_4(\tau_1-\tau_2)+\tau_1+2}}\left\{\alpha_{U\max 2}N_U\left(\dfrac{A_1}{A_2}\right)^{x_4}\left(0.769R_m^{0.059}\right)^{\tau_2x_4}\dfrac{A_1}{\Delta_{U\lim}}\right\}^{\frac{2}{x_3(\tau_1-\tau_2)+\tau_1+2}} & \dfrac{k_{U01}\left(T_S^{'}\right)^2}{0.25}\le k_{\alpha U\max}<\dfrac{k_{U02}\left(T_S^{'}\right)^2}{0.25}\\ m_U\left(\dfrac{2\pi}{\bar{\omega}_{1U}}\right)^{2-\frac{4}{\tau_2+2}}\left\{\alpha_{U\max 2}N_U\left[\dfrac{S_a(0.2)}{A_1}\right]^{x_4}\left(0.769R_m^{0.059}\right)^{\tau_2x_4}\dfrac{A_2}{\Delta_{U\lim}}\right\}^{\frac{2}{\tau_2+2}} & k_{U02}\left(T_S^{'}\right)^2\le k_{\alpha U\max}<\dfrac{k_{U01}\left(T_S^{'}\right)^2}{0.25}\\ m_U\left(\dfrac{2\pi}{\bar{\omega}_{1U}}\right)^{2-\frac{4}{x_4(\tau_2-\tau_3)+\tau_2+2}}\left\{\alpha_{U\max 2}N_U\left(\dfrac{A_2}{A_3}\right)^{x_4}\left(0.769R_m^{0.059}\right)^{\tau_3x_4}\dfrac{A_2}{\Delta_{U\lim}}\right\}^{\frac{2}{x_3(\tau_2-\tau_3)+\tau_2+2}} & k_{U01}\left(T_S^{'}\right)^2\le k_{\alpha U\max}<k_{U02}\left(T_S^{'}\right)^2\\ m_U\left(\dfrac{2\pi}{\bar{\omega}_{1U}}\right)^{2-\frac{4}{\tau_3+2}}\left\{\alpha_{U\max 2}N_U\left[\dfrac{S_a(0.2)}{A_1}\right]^{x_4}\left(0.769R_m^{0.059}\right)^{\tau_3x_4}\dfrac{A_3}{\Delta_{U\lim}}\right\}^{\frac{2}{\tau_3+2}} & \dfrac{k_{U02}\left(T_S^{'}\right)^2}{4}\le k_{\alpha U\max}<k_{U01}\left(T_S^{'}\right)^2\\ m_U\left(\dfrac{2\pi}{\bar{\omega}_{1U}}\right)^{2-\frac{4}{x_4(\tau_3-\tau_4)+\tau_3+2}}\left\{\alpha_{U\max 2}N_U\left(\dfrac{A_3}{A_4}\right)^{x_3}\left(0.769R_m^{0.059}\right)^{\tau_3x_4}\dfrac{A_3}{\Delta_{U\lim}}\right\}^{\frac{2}{x_4(\tau_3-\tau_4)+\tau_3+2}} & \\ & \dfrac{k_{U01}\left(T_S^{'}\right)^2}{4}\le k_{\alpha U\max}<\dfrac{k_{U02}\left(T_S^{'}\right)^2}{4}\end{cases}$$

(E.9)

$$k_{\alpha U2stg}=\begin{cases}\alpha_{U2stg}m_U N_U\dfrac{S_a(0.2)}{\Delta_{U\lim}} & k_{\alpha U2stg}\ge k_{U01}\\ m_U\left(\dfrac{2\pi}{\bar{\omega}_{1U}}\right)^{2-\frac{4}{\tau_1+2}}\left(\alpha_{U2stg}N_U\dfrac{A_1}{\Delta_{U\lim}}\right)^{\frac{2}{\tau_1+2}} & \dfrac{k_{U01}\left(T_S^{'}\right)^2}{0.25}\le k_{\alpha U2stg}<k_{U01}\\ m_U\left(\dfrac{2\pi}{\bar{\omega}_{1U}}\right)^{2-\frac{4}{\tau_2+2}}\left(\alpha_{U2stg}N_U\dfrac{A_2}{\Delta_{U\lim}}\right)^{\frac{2}{\tau_2+2}} & k_{U01}\left(T_S^{'}\right)^2\le k_{\alpha U2stg}<\dfrac{k_{U01}\left(T_S^{'}\right)^2}{0.25}\\ m_U\left(\dfrac{2\pi}{\bar{\omega}_{1U}}\right)^{2-\frac{4}{\tau_3+2}}\left(\alpha_{U2stg}N_U\dfrac{A_3}{\Delta_{U\lim}}\right)^{\frac{2}{\tau_3+2}} & \dfrac{k_{U01}\left(T_S^{'}\right)^2}{4}\le k_{\alpha U2stg}<k_{U01}\left(T_S^{'}\right)^2\end{cases}$$

(E.10)

where

$$k_{U01} = m_U \left[2\pi / \left(\bar{\omega}_{1U} T_S^{'} \right) \right]^2 \tag{E.11}$$

$$k_{U02} = 1.691 \left(R_m \right)^{-0.118} k_{U01} \tag{E.12}$$

$$k_{U03} = \left[\left(N_U + N_L \right) / \left(N_U + 0.12 N_L \right) \right] k_{U01} \tag{E.13}$$

E.3.2 Exponential function

If each linear segment of the NBCC 2010 spectrum is approximated by the exponential function as shown in Eq. (5.9), the spectral ratio $S_a(T_1)/S_a(T_U)$ can be evaluated as follows:

$$\frac{S_a(T_1)}{S_a(T_U)} = \begin{cases} 1 & T_U \le T_S^{'} \left(T_U / T_1 \right) \\ \dfrac{A_1}{S_a(0.2)} \exp\left[\tau_1 \left(T_1 / T_U \right) T_U \right] & T_S^{'} \left(T_U / T_1 \right) < T_U \le T_S^{'} \\ \exp\left[\left(T_1 / T_U - 1 \right) \tau_1 T_U \right] & T_S^{'} < T_U \le 0.5 \left(T_U / T_1 \right) \text{ s} \\ \dfrac{A_2}{A_1} \exp\left[\left(\tau_2 T_1 / T_U - \tau_1 \right) T_U \right] & 0.5 \left(T_U / T_1 \right) \text{ s} < T_U \le 0.5 \text{ s} \\ \exp\left[\left(T_1 / T_U - 1 \right) \tau_2 T_U \right] & 0.5 \text{ s} < T_U \le 1.0 \left(T_U / T_1 \right) \text{ s} \\ \dfrac{A_3}{A_2} \exp\left[\left(\tau_3 T_1 / T_U - \tau_2 \right) T_U \right] & 1.0 \left(T_U / T_1 \right) \text{ s} < T_U \le 1.0 \text{ s} \\ \exp\left[\left(T_1 / T_U - 1 \right) \tau_3 T_U \right] & 1.0 \text{ s} < T_U \le 2.0 \left(T_U / T_1 \right) \text{ s} \\ \dfrac{A_4}{A_3} \exp\left[\left(\tau_4 T_1 / T_U - \tau_3 \right) T_U \right] & 2.0 \left(T_U / T_1 \right) \text{ s} < T_U \le 2.0 \text{ s} \end{cases} \tag{E.14}$$

Periods T_U and T_1 in Eq. (E.14) are assumed to be located either in the same linear segment or in the adjacent linear segments of the spectrum. By: (1) using Eq. (5.9) to express S_a (T_U) and Eq. (E.14) to express $S_a(T_1)/S_a(T_U)$, (2) using Eq. (E.6) to express α_{U1} and Eq. (E.7) to express $\alpha_{U\max}$, and (3) following the same procedure discussed in section 3.4, analytical solutions for the critical storey-stiffnesses $k_{\alpha U}$, $k_{\alpha U\max}$ and $k_{\alpha U2stg}$ are obtained as follows:

$$k_{\alpha U1}=\begin{cases}\alpha_{U12}m_U N_U\dfrac{S_a(0.2)}{\Delta_{U\lim}} & k_{\alpha U1}\geq k_{U03}\\ m_U\left(\dfrac{2\pi}{\bar{\omega}_{1U}}\right)^2\dfrac{N_U+N_L}{N_U+0.12N_L}\left(\dfrac{\tau_1 x_3}{y_1}\right)^2 & k_{U01}\leq k_{\alpha U1}<k_{U03}\\ m_U\left(\dfrac{2\pi}{\bar{\omega}_{1U}}\right)^2\left[\left(1-\sqrt{\dfrac{N_U+N_L}{N_U+0.12N_L}}\right)x_3+1\right]^2\left(\dfrac{\tau_1}{y_2}\right)^2 & \dfrac{k_{U03}\left(T_S^{'}\right)^2}{0.25}\leq k_{\alpha U1}<k_{U01}\\ m_U\left(\dfrac{2\pi}{\bar{\omega}_{1U}}\right)^2\left[\left(\tau_1-\tau_2\sqrt{\dfrac{N_U+N_L}{N_U+0.12N_L}}\right)x_3+\tau_1\right]^2\left(\dfrac{1}{y_3}\right)^2 & \dfrac{k_{U01}\left(T_S^{'}\right)^2}{0.25}\leq k_{\alpha U1}<\dfrac{k_{U03}\left(T_S^{'}\right)^2}{0.25}\\ m_U\left(\dfrac{2\pi}{\bar{\omega}_{1U}}\right)^2\left[\left(1-\sqrt{\dfrac{N_U+N_L}{N_U+0.12N_L}}\right)x_3+1\right]^2\left(\dfrac{\tau_2}{y_4}\right)^2 & k_{U03}\left(T_S^{'}\right)^2\leq k_{\alpha U1}<\dfrac{k_{U01}\left(T_S^{'}\right)^2}{0.25}\\ m_U\left(\dfrac{2\pi}{\bar{\omega}_{1U}}\right)^2\left[\left(\tau_2-\tau_3\sqrt{\dfrac{N_U+N_L}{N_U+0.12N_L}}\right)x_3+\tau_2\right]^2\left(\dfrac{1}{y_5}\right)^2 & k_{U01}\left(T_S^{'}\right)^2\leq k_{\alpha U1}<k_{U03}\left(T_S^{'}\right)^2\\ m_U\left(\dfrac{2\pi}{\bar{\omega}_{1U}}\right)^2\left[\left(1-\sqrt{\dfrac{N_U+N_L}{N_U+0.12N_L}}\right)x_3+1\right]^2\left(\dfrac{\tau_3}{y_6}\right)^2 & \dfrac{k_{U03}\left(T_S^{'}\right)^2}{4}\leq k_{\alpha U1}<k_{U01}\left(T_S^{'}\right)^2\\ m_U\left(\dfrac{2\pi}{\bar{\omega}_{1U}}\right)^2\left[\left(\tau_3-\tau_4\sqrt{\dfrac{N_U+N_L}{N_U+0.12N_L}}\right)x_3+\tau_3\right]^2\left(\dfrac{1}{y_7}\right)^2 & \dfrac{k_{U01}\left(T_S^{'}\right)^2}{4}\leq k_{\alpha U1}<\dfrac{k_{U03}\left(T_S^{'}\right)^2}{4}\end{cases} \quad \text{(E.15)}$$

$$k_{\alpha U\max}=\begin{cases}\alpha_{U12}m_U N_U\dfrac{S_a(0.2)}{\Delta_{U\lim}} & k_{\alpha U\max}\geq k_{U02}\\ m_U\left(\dfrac{2\pi}{\bar{\omega}_{1U}}\right)^2\left(1.691R_m^{-0.118}\right)\left(\dfrac{\tau_1 x_4}{y_1}\right)^2 & k_{U01}\leq k_{\alpha U\max}<k_{U02}\\ m_U\left(\dfrac{2\pi}{\bar{\omega}_{1U}}\right)^2\left[\left(1-1.30R_m^{-0.059}\right)x_4+1\right]^2\left(\dfrac{\tau_1}{y_2}\right)^2 & \dfrac{k_{U02}\left(T_S^{'}\right)^2}{0.25}\leq k_{\alpha U\max}<k_{U01}\\ m_U\left(\dfrac{2\pi}{\bar{\omega}_{1U}}\right)^2\left[\left(\tau_1-1.30\tau_2R_m^{-0.059}\right)x_4+\tau_1\right]^2\left(\dfrac{1}{y_3}\right)^2 & \dfrac{k_{U01}\left(T_S^{'}\right)^2}{0.25}\leq k_{\alpha U\max}<\dfrac{k_{U02}\left(T_S^{'}\right)^2}{0.25}\\ m_U\left(\dfrac{2\pi}{\bar{\omega}_{1U}}\right)^2\left[\left(1-1.30R_m^{-0.059}\right)x_4+1\right]^2\left(\dfrac{\tau_2}{y_4}\right)^2 & k_{U02}\left(T_S^{'}\right)^2\leq k_{\alpha U\max}<\dfrac{k_{U01}\left(T_S^{'}\right)^2}{0.25}\\ m_U\left(\dfrac{2\pi}{\bar{\omega}_{1U}}\right)^2\left[\left(\tau_2-1.301\tau_3R_m^{-0.059}\right)x_4+\tau_2\right]^2\left(\dfrac{1}{y_5}\right)^2 & k_{U01}\left(T_S^{'}\right)^2\leq k_{\alpha U\max}<k_{U02}\left(T_S^{'}\right)^2\\ m_U\left(\dfrac{2\pi}{\bar{\omega}_{1U}}\right)^2\left[\left(1-1.30R_m^{-0.059}\right)x_4+1\right]^2\left(\dfrac{\tau_3}{y_6}\right)^2 & k_{U02}\left(T_S^{'}\right)^2\leq k_{\alpha U\max}<k_{U01}\left(T_S^{'}\right)^2\\ m_U\left(\dfrac{2\pi}{\bar{\omega}_{1U}}\right)^2\left[\left(\tau_3-1.301\tau_4R_m^{-0.059}\right)x_4+\tau_3\right]^2\left(\dfrac{1}{y_7}\right)^2 & \dfrac{k_{U01}\left(T_S^{'}\right)^2}{4}\leq k_{\alpha U\max}<\dfrac{k_{U02}\left(T_S^{'}\right)^2}{4}\end{cases}$$

(E.16)

$$k_{\alpha U2stg}=\begin{cases}\alpha_{U2stg}m_U N_U\dfrac{S_a(0.2)}{\Delta_{U\lim}} & k_{\alpha U2stg}\ge k_{U01}\\ m_U\left(\dfrac{2\pi}{\bar{\omega}_{1U}}\right)^2\left(\dfrac{\tau_1}{y_1}\right)^2 & \dfrac{k_{U01}\left(T_S^{'}\right)^2}{0.25}\le k_{\alpha U2stg}<k_{U01}\\ m_U\left(\dfrac{2\pi}{\bar{\omega}_{1U}}\right)^2\left(\dfrac{\tau_2}{y_2}\right)^2 & k_{U01}\left(T_S^{'}\right)^2\le k_{\alpha U2stg}<\dfrac{k_{U01}\left(T_S^{'}\right)^2}{0.25}\\ m_U\left(\dfrac{2\pi}{\bar{\omega}_{1U}}\right)^2\left(\dfrac{\tau_3}{y_3}\right)^2 & \dfrac{k_{U01}\left(T_S^{'}\right)^2}{4}\le k_{\alpha U2stg}<k_{U01}\left(T_S^{'}\right)^2\end{cases} \tag{E.17}$$

where k_{U01}, k_{U02} and k_{U03} are computed based on Eqs. (E.11) ~ (E.13), respectively, and the parameter y_i, where i=1,2…., is the numerical solution of the following equation:

$$\exp(y_i)y_i^2=b_i \tag{E.18}$$

Use $b_{\alpha U1,i}$, $b_{\alpha U\max,i}$ and $b_{\alpha U2stg,i}$ to denote the b_i of Eq. (E.18) that is applied to solve the y_i in Eqs. (E.15), (E.16) and (E.17), respectively. They are calculated as follows:

$$b_{\alpha U1,i}=\begin{cases}\dfrac{N_U+N_L}{N_U+0.12N_L}\tau_1^2\left(\dfrac{2\pi}{\bar{\omega}_{1U}}\right)^2\left[\dfrac{A_1}{S_a(0.2)}\right]^{x_3}\dfrac{\Delta_{U\lim}}{\alpha_{U12}N_U S_a(0.2)} & i=1\\ \left[\left(1-\sqrt{\dfrac{N_U+N_L}{N_U+0.12N_L}}\right)x_3+1\right]^2\tau_1^2\left(\dfrac{2\pi}{\bar{\omega}_{1U}}\right)^2\dfrac{\Delta_{U\lim}}{\alpha_{U12}N_U A_1} & i=2\\ \left[\left(\tau_1-\tau_2\sqrt{\dfrac{N_U+N_L}{N_U+0.12N_L}}\right)x_3+\tau_1\right]^2\left(\dfrac{2\pi}{\bar{\omega}_{1U}}\right)^2\left[\dfrac{A_2}{A_1}\right]^{x_3}\dfrac{\Delta_{U\lim}}{\alpha_{U12}N_U A_1} & i=3\\ \left[\left(1-\sqrt{\dfrac{N_U+N_L}{N_U+0.12N_L}}\right)x_3+1\right]^2\tau_2^2\left(\dfrac{2\pi}{\bar{\omega}_{1U}}\right)^2\dfrac{\Delta_{U\lim}}{\alpha_{U12}N_U A_2} & i=4\\ \left[\left(\tau_2-\tau_3\sqrt{\dfrac{N_U+N_L}{N_U+0.12N_L}}\right)x_3+\tau_2\right]^2\left(\dfrac{2\pi}{\bar{\omega}_{1U}}\right)^2\left[\dfrac{A_3}{A_2}\right]^{x_3}\dfrac{\Delta_{U\lim}}{\alpha_{U12}N_U A_2} & i=5\\ \left[\left(1-\sqrt{\dfrac{N_U+N_L}{N_U+0.12N_L}}\right)x_3+1\right]^2\tau_3^2\left(\dfrac{2\pi}{\bar{\omega}_{1U}}\right)^2\dfrac{\Delta_{U\lim}}{\alpha_{U12}N_U A_3} & i=6\\ \left[\left(\tau_3-\tau_4\sqrt{\dfrac{N_U+N_L}{N_U+0.12N_L}}\right)x_3+\tau_3\right]^2\left(\dfrac{2\pi}{\bar{\omega}_{1U}}\right)^2\left[\dfrac{A_4}{A_3}\right]^{x_3}\dfrac{\Delta_{U\lim}}{\alpha_{U12}N_U A_3} & i=7\end{cases} \tag{E.19}$$

$$b_{\alpha U\max,i}=\begin{cases}1.169R_m^{-0.118}\tau_1^2x_4^2\left(\dfrac{2\pi}{\bar{\omega}_{1U}}\right)^2\left[\dfrac{A_1}{S_a(0.2)}\right]^{x_4}\dfrac{\Delta_{U\lim}}{\alpha_{U\max 2}N_US_a(0.2)} & i=1\\ \left[\left(1-1.3R_m^{-0.059}\right)x_4+1\right]^2\tau_1^2\left(\dfrac{2\pi}{\bar{\omega}_{1U}}\right)^2\dfrac{\Delta_{U\lim}}{\alpha_{U\max 2}N_UA_1} & i=2\\ \left[\left(\tau_1-1.3\tau_2R_m^{-0.059}\right)x_4+\tau_1\right]^2\left(\dfrac{2\pi}{\bar{\omega}_{1U}}\right)^2\left[\dfrac{A_2}{A_1}\right]^{x_4}\dfrac{\Delta_{U\lim}}{\alpha_{U\max 2}N_UA_1} & i=3\\ \left[\left(1-1.3R_m^{-0.059}\right)x_4+1\right]^2\tau_2^2\left(\dfrac{2\pi}{\bar{\omega}_{1U}}\right)^2\dfrac{\Delta_{U\lim}}{\alpha_{U\max 2}N_UA_2} & i=4\\ \left[\left(\tau_2-1.3\tau_3R_m^{-0.059}\right)x_4+\tau_2\right]^2\left(\dfrac{2\pi}{\bar{\omega}_{1U}}\right)^2\left[\dfrac{A_3}{A_2}\right]^{x_4}\dfrac{\Delta_{U\lim}}{\alpha_{U\max 2}N_UA_2} & i=5\\ \left[\left(1-1.3R_m^{-0.059}\right)x_4+1\right]^2\tau_3^2\left(\dfrac{2\pi}{\bar{\omega}_{1U}}\right)^2\dfrac{\Delta_{U\lim}}{\alpha_{U\max 2}N_UA_3} & i=6\\ \left[\left(\tau_3-1.3\tau_4R_m^{-0.059}\right)x_4+\tau_3\right]^2\left(\dfrac{2\pi}{\bar{\omega}_{1U}}\right)^2\left[\dfrac{A_4}{A_3}\right]^{x_4}\dfrac{\Delta_{U\lim}}{\alpha_{U\max 2}N_UA_3} & i=7\end{cases} \tag{E.20}$$

$$b_{\alpha U2stg,i}=\begin{cases}\tau_1^2\left(\dfrac{2\pi}{\bar{\omega}_{1U}}\right)^2\dfrac{\Delta_{U\lim}}{\alpha_{U2stg}N_UA_1} & i=1\\ \tau_2^2\left(\dfrac{2\pi}{\bar{\omega}_{1U}}\right)^2\dfrac{\Delta_{U\lim}}{\alpha_{U2stg}N_UA_2} & i=2\\ \tau_3^2\left(\dfrac{2\pi}{\bar{\omega}_{1U}}\right)^2\dfrac{\Delta_{U\lim}}{\alpha_{U2stg}N_UA_3} & i=3\end{cases} \tag{E.21}$$

Once b_i in calculated based on Eq. (E.18), the numerical solution of y_i can be solved by iteration. As to typical values of b_i that will be encountered in the combined framing system, the numerical solution of y_i is provided in Table E.8 for convenience. For other values of b_i not listed in the table, the value of y_i can be determined through the linear interpolation by the magnitude of b_i.

Table E.8: Numerical solution of the y_i

y_i	b_i	y_i	b_i
-0.100	0.009	-1.100	0.403
-0.200	0.033	-1.200	0.434
-0.300	0.067	-1.300	0.461
-0.400	0.107	-1.400	0.483
-0.500	0.152	-1.500	0.502
-0.600	0.198	-1.600	0.517
-0.700	0.243	-1.700	0.528
-0.800	0.288	-1.800	0.536
-0.900	0.329	-1.900	0.540
-1.000	0.368	-2.000	0.541

E.4 Suggested spectrum approximation techniques

Two different techniques are proposed to determine curve approximation parameters of the power and exponential functions, as shown in Figures E.2 (a) ~ (b). For the sake of convenience, each approximation is designated as a combination of the approximation function and the approximation technique, as shown in Table E.9. For example, the designation "EXP-1" represents the exponential function is selected to fit the NBCC 2010 spectrum and the curving fitting parameters of the exponential function are determined by the approximation technique 1. Equations to compute the curve fitting parameters for each approximation, which are discussed in the following Appendices E.4.1 and E.4.2, are also summarized in the table. In addition, the pros and cons for each approximation is discussed in Appendix E.6.

E.4.1 Power function

PWR-1

As shown in Figure E.2 (a), the first approximation technique determines values of A_i and τ_i based on the spectral values at the starting and ending points of each linear segment. In accordance with this approximation technique:

Table E.9: Designation rules of spectrum approximation schemes

Designation	approximation function	approximation technique	curve fitting equations
PWR-1	power function (Eq.(5.8))	1	Eqs.(E.22) ~ (E.24)
PWR-2		2	Eqs. (E.25) ~ (E.27)
EXP-1	exponential function (Eq. (5.9))	1	Eqs. (E.28) ~ (E.30)
EXP-2		2	Eqs. (E.31) ~ (E.33)

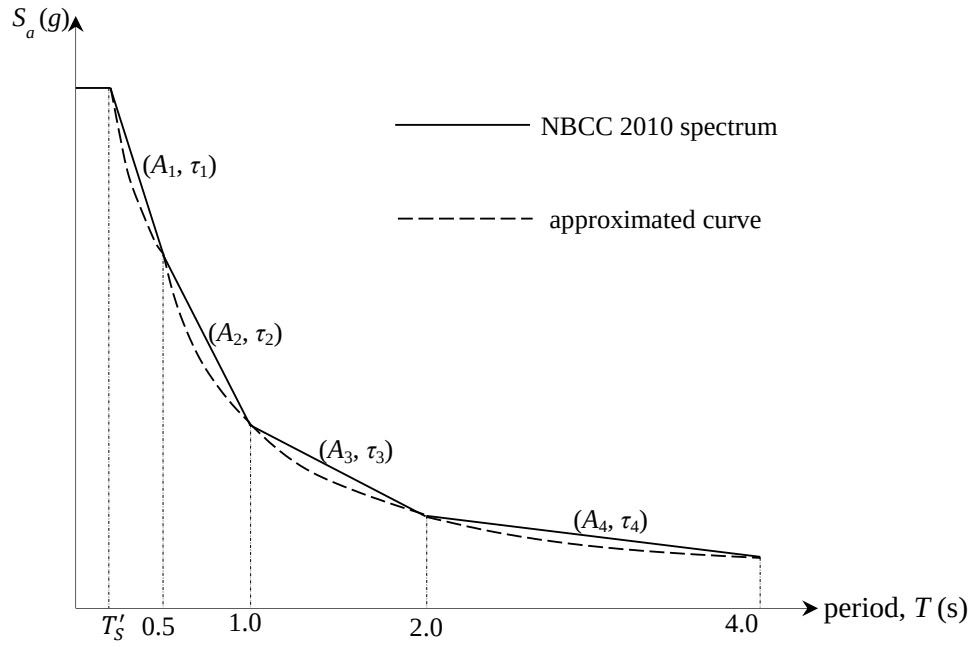

(a) approximation technique 1

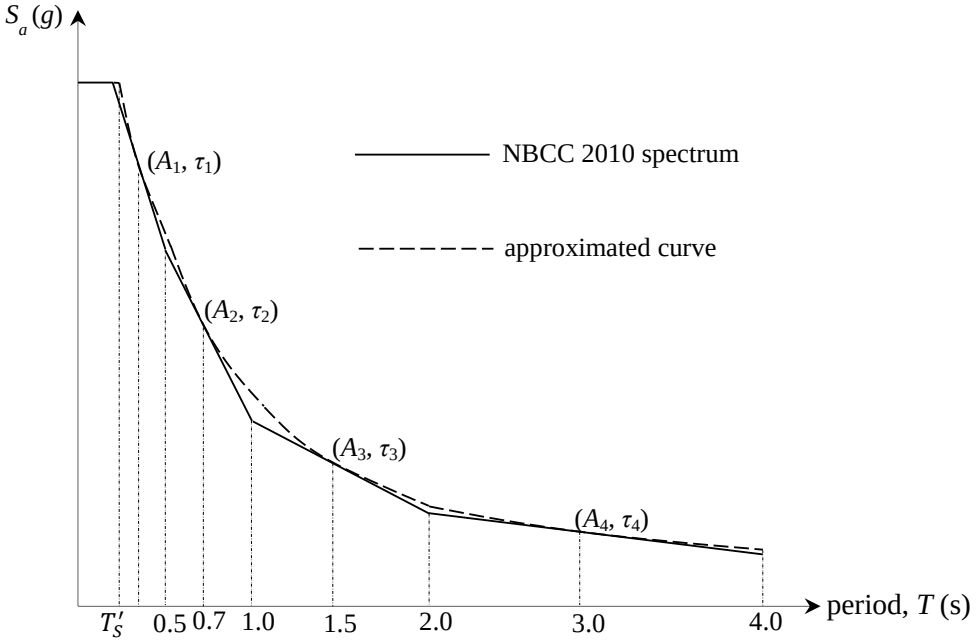

(b) approximation technique 2

Figure E.2: Illustration of approximation techniques

$$T_S^{'} = 0.2 \text{ s} \tag{E.22}$$

$$\tau_i = \begin{cases} \dfrac{\ln\left[S_a(0.2)/S_a(0.5)\right]}{\ln[0.2/0.5]} & i=1 \\ \dfrac{\ln\left[S_a(0.5)/S_a(1.0)\right]}{\ln[0.5/1.0]} & i=2 \\ \dfrac{\ln\left[S_a(1.0)/S_a(2.0)\right]}{\ln[1.0/2.0]} & i=3 \\ \dfrac{\ln\left[S_a(2.0)/S_a(4.0)\right]}{\ln[2.0/4.0]} & i=4 \end{cases} \tag{E.23}$$

$$A_i = \begin{cases} S_a(0.2)(0.2)^{-\tau_i} & i=1 \\ S_a(0.5)(0.5)^{-\tau_i} & i=2 \\ S_a(1.0)(1.0)^{-\tau_i} & i=3 \\ S_a(2.0)(2.0)^{-\tau_i} & i=4 \end{cases} \tag{E.24}$$

PWR-2

As shown in Figure E.2 (b), parameters A_1 and τ_1 for the first linear segment are determined by the slope and spectral value at the midpoint, where the period T_U=0.35 second. For other linear segments, values of A_i and τ_i are determined by spectral values at the starting point and midpoint of each linear segment. Values of τ_i and A_i are computed as follows:

$$\tau_i = \begin{cases} \dfrac{S_a(0.5)-S_a(0.2)}{S_a(0.35)}\dfrac{0.35}{0.3} & i=1 \\ \dfrac{\ln\left[S_a(0.75)/S_a(0.35)/(0.5/0.35)^{\tau_{i-1}}\right]}{\ln[0.75/0.5]} & i=2 \\ \dfrac{\ln\left[S_a(1.5)/S_a(0.75)/(1.0/0.75)^{\tau_{i-1}}\right]}{\ln[1.5/1.0]} & i=3 \\ \dfrac{\ln\left[S_a(3.0)/S_a(1.5)/(2.0/1.5)^{\tau_{i-1}}\right]}{\ln[3.0/2.0]} & i=4 \end{cases} \tag{E.25}$$

$$A_i = \begin{cases} \dfrac{S_a(0.35)}{0.35^{\tau_i}} & i=1 \\ \dfrac{S_a(0.75)}{0.75^{\tau_i}} & i=2 \\ \dfrac{S_a(1.5)}{1.5^{\tau_i}} & i=3 \\ \dfrac{S_a(3.0)}{3.0^{\tau_i}} & i=4 \end{cases} \tag{E.26}$$

In addition, the value of T_S' is determined by the intersection between the flat portion and the approximated first linear segment, as shown in Figure E.2 (b). Value of T_S' are calculated as follows:

$$T_S^{'} = \left[\frac{S_a(0.2)}{A_1}\right]^{1/\tau_1} \tag{E.27}$$

E.4.2 Exponential function

EXP-1

The two approximation techniques shown in Figures E.2 (a) and (b) are also applied to determine values of T_S', A_i and τ_i in Eq. (5.9). If the first approximation technique shown in Figure E.2 (a) is adopted, values of T_S', A_i and τ_i are calculated as follows:

$$T_S^{'} = 0.2 \text{ s} \tag{E.28}$$

$$\tau_i = \begin{cases} \dfrac{\ln\left[S_a(0.2)/S_a(0.5)\right]}{0.2-0.5} & i=1 \\ \dfrac{\ln\left[S_a(0.5)/S_a(1.0)\right]}{0.5-1.0} & i=2 \\ \dfrac{\ln\left[S_a(1.0)/S_a(2.0)\right]}{1.0-2.0} & i=3 \\ \dfrac{\ln\left[S_a(2.0)/S_a(4.0)\right]}{2.0-4.0} & i=4 \end{cases} \tag{E.29}$$

$$A_i = \begin{cases} S_a(0.2)\exp(-0.2\tau_i) & i=1 \\ S_a(0.5)\exp(-0.5\tau_i) & i=2 \\ S_a(1.0)\exp(-1.0\tau_i) & i=3 \\ S_a(2.0)\exp(-2.0\tau_i) & i=4 \end{cases} \tag{E.30}$$

EXP-2

If the second approximation technique shown in Figure E.2 (b) is applied, values of τ_i, A_i and T_S' in Eq.(5.9) are evaluated as follows:

$$\tau_i = \begin{cases} \dfrac{S_a(0.5)-S_a(0.2)}{0.3S_a(0.35)} & i=1 \\ \dfrac{\ln\left[\exp(0.5\tau_{i-1})S_a(0.75)/S_a(0.35)\right]}{0.75-0.5} & i=2 \\ \dfrac{\ln\left[\exp(1.0\tau_{i-1})S_a(1.5)/S_a(0.75)\right]}{1.5-1.0} & i=3 \\ \dfrac{\ln\left[\exp(2.0\tau_{i-1})S_a(3.0)/S_a(1.5)\right]}{3.5-2.0} & i=4 \end{cases} \tag{E.31}$$

$$A_i = \begin{cases} S_a(0.35)\exp(-0.35\tau_i) & i=1 \\ S_a(0.75)\exp(-0.75\tau_i) & i=2 \\ S_a(1.5)\exp(-1.5\tau_i) & i=3 \\ S_a(3.0)\exp(-3.0\tau_i) & i=4 \end{cases} \quad \text{(E.32)}$$

$$T_S^{'} = \frac{\ln\left[S_a(0.2)/A_1\right]}{\tau_1} \quad \text{(E.33)}$$

E.5 Error of proposed factor α_U

By considering all possible combinations of r_m, r_k, T_{singU} and T_{singL} that are presented in section 1.3.2, the maximum and minimum errors of the proposed factor α_U for the three representative seismic cities, i.e., Vancouver, Montreal and Halifax, are listed in Tables E.10 ~ E.15.

Table E.10: Maximum errors of the proposed factor α_U (Vancouver spectrum)

N_L \ N_U	1	2	3	4	5	6	7	8	9
1	13.7%	15.7%	18.6%	22.5%	24.4%	25.7%	27.2%	26.9%	27.5%
2	16.9%	18.4%	22.7%	28.0%	27.5%	27.4%	29.9%	27.6%	N/A
3	18.1%	23.4%	30.7%	28.3%	25.5%	29.1%	25.7%	N/A	N/A
4	18.8%	22.4%	26.8%	32.3%	31.9%	23.9%	N/A	N/A	N/A
5	20.6%	24.0%	26.1%	29.8%	31.5%	N/A	N/A	N/A	N/A
6	18.4%	23.4%	25.6%	28.4%	N/A	N/A	N/A	N/A	N/A
7	10.8%	21.4%	27.2%	N/A	N/A	N/A	N/A	N/A	N/A
8	11.7%	23.6%	N/A	N/A	N/A	N/A	N/A	N/A	N/A
9	11.4%	N/A	N/A	N/A	N/A	N/A	N/A	N/A	N/A

Note: N/A denotes the proposed approach is not applicable for the combination of the lower and upper structures.

Table E.11: Minimum errors of the proposed factor α_U (Vancouver spectrum)

N_L \ N_U	1	2	3	4	5	6	7	8	9
1	-0.4%	3.2%	5.3%	6.0%	9.0%	11.9%	14.5%	16.8%	17.8%
2	6.9%	2.1%	4.6%	6.2%	4.0%	7.3%	7.5%	7.9%	N/A
3	6.7%	3.4%	0.5%	0.7%	-3.5%	3.0%	-3.1%	N/A	N/A
4	6.5%	9.2%	0.0%	0.0%	4.1%	-3.3%	N/A	N/A	N/A
5	6.9%	8.7%	0.0%	3.6%	2.5%	N/A	N/A	N/A	N/A
6	7.1%	7.8%	0.0%	1.6%	N/A	N/A	N/A	N/A	N/A
7	-1.0%	7.1%	N/A	N/A	N/A	N/A	N/A	N/A	N/A
8	-1.0%	6.5%	N/A	N/A	N/A	N/A	N/A	N/A	N/A
9	-0.9%	N/A	N/A	N/A	N/A	N/A	N/A	N/A	N/A

Note: N/A denotes the proposed approach is not applicable for the combination of the lower and upper structures.

Table E.12: Maximum errors of the proposed factor α_U (Montreal spectrum)

N_L \ N_U	1	2	3	4	5	6	7	8	9
1	13.7%	17.9%	20.7%	23.6%	24.4%	25.6%	28.2%	27.9%	28.3%
2	18.6%	30.4%	24.2%	31.3%	30.7%	29.4%	31.8%	28.5%	N/A
3	20.0%	29.6%	34.9%	29.0%	31.5%	32.9%	25.6%	N/A	N/A
4	19.9%	27.4%	29.4%	37.3%	35.3%	25.5%	N/A	N/A	N/A
5	20.6%	25.5%	26.1%	31.7%	35.2%	N/A	N/A	N/A	N/A
6	20.5%	24.4%	25.7%	28.4%	N/A	N/A	N/A	N/A	N/A
7	14.9%	23.8%	27.2%	N/A	N/A	N/A	N/A	N/A	N/A
8	14.9%	23.7%	N/A	N/A	N/A	N/A	N/A	N/A	N/A
9	15.6%	N/A	N/A	N/A	N/A	N/A	N/A	N/A	N/A

Note: N/A denotes the proposed approach is not applicable for the combination of the lower and upper structures.

Table E.13: Minimum errors of the proposed factor α_U (Montreal spectrum)

N_L \ N_U	1	2	3	4	5	6	7	8	9
1	-0.4%	0.7%	1.4%	1.3%	3.3%	7.2%	9.6%	8.3%	3.0%
2	5.8%	1.5%	3.1%	2.4%	-2.6%	0.6%	0.5%	1.7%	N/A
3	4.6%	2.6%	0.5%	-0.8%	-4.6%	-4.6%	-3.1%	N/A	N/A
4	3.8%	4.9%	-1.3%	0.0%	-5.8%	-4.3%	N/A	N/A	N/A
5	4.1%	3.7%	0.0%	0.3%	-5.1%	N/A	N/A	N/A	N/A
6	5.4%	2.9%	0.0%	1.4%	N/A	N/A	N/A	N/A	N/A
7	-1.0%	2.2%	N/A	N/A	N/A	N/A	N/A	N/A	N/A
8	-1.0%	1.6%	N/A	N/A	N/A	N/A	N/A	N/A	N/A
9	-0.9%	N/A	N/A	N/A	N/A	N/A	N/A	N/A	N/A

Note: N/A denotes the proposed approach is not applicable for the combination of the lower and upper structures.

Table E.14: Maximum errors of the proposed factor α_U (Halifax spectrum)

N_L \ N_U	1	2	3	4	5	6	7	8	9
1	13.7%	15.7%	18.7%	21.4%	23.4%	24.8%	26.0%	26.8%	27.5%
2	16.9%	19.4%	20.3%	23.6%	23.0%	24.6%	25.3%	28.9%	N/A
3	18.1%	23.4%	25.6%	25.2%	21.3%	29.1%	24.6%	N/A	N/A
4	18.8%	22.4%	24.2%	27.1%	29.6%	31.9%	N/A	N/A	N/A
5	20.6%	24.0%	26.1%	25.8%	33.6%	N/A	N/A	N/A	N/A
6	19.1%	23.4%	25.6%	28.4%	N/A	N/A	N/A	N/A	N/A
7	12.1%	21.4%	27.2%	N/A	N/A	N/A	N/A	N/A	N/A
8	12.8%	23.6%	N/A	N/A	N/A	N/A	N/A	N/A	N/A
9	12.4%	N/A	N/A	N/A	N/A	N/A	N/A	N/A	N/A

Note: N/A denotes the proposed approach is not applicable for the combination of the lower and upper structures.

Table E.15: Minimum errors of the proposed factor α_U (Halifax spectrum)

N_L \ N_U	1	2	3	4	5	6	7	8	9
1	-0.4%	3.2%	6.6%	7.8%	8.1%	11.7%	15.4%	16.7%	12.6%
2	6.9%	2.1%	4.6%	6.2%	6.3%	3.8%	3.9%	5.5%	N/A
3	6.6%	3.4%	0.5%	0.7%	-3.5%	5.3%	-3.1%	N/A	N/A
4	6.2%	9.2%	0.0%	0.0%	4.7%	-3.3%	N/A	N/A	N/A
5	6.7%	8.4%	0.0%	3.6%	2.5%	N/A	N/A	N/A	N/A
6	6.9%	7.7%	0.0%	1.6%	N/A	N/A	N/A	N/A	N/A
7	-1.0%	7.1%	0.0%	N/A	N/A	N/A	N/A	N/A	N/A
8	-1.0%	6.7%	N/A	N/A	N/A	N/A	N/A	N/A	N/A
9	-0.9%	N/A	N/A	N/A	N/A	N/A	N/A	N/A	N/A

Note: N/A denotes the proposed approach is not applicable for the combination of the lower and upper structures.

E.6 Error of $\alpha_U S_a(T_U)$

By considering all possible combinations of r_m, r_k, T_{singU} and T_{singL} that are presented in section 1.3.2, the maximum and minimum errors of the estimated $\alpha_U S_a(T_U)$ for each approximation listed in Table E.9 and the three representative seismic cities are listed in Tables E.16 ~ E.39.

Table E.16: Maximum errors of the estimated $\alpha_U S_a(T_U)$ (Vancouver spectrum, PWR-1)

N_L \ N_U	1	2	3	4	5	6	7	8	9
1	13.7%	15.7%	18.1%	18.9%	22.2%	23.5%	23.2%	22.9%	25.1%
2	16.9%	17.6%	17.5%	18.1%	20.4%	21.6%	22.0%	21.9%	N/A
3	18.1%	23.4%	20.1%	19.2%	19.5%	19.5%	19.9%	N/A	N/A
4	18.8%	22.4%	22.1%	21.7%	22.9%	21.0%	N/A	N/A	N/A
5	19.1%	20.7%	24.4%	21.3%	20.8%	N/A	N/A	N/A	N/A
6	17.3%	19.0%	21.4%	22.6%	N/A	N/A	N/A	N/A	N/A
7	9.3%	17.7%	21.6%	N/A	N/A	N/A	N/A	N/A	N/A
8	7.0%	19.3%	N/A	N/A	N/A	N/A	N/A	N/A	N/A
9	7.7%	N/A	N/A	N/A	N/A	N/A	N/A	N/A	N/A

Note: N/A denotes the proposed approach is not applicable for the combination of the lower and upper structures.

Table E.17: Minimum errors of the estimated $\alpha_U S_a(T_U)$ (Vancouver spectrum, PWR-1)

N_L \ N_U	1	2	3	4	5	6	7	8	9
1	-4.8%	-1.8%	-3.0%	-1.1%	-0.7%	1.1%	2.7%	4.7%	6.3%
2	2.0%	-3.4%	-3.8%	-3.4%	-0.8%	-1.7%	-1.6%	-1.2%	N/A
3	1.6%	-2.2%	-4.4%	-3.1%	-3.6%	-5.4%	-5.7%	N/A	N/A
4	0.5%	2.0%	-4.0%	-3.3%	-2.1%	-7.0%	N/A	N/A	N/A
5	1.2%	1.6%	-4.6%	-2.5%	-4.2%	N/A	N/A	N/A	N/A
6	1.6%	1.6%	-6.2%	-4.1%	N/A	N/A	N/A	N/A	N/A
7	-3.7%	1.5%	-5.9%	N/A	N/A	N/A	N/A	N/A	N/A
8	-3.8%	1.4%	N/A	N/A	N/A	N/A	N/A	N/A	N/A
9	-3.5%	N/A	N/A	N/A	N/A	N/A	N/A	N/A	N/A

Note: N/A denotes the proposed approach is not applicable for the combination of the lower and upper structures.

Table E.18: Maximum errors of the estimated $\alpha_U S_a(T_U)$ (Montreal spectrum, PWR-1)

N_L \ N_U	1	2	3	4	5	6	7	8	9
1	13.7%	15.7%	17.7%	18.4%	21.4%	22.2%	23.3%	18.6%	24.7%
2	16.9%	19.0%	17.5%	17.1%	19.4%	20.1%	22.1%	17.4%	N/A
3	18.1%	23.4%	20.5%	19.5%	16.8%	19.1%	20.1%	N/A	N/A
4	18.8%	22.4%	19.8%	21.3%	22.7%	16.7%	N/A	N/A	N/A
5	18.1%	20.9%	22.5%	20.7%	20.9%	N/A	N/A	N/A	N/A
6	16.9%	16.0%	21.0%	18.8%	N/A	N/A	N/A	N/A	N/A
7	7.4%	14.0%	15.3%	N/A	N/A	N/A	N/A	N/A	N/A
8	4.5%	14.5%	N/A	N/A	N/A	N/A	N/A	N/A	N/A
9	5.9%	N/A	N/A	N/A	N/A	N/A	N/A	N/A	N/A

Note: N/A denotes the proposed approach is not applicable for the combination of the lower and upper structures.

Table E.19: Minimum errors of the estimated $\alpha_U S_a(T_U)$ (Montreal spectrum, PWR-1)

N_L \ N_U	1	2	3	4	5	6	7	8	9
1	-10.9%	-8.6%	-9.1%	-6.7%	-9.4%	-11.8%	-11.8%	-12.2%	-11.2%
2	-7.9%	-8.3%	-10.0%	-10.6%	-12.1%	-17.4%	-17.2%	-17.4%	N/A
3	-7.9%	-8.7%	-9.9%	-8.9%	-12.7%	-18.8%	-21.9%	N/A	N/A
4	-7.9%	-4.9%	-9.7%	-9.2%	-16.9%	-22.0%	N/A	N/A	N/A
5	-6.5%	-5.2%	-9.4%	-9.8%	-16.5%	N/A	N/A	N/A	N/A
6	-5.7%	-5.2%	-11.6%	-11.3%	N/A	N/A	N/A	N/A	N/A
7	-10.5%	-5.1%	-11.5%	N/A	N/A	N/A	N/A	N/A	N/A
8	-10.9%	-5.1%	N/A	N/A	N/A	N/A	N/A	N/A	N/A
9	-10.9%	N/A	N/A	N/A	N/A	N/A	N/A	N/A	N/A

Note: N/A denotes the proposed approach is not applicable for the combination of the lower and upper structures.

Table E.20: Maximum errors of the estimated $\alpha_U S_a(T_U)$ (Halifax spectrum, PWR-1)

N_L \ N_U	1	2	3	4	5	6	7	8	9
1	13.7%	15.7%	18.1%	19.1%	22.2%	23.3%	23.1%	23.1%	25.0%
2	16.9%	17.6%	17.5%	17.4%	20.3%	21.3%	22.0%	22.1%	N/A
3	18.1%	23.4%	19.8%	19.1%	19.1%	19.1%	19.9%	0.0%	N/A
4	18.8%	22.4%	21.8%	19.9%	21.4%	20.4%	N/A	N/A	N/A
5	18.9%	20.7%	24.2%	21.2%	19.8%	N/A	N/A	N/A	N/A
6	17.2%	18.7%	21.3%	21.7%	N/A	N/A	N/A	N/A	N/A
7	9.1%	17.2%	20.7%	N/A	N/A	N/A	N/A	N/A	N/A
8	6.9%	18.7%	N/A	N/A	N/A	N/A	N/A	N/A	N/A
9	7.9%	N/A	N/A	N/A	N/A	N/A	N/A	N/A	N/A

Note: N/A denotes the proposed approach is not applicable for the combination of the lower and upper structures.

Table E.21: Minimum errors of the estimated $\alpha_U S_a(T_U)$ (Halifax spectrum, PWR-1)

N_L \ N_U	1	2	3	4	5	6	7	8	9
1	-5.5%	-2.5%	-0.7%	1.2%	-7.0%	-10.4%	-10.1%	-8.2%	-7.6%
2	0.9%	-2.7%	-2.5%	-2.0%	-10.6%	-16.7%	-13.9%	-13.1%	N/A
3	0.9%	-1.4%	-2.4%	-1.3%	-10.9%	-14.7%	-16.2%	N/A	N/A
4	-0.1%	3.1%	-2.1%	-3.8%	-15.6%	-21.9%	0.0%	N/A	N/A
5	1.0%	2.7%	-2.7%	-5.7%	-14.9%	N/A	N/A	N/A	N/A
6	1.6%	2.7%	-4.4%	-6.9%	0.0%	N/A	N/A	N/A	N/A
7	-3.2%	2.6%	-4.2%	N/A	N/A	N/A	N/A	N/A	N/A
8	-3.3%	2.6%	N/A	N/A	N/A	N/A	N/A	N/A	N/A
9	-3.0%	N/A	N/A	N/A	N/A	N/A	N/A	N/A	N/A

Note: N/A denotes the proposed approach is not applicable for the combination of the lower and upper structures.

Table E.22: Maximum errors of the estimated $\alpha_U S_a(T_U)$ (Vancouver spectrum, PWR-2)

N_L \ N_U	1	2	3	4	5	6	7	8	9
1	16.5%	20.0%	24.6%	30.3%	39.8%	41.1%	41.8%	42.4%	43.2%
2	20.2%	20.7%	28.2%	34.3%	38.6%	39.7%	40.1%	41.3%	N/A
3	21.9%	26.9%	35.4%	36.3%	35.2%	37.0%	38.4%	N/A	N/A
4	22.7%	26.1%	32.3%	38.2%	40.3%	34.5%	N/A	N/A	N/A
5	25.1%	27.8%	29.4%	35.9%	37.4%	N/A	N/A	N/A	N/A
6	22.6%	25.4%	28.4%	33.6%	N/A	N/A	N/A	N/A	N/A
7	13.8%	27.8%	28.7%	N/A	N/A	N/A	N/A	N/A	N/A
8	13.8%	27.5%	N/A	N/A	N/A	N/A	N/A	N/A	N/A
9	14.5%	N/A	N/A	N/A	N/A	N/A	N/A	N/A	N/A

Note: N/A denotes the proposed approach is not applicable for the combination of the lower and upper structures.

Table E.23: Minimum errors of the estimated $\alpha_U S_a(T_U)$ (Vancouver spectrum, PWR-2)

N_L \ N_U	1	2	3	4	5	6	7	8	9
1	-0.4%	3.2%	7.8%	10.2%	10.9%	14.0%	14.9%	17.5%	18.9%
2	6.9%	3.1%	6.2%	7.0%	9.7%	10.3%	9.6%	9.5%	N/A
3	7.8%	3.4%	0.5%	4.9%	0.9%	7.3%	4.2%	N/A	N/A
4	7.0%	9.2%	4.6%	6.4%	9.8%	3.9%	N/A	N/A	N/A
5	7.3%	9.5%	5.9%	7.3%	7.3%	N/A	N/A	N/A	N/A
6	7.4%	10.5%	4.0%	6.7%	N/A	N/A	N/A	N/A	N/A
7	0.7%	10.6%	4.3%	N/A	N/A	N/A	N/A	N/A	N/A
8	2.4%	10.7%	N/A	N/A	N/A	N/A	N/A	N/A	N/A
9	2.6%	N/A	N/A	N/A	N/A	N/A	N/A	N/A	N/A

Note: N/A denotes the proposed approach is not applicable for the combination of the lower and upper structures.

Table E.24: Maximum errors of the estimated $\alpha_U S_a(T_U)$ (Montreal spectrum, PWR-2)

N_L \ N_U	1	2	3	4	5	6	7	8	9
1	20.3%	30.3%	35.1%	34.5%	39.4%	40.2%	41.6%	37.6%	43.2%
2	27.8%	37.0%	32.2%	36.5%	37.1%	37.9%	40.2%	36.2%	N/A
3	26.7%	35.6%	39.4%	38.3%	35.2%	38.0%	38.0%	N/A	N/A
4	27.5%	32.8%	32.6%	40.4%	42.2%	34.7%	N/A	N/A	N/A
5	29.0%	30.8%	30.7%	36.6%	40.0%	N/A	N/A	N/A	N/A
6	28.4%	30.7%	31.5%	33.6%	N/A	N/A	N/A	N/A	N/A
7	19.6%	31.0%	32.4%	N/A	N/A	N/A	N/A	N/A	N/A
8	20.7%	31.6%	N/A	N/A	N/A	N/A	N/A	N/A	N/A
9	22.1%	N/A	N/A	N/A	N/A	N/A	N/A	N/A	N/A

Note: N/A denotes the proposed approach is not applicable for the combination of the lower and upper structures.

Table E.25: Minimum errors of the estimated $\alpha_U S_a(T_U)$ (Montreal spectrum, PWR-2)

N_L \ N_U	1	2	3	4	5	6	7	8	9
1	-0.4%	3.2%	5.0%	7.9%	8.1%	8.7%	10.5%	11.7%	12.7%
2	6.4%	3.5%	3.9%	3.3%	6.9%	3.8%	3.8%	5.5%	N/A
3	6.4%	3.4%	0.5%	5.2%	0.9%	-1.0%	-2.2%	N/A	N/A
4	6.3%	9.2%	4.3%	5.0%	2.5%	-1.2%	N/A	N/A	N/A
5	6.5%	9.3%	4.6%	6.3%	2.4%	N/A	N/A	N/A	N/A
6	6.3%	9.4%	2.2%	5.1%	N/A	N/A	N/A	N/A	N/A
7	1.6%	9.4%	2.2%	N/A	N/A	N/A	N/A	N/A	N/A
8	2.9%	9.4%	N/A	N/A	N/A	N/A	N/A	N/A	N/A
9	2.9%	N/A	N/A	N/A	N/A	N/A	N/A	N/A	N/A

Note: N/A denotes the proposed approach is not applicable for the combination of the lower and upper structures.

Table E.26: Maximum errors of the estimated $\alpha_U S_a(T_U)$ (Halifax spectrum, PWR-2)

N_L \ N_U	1	2	3	4	5	6	7	8	9
1	17.1%	20.9%	25.6%	26.9%	34.2%	35.7%	36.0%	36.8%	55.3%
2	20.5%	22.2%	24.2%	27.0%	33.1%	34.5%	34.6%	38.2%	N/A
3	22.2%	27.2%	28.8%	31.6%	30.3%	33.6%	41.0%	N/A	N/A
4	23.3%	26.5%	26.5%	32.0%	34.0%	36.7%	N/A	N/A	N/A
5	25.5%	28.1%	27.9%	29.9%	33.3%	N/A	N/A	N/A	N/A
6	23.1%	25.8%	28.0%	31.3%	N/A	N/A	N/A	N/A	N/A
7	14.1%	24.8%	28.5%	N/A	N/A	N/A	N/A	N/A	N/A
8	14.9%	26.2%	N/A	N/A	N/A	N/A	N/A	N/A	N/A
9	15.9%	N/A	N/A	N/A	N/A	N/A	N/A	N/A	N/A

Note: N/A denotes the proposed approach is not applicable for the combination of the lower and upper structures.

Table E.27: Minimum errors of the estimated $\alpha_U S_a(T_U)$ (Halifax spectrum, PWR-2)

N_L \ N_U	1	2	3	4	5	6	7	8	9
1	-0.4%	3.2%	7.8%	10.6%	10.9%	11.5%	12.9%	17.5%	19.1%
2	6.9%	3.1%	5.9%	6.7%	9.1%	7.7%	9.8%	6.6%	N/A
3	7.8%	3.4%	0.5%	5.2%	0.9%	5.9%	2.6%	N/A	N/A
4	7.1%	9.2%	4.7%	6.8%	5.1%	2.9%	N/A	N/A	N/A
5	7.2%	9.5%	6.0%	7.6%	5.0%	N/A	N/A	N/A	N/A
6	7.2%	10.5%	4.1%	7.2%	N/A	N/A	N/A	N/A	N/A
7	0.8%	10.6%	4.2%	N/A	N/A	N/A	N/A	N/A	N/A
8	2.8%	10.9%	N/A	N/A	N/A	N/A	N/A	N/A	N/A
9	2.9%	N/A	N/A	N/A	N/A	N/A	N/A	N/A	N/A

Note: N/A denotes the proposed approach is not applicable for the combination of the lower and upper structures.

Table E.28: Maximum errors of the estimated $\alpha_U S_a(T_U)$ (Vancouver spectrum, EXP-1)

N_L \ N_U	1	2	3	4	5	6	7	8	9
1	13.7%	15.7%	18.4%	20.1%	22.7%	23.6%	24.6%	24.0%	25.9%
2	16.9%	17.6%	18.0%	23.0%	22.0%	24.0%	24.4%	23.0%	N/A
3	18.1%	23.4%	25.2%	22.7%	19.9%	24.0%	21.6%	N/A	N/A
4	18.8%	22.4%	23.5%	26.3%	26.7%	21.1%	0.0%	N/A	N/A
5	20.3%	22.9%	25.6%	24.2%	25.1%	N/A	N/A	N/A	N/A
6	18.2%	21.3%	23.5%	25.5%	N/A	N/A	N/A	N/A	N/A
7	10.4%	19.3%	23.2%	N/A	N/A	N/A	N/A	N/A	N/A
8	9.5%	20.6%	N/A	N/A	N/A	N/A	N/A	N/A	N/A
9	9.7%	N/A	N/A	N/A	N/A	N/A	N/A	N/A	N/A

Note: N/A denotes the proposed approach is not applicable for the combination of the lower and upper structures.

Table E.29: Minimum errors of the estimated $\alpha_U S_a(T_U)$ (Vancouver spectrum, EXP-1)

N_L \ N_U	1	2	3	4	5	6	7	8	9
1	-0.6%	2.6%	1.0%	2.8%	3.8%	6.1%	8.2%	10.5%	12.5%
2	6.1%	2.3%	1.7%	2.2%	2.6%	3.3%	3.3%	3.6%	N/A
3	5.3%	2.8%	0.0%	1.4%	0.6%	-0.4%	-1.3%	N/A	N/A
4	4.7%	6.3%	0.4%	0.8%	1.5%	-2.5%	N/A	N/A	N/A
5	5.6%	5.4%	0.3%	1.9%	0.8%	N/A	N/A	N/A	N/A
6	6.2%	4.9%	-1.1%	0.8%	N/A	N/A	N/A	N/A	N/A
7	0.0%	4.5%	-0.8%	N/A	N/A	N/A	N/A	N/A	N/A
8	0.4%	4.1%	N/A	N/A	N/A	N/A	N/A	N/A	N/A
9	0.6%	N/A	N/A	N/A	N/A	N/A	N/A	N/A	N/A

Note: N/A denotes the proposed approach is not applicable for the combination of the lower and upper structures.

Table E.30: Maximum errors of the estimated $\alpha_U S_a(T_U)$ (Montreal spectrum, EXP-1)

N_L \ N_U	1	2	3	4	5	6	7	8	9
1	13.7%	15.7%	18.3%	19.3%	22.2%	22.4%	25.4%	21.5%	26.3%
2	16.9%	24.7%	19.4%	23.4%	21.9%	23.8%	24.2%	22.1%	N/A
3	18.1%	23.6%	26.7%	24.5%	22.0%	24.6%	22.2%	N/A	N/A
4	18.8%	22.4%	22.4%	26.8%	27.3%	20.0%	N/A	N/A	N/A
5	19.5%	20.9%	24.8%	23.5%	26.1%	N/A	N/A	N/A	N/A
6	18.6%	20.0%	22.7%	20.9%	N/A	N/A	N/A	N/A	N/A
7	9.5%	17.4%	19.7%	N/A	N/A	N/A	N/A	N/A	N/A
8	10.0%	17.6%	N/A	N/A	N/A	N/A	N/A	N/A	N/A
9	10.1%	N/A	N/A	N/A	N/A	N/A	N/A	N/A	N/A

Note: N/A denotes the proposed approach is not applicable for the combination of the lower and upper structures.

Table E.31: Minimum errors of the estimated $\alpha_U S_a(T_U)$ (Montreal spectrum, EXP-1)

N_L \ N_U	1	2	3	4	5	6	7	8	9
1	-4.0%	-1.9%	-4.6%	-2.9%	-4.1%	-4.5%	-3.9%	-5.5%	-5.1%
2	-0.5%	-2.7%	-3.8%	-4.6%	-5.7%	-10.8%	-9.8%	-11.2%	N/A
3	-0.5%	-2.9%	-4.5%	-2.7%	-8.0%	-11.9%	-14.5%	N/A	N/A
4	-1.0%	-0.1%	-4.7%	-4.8%	-9.8%	-15.2%	N/A	N/A	N/A
5	0.3%	-0.9%	-4.0%	-3.4%	-9.7%	N/A	N/A	N/A	N/A
6	1.2%	-1.1%	-5.8%	-4.3%	N/A	N/A	N/A	N/A	N/A
7	-4.2%	-1.4%	-5.7%	N/A	N/A	N/A	N/A	N/A	N/A
8	-4.4%	-1.6%	N/A	N/A	N/A	N/A	N/A	N/A	N/A
9	-4.2%	N/A	N/A	N/A	N/A	N/A	N/A	N/A	N/A

Note: N/A denotes the proposed approach is not applicable for the combination of the lower and upper structures.

Table E.32: Maximum errors of the estimated $\alpha_U S_a(T_U)$ (Halifax spectrum, EXP-1)

N_L \ N_U	1	2	3	4	5	6	7	8	9
1	13.7%	15.7%	18.4%	20.1%	22.6%	23.5%	24.4%	24.1%	26.0%
2	16.9%	17.6%	17.5%	18.8%	20.7%	21.4%	23.3%	23.1%	N/A
3	18.1%	23.4%	21.7%	22.0%	19.6%	21.3%	21.3%	N/A	N/A
4	18.8%	22.4%	23.4%	23.8%	24.6%	20.6%	N/A	N/A	N/A
5	20.2%	22.7%	25.5%	22.1%	23.5%	N/A	N/A	N/A	N/A
6	18.3%	21.1%	23.1%	25.0%	N/A	N/A	N/A	N/A	N/A
7	10.3%	19.1%	22.5%	N/A	N/A	N/A	N/A	N/A	N/A
8	10.5%	20.3%	N/A	N/A	N/A	N/A	N/A	N/A	N/A
9	10.6%	N/A	N/A	N/A	N/A	N/A	N/A	N/A	N/A

Note: N/A denotes the proposed approach is not applicable for the combination of the lower and upper structures.

Table E.33: Minimum errors of the estimated $\alpha_U S_a(T_U)$ (Halifax spectrum, EXP-1)

N_L \ N_U	1	2	3	4	5	6	7	8	9
1	-0.9%	2.3%	3.5%	5.0%	-1.2%	-2.5%	-1.8%	-0.2%	0.5%
2	5.5%	2.1%	2.3%	2.9%	-3.5%	-9.6%	-7.3%	-5.8%	N/A
3	4.9%	3.0%	0.5%	2.7%	-4.3%	-7.3%	-8.8%	N/A	N/A
4	4.4%	6.8%	2.2%	2.5%	-7.9%	-14.6%	N/A	N/A	N/A
5	5.4%	6.0%	1.6%	2.5%	-7.4%	N/A	N/A	N/A	N/A
6	6.1%	5.6%	0.0%	1.1%	0.0%	N/A	N/A	N/A	N/A
7	0.0%	5.2%	0.2%	N/A	N/A	N/A	N/A	N/A	N/A
8	0.4%	5.0%	N/A	N/A	N/A	N/A	N/A	N/A	N/A
9	0.6%	N/A	N/A	N/A	N/A	N/A	N/A	N/A	N/A

Note: N/A denotes the proposed approach is not applicable for the combination of the lower and upper structures.

Table E.34: Maximum errors of the estimated $\alpha_U S_a(T_U)$ (Vancouver spectrum, EXP-2)

N_L \ N_U	1	2	3	4	5	6	7	8	9
1	14.1%	16.5%	20.9%	26.4%	31.9%	32.6%	35.1%	34.8%	35.9%
2	17.7%	19.2%	25.7%	31.8%	30.8%	31.6%	33.5%	33.7%	N/A
3	19.3%	23.8%	33.2%	31.8%	28.3%	33.0%	31.9%	N/A	N/A
4	20.2%	23.5%	29.2%	34.6%	36.0%	28.9%	N/A	N/A	N/A
5	22.3%	25.0%	27.7%	33.0%	35.2%	N/A	N/A	N/A	N/A
6	19.8%	24.7%	26.99%	29.2%	N/A	N/A	N/A	N/A	N/A
7	11.6%	24.2%	28.9%	N/A	N/A	N/A	N/A	N/A	N/A
8	12.0%	24.7%	N/A	N/A	N/A	N/A	N/A	N/A	N/A
9	12.1%	N/A	N/A	N/A	N/A	N/A	N/A	N/A	N/A

Note: N/A denotes the proposed approach is not applicable for the combination of the lower and upper structures.

Table E.35: Minimum errors of the estimated $\alpha_U S_a(T_U)$ (Vancouver spectrum, EXP-2)

N_L \ N_U	1	2	3	4	5	6	7	8	9
1	-0.4%	3.2%	7.5%	9.9%	11.2%	14.5%	15.3%	16.9%	17.7%
2	6.9%	2.1%	4.6%	6.2%	7.5%	9.1%	8.0%	8.1%	N/A
3	7.0%	3.4%	0.5%	0.7%	-3.5%	6.6%	-3.1%	N/A	N/A
4	6.8%	9.2%	0.0%	0.0%	6.8%	-3.3%	N/A	N/A	N/A
5	7.0%	9.0%	0.0%	3.6%	2.5%	N/A	N/A	N/A	N/A
6	7.2%	8.9%	0.0%	1.6%	N/A	N/A	N/A	N/A	N/A
7	-1.0%	8.7%	0.0%	N/A	N/A	N/A	N/A	N/A	N/A
8	-1.0%	8.6%	N/A	N/A	N/A	N/A	N/A	N/A	N/A
9	-0.9%	N/A	N/A	N/A	N/A	N/A	N/A	N/A	N/A

Note: N/A denotes the proposed approach is not applicable for the combination of the lower and upper structures.

Table E.36: Maximum errors of the estimated $\alpha_U S_a(T_U)$ (Montreal spectrum, EXP-2)

N_L \ N_U	1	2	3	4	5	6	7	8	9
1	16.5%	24.1%	28.0%	28.6%	32.2%	33.1%	35.5%	31.5%	36.5%
2	23.6%	34.0%	28.7%	33.7%	32.2%	31.9%	34.2%	31.3%	N/A
3	23.3%	32.8%	36.8%	31.3%	33.6%	35.1%	32.8%	N/A	N/A
4	23.1%	30.2%	30.9%	39.1%	38.3%	29.5%	N/A	N/A	N/A
5	24.3%	28.2%	28.7%	33.3%	37.7%	N/A	N/A	N/A	N/A
6	23.9%	27.5%	28.3%	29.7%	N/A	N/A	N/A	N/A	N/A
7	16.8%	26.2%	30.3%	N/A	N/A	N/A	N/A	N/A	N/A
8	17.7%	27.3%	N/A	N/A	N/A	N/A	N/A	N/A	N/A
9	17.7%	N/A	N/A	N/A	N/A	N/A	N/A	N/A	N/A

Note: N/A denotes the proposed approach is not applicable for the combination of the lower and upper structures.

Table E.37: Minimum errors of the estimated $\alpha_U S_a(T_U)$ (Montreal spectrum, EXP-2)

N_L \ N_U	1	2	3	4	5	6	7	8	9
1	-0.4%	3.2%	3.0%	4.8%	7.1%	9.0%	10.5%	10.9%	12.1%
2	6.2%	2.1%	3.9%	3.0%	2.7%	2.6%	3.8%	4.2%	N/A
3	6.1%	3.4%	0.5%	0.7%	-3.5%	-1.6%	-3.1%	N/A	N/A
4	5.6%	8.0%	0.0%	0.0%	-0.9%	-3.3%	N/A	N/A	N/A
5	5.9%	7.2%	0.0%	3.6%	-0.8%	N/A	N/A	N/A	N/A
6	5.8%	6.9%	0.0%	1.6%	N/A	N/A	N/A	N/A	N/A
7	-1.0%	6.6%	0.0%	N/A	N/A	N/A	N/A	N/A	N/A
8	-1.0%	6.3%	N/A	N/A	N/A	N/A	N/A	N/A	N/A
9	-0.9%	N/A	N/A	N/A	N/A	N/A	N/A	N/A	N/A

Note: N/A denotes the proposed approach is not applicable for the combination of the lower and upper structures.

Table E.38: Maximum errors of the estimated $\alpha_U S_a(T_U)$ (Halifax spectrum, EXP-2)

N_L \ N_U	1	2	3	4	5	6	7	8	9
1	14.4%	17.1%	21.5%	23.6%	27.9%	28.8%	30.7%	30.7%	44.4%
2	17.9%	20.5%	22.1%	25.3%	26.9%	27.7%	29.3%	36.8%	N/A
3	19.4%	24.0%	27.1%	28.0%	24.1%	32.1%	36.0%	N/A	N/A
4	20.5%	23.7%	25.9%	28.4%	30.4%	34.8%	N/A	N/A	N/A
5	22.5%	25.2%	27.9%	27.6%	34.4%	N/A	N/A	N/A	N/A
6	20.0%	25.0%	27.1%	29.3%	N/A	N/A	N/A	N/A	N/A
7	12.6%	22.9%	29.2%	N/A	N/A	N/A	N/A	N/A	N/A
8	13.4%	25.0%	N/A	N/A	N/A	N/A	N/A	N/A	N/A
9	13.4%	N/A	N/A	N/A	N/A	N/A	N/A	N/A	N/A

Note: N/A denotes the proposed approach is not applicable for the combination of the lower and upper structures.

Table E.39: Minimum errors of the estimated $\alpha_U S_a(T_U)$ (Halifax spectrum, EXP-2)

N_L \ N_U	1	2	3	4	5	6	7	8	9
1	-0.4%	3.2%	7.8%	10.2%	10.6%	12.7%	16.2%	18.9%	19.8%
2	6.9%	2.1%	4.6%	6.2%	7.5%	6.4%	9.1%	8.1%	N/A
3	6.9%	3.4%	0.5%	0.7%	-3.5%	6.1%	-3.1%	N/A	N/A
4	6.7%	9.2%	0.0%	0.0%	5.4%	-3.3%	N/A	N/A	N/A
5	6.8%	9.0%	0.0%	3.6%	2.5%	N/A	N/A	N/A	N/A
6	7.0%	8.9%	0.0%	1.6%	N/A	N/A	N/A	N/A	N/A
7	-1.0%	8.8%	N/A	N/A	N/A	N/A	N/A	N/A	N/A
8	-1.0%	8.7%	N/A	N/A	N/A	N/A	N/A	N/A	N/A
9	-0.9%	N/A	N/A	N/A	N/A	N/A	N/A	N/A	N/A

Note: N/A denotes the proposed approach is not applicable for the combination of the lower and upper structures.

As shown in Tables E.16 ~ E.39, not all approximations of the spectrum listed in Table E.9 have acceptable errors for all possible storey combinations of lower and upper structures. Errors of the estimated $\alpha_U S_a(T_U)$ for each one of the four approximations listed in Table E.9 have the following characteristics:

(1)The primary disadvantage for the first approximation technique is that the it may greatly underestimate the value of $\alpha_U S_a(T_U)$ for certain storey combinations. For example, when N_L=4, N_U=6 and the Montreal spectrum is used, the maximum underestimation of $\alpha_U S_a(T_U)$ can be as large as 22.0% and 15.2% if the power and exponential functions are selected to approximate the spectrum, respectively, as shown in Tables E.19 and E.31. On the other hand, the primary disadvantage for the second approximation technique is that it may greatly overestimate the value of $\alpha_U S_a(T_U)$ for certain storey combinations of lower and upper structures. For example, when N_L=1, N_U=9 and the Halifax

spectrum is used, the maximum overestimation of $\alpha_U S_a(T_U)$ can be as large as 55.3% and 44.4% if the power and exponential functions are selected to approximate the spectrum, respectively, as shown in Tables E.26 and E.38.

Such disadvantages associated with the first and second approximation techniques are resulted from the inherent characteristics of the power and exponential functions. With the positive value for A_i and negative value for τ_i, the power or exponential function is a convex function. If such convex function matches the spectrum values at the beginning and ending points of each linear segment, i.e., the first approximation technique, the spectral values at intermediate periods will be underestimated, as shown in Figure E.2 (a). On the other hand, if such convex function matches the spectral value at the midpoint of each linear segment, i.e., the second approximation technique, although the spectrum values at all periods will not be underestimated, the spectrum values at the starting and ending points may be greatly overestimated, as shown in Figure E.2 (b). Therefore, the value of $\alpha_U S_a(T_U)$ may be greatly underestimated if the first approximation technique is adopted due to the underestimation of the spectrum value $S_a(T_U)$, and the value of $\alpha_U S_a(T_U)$ and may be greatly overestimated if the second approximation technique is adopted due to the overestimation of the spectrum value $S_a(T_U)$.

(2) From a general aspect, the exponential function is a better approximation of the spectrum than the power function. If the first approximation technique is adopted to approximate the spectrum, the magnitude of underestimation associated with the power function is larger than that of the exponential function. For example, when N_L=4, N_U=6 and using the first approximation technique to approximate the Montreal spectrum, the underestimation of $\alpha_U S_a(T_U)$ associated with the power function is 22.0% while that associated with the exponential function is 15.2%, as shown in Tables E.19 and E.31, respectively. On the other hand, if the second approximation technique is adopted to approximate the spectrum, the magnitude of overestimation associated with the power function is also larger than that of the exponential function. For example, when N_L=1, N_U=9 and the second approximation technique is adopted to fit the Halifax spectrum, the maximum overestimation of $\alpha_U S_a(T_U)$ associated with the power function is 55.3% while that associated with the exponential function is 44.4%, as shown in Tables E.26 and E.38.

(3) Considering all possible combinations of lower and upper structures, the "EXP-2" approximation, which adopts the exponential function and the second approximation technique to obtain the curve approximation parameters as listed in Table E.9, provides the most reasonable values of $\alpha_U S_a(T_U)$ from a general aspect. However, the "EXP-2" approximation does not always provide the best estimated $\alpha_U S_a(T_U)$ for all storey combinations of lower and upper structures. For example, when

N_L=6 and N_U=3, as shown in Tables E. 22 ~ E. 27, the "PWR-2" approximation also provides reasonable estimation of $\alpha_U S_a(T_U)$.

E.7 Error of modified ELF procedure based on NBCC 2010

Table E.40: Errors associated with modified ELF procedure (Vancouver spectrum)

N_L	N_U	lower structure		upper structure	
		maximum	minimum	maximum	minimum
2	1	23.6%	12.8%	15.2%	7.7%
3	1	28.1%	13.7%	16.0%	6.7%
4	1	31.7%	14.5%	16.2%	6.6%
5	1	33.7%	15.0%	16.6%	6.9%
6	1	35.3%	15.5%	18.1%	7.1%
7	1	36.4%	15.9%	10.8%	-1.0%
8	1	35.6%	16.3%	11.7%	-1.0%
9	1	39.0%	16.8%	11.4%	-0.9%

Table E.41: Errors associated with modified ELF procedure (Montreal spectrum)

N_L	N_U	lower structure		upper structure	
		maximum	minimum	maximum	minimum
2	1	23.6%	11.2%	18.7%	6.4%
3	1	28.1%	12.4%	20.0%	4.7%
4	1	31.7%	13.0%	19.9%	4.1%
5	1	33.7%	13.4%	19.4%	4.1%
6	1	35.3%	13.7%	20.5%	5.4%
7	1	36.4%	13.9%	14.9%	-1.0%
8	1	35.6%	14.2%	14.9%	-1.0%
9	1	31.8%	14.3%	11.4%	-0.9%

Table E.42: Errors associated with modified ELF procedure (Halifax spectrum)

N_L	N_U	lower structure		upper structure	
		maximum	minimum	maximum	minimum
2	1	23.6%	12.7%	15.7%	7.6%
3	1	28.1%	13.6%	16.6%	6.6%
4	1	31.7%	14.4%	16.8%	6.5%
5	1	33.7%	14.9%	17.1%	6.7%
6	1	35.3%	15.4%	19.1%	6.9%
7	1	36.4%	15.8%	12.1%	-1.0%
8	1	35.6%	16.2%	12.8%	-1.0%
9	1	38.8%	16.7%	12.4%	-0.9%

E.8 Error of proposed two-stage analysis procedure based on NBCC 2010

Table E.43: Errors associated with proposed two-stage procedure (Vancouver spectrum)

N_L	N_U	upper structure		lower structure	
		maximum	minimum	maximum	maximum
1	1	9.7%	-0.4%	8.6%	3.0%
1	2	22.7%	3.2%	21.1%	0.1%
2	2	18.9%	2.1%	29.8%	1.7%
3	2	14.5%	4.4%	31.6%	4.2%
1	3	31.0%	7.8%	33.1%	12.2%
2	3	28.5%	4.6%	47.4%	11.0%
3	3	26.8%	4.3%	52.5%	9.0%
4	3	21.9%	4.2%	54.5%	8.1%
1	4	36.0%	12.0%	40.3%	13.7%
2	4	34.1%	6.2%	51.6%	12.4%
3	4	30.7%	5.9%	58.8%	10.0%
4	4	35.4%	5.8%	62.4%	8.0%
5	4	24.7%	5.7%	64.4%	6.9%
1	5	39.6%	8.0%	41.8%	13.8%
2	5	38.1%	4.0%	53.4%	13.2%
3	5	35.0%	3.3%	60.9%	10.6%
4	5	36.3%	4.1%	64.7%	8.9%
5	5	36.6%	3.2%	66.6%	7.6%
1	6	42.0%	7.5%	42.7%	14.4%
2	6	40.6%	5.1%	55.3%	13.7%
3	6	39.6%	3.0%	62.7%	11.0%
4	6	37.9%	4.1%	66.8%	9.2%
1	7	43.9%	5.1%	44.3%	14.8%
2	7	42.7%	5.2%	57.4%	14.1%
3	7	40.4%	-0.5%	64.6%	11.4%
1	8	45.4%	7.3%	45.9%	14.8%
2	8	44.4%	6.6%	59.8%	14.5%
1	9	46.6%	7.1%	48.3%	14.6%

Table E.44: Errors associated with proposed two-stage procedure (Montreal spectrum)

N_L	N_U	upper structure		lower structure	
		maximum	minimum	maximum	maximum
1	1	10.4%	-0.4%	8.6%	3.0%
1	2	23.1%	-3.6%	21.1%	0.1%
2	2	19.6%	-2.8%	29.8%	1.7%
3	2	15.3%	-0.2%	31.6%	4.2%
1	3	31.2%	3.3%	33.1%	12.2%
2	3	28.8%	1.9%	47.4%	11.0%
3	3	29.0%	1.9%	52.5%	9.0%
4	3	25.0%	4.2%	54.5%	8.1%
1	4	36.0%	0.8%	40.3%	13.7%
2	4	34.2%	-0.8%	51.6%	12.4%
3	4	31.8%	-1.4%	58.8%	10.0%
4	4	34.9%	-1.6%	62.4%	8.0%
5	4	26.1%	-1.4%	64.4%	6.9%
1	5	39.7%	-1.6%	41.8%	13.8%
2	5	38.3%	-5.0%	53.4%	13.2%
3	5	35.3%	-6.3%	60.9%	10.6%
4	5	35.7%	-5.4%	64.7%	8.9%
5	5	35.7%	-5.7%	66.6%	7.6%
1	6	42.0%	0.1%	42.7%	14.4%
2	6	40.6%	-4.9%	55.3%	13.7%
3	6	37.9%	-6.0%	62.7%	11.0%
4	6	35.3%	-6.4%	66.8%	9.2%
1	7	43.9%	-0.5%	44.3%	14.8%
2	7	42.7%	-3.3%	57.4%	14.1%
3	7	40.4%	-4.7%	64.6%	11.4%
1	8	45.4%	-0.4%	45.9%	14.8%
2	8	44.4%	-4.1%	59.8%	14.5%
1	9	46.6%	0.3%	48.3%	14.6%

Table E.45: Errors associated with proposed two-stage procedure (Halifax spectrum)

N_L	N_U	upper structure		lower structure	
		maximum	minimum	maximum	maximum
1	1	9.8%	-0.4%	8.7%	3.0%
1	2	22.7%	3.2%	22.1%	0.1%
2	2	19.0%	2.1%	31.0%	1.7%
3	2	14.6%	4.4%	33.0%	4.2%
1	3	31.0%	7.8%	33.4%	12.2%
2	3	28.5%	4.6%	47.6%	11.0%
3	3	26.2%	4.3%	52.9%	9.0%
4	3	21.5%	4.2%	54.6%	8.1%
1	4	36.0%	12.0%	39.6%	13.7%
2	4	34.1%	6.2%	51.0%	12.4%
3	4	30.7%	5.9%	57.8%	10.0%
4	4	35.0%	5.8%	61.1%	8.0%
5	4	24.3%	5.7%	62.8%	6.9%
1	5	39.6%	11.0%	41.4%	14.0%
2	5	38.1%	6.3%	53.2%	13.2%
3	5	35.1%	5.7%	60.6%	10.6%
4	5	36.1%	6.7%	64.4%	8.9%
5	5	36.5%	5.6%	66.3%	7.6%
1	6	42.0%	8.3%	43.9%	14.5%
2	6	40.6%	7.5%	56.6%	13.7%
3	6	39.6%	5.3%	63.9%	11.0%
4	6	38.1%	6.6%	68.0%	9.2%
1	7	43.9%	4.9%	47.3%	14.5%
2	7	42.7%	5.1%	60.8%	14.1%
3	7	40.4%	2.6%	67.8%	11.4%
1	8	45.4%	6.6%	51.4%	13.9%
2	8	44.4%	4.5%	66.2%	14.5%
1	9	46.6%	7.8%	57.2%	12.5%

E.9. Modal parameters of RC column

E.9.1 Elastic stiffness

As suggested by FEMA 356 (FEMA, 2000), the flexural stiffness $(EI)_{stf}$ of the RC column should be 0.5 times of the actual component flexural stiffness if the axial load ratio is not greater than 0.3. With

the rigid floor assumption, the initial stiffness of the RC column in the moment frame can be calculated as

$$k_e = 12\frac{(EI)_{stf}}{h_n^3} = 12\frac{0.5E_cI_g}{h_n^3} \tag{E.34}$$

where E_c is the elastic modulus of the concrete, h_n is the storey height, and I_g is the moment inertia of the gross section. The elastic stiffness of the concrete adopted in Examples 5-1 and 5-2 is E=3.0×10^{4}MPa. The column size is 600mm×600mm. By substituting E_c=3.0×10^4 MPa, h_n=3.3 m and the 600mm×600mm column section into Eq. (E.34), the initial stiffness can be calculated. The calculated initial stiffness is listed in Table 5.14.

E.9.2 Yield shear force

In accordance with FEMA P695 (FEMA, 2009), the yield flexural strength of the RC column (M_y) can be approximated as 0.97 times that calculated by the equations proposed by Panagiotakos and Fradis (2001), i.e., $M_{y,\text{Fradis}}$. The yield moment $M_{y,\text{Fradis}}$ is computed as follows:

$$\frac{M_{y,Fradis}}{bd^3} = \phi_y\left\{E_c\frac{\kappa_y^2}{2}\left[0.5\left(1+\frac{d'}{d}\right)-\frac{\kappa_y}{3}\right]+\frac{E_s}{2}\left[\left(1-\kappa_y\right)\rho_t+\left(\kappa_y-\frac{d'}{d}\right)\rho_c+\frac{\rho_v}{6}\left(1-\frac{d'}{d}\right)\right]\left(1-\frac{d'}{d}\right)\right\} \tag{E.35}$$

where E_s is the elastic modulus of the reinforcement; b is the width of the compression zone; d is the effective depth of the cross section; d' is the distance from the center of the compression reinforcement to the extreme compression fiber; ρ_t and ρ_c are the tension and compression reinforcement ratio, respectively; ρ_v is the ratio of the total web area of the longitudinal reinforcement between tension and compression steel to the product of b and d (bd); ϕ_y is the yield curvature; and κ_y is the normalized compression zone depth at yield. The yield curvature ϕ_y and the normalized compression zone depth at yield κ_y are computed as follows:

$$\phi_y = \frac{f_y}{E_s\left(1-\kappa_y\right)d} \tag{E.36}$$

$$\kappa_y = \sqrt{n^2A^2+2nB}-nA \tag{E.37}$$

where

$$A = \rho_t+\rho_c+\rho_v+\frac{N}{bdf_y} \tag{E.38}$$

$$B = \rho_t+\rho_c\frac{d'}{d}+0.5\rho_v\left(1+\frac{d'}{d}\right)+\frac{N}{bdf_y} \tag{E.39}$$

Table E.46: Design parameters of the RC column in the moment frame

design parameter	E_s (MPa)	f_y (MPa)	$f_{y,sh}$ (MPa)	ρ_t	ρ_c	ρ_v
value	2.00×10^5	235	235	0.009	0.009	0.0
design parameter	ρ_{sh}	v	α_{sl}	s_n	s/d	V_P/V_n
value	0.0121	0.06	1.0	7.5	0.14	0.88

$$n = E_s / E_c \tag{E.40}$$

where N is the axial load. The axial load in this study is approximated as follows:

$$N = \nu A_g f_c \tag{E.41}$$

where ν is the axial load ratio and A_g is the gross area of the column section.

As discussed in section 3.6.1, the column size is 600mm×600mm. By setting $d' = 25$ mm, it is obtained that $d = 600 - d' = 575$ mm. Then, by referring to the configuration of the eight-sotrey RC column in the moment frame that is listed in Table E-2 of FEMA P695 (FEMA, 2009), the design parameters E_s, f_y, ρ_t, ρ_c, ρ_v and ν are listed in Table E.46. With the values of these parameters, the yield moment $M_{y,\text{Fradis}}$ can be calculated through Eqs. (E.35) ~ (E.41). The calculated $M_{y,\text{Fradis}}$ is 537.6kN.m. The yield moment M_y =0.97$M_{y,\text{Fradis}}$=521.4 kN.m.

With the rigid floor assumption, the inflection point is set at the mid-height of the column. The yield shear force V_y is computed as

$$V_y = \frac{2M_y}{h_n} \tag{E.42}$$

Based on Eq. (E.42), the yield shear force can be evaluated. The calculated value of V_y is listed in Table 5.14.

E.9.3 Other parameters

In accordance with the empirical equations provided in Appendix E of FEMA P695 (FEMA, 2009), it is suggested that c=1.0 is acceptable for columns failing in flexure and flexure-shear mode. In addition, δ_p, δ_{pc} and λ are computed as follows:

$$\frac{\delta_p}{0.5h_n} = 0.12\left(1+0.55\alpha_{sl}\right)(0.16)^{\nu}(0.02+40\rho_{sh})^{0.43}\left(0.54\right)^{0.01 f_c}\left(0.66\right)^{0.1 s_n}(2.27)^{10.0\rho} \tag{E.43}$$

$$\frac{\delta_{pc}}{0.5h_n} = 0.76\left(0.031\right)^{\nu}(0.02+40\rho_{sh})^{1.02} \le 0.10 \tag{E.44}$$

$$\lambda = 131\left(0.18\right)^{\nu}\left(0.26\right)^{s/d}\left(0.57\right)^{V_P/V_n}\left(61.4\right)^{\rho_{sh.eff}} \tag{E.45}$$

where α_{sl} is the indicator variable (0 or 1) to signify the possibility of the longitudinal rebar slip past the column end, with α_{sl}=1 if slip is possible; ρ_{sh} is the area ratio of the transverse reinforcement; s_n is the rebar buckling coefficient; ρ is the ratio of total area of the longitudinal reinforcement and $\rho=\rho_t+\rho_c$; s is the spacing of the transverse reinforcement; V_P is the shear demand at the point of flexure yielding; V_n is the shear capacity; and $\rho_{sh,\text{eff}}$ is the effective ratio of the transverse reinforcement evaluated as follows:

$$\rho_{sh,eff} = \rho_{sh} \frac{f_{y,sh}}{f_c} \tag{E.46}$$

where $f_{y,sh}$ is the yield stress of the transverse reinforcement. Still, by referring to the configuration of the eight-storey RC column in the moment frame that is listed in Table E-2 of FEMA P695 (FEMA, 2009), values of the design parameters α_{sl}, ρ_{sh}, s_n, s/d, V_P/V_n and $f_{y,sh}$ are listed in Table E.46. With these values, δ_p, δ_{pc} and λ can be further calculated based on Eqs. (E.43) , (E.44) and (E.45), respectively. The calculated values of δ_p, δ_{pc} and λ are listed in Table 5.14.

In addition, a constant value 1.13 is suggested for V_c/V_y , i.e., V_c/V_y=1.13. Therefore, based on Figure 5.14, the parameter α_s can be computed as follows:

$$\alpha_s = \frac{0.13V_y}{k_e\delta_p} \tag{E.47}$$

The calculated value of α_s is listed in Table 5.14.

Appendix F Estimation of ε_i

F.1 Estimation of ε_i

Recall Eq.(6.9):

$$\ddot{\mathbf{D}} + \boldsymbol{\Xi}\dot{\mathbf{D}} + \boldsymbol{\Omega}^2\mathbf{D} = -\boldsymbol{\tau}\ddot{x}_g \tag{F.1}$$

where $\mathbf{D} = [D_1 \quad D_2 \quad \cdots \quad D_N]^T$. Let

$$\mathbf{Z}^T = \left[\mathbf{D}^T \quad \dot{\mathbf{D}}^T\right]^T \tag{F.2}$$

Substitution of Eq.(F.2) into Eq.(F.1) leads to

$$\dot{\mathbf{Z}} = \mathbf{A}\mathbf{Z} + \boldsymbol{\upsilon}\ddot{x}_g \tag{F.3}$$

where

$$\mathbf{A} = \begin{bmatrix} \mathbf{0}_{N\times N} & \mathbf{I}_{N\times N} \\ \boldsymbol{\Omega}^2 & -\boldsymbol{\Xi} \end{bmatrix} \tag{F.4}$$

$$\boldsymbol{\upsilon} = \begin{bmatrix} \mathbf{0}_{N\times 1} \\ -\boldsymbol{\tau} \end{bmatrix} \tag{F.5}$$

In Eqs.(F.4) and (F.5), $\mathbf{0}_{N\times N}$ and $\mathbf{I}_{N\times N}$ represent the zero and identity matrices with the order of ($N\times N$). The subscript $a_0\times b_0$ indicates the zero or identity matrix has "a_0" rows and "b_0" columns. Assume the earthquake ground motion is a white noise with a constant power spectrum density being S_0. The stationary covariance of $\mathbf{Z}^{[2]}$ can be written as follows (Falsone & Muscolino, 1999):

$$E\left[\mathbf{Z}^{[2]}\right] = -2S_0\mathbf{A}_2^{-1}\boldsymbol{\upsilon}^{[2]} \tag{F.6}$$

where the operation "-1" represents the inverse of a matrix; the exponent in square brackets, i.e.,[2], indicates the power made by the Kronecker block product, that is

$$\mathbf{Z}^{[2]} = \mathbf{Z}\odot\mathbf{Z} = \begin{bmatrix} \mathbf{D}\otimes\mathbf{D} \\ \mathbf{D}\otimes\dot{\mathbf{D}} \\ \dot{\mathbf{D}}\otimes\mathbf{D} \\ \dot{\mathbf{D}}\otimes\dot{\mathbf{D}} \end{bmatrix} \tag{F.7}$$

and the matrix $\mathbf{A}_2$ is given by

$$\mathbf{A}_2 = \mathbf{A}\otimes\mathbf{I}_{2N\times 2N} + \mathbf{I}_{2N\times 2N}\otimes\mathbf{A} = \mathbf{A}\oplus\mathbf{A} \tag{F.8}$$

In Eqs.(F.7) and (F.8), symbols $\otimes$ and $\odot$ represent the Kronecker product and Kronecker block product, respectively. Detail introduction on the Kronecker algebra is discussed in the following Appendix F.3.

Split the modal damping matrix $\boldsymbol{\Xi}$ into two that only contain diagonal terms and off-diagonal terms, respectively, that is

$$\boldsymbol{\Xi} = \boldsymbol{\Xi}_d + \boldsymbol{\Xi}_f \tag{F.9}$$

where

$$\boldsymbol{\Xi}_d = \begin{bmatrix} \Xi_{11} & 0 & \cdots & 0 \\ 0 & \Xi_{22} & \cdots & 0 \\ \vdots & \vdots & \ddots & \vdots \\ 0 & 0 & \cdots & \Xi_{NN} \end{bmatrix} \tag{F.10}$$

$$\boldsymbol{\Xi}_f = \begin{bmatrix} 0 & \Xi_{12} & \cdots & \Xi_{1N} \\ \Xi_{21} & 0 & \cdots & \Xi_{2N} \\ \vdots & \vdots & \ddots & \vdots \\ \Xi_{N1} & \Xi_{N2} & \cdots & 0 \end{bmatrix} \tag{F.11}$$

With the substitution of Eq.(F.9) into Eq.(F.4) and then the substitution of (F.4) into Eq. (F.8), it is obtained that

$$\mathbf{A}_2 = \mathbf{A}_{2,d} + \mathbf{A}_{2,f} \tag{F.12}$$

where

$$\mathbf{A}_{2,d} = \mathbf{A}_d \oplus \mathbf{A}_d = \begin{bmatrix} \mathbf{0}_{N^2\times N^2} & \mathbf{I}_{N^2\times N^2} & \mathbf{I}_{N^2\times N^2} & \mathbf{0}_{N^2\times N^2} \\ -\mathbf{I}_{n\times n}\otimes\boldsymbol{\Omega}^2 & -\mathbf{I}_{N\times N}\otimes\boldsymbol{\Xi}_d & \mathbf{0}_{N^2\times N^2} & \mathbf{I}_{N^2\times N^2} \\ -\boldsymbol{\Omega}^2\otimes\mathbf{I}_{N\times N} & \mathbf{0}_{N^2\times N^2} & -\boldsymbol{\Xi}_d\otimes\mathbf{I}_{N\times N} & \mathbf{I}_{N^2\times N^2} \\ \mathbf{0}_{N^2\times N^2} & -\boldsymbol{\Omega}^2\otimes\mathbf{I}_{N\times N} & -\mathbf{I}_{N\times N}\otimes\boldsymbol{\Omega}^2 & -\boldsymbol{\Xi}_d\oplus\boldsymbol{\Xi}_d \end{bmatrix} \tag{F.13}$$

$$\mathbf{A}_{2,f} = \mathbf{A}_f \oplus \mathbf{A}_f = \begin{bmatrix} \mathbf{0}_{N^2\times N^2} & \mathbf{0}_{N^2\times N^2} & \mathbf{0}_{N^2\times N^2} & \mathbf{0}_{N^2\times N^2} \\ \mathbf{0}_{N^2\times N^2} & -\mathbf{I}_{N\times N}\otimes\boldsymbol{\Xi}_f & \mathbf{0}_{N^2\times N^2} & \mathbf{0}_{N^2\times N^2} \\ \mathbf{0}_{N^2\times N^2} & \mathbf{0}_{N^2\times N^2} & -\boldsymbol{\Xi}_f\otimes\mathbf{I}_{N\times N} & \mathbf{I}_{N^2\times N^2} \\ \mathbf{0}_{N^2\times N^2} & \mathbf{0}_{N^2\times N^2} & \mathbf{0}_{N^2\times N^2} & -\boldsymbol{\Xi}_f\oplus\boldsymbol{\Xi}_f \end{bmatrix} \tag{F.14}$$

In Eqs.(F.13) and (F.14),

$$\mathbf{A}_d = \begin{bmatrix} \mathbf{0}_{N\times N} & \mathbf{I}_{N\times N} \\ \boldsymbol{\Omega}^2 & -\boldsymbol{\Xi}_d \end{bmatrix} \tag{F.15}$$

$$\mathbf{A}_f = \begin{bmatrix} \mathbf{0}_{N\times N} & \mathbf{0}_{N\times N} \\ \mathbf{0}_{N\times N} & -\boldsymbol{\Xi}_f \end{bmatrix} \tag{F.16}$$

Substitute Eq.(F.12) into (F.6). It is derived that

$$E\left[\mathbf{Z}^{[2]}\right] = E\begin{bmatrix} \mathbf{D}\otimes\mathbf{D} \\ \mathbf{D}\otimes\dot{\mathbf{D}} \\ \dot{\mathbf{D}}\otimes\mathbf{D} \\ \dot{\mathbf{D}}\otimes\dot{\mathbf{D}} \end{bmatrix} = -2S_0\mathbf{B}\mathbf{A}_{2,d}^{-1}\boldsymbol{\upsilon}^{[2]} = \mathbf{B}E\begin{bmatrix} \mathbf{D}_0\otimes\mathbf{D}_0 \\ \mathbf{D}_0\otimes\dot{\mathbf{D}}_0 \\ \dot{\mathbf{D}}_0\otimes\mathbf{D}_0 \\ \dot{\mathbf{D}}_0\otimes\dot{\mathbf{D}}_0 \end{bmatrix} \tag{F.17}$$

where $\mathbf{D}_0$ represents the displacement vector for the classically-damped system, in which the off-diagonal terms of the modal damping matrix $\boldsymbol{\Xi}$ are zero, as shown in Eq.(6.26); and

$$\mathbf{B} = \left[\mathbf{I}_{4N^2 \times 4N^2} + \mathbf{A}_{2,d}^{-1} \mathbf{A}_{2,f} \right]^{-1} \tag{F.18}$$

Assume the matrix $\mathbf{B}$ has the following format:

$$\mathbf{B} = \begin{bmatrix} \mathbf{B}_0 & \mathbf{B}_1 & \mathbf{B}_2 & \mathbf{B}_3 \\ \mathbf{B}_4 & \mathbf{B}_5 & \mathbf{B}_6 & \mathbf{B}_7 \\ \mathbf{B}_8 & \mathbf{B}_9 & \mathbf{B}_{10} & \mathbf{B}_{11} \\ \mathbf{B}_{12} & \mathbf{B}_{13} & \mathbf{B}_{14} & \mathbf{B}_{15} \end{bmatrix} \tag{F.19}$$

Substitute Eq.(F.19) into Eq.(F.17). Then, it is derived that

$$\begin{aligned} E\left[D_i D_j \right] = & \sum_{u=1}^{N} \sum_{v=1}^{N} B_{0,t_1 t_2} E\left[D_{0,u} D_{0,v} \right] + \sum_{u=1}^{N} \sum_{v=1}^{N} B_{1,t_1 t_2} E\left[D_{0,u} \dot{D}_{0,v} \right] + \sum_{u=1}^{N} \sum_{v=1}^{N} B_{2,t_1 t_2} E\left[\dot{D}_{0,u} D_{0,v} \right] \\ & + \sum_{u=1}^{N} \sum_{v=1}^{N} B_{3,t_1 t_2} E\left[\dot{D}_{0,u} \dot{D}_{0,v} \right] \end{aligned} \tag{F.20}$$

where $t_1 = i + N(j-1)$ and $t_2 = u + N(v-1)$. Re-organize Eq.(F.20) as follows:

$$E\left[D_i D_j \right] = E\left[D_{0,i} D_{0,j} \right] \left(1 + \varepsilon_{ij} \right) \tag{F.21}$$

where

$$\varepsilon_{ij} = \frac{\sum_{u=1}^{N} \sum_{v=1}^{N} \left\{ B_{0,t_1 t_2} E\left[D_{0,u} D_{0,v} \right] + B_{1,t_1 t_2} E\left[D_{0,u} \dot{D}_{0,v} \right] + B_{2,t_1 t_2} E\left[\dot{D}_{0,u} D_{0,v} \right] + B_{3,t_1 t_2} E\left[\dot{D}_{0,u} \dot{D}_{0,v} \right] \right\}}{E\left[D_{0,i} D_{0,j} \right]} - 1 \tag{F.22}$$

From Eq.(F.21), it is seen the parameter ε_{ij} represents the error of $E[D_i D_j]$ introduced by ignoring the off-diagonal terms of the modal damping matrix $\boldsymbol{\Xi}$. For the classically-damped system, the expected value $E\left[D_{0,i} D_{0,j} \right]$, $E\left[D_{0,i} \dot{D}_{0,j} \right]$, $E\left[\dot{D}_{0,i} D_{0,j} \right]$ and $E\left[\dot{D}_{0,i} \dot{D}_{0,j} \right]$ can be theoretically solved for, as discussed in Appendix F.2. Based on Eqs.(F.38) and (F.39) in Appendix F.2, the following relationship can be obtained:

$$\begin{aligned} E\left[D_{0,u} D_{0,u} \right] &= \rho_{vu} \sqrt{E\left[D_{0,u}^2 \right] E\left[D_{0,v}^2 \right]} \\ E\left[D_{0,u} \dot{D}_{0,v} \right] &= \rho_{1,uv} \omega_v \sqrt{E\left[D_{0,u}^2 \right] E\left[D_{0,v}^2 \right]} \\ E\left[\dot{D}_{0,u} D_{0,v} \right] &= \rho_{1,vu} \omega_u \sqrt{E\left[D_{0,u}^2 \right] E\left[D_{0,v}^2 \right]} \\ E\left[\dot{D}_{0,u} \dot{D}_{0,v} \right] &= \rho_{vu} \omega_u \omega_v \sqrt{E\left[D_{0,u}^2 \right] E\left[D_{0,v}^2 \right]} \end{aligned} \tag{F.23}$$

where $\rho_{1,uv}$ and ρ_{uv} are correlation coefficients associated with the *u*-th and *v*-th modes and are presented in Eq.(F.40) . Meanwhile, by using the first order Taylor Series to expand matrix **B** in Eq. (F.18), it is obtained that

$$\mathbf{B} \approx \mathbf{I}_{4N^2 \times 4N^2} - \mathbf{A}_{2,d}^{-1}\mathbf{A}_{2,f} \tag{F.24}$$

The inverse of matrix $\mathbf{A}_{2,d}$ is presented in Eqs.(F.33) and (F.34) of Appendix F.2. With the substitution of Eqs.(F.14) and (F.33) into Eq.(F.24), it is derived that

$$\mathbf{B}_0 = \mathbf{I}_{N^2 \times N^2}\ ,\ \mathbf{B}_1 = \hat{\mathbf{b}}_0\left(\mathbf{I}_{N\times N} \otimes \mathbf{\Xi}_f\right),\ \mathbf{B}_2 = \hat{\mathbf{c}}_0\left(\mathbf{\Xi}_f \otimes \mathbf{I}_{N\times N}\right),\ \mathbf{B}_3 = \hat{\mathbf{d}}_0\left(\mathbf{\Xi}_f \otimes \mathbf{\Xi}_f\right) \tag{F.25}$$

where diagonal matrices $\hat{\mathbf{b}}_0$, $\hat{\mathbf{c}}_0$, $\hat{\mathbf{d}}_0$ are presented in Eq. (F.34). Substitute Eqs.(F.23) and (F.25) into Eq.(F.22). It is derived that

$$\begin{aligned}\varepsilon_{ij} = &\sum_{u=1}^{N}\left\{\left[\frac{\rho_{1,uj}}{\rho_{ij}} b_{0,tt}\omega_j + \omega_u\omega_j d_{0,tt}\frac{\rho_{uj}}{\rho_{ij}}\right]\Xi_{f,iu}\sqrt{\frac{E\left[D_{0,u}^2\right]}{E\left[D_{0,i}^2\right]}}\right\} \\ &\sum_{u=1}^{N}\left\{\left[\frac{\rho_{1,ui}}{\rho_{ij}} c_{0,tt}\omega_i + \omega_u\omega_i d_{0,tt}\frac{\rho_{ui}}{\rho_{ij}}\right]\Xi_{f,ju}\sqrt{\frac{E\left[D_{0,u}^2\right]}{E\left[D_{0,j}^2\right]}}\right\}\end{aligned} \tag{F.26}$$

where $t=i+N(j-1)$. For the case where $i=j$, based on Eq. (F.34), it is obtained that

$$b_{0,tt} = c_{0,tt} = \frac{-1}{2\omega_i^2},\quad d_{0,tt} = \frac{-1}{4\varsigma_i\omega_i^3} \tag{F.27}$$

where $t=i+N(i-1)$. With the substitution of Eqs.(F.27) and (F.37) into Eq.(F.26), the following can be derived:

$$\varepsilon_{ii} = -\sum_{u=1}^{N}\frac{\Xi_{f,iu}}{\sqrt{\Xi_{ii}\Xi_{uu}}}\left(\frac{2\rho_{1,ui}\varsigma_i\omega_i}{\omega_u} + \rho_{ui}\right) \tag{F.28}$$

Based on Eqs.(F.41) in Appendix F.2, it is obtained that

$$\frac{2\rho_{1,ui}\varsigma_i\omega_i}{\omega_u} = \frac{\varsigma_i\left(1-\beta_{iu}^2\right)}{\varsigma_u + \varsigma_i\beta_{iu}}\rho_{ui} \tag{F.29}$$

where β_{iu} is the ratio of natural frequency between the *i*th- and *u*th-modes, as defined in Eq.(F.42) of Appendix F.2. Note both correlation coefficients ρ_{iu} and $\rho_{1,iu}$ only become significant when β_{iu}=1, as shown in Figure E.1 of Appendix F.2. However, in practice for a combined framing system, when β_{iu} is close to unity, the mode shape of the *i*th-mode will be very similar to that of the *u*th-mode, i.e., $\boldsymbol{\varphi}_i \approx \boldsymbol{\varphi}_u$ In such case, $\varsigma_i \approx \varsigma_u$ based on Eqs.(6.16 a)~ (5.16 c).Therefore, when β_{iu} is close to unity, it is concluded that

$$\frac{\varsigma_i\left(1-\beta_{iu}^2\right)}{\varsigma_u+\varsigma_i\beta_{iu}}\approx 1-\beta_{iu}\approx 0 \tag{F.30}$$

Therefore, the modal error ε_{ii} in Eq.(F.28) can be further simplified as

$$\varepsilon_{ii}=-\sum_{u=1}^{N}\rho_{ui}\frac{\Xi_{f,iu}}{\sqrt{\Xi_{ii}\Xi_{uu}}} \tag{F.31}$$

Note the modal error ε_{ii} is denoted as ε_i for simplicity in Chapter 5.

F.2 Classically-damped structure

When the structure is classically damped, i.e., the off-diagonal terms of the modal damping matrix $\mathbf{\Xi}$ are zero, Eq.(F.17) becomes as

$$E\begin{bmatrix}\mathbf{D}_0\otimes\mathbf{D}_0\\ \mathbf{D}_0\otimes\dot{\mathbf{D}}_0\\ \dot{\mathbf{D}}_0\otimes\mathbf{D}_0\\ \dot{\mathbf{D}}_0\otimes\dot{\mathbf{D}}_0\end{bmatrix}=-2S_0\mathbf{A}_{2,d}^{-1}\boldsymbol{\upsilon}^{[2]} \tag{F.32}$$

Based on Eq.(F.13), the inverse matrix of $\mathbf{A}_{2,d}$ can be solved for as follows:

$$\mathbf{A}_{2,d}^{-1}=\begin{bmatrix}\hat{\mathbf{a}}_0 & \hat{\mathbf{b}}_0 & \hat{\mathbf{c}}_0 & \hat{\mathbf{d}}_0\\ \hat{\mathbf{e}}_0 & \hat{\mathbf{f}}_0 & \hat{\mathbf{g}}_0 & \hat{\mathbf{h}}_0\\ \hat{\mathbf{I}}_0 & \hat{\mathbf{m}}_0 & \hat{\mathbf{n}}_0 & \hat{\mathbf{r}}_0\\ \hat{\mathbf{s}}_0 & \hat{\mathbf{t}}_0 & \hat{\mathbf{v}}_0 & \hat{\mathbf{w}}_0\end{bmatrix} \tag{F.33}$$

where $\hat{\mathbf{a}}_0=\mathbf{I}_{N^2\times N^2}$, and all other submatrices are diagonal. The diagonal terms of $\hat{\mathbf{b}}_0$, $\hat{\mathbf{c}}_0$, $\hat{\mathbf{d}}_0$, $\hat{\mathbf{h}}_0$, $\hat{\mathbf{r}}_0$ and $\hat{\mathbf{w}}_0$ are calculated as follows (Falsone & Muscolino, 2004):

$$\hat{b}_{0,tt}=\frac{-\mu_{ij}}{\chi_{ij}}\ ,\quad \hat{c}_{0,tt}=\frac{-\mu_{ji}}{\chi_{ij}}\ ,\quad \hat{d}_{0,tt}=-\frac{2\varsigma_i\omega_i+2\varsigma_i\omega_j}{\chi_{ij}}\ ,\quad \hat{h}_{0,tt}=\frac{\omega_i^2-\omega_j^2}{\chi_{ij}}$$

$$\hat{r}_{0,tt}=\frac{\omega_j^2-\omega_i^2}{\chi_{ij}},\quad \hat{w}_{0,tt}=-\frac{\omega_i\omega_j\left(2\varsigma_i\omega_i+2\varsigma_i\omega_j\right)}{\chi_{ij}} \tag{F.34}$$

where $t=i+(n-1)j$, and

$$\varsigma_i=\frac{\Xi_{ii}}{2\omega_i} \tag{F.35}$$

$$\mu_{ij}=\omega_i^2-\omega_j^2\left(1-4\varsigma_j^2\right)+4\varsigma_i\varsigma_j\omega_i\omega_j\ ,\quad \chi_{ij}=\omega_i^2\mu_{ij}+\omega_j^2\mu_{ji} \tag{F.36}$$

With the substitution of Eqs.(F.33) and (F.34) into Eq.(F.32), it is obtained that

$$
\begin{aligned}
E\left[D_{0,i}D_{0,j}\right] &= -2S_0\hat{d}_{0,tt} = 2S_0\frac{2\varsigma_i\omega_i + 2\varsigma_i\omega_j}{\chi_{ij}} \\
E\left[D_{0,i}\dot{D}_{0,j}\right] &= -2S_0\hat{h}_{0,tt} = -2S_0\frac{\omega_i^2 - \omega_j^2}{\chi_{ij}} \\
E\left[\dot{D}_{0,i}D_{0,j}\right] &= -2S_0\hat{r}_{0,tt} = 2S_0\frac{\omega_i^2 - \omega_j^2}{\chi_{ij}} \\
E\left[\dot{D}_{0,i}\dot{D}_{0,j}\right] &= -2S_0\hat{w}_{0,tt} = 2S_0\frac{\omega_i\omega_j\left(2\varsigma_i\omega_i + 2\varsigma_i\omega_j\right)}{\chi_{ij}}
\end{aligned}
\tag{F.37}
$$

Define

$$
\rho_{ij} = \frac{E\left(D_{0,i}D_{0,j}\right)}{\sqrt{E\left(D_{0,i}^2\right)E\left(D_{0,j}^2\right)}},\quad \rho_{1,ij} = \frac{E\left(D_{0,i}\dot{D}_{0,j}\right)}{\sqrt{E\left(D_{0,i}^2\right)E\left(\dot{D}_{0,j}^2\right)}},\quad \rho_{2,ij} = \frac{E\left(\dot{D}_{0,i}\dot{D}_{0,j}\right)}{\sqrt{E\left(\dot{D}_{0,i}^2\right)E\left(\dot{D}_{0,j}^2\right)}} \tag{F.38}
$$

Meanwhile, from Eq.(F.37) it is obtained that

$$
E\left(\dot{D}_{0,i}^2\right) = \omega_i^2 E\left(D_{0,i}^2\right) \tag{F.39}
$$

By substituting of Eqs.(F.34) and (F.39) into Eq.(F.38), it is obtained that

$$
\begin{aligned}
\rho_{ij} &= \frac{4\left(\omega_i\omega_j\right)^{1.5}\left(\varsigma_i\varsigma_j\right)\left(2\varsigma_i\omega_i + 2\varsigma_j\omega_j\right)}{\chi_{ij}} \\
\rho_{1,ij} &= \frac{4\omega_i\left(\omega_i\omega_j\varsigma_i\varsigma_j\right)\left(\omega_i^2 - \omega_j^2\right)}{\chi_{ij}} \\
\rho_{2,ij} &= \rho_{ij}
\end{aligned}
\tag{F.40}
$$

With the substitution of Eq.(F.36) into Eq.(F.40), it is obtained that

$$
\rho_{ij} = \rho_{2,ij} = \frac{8\left(\beta_{ij}\right)^{1.5}\left(\varsigma_i\varsigma_j\right)^{0.5}\left(\varsigma_i + \varsigma_j\beta_{ij}\right)}{\left[1-\left(\beta_{ij}\right)^2\right]^2 + 4\varsigma_i\varsigma_j\beta_{ij}\left[1+\left(\beta_{ij}\right)^2\right] + 4\left(\beta_{ij}\right)^2\left[\left(\varsigma_i\right)^2 + \left(\varsigma_j\right)^2\right]} \tag{F.41}
$$

$$
\rho_{1,ij} = \frac{\left[\left(\beta_{ij}\right)^2 - 1\right]\left(\beta_{ij}\right)^{0.5}\left(\varsigma_i\varsigma_j\right)^{0.5}}{\left[1-\left(\beta_{ij}\right)^2\right]^2 + 4\varsigma_i\varsigma_j\beta_{ij}\left[1+\left(\beta_{ij}\right)^2\right] + 4\left(\beta_{ij}\right)^2\left[\left(\varsigma_i\right)^2 + \left(\varsigma_j\right)^2\right]}
$$

where

$$
\beta_{ij} = \omega_i / \omega_j \tag{F.42}
$$

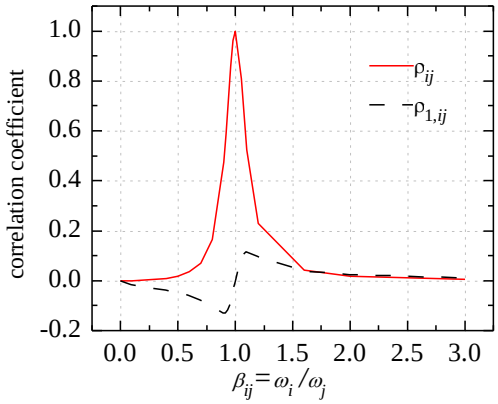

Figure F.1: Variation of correlation coefficients with natural frequency ratio β_{ij} ($\varsigma_i = \varsigma_j = 0.05$)

As shown in Figure F.1, both correlation coefficients ρ_{ij} and $\rho_{1,ij}$ only become significant near to $\beta_{ij} = 1$ and the magnitudes of the both coefficients diminish rapidly as the two natural frequencies move farther apart. However, the magnitude of ρ_{ij} is far greater than that of $\rho_{1,ij}$. The maximum value for ρ_{ij} is unity while the maximum magnitude for $\rho_{1,ij}$ is only 0.12, as shown in Figure F.1.

F.3 Kronecker algebra

Give two matrices **P** and **Q**. Suppose the matrix **P** is as follows:

$$\mathbf{P} = \begin{bmatrix} p_{11} & p_{12} & \cdots & p_{1n} \\ p_{21} & p_{22} & \cdots & p_{2n} \\ \vdots & \vdots & \ddots & \vdots \\ p_{m1} & p_{m2} & \cdots & p_{mn} \end{bmatrix} \tag{F.43}$$

The Kronecker product $\mathbf{P} \otimes \mathbf{Q}$ is as calculated as follows (Falsone & Muscolino, 1999):

$$\mathbf{R} = \mathbf{P} \otimes \mathbf{Q} = \begin{bmatrix} p_{11}\mathbf{Q} & p_{12}\mathbf{Q} & \cdots & p_{1n}\mathbf{Q} \\ p_{21}\mathbf{Q} & p_{22}\mathbf{Q} & \cdots & p_{2n}\mathbf{Q} \\ \vdots & \vdots & \ddots & \vdots \\ p_{m1}\mathbf{Q} & p_{m2}\mathbf{Q} & \cdots & p_{mn}\mathbf{Q} \end{bmatrix} \tag{F.44}$$

Therefore, if **P** and **Q** are of order $(m \times n)$ and $(r \times s)$, respectively, the Kronecker product $\mathbf{P} \otimes \mathbf{Q}$ is of order $(mr \times ns)$.

Now, if **P** and **Q** are matrices built by submatrices as follows:

$$\mathbf{P} = \begin{bmatrix} \mathbf{P}_{11} & \mathbf{P}_{12} \\ \mathbf{P}_{21} & \mathbf{P}_{22} \end{bmatrix}, \quad \mathbf{Q} = \begin{bmatrix} \mathbf{Q}_{11} & \mathbf{Q}_{12} \\ \mathbf{Q}_{21} & \mathbf{Q}_{22} \end{bmatrix} \tag{F.45}$$

Beyond the classical Kronecker product as introduced in Eq.(F.44), the block Kronecker product $\mathbf{P} \odot \mathbf{Q}$ is calculated is follows:

$$\mathbf{R} = \mathbf{P} \odot \mathbf{Q} = \begin{bmatrix} \mathbf{P}_{11} \otimes \mathbf{Q}_{11} & \mathbf{P}_{11} \otimes \mathbf{Q}_{12} & \mathbf{P}_{12} \otimes \mathbf{Q}_{11} & \mathbf{P}_{12} \otimes \mathbf{Q}_{12} \\ \mathbf{P}_{11} \otimes \mathbf{Q}_{21} & \mathbf{P}_{11} \otimes \mathbf{Q}_{22} & \mathbf{P}_{12} \otimes \mathbf{Q}_{21} & \mathbf{P}_{12} \otimes \mathbf{Q}_{22} \\ \mathbf{P}_{21} \otimes \mathbf{Q}_{11} & \mathbf{P}_{21} \times \mathbf{Q}_{12} & \mathbf{P}_{22} \times \mathbf{Q}_{11} & \mathbf{P}_{22} \otimes \mathbf{Q}_{12} \\ \mathbf{P}_{21} \otimes \mathbf{Q}_{21} & \mathbf{P}_{21} \otimes \mathbf{Q}_{22} & \mathbf{P}_{22} \otimes \mathbf{Q}_{21} & \mathbf{P}_{22} \otimes \mathbf{Q}_{22} \end{bmatrix} \tag{F.46}$$